The evaluation of data filtering criteria in wind turbine power performance assessment

Brian Davison

A thesis submitted in partial fulfilment of the requirements of Edinburgh Napier University, for the award of Doctor of Philosophy

August 2019

Abstract

The post-installation verification of wind turbine performance is an essential part of a wind energy project. Data collected from meteorological instruments and from the turbine is analysed to produce an estimate of the annual energy production (AEP) which is compared against expectations. However, turbine warranties can impose very strict data filtering criteria which can lead to high rates of data loss. As a consequence, measurement campaigns may last longer than expected and incur additional costs for the development.

This project aims to investigate the extent of the problem and the potential of alternative data filtering strategies with respect to data loss, AEP estimates and the dispersion of points in the power curve scatter plot. In doing so, it targets a wide range of meteorological parameters with theoretical relationships to wind turbine power production with particular interest in those not accounted for in the current standard. The identification of viable filtering strategies with lower data loss would provide significant benefits to wind energy development projects in terms of greater control over timescales and reduced costs.

Data from a sample of power performance tests is analysed to explore the range and severity of the problem of data loss. It confirms the wide variation in warranty conditions, demonstrates the extent and likelihood of data losses and quantifies the financial implications within the limits of commercial sensitivity. When indirect costs are taken into consideration, the impact of extended measurement campaigns can theoretically reach tens of millions of pounds.

A new, high-fidelity dataset is then compiled so that the effects of alternative filtering strategies can be examined. The dataset covers the whole of 2017 and consists of over 700 parameters of which 74 are selected for investigation here. The eFAST method of global sensitivity analysis is used in combination with correlation analysis to reduce this number to 11 parameters which are then used to define alternative filtering criteria.

Similar AEP estimates are obtained by application of conventional and experimental criteria to the research dataset. In the case of the experimental filters, however, the data loss was 11% compared to 63% data loss with conventional filters. Conventional filters were also shown to increase the dispersion in the power curve scatter plot by over 10%, while dispersion did not increase significantly with the experimental filters.

Acknowledgements

First of all, I would like to recognise the major contribution to this work made by my partner Bridget with her patience and forbearance over the course of the whole process. It is largely through her support that I have been able to complete this project.

I would also like to extend my thanks to past and present staff at Wood Clean Energy (previously Sgurr Energy) who first proposed the topic to me and then supported me to complete the project. Special mention goes to Richard Boddington, Gabriele Calvo, Peter Clive, Katie Gracie-Orr, Pablo Olmos, Florin Pintilie and Dave Robb. (NB. Alphabetical order!)

The data used in the project was provided by the University of Minnesota, and I would like to thank Chris Milliren for accommodating all of my requests with no hint of impatience.

Throughout the project, I have communicated with several authors and researchers. Some of their work and comments became part of this project while others did not, but without exception they were open, encouraging and helpful and I would like to add their names to this section:

Dale Dolan	Kurt S. Hansen	Eric Lebigot
Stefan Emeis	Gerhard Heinzel	Mike Optis
Thomas Foken	Jason Jonkman	Olaf Outzen
Breanne Gellatly	Estate Khmaladze	Joris Peeters

The people who read drafts and gave me feedback were also important, so thanks to Richard Dixon, Murray MacCallum and Tim Read for their support. Also, thanks to Steph Archibald for helping deliver the draft!

Finally, I would like to thank my supervisory team, Ahmed Al-Dubai, Alistair Armitage and Tariq Muneer. I am sure they would have preferred a more conventional student.

Declaration

I hereby declare that the work presented in this thesis was carried out entirely by myself at Edinburgh Napier University, except where due acknowledgement is made, and that it has not been submitted for any other degree or professional qualification.

[redacted]

Brian Davison (Candidate)

Date 8 Aug 2019

TABLE OF CONTENTS

Table of figures

Table of tables

Symbols and abbreviations

$\bar{a}$	Mean value of quantity a
a'	Perturbation of quantity a
a_0	Value of a at the surface
a_t	Value of a at time t
a_U	Stationarity of horizontal wind speed
a_z	Value of a at height z; Stationarity of vertical wind speed
$\|a\|$	Absolute value of a
Δa	Difference in two values of a, typically at the top and bottom of an atmospheric layer
a_h	Quantity a measured at hub height
a_{max}	Maximum value of quantity a
a_{min}	Minimum value of quantity a
a_{ref}	Quantity a measured at reference height
$\hat{a}$	Expected value of quantity a
A	Area swept by the turbine rotor
ABL	Atmospheric boundary layer
ADF	Augmented Dickey-Fuller test p-value
AEP	Annual Energy Production
A_i	Area of the i^{th} rotor segment
ANN	Artificial neural network
ASL	Atmospheric surface layer
ASOS	Automated Surface Observing Systems
B	Barometric pressure
BEM	Blade element momentum
c	Speed of sound
c, k	Parameters to the Weibull function
CFD	Computational Fluid Dynamics
C_p	Coefficient of performance; Power coefficient; Specific heat of air at constant pressure
C_K	Kolmogorov constant ≅ 2
C_{RM}	Rossby-Montgomery coefficient
d	Wind direction
D	Rotor diameter; Campaign duration
DAQ	Data acquisition
eFAST	Extended Fourier amplitude sensitivity test
FAST	Fourier amplitude sensitivity test
f	Coriolis parameter; Neural network activation function
F	Vertical momentum flux
$F(\,)$	Cumulative probability function
$f(u)$	Wind speed probability density distribution
f_{loss}	Fraction of data lost
G	Geostrophic wind speed
G_{sz}, G_{sm}	Zonal/meridional surface geostrophic wind speed
g	Acceleration due to gravity; Neural network integration function
G_{tz}, G_{tm}	Zonal and meridional components of the thermal wind
GW	Gigawatt
GWh	Gigawatt hour
H	Hub height
h	Height of the boundary layer
hPa	hectopascal
IEC	International Electrotechnical Commission
IEC2005	IEC 61400-12-1 2005 edition
IEC2017	IEC 61400-12-1 2017 edition
$\boldsymbol{i_U}$	Intermittency of horizontal wind speed
JB	Jarque-Bera test p-value
K	Kurtosis

$KPSS$	Kwiatkowski-Phillips-Schmidt-Shin test p-value
kW	kilowatt
L	Obukhov length; Distance from turbine to measurement equipment
$Lidar$	Light Detection And Ranging
M	Number of harmonics
MA	Mean error
MAE	Mean absolute error
$MAIC$	Modified Akaike information criterion
MW	Megawatt
MWh	Megawatt hour
n	Number of moles of gas
N	Number of bins; Number of values in series; Brunt-Väisälä frequency
N_h	Number of hours in one year = 8760
N_i	Number of TMA power values in bin i
N_s	Number of samples
$\boldsymbol{n_U}$	Normality of horizontal wind speed
$\boldsymbol{n_z}$	Normality of vertical wind speed
P	Power
$P(u)$	Power output: function of wind speed (i.e. the turbine power curve)
Pa	Pascal
$PCWG$	Power Curve Working Group
P	Electrical power output; Pressure
P_i	Power output in bin i
$P_{I=0}(u)$	Zero turbulence power curve
$P_{Iref}(u)$	power output normalised to reference turbulence intensity I_{ref}
P_{sim}	Simulated power output
$P_{sim.I}(u)$	Simulated power output for measured turbulence intensity
$P_{sim.Iref}(u)$	Simulated power output for the reference turbulence intensity
PPT	Power Performance Test
P_w	Power available in the wind; Vapour pressure
Q	Kinematic sensible heat flux
QA	Quality assurance
QC	Quality control
q	Specific humidity
r	Autocorrelation function
R	Rotor radius; Universal gas constant
R_d	Gas constant for dry air
R_w	Gas constant for water vapour
$REWS$	Rotor equivalent wind speed
Ri_b	Bulk Richardson number
$RMSE$	Root mean square error
RSD	Remote sensing device
r^2	Coefficient of determination/Pearson correlation coefficient
s	Slope of the best-fit line in a correlation; standard uncertainty; sampling frequency
S	Skew; Sensitivity index
SA	Sensitivity analysis
$SCADA$	Supervisory Control And Data Acquisition
$Sodar$	Sound detection and ranging
$s_{P,i}$	Normalised mean power in bin i
S_T	Total effect
T	Measured temperature
TI	Turbulence intensity
TKE	Turbulent kinetic energy
TMA	Ten-minute average
T_s	Sonic temperature
T_v	Virtual temperature
U	Horizontal TMA wind speed perpendicular to the rotor

u, v, w	Zonal, meridional and vertical wind components
U_i	Wind speed measured at height z_i; Normalized and averaged wind speed in bin i; Wind speed corresponding to ith segment
U_n	Normalized wind speed
U_{eq}	Rotor equivalent wind speed
u_*	Friction velocity
$\bar{U}$	Annual average hub height wind speed
V	Volume; Coefficient of variation; Variance
V_2	Second-order coefficient of variation
$\overline{w'u'}$	Kinematic vertical flux of horizontal momentum
$\overline{w'\theta'}$	Kinematic vertical flux of sensible heat
x, y, z	Zonal, meridional and vertical axes
z	Altitude/height
z_0	Aerodynamic roughness length
α	Wind shear exponent; Angle of attack
α_0	Cross-isobar angle
β	Bowen ratio; Solar elevation; Constant representing linear trend
Γ_d	Dry adiabatic lapse rate
Γ_e	Environmental lapse rate
δ	Value increment; Solar declination
$\Delta P_z, \Delta P_m$	Zonal and meridional pressure gradients
$\Delta T_{vz}, \Delta T_{vm}$	Zonal and meridional gradients of virtual temperature
ϵ	Rate of dissipation of TKE through viscous processes; stochastic noise
ζ	Obukhov stability parameter $= z/L$
θ	Potential temperature
θ_v	Potential virtual temperature
κ	von Kármán constant (≈ 0.4)
λ	Latitude; tip-speed ratio; Latent heat of condensation for water
μ	Mean
ρ	Density of the air
ρ_0	Reference density
$\sigma u, \sigma v, \sigma z$	Standard deviation of zonal, meridional and vertical wind speed
$\sigma_{P,i}$	Standard deviation of TMA power values in bin i
σ	Standard deviation of wind speed
ϕ	Inflow angle; Relative humidity
φ_i	Angle difference
Ψ_m	Stability correction
ω	Frequency

1 Introduction

1.1 Problem outline

Following the installation of wind energy generation equipment in the form of one or more wind turbines, the satisfactory performance of the equipment is assured through a power performance test (PPT) as defined in the International Electrotechnical Commission (IEC) standard IEC61400-12-1 (IEC, 2017). The existence of an agreed standard and associated procedures is crucial in mediating the relationships among manufacturers, operators, investors and regulators. During a test, data is collected from meteorological instruments and from the turbine supervisory control and data acquisition (SCADA) system. The data is analysed to produce an estimate of the annual energy production (AEP) in megawatt-hours (MWh) which is compared against the expected output of the turbine as defined in the warranty. If the AEP estimate is satisfactory, the project proceeds to completion. If not, additional remedial technical work may be required and the developer may have a financial claim against the manufacturer.

The standard procedure calls for the identification and control of any extraneous influences that might distort the test results. These include, for example, extreme meteorological conditions, turbine faults, unwanted interactions between turbines, and situations where turbine output is deliberately curtailed for practical or financial reasons. Methods are provided in the standard for normalising some aspects of the data in certain circumstances to eliminate unwanted influences; however, the more common approach is to filter the data to reject any affected records so that they are excluded from the final analysis. The standard PPT procedure therefore tests the operation of a turbine under a set of ideal conditions, only some of which can be defined objectively. For example, deterministic procedures are specified for identifying the *free-stream* or *measurement* sector, a range of wind directions where the turbine under test is free from turbulence due to nearby obstacles and the wakes of other turbines. Other conditions, such as the permitted levels of turbulence and wind shear, are the subject of negotiation between the parties commissioning the test. Two types of data filter can therefore be identified, *quality* filters which are defined objectively, and *contractual* filters which can be more or less restrictive depending on the concerns of the negotiating parties. Where contractual filters impose narrow limits on the data, up to 90% may be rejected in extreme cases (Bunse & Mellinghoff, 2008; Rareshide et al., 2009). Large data losses mean that it takes longer to accumulate the minimum quantity of data required by the standard and a longer measurement campaign incurs additional costs for the project. Since the additional costs are a direct consequence of the lost data, finding ways of avoiding data rejection is desirable. The question pursued here is whether alternative filtering strategies can be defined which reject less data but which still deliver AEP estimates similar to those obtained with conventional filters.

A major constraint on the standard procedure is that it must be reliable in the sense that it must produce comparable results in the same physical circumstances irrespective of the organisation that is carrying it out. Because of the complex interactions between the turbine machinery and the atmosphere, precise numerical calculations are not feasible. PPT therefore relies on simplified mathematical models of atmospheric and mechanical behaviour. In particular, the main model used to represent turbine performance, the power curve, is a simple bivariate relationship between a characteristic wind speed and turbine power output. Such a model disregards the effects of many meteorological parameters that are known to have an impact on power production. The effects of these parameters are treated as uncertainty which appears as unwanted dispersion in the power curve scatter plot (Bandi & Apt, 2016; Courtney et al., 2011). The degree of dispersion in the power curve can therefore be used as an evaluation criterion for a data filters assuming that an effective filter would produce a significant reduction in dispersion.

Research on wind turbine performance tends to be selective, focussing on specific combinations of parameters. Often, the data is conditioned for very restrictive criteria and the resulting idealised circumstances are not representative of the real contexts in which turbines operate. In order to achieve a comprehensive overview, individual results have to be combined in a piecemeal fashion and this may overlook unexpected influences and interaction between parameters (Kwon, 2010; Morshedizadeh et al., 2017). Some parameters such as turbulence and shear appear often in the literature, although the measures typically used to quantify them do not necessarily represent the full complexity of the phenomenon. This is particularly true for turbulence which is usually represented by *turbulence intensity*, a measure based on the mean and standard deviation of wind speed. As one-point statistics, the mean and standard deviation introduce assumptions about the distribution of wind speeds within a given averaging period, and fail to capture temporal dynamics that could affect power output (Kelley et al., 2005; Morales et al., 2010; Wächter et al., 2012). Other measured or statistical parameters that may have an impact such as atmospheric stability (Motta et al., 2005; St. Martin et al., 2016; Sumner & Masson, 2006b; Van Den Berg, 2008; Wharton & Lundquist, 2012), wind veer (Bulaevskaya et al., 2015; Rareshide et al., 2009; Sakagami et al., 2015), isotropy (Wächter et al., 2012) and intermittency of turbulence (Schottler et al., 2016) are much less common. The significance of stationarity of the wind velocity has been acknowledged insofar as it is occasionally used as to condition data before analysis (Peña & Floors, 2014), but no studies directly examine its impact on power production. The assumption that wind speeds are Gaussian-distributed within the standard ten-minute averaging period is noted (Brand et al., 2011), but no studies appear even to filter the data according to this criterion. A gap in the literature therefore exists around the identification of potentially influential parameters that are not traditionally accommodated in established procedures, their main effects and their interactions.

Measurement campaigns are expensive, and to avoid unnecessary costs it is common for data collection to satisfy only the minimum requirements of the PPT standard and analyses rely on mathematical models to provide information about parameters that are not directly observed. Consequently, existing PPT datasets are highly constrained and offer few opportunities to examine novel parameters that could improve its accuracy or reduce the amount of data discarded through filtering. A need therefore exists for a research dataset that supports a wider range of analyses than those currently available.

1.2 Aim and objectives

In the light of the foregoing discussion of the PPT process, this project aims to investigate the potential of alternative data filtering strategies with respect to data loss, AEP estimates and the dispersion of points in the power curve scatter plot.

In doing so, it targets a wide range of meteorological parameters with theoretical relationships to wind turbine power production with particular interest in those not accounted for in the current standard. The identification of viable filtering strategies with lower data loss would provide significant benefits to wind energy development projects in terms of greater control over timescales and reduced costs.

The following objectives are addressed in order to achieve the overall aim of the project:

1. Explore and quantify the loss of data through filtering in real PPT contracts with an emphasis on the requirements of the standard, the associated costs and the potential for savings
2. Compile a new, high-fidelity dataset corresponding to the wind regime impacting on turbine performance which incorporates a wide range of parameters that is not constrained by the assumptions embodied in the current PPT standard
3. Evaluate traditional and novel filtering strategies in terms of data loss, dispersion in the power curve and estimated AEP

1.3 Justification

The discussion in §1.1 identifies the risk of significant data losses through restrictive filtering criteria, and the first aim of the project is to compare that risk with reality. If significant data losses are identified and the associated costs are shown to be significant, then there is clear motivation for improving the PPT process which reinforces the rationale for the remainder of the project.

Existing PPT datasets are optimised to support the current PPT standard. Data related to parameters other than those specifically required by the current standard is therefore absent. Any empirical investigation into the relationship of such parameters to power output therefore requires an appropriate dataset to be expressly compiled. The overall strategy in this project is to cast as wide a net as possible in the search for overlooked influences on power performance, and to avoid making assumptions based on a small number of known influences from previous works.

The assumption underlying the bivariate power curve is that points should lie neatly on a roughly sigmoid curve once the characteristic wind speed and power output are plotted. In practice, there is significant dispersion in a scatter plot based on real data. Some of this can be attributed to natural variation, but since the power curve does not consider parameters other than a characteristic wind speed on power output, their impacts can only appear as a contribution to the dispersion (Hwangbo et al., 2015; Paiva et al., 2013). Filtering on a parameter with a significant impact should therefore reduce the dispersion of the points in the traditional power curve scatter plot. Some authors have crystallised this idea by suggesting that an acceptance band should be defined to eliminate outlying values in the power curve (Barthelmie et al., 2011; Hernandez et al., 2016). The experimental filtering strategies explored here are carried out with this in mind and the dispersion evident in the power curve is used as a major evaluation criterion.

1.4 Approach

The analysis of real PPT projects is carried out in cooperation with Wood Clean Energy[1] (previously Sgurr Energy). Suitably anonymised data is extracted from the project documentation and summarised to produce the required results.

[1] https://www.woodgroup.com/what-we-do/view-by-products-and-services/clean-energy

A new, high-fidelity research dataset is created, based primarily on measured data from a well-instrumented research turbine operated by the University of Minnesota[2] synchronised with data from other sources. Significant effort is made to ensure the quality of the dataset so that later analyses may be seen as reliable including a set of stringent tests usually employed only in the analysis of atmospheric fluxes. Statistical quantities associated with various physical phenomena are calculated over a standard ten-minute averaging period. The final output is a two-layer dataset whose main component is a single file of ten-minute average (TMA) values for over 700 parameters covering the whole of 2017. The second layer consists of a comprehensive set of ten-minute data samples each of which corresponds to one record in the main TMA file.

Global sensitivity analysis and correlation analysis are used to identify those parameters in the TMA dataset most strongly related to power output. Experimental filters based on these parameters are then evaluated for their impact on data loss, predicted AEP, and the dispersion of points in a traditional bivariate power curve scatter plot.

1.5 Limitations

Although the data covers the whole of 2017, the fact that results are based on a single data source limit the generality of any results and conclusions. The project therefore shares features with case studies which provide detailed analysis of a single case, but which require further validation to achieve generality.

The traditional ten-minute averaging period is adopted in this work. No use is made of unaggregated data sampled at 1 Hz or above, and no attempt is made to investigate aggregation periods of alternative or variable durations.

The focus of the study is on the meteorological influences on power production; therefore, no attempt is made to incorporate data on the turbine machinery, control system or grid connection.

---

[2] http://eolos.umn.edu/

The study is carried out in the context of power performance testing as envisaged in the relevant international standard, IEC-61400-12-1 (IEC, 2017). The scenario involves the evaluation of a single turbine under normal flow conditions. Turbine interactions and wake effects are therefore not treated.

Because the intention is to examine novel parameters that are unlikely to be implemented in existing tools, the work is not benchmarked against supposedly objective models such as those produced using blade-element/momentum (BEM) or computational fluid dynamics (CFD) approaches. Instead, a baseline power curve is created from the data using the relevant international standard. Later results are compared with this self-referential benchmark. This also limits the generality of the results and conclusions, and commentary is offered on this issue at various points during the report.

1.6 Structure of the report

Chapter 2 reviews relevant background topics starting with a discussion of the economic, technological, meteorological and regulatory contexts. It continues with an overview of wind turbine performance and a summary of important concepts from the international standard IEC-61400-12-1 as background to later practical work. A more detailed coverage of relevant micrometeorological phenomena is then provided. This includes the formulae for derived parameters that are included in the research dataset. Finally, several important methodological topics are reviewed including the use of artificial neural networks to model complex system behaviour, the use of correlation analysis for eliminating redundant parameters and variance-based global sensitivity analysis. The eFAST method is covered in detail.

Chapter 3 outlines the process adopted and provides details on methods used in the practical work of the project

Chapter 4 present the results of the review of commercial PPT contracts focussing on the variation in warranty conditions and the effect of more or less restrictive conditions on project duration. The novel concept of effective duration is introduced to allow comparison across projects. The cost implications of extended measurement campaign durations are also explored. The detail of PPT projects has not previously been reported in this form, and this section therefore constitutes one of the novel contributions from this project.

Chapter 5 describes in detail the construction of the research dataset. It includes a detailed description of the wind regime at the Eolos turbine site, and discusses issues related to data quality control, the removal of spurious data, the conflation of data from different sources, the reduction of raw data to ten-minute averages and the addition of derived parameters. No extant datasets with appropriate characteristics were identified, and the publication of the dataset created here is a further contribution from this project.

Chapter 6 presents the results of the investigation into alternative filtering strategies. It describes the identification of the parameters with the strongest relationship with the variance in the turbine power output, the creation of comparator power curves using the IEC2017 procedure, the specification of alternative filters, and the results of applying them to the research dataset. The results from conventional and experimental filters are compared and contrasted, and the implications of the alternative strategies on the costs of wind energy projects are discussed. For several of the parameters examined here, their relationship with power performance has not previously been investigated. In addition, the effect of conventional filters on the dispersion of points in the power curve scatter plot is presented here for the first time. The results in this chapter also constitute a novel contribution from the current work.

Chapter 7 concludes the report by revisiting the key objectives and explaining how these were met. It highlights research limitations and provides recommendations for progressing the future work.

2 Literature review

2.1 Introduction

2.1.1 Economic context

Amid concerns about global climate change, pollution caused by hydrocarbon-based materials and the finite nature of fossil fuels, the generation of energy from renewable sources has garnered much attention since the start of the century. The majority of developed countries have adopted targets for the reduction of greenhouse emissions. Scotland, for example, aims to source 100% of its domestic electricity from renewable sources by 2020, and 50% of energy consumption including electricity, heat and transport from renewables by 2030 (Scottish Government, 2017). As a mature renewable energy source, wind stands to contribute significantly to the achievement of such targets. Indeed, the wind industry has seen very strong growth in recent years as illustrated by Fig. 1.

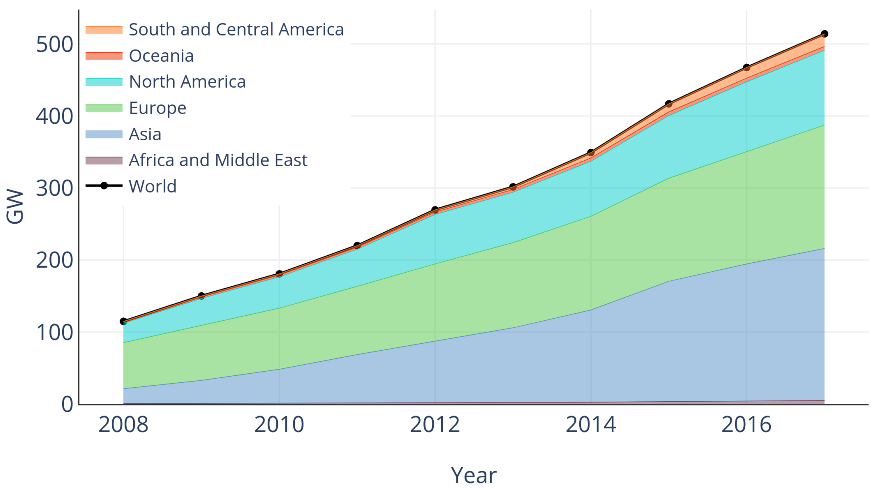

Figure 1: Global installed wind capacity (IRENA, 2018)

While the wind resource itself is essentially without cost, the equipment to extract energy from the wind is expensive to develop, manufacture, install, operate and maintain. For onshore wind projects at the end of 2017, the global average installation cost was $1477 per kW with turbine purchase accounting for 66-84% (IRENA, 2018). While the cost of onshore wind projects is on a downward trend, offshore costs are increasing due to the exploitation of more remote sites which entail higher grid connection expenses. In 2016, the global average installation cost for offshore projects was $4487 per kW with turbine purchase accounting for 30-50% (IRENA, 2018). PPT ensures that the installed turbines operate according to their specifications; however, the testing procedure adds additional costs to the project. Not only does PPT entail costs directly related to its management and operation including specialist measurement equipment and staffing costs, the duration of a measurement campaign can also impact the overall construction schedule for a wind energy project. This is especially true where a campaign takes longer than expected.

2.1.2 Turbine technology

All wind turbines operate by using a proportion of the kinetic energy in an air flow to develop torque in a shaft. Current designs rely on the aerodynamic properties of rotors comprised of two or three rigid blades mounted on a horizontal axis. Vertical-axis designs are also in use, but they are less popular due to their lower efficiencies and higher cost (Gross, 2007, p.104). Experimental designs include wind concentrators (Allaei, 2012), tethered wings (Goldstein, 2013) and airborne generators (Castellani & Garinei, 2013). The remainder of this report will only be concerned with the most widely-used design involving three horizontally-mounted blades.

The aerodynamic profile of the blades is a key aspect in the design of a wind turbine. Blades have an aerofoil shape in cross-section and are set at an angle to the oncoming wind so that the induced aerodynamic lift causes the rotor to rotate. The angle at which the flow of air strikes an aerofoil, known as the *angle of attack*, determines the magnitude of aerodynamic lift. Since the tangential speed of a rotating blade is greater the further it is measured from the hub, the apparent angle of attack is also larger. Blade design therefore includes a twist to compensate so that the angle of attack is optimised to extract maximum energy from the air flow along the whole length of the blade. Because the blade design is crucial to the machine's performance, it is kept confidential by manufacturers (Niebsch, 2011).

A disadvantage of a fixed blade profile is that it cannot accommodate variations in flow conditions in different parts of the rotor swept area (Chavan et al., 2017). Although horizontal homogeneity is a reasonable assumption, many meteorological quantities vary naturally in the vertical dimension. The greater these variations, the more the conditions will diverge from those for which the blade profile is optimal leading to a degradation in performance. This problem is exacerbated by the trend towards larger turbines because as the size of the rotor increases, meteorological measurements taken at hub height become less representative of the general conditions across the rotor disk. This affects the apparent angle of attack seen at a point on the blade since the air flow it experiences is the vector sum of the actual air flow and its own tangential velocity. Over the past two decades, hub-heights and power ratings have also increased along with rotor diameters. Between 2010 and 2016, the typical power rating has increased from 2 MW or below to nearly 3 MW, while typical rotors have increased from 80 m or below to around 100 m, with some reaching 110 m (IRENA, 2018).

The operation of a wind turbine is constrained by its connection to the electrical grid. When the transmission system is not capable of accommodating the full amount of power being generated, power production is *curtailed*. The mechanism for this is to set a limit on the maximum power output of the turbine at a level below rated capacity using the turbine's control system. As well as situations of involuntary curtailment due to grid capacity, output can also be voluntarily curtailed for economic reasons (Fine et al., 2017). In either case, a curtailed turbine deliberately operating below its normal level is not indicative of its optimum performance.

Performance assessment can be applied to a single turbine or to an entire wind farm where the impact of turbine wakes on other units in the wind farm layout needs to be considered. The rotational turbulence in the wake of one turbine can significantly disrupt the inflow to its neighbours. The Park model is one approach to modelling wake interactions, taking into account turbine spacing and the expected rate of decay of the wake (Katic et al., 1986). The model was later updated to incorporate considerations of atmospheric stability (Peña et al., 2014). The study of wake effects is an important topic in the wind industry, as evidenced by the growing number of Google Scholar results from 2000 to 2018 shown in Fig. 2. However, wake interactions are not accommodated in the international standard for PPT since it is concerned with the correct operation of a single turbine under normal operating conditions. Indeed, the procedure specifically excludes wind directions where wake interactions might occur. The intention in this project is to investigate parameters that vary naturally in the free-stream wind, and which could be used to improve the PPT process. For this reason, wake interactions are not pursued.

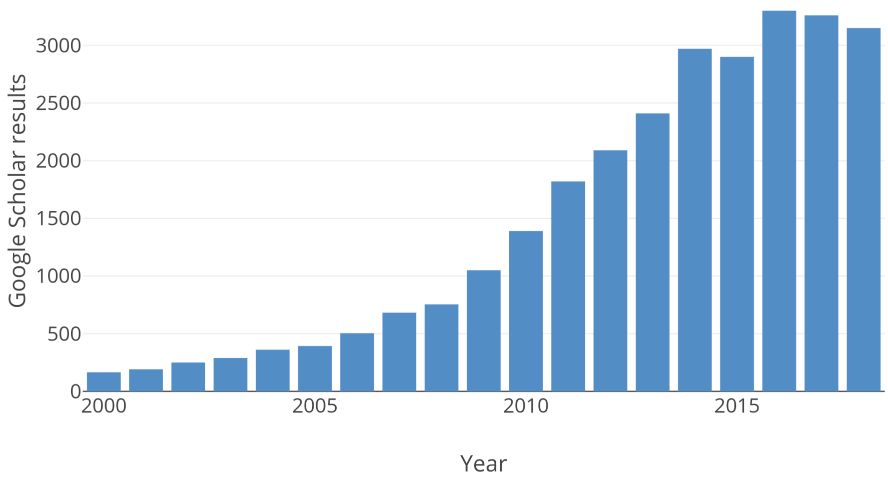

Figure 2: Number of Google Scholar references to turbine wakes by year of publication
Source: Searches performed on Google Scholar 24 Mar 2019

2.1.3 Regulatory context

IEC-61400, published by the International Electrotechnical Committee (IEC), defines a family of standards for the specification and operation of wind turbines[3]. The purpose of IEC-61400-12-1 is "to provide a uniform methodology that will ensure consistency, accuracy and reproducibility in the measurement and analysis of power performance by wind turbines" (IEC, 2017). The current version (henceforward IEC2017) supersedes the 2005 edition (henceforward IEC2005) which constituted a technical revision of the original IEC-61400-12, published in 1998. The procedures specified in IEC2005 were all based on meteorological measurements by approved and calibrated sensors mounted on a hub-height meteorological mast (met mast). IEC2017 adds provision for the use of ground-based remote sensing devices under certain circumstances as a complement to traditional instruments, but still maintains an emphasis on hub-height wind speed measurements. IEC-61400-12-2 published in 2013, specifies PPT procedures for large turbines using nacelle-mounted anemometers (IEC, 2013). PPT of small turbines – those with a swept rotor area smaller than 200 m^2 and an AC voltage less than 1000 V or DC voltage less than 1500 V – is covered by IEC-61400-2. Other related standards concern electromagnetic compatibility (IEC-61400-1), acoustic noise measurement (IEC-61400-11) and load measurements (IEC-61400-13), and form part of a comprehensive testing and certification regime defined in IEC-61400-22.

With specific reference to PPT for large turbines, IEC-61400-12-1 was intended to address the needs of a wide variety of interests including manufacturers, purchasers, operators, planners and regulators, in order to facilitate communication and agreement among them. A major output from PPT is an estimate of annual energy production (AEP), a theoretical quantity calculated for the purposes of verifying correct operation of the turbine under test. It can be estimated based on the distribution of wind speeds at the site using either a velocity exceedance curve, or the more involved process defined in IEC2017. Both methods assume 100% turbine availability, and therefore do not represent a predicted yield from the turbine. For this, a further net AEP value must

[3] https://collections.iec.ch/std/catalog.nsf/collection.xsp?open&col=IEC%2061400

be estimated which takes account of wake effects where a turbine is located in close proximity to others, and technical losses including curtailment, turbine faults and downtime for maintenance (Mortensen et al., 2015).

Other notable organisations include MEASNET[4], an association of European wind test centres which cooperate on the development of common approaches to measurement in the wind industry. In particular, MEASNET aims to ensure high-quality, reliable measurements to the wind industry, and in order to do so offers additional interpretations of international standards such as IEC-61400-12 and guidance on their application.

Another function of MEASNET is the certification of measurement instruments such as anemometers. A small number of test centres are certified by MEASNET to carry out calibration tests and to provide the associated documentation.

The Power Curve Working Group (PCWG)[5] is a grouping of industry stakeholders who came together following the European Wind Energy conference in 2012. Their aim is "… to help identify and develop ways to improve the modelling of turbine performance in real world wind conditions".

2.1.4 Meteorological context

Wind turbines operate in the atmospheric boundary layer (ABL) where the flow of air is affected by interactions with the ground. The ABL varies in height from around 100 m to around 3 km, expanding during the daytime as solar warming stimulates convection and sinking back during the night as the cold ground absorbs energy from below (Stull, 1988, p. 9). A horizontal flow of air near the ground encounters roughness elements such as vegetation, buildings and changes in topology that create turbulent eddies and reduce its velocity. This leads to an increase in wind speed with height known as wind shear. As well as mechanically-driven turbulence, eddies are also created as air rises

[4] http://www.measnet.com/corporate-information/
[5] http://www.pcwg.org/

from a warmed surface during the daytime. The largest eddies are of a size comparable to the ABL height and break down into smaller eddies over time as they are stretched and distorted by stress forces (Davidson, 2004, p. 17).

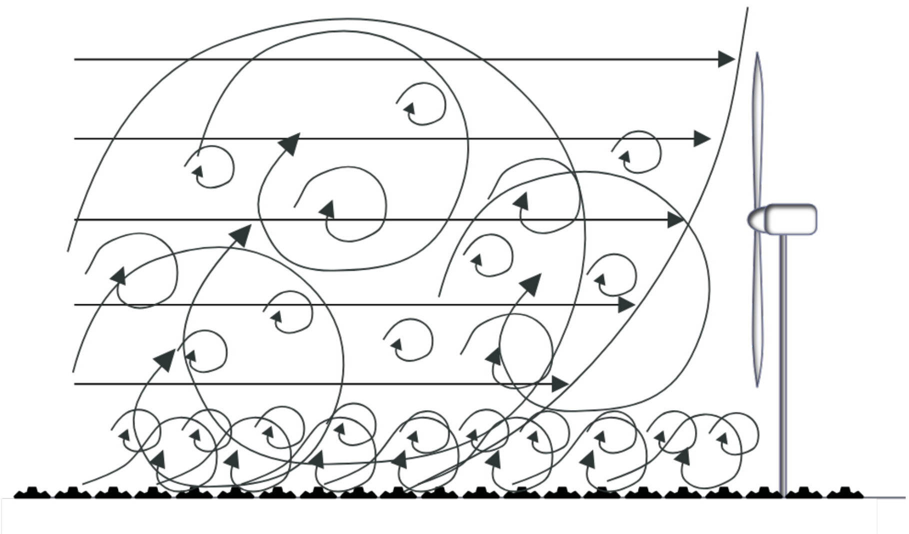

Figure 3: Turbulence visualised as eddies of different sizes superimposed onto a sheared horizontal air flow

A turbulent atmosphere is composed of many overlapping eddies of different sizes as illustrated in Fig. 3. This complexity is extremely challenging to model mathematically and the usual approach is to rely on a statistical description (Pope, 2000, p. 8; Roy, 2012). There is a rough inverse relationship between shear and turbulence. The dynamic condition that results from solar warming in which a parcel of air will continue to rise if displaced from its original position is known as an unstable atmospheric regime. Unstable conditions are characterised by low shear and high turbulence. In contrast, a stable regime characterised by relatively low turbulence and high shears is usually found at night. A neutral regime can also be found either as a transition between stable and unstable atmospheres, or during overcast conditions where solar warming of the surface is suppressed (Emeis, 2011, p. 11).

The daily passage of the sun is one source of heating and cooling of the surface, and the changes in day length and solar declination over the course of a year modify the main solar effect. Local weather conditions, and cloud cover in particular, modify the overall degree of heating and cooling at a location. Since cloud cover can vary considerably over a relatively short distance, different locations may experience different levels of heating or cooling at any given moment. Thus, warm air from one location can be transported, or *advected*, over a neighbouring location by the mean flow of wind. This gives rise to a second source of temperature differences at the surface, and the reverse can obviously occur with cold air being advected over a warmer surface.

Differences in temperature cause changes in the density of the air which in turn lead to differences in pressure. Large-scale pressure differences are a major driver for synoptic weather patterns while local horizontal pressure gradients are responsible for winds at smaller scales (Sun et al., 2013). Because of the greater level of solar heating close to the equator, the main pressure gradient induces winds from south to north in the northern hemisphere, and from north to south in the southern hemisphere. The rotation of the Earth is another large-scale influence on the behaviour of the wind. Through the Coriolis effect, winds in the northern hemisphere are turned clockwise with increasing height while those in the southern hemisphere are turned anticlockwise, a phenomenon known as wind veer. The notional geostrophic wind, G, is a theoretical wind which represents a balance between the horizontal pressure gradient and the Coriolis force. Within the ABL winds are rarely geostrophic, but they approach geostrophic just above the ABL where the isobars on a weather map are relatively straight (Stull, 2015, p. 303).

2.2 Wind turbine performance

2.2.1 Energy extraction

As an energy conversion device, the efficiency of a wind turbine is expressed in terms of the power generated compared to the power available. Rotor disc theory treats the swept area of a wind turbine rotor as the cross-section of a cylindrical stream of air travelling longitudinally at a constant speed (Burton et al., 2011). This simple model, captured in Eq. 1, provides the means of quantifying the power available in the wind and is the model used by IEC2017.

$$P_w = \frac{1}{2}\rho A U^3 \tag{1}$$

where
P_w = power available in the wind (kW)
ρ = density of the air (kg m^{-3})
A = area swept by the turbine rotor (m^2)
U = horizontal wind speed (ms^{-1})
(Burton et al., 2011, p. 43)

Not all available power can be converted, and the ratio of the actual power production of the machine to the available power gives a dimensionless power coefficient, C_p, whose formula is given by Eq. 2. By optimising the formula for C_p, it can be shown that the maximum possible value is 0.593, known as the Lanchester-Betz limit (Burton et al., 2011, p. 43). Because it is derived from theoretical principles rather than with reference to any particular turbine design, the Lanchester-Betz limit provides a fixed upper bound for the efficiency of any horizontal axis turbine.

$$C_p = \frac{P}{\frac{1}{2}\rho U^3 A} \tag{2}$$

where
P = Output power (W)
(Burton et al., 2011, p. 43)

Rotor disc theory is simple to conceptualise and easy to apply. However, it ignores complexities such as the precise aerodynamics of the blades, variations in the wind flow and interactions with the turbine machinery such as blockage effects, vortex shedding and wake rotations. The impacts of all excluded phenomena are subsumed into the power coefficient. To accommodate unmodeled variation, IEC2017 provides a set of procedures for calculating the uncertainty in its output predictions.

2.2.2 The power curve

The behaviour of a wind turbine is traditionally described by a power curve in which power output is plotted as a function of wind speed. The version provided in table and graphical form in manufacturers' product brochures is referred to as the *sales power curve* and Fig. 4 shows an example for a typical multi-megawatt variable pitch/variable speed turbine. As part of a wind energy development, the manufacturer will provide the developer with a *warranted power curve* which reflects the wind regime at the site. During PPT, a *measured power curve* is created, and the main output of the test is a comparison between the warranted and measured power curves.

Power Curve Gamesa G90-2.0 MW (for an air density of 1,225 kg/m³)

Power curve calculation based on DU (Delft University) and FFAW3 airfoils.

Calculation parameters: 50 Hz grid frequency; tip angle pitch regulated; 10% turbulence intensity and a variable rotor speed ranging from 9.0-19.0 rpm.

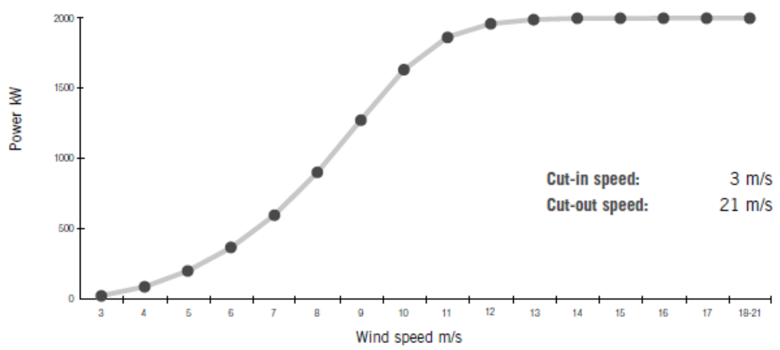

Speed (m/s)	Power (kW)
3	21.3
4	84.9
5	197.3
6	363.8
7	594.9
8	900.8
9	1274.4
10	1633.0
11	1863.0
12	1960.4
13	1990.4
14	1997.9
15	1999.6
16	1999.9
17	2000.0
18-21	2000.0

Figure 4: Typical manufacturer's power curve[6]

[6] http://www.wind-power-program.com/Library/Turbine%20leaflets/Gamesa/Gamesa%20G90%202mw.pdf

The power curve can be divided into four main regions as shown schematically in Fig. 5. In regions I and IV there is no power output because the wind speed is below cut-in or above cut-out wind speed respectively. As the wind speed increases above cut-in, the power output of the turbine also increases until the generator is operating at its rated capacity. The curve is not linear in region II because the power output is proportional to the cube of the wind speed (see Eq. 1). For most of region II therefore the curve is slightly concave. As wind speed approaches rated the curve becomes convex and it is sometimes useful to refer to this transitional part of region II separately as region IIa. Region III covers speeds between rated and cut-out during which the power output remains at rated thanks to regulation by the control system. The critical characteristics – cut-in wind speed, cut-out wind speed, rated speed and rated capacity – vary from one model of turbine to another.

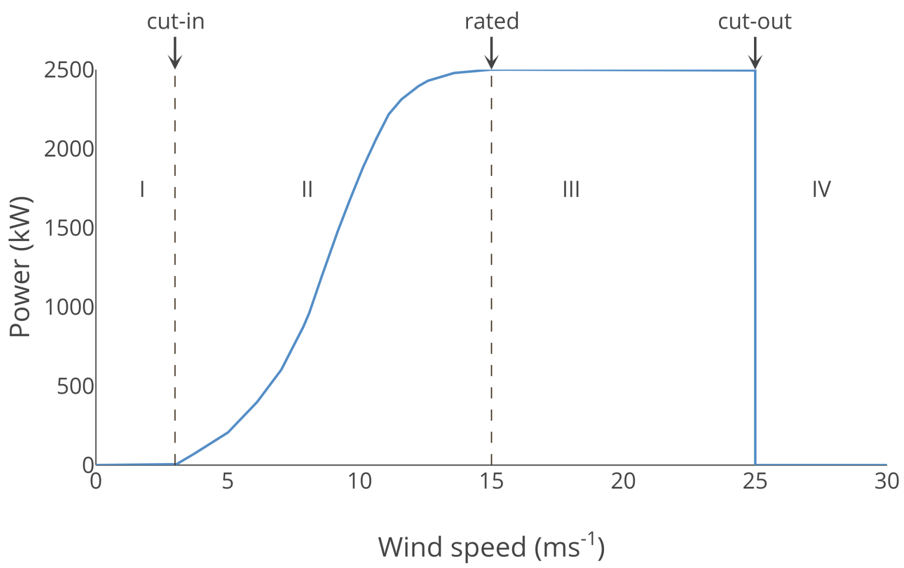

Figure 5: Regions of the power curve

As a simple bivariate relationship between mean horizontal wind speed and power output, the power curve has an intuitive appeal. Although the wind speed in question is usually assumed to refer to the horizontal wind at hub height, wind speed actually varies in three dimensions across the rotor and the power output reflects this heterogeneity. In practice, many of the parameters mentioned in §2.1.4 also influence power output.

The power curve model also assumes that turbine performance can be adequately described with reference to the mean and standard deviation of wind speed and power. Since the mean and standard deviation are one-point statistics, they cannot take account of dynamic variations over time (Clive, 2012; Hedevang, 2014; Katul et al., 1994; Morales et al., 2012; Schottler et al., 2016). With dynamic variations excluded, their influence appears as increased uncertainty in the PPT results and are visible as unwanted dispersion in the measured power curve scatter plot.

2.2.3 Annual Energy Production

All industry stakeholders rely on an estimate of the expected energy yield from a turbine for business and technical decision making. PPT therefore yields an estimate of annual energy production (AEP) for comparison with the pre-installation estimate based on the warranted power curve and the technical specification of the turbine in question. The formula, shown as Eq. 3, treats AEP as a function of the measured power curve and the wind distribution at the site. It is well-known that the spread of natural wind speed is well approximated by a two-parameter Weibull distribution (Burton et al., 2011, p. 12). The distribution's scale parameter, c, and the shape parameter, k, can be adjusted to fit the observed wind distribution at a site (G. L. Johnson, 2001). *Generic* AEP is calculated in IEC2017 using the one-parameter Rayleigh distribution, which is identical to the Weibull with a fixed shape parameter value of 2 despite the loss in accuracy (Celik et al., 2010). Where more detailed information about the local wind regime is known, IEC2017 allows for *site-specific* AEP to be calculated and reported using the Weibull distribution in addition to the generic AEP.

$$AEP = N_h \sum_{i=1}^{N} [F(U_i) - F(U_{i-1})] \left(\frac{P_{i-1}+P_i}{2}\right) \tag{3}$$

where

N_h	=	number of hours in a year = 8760
N	=	number of wind speed bins
U_i	=	normalised and averaged wind speed in bin i
P_i	=	normalised and averaged power in bin i
$F(\cdot)$	=	cumulative probability distribution either Rayleigh, R_c, or Weibull, W_c given by

$$R_c = 1 - \exp\left[-\frac{\pi}{4}\left(\frac{U}{\overline{U}}\right)^2\right]$$

$$W_c = 1 - exp\left[-\left(\frac{U}{c}\right)^k\right]$$

where

$\overline{U}$	=	annual average hub height wind speed
c	=	Weibull scale parameter
k	=	Weibull shape parameter

The IEC2017 procedure requires that AEP is calculated for a range of mean hub height wind speeds from 4 ms^{-1} to 11 ms^{-1}, and is presented in two forms, *measured* and *extrapolated*. To calculate measured AEP, only valid wind speed bins are included and zero power output is assumed for all other bins below and above this range. A wind speed bin is considered valid in IEC2017 if it contains at least 30 minutes of data. Where the set of valid bins does not extend up to turbine cut-out, extrapolated AEP is calculated by assuming the value of the highest measured bin for all bins between the top of the measured range and cut-out wind speed.

The warranted power curve is intended to represent the prevailing wind regime at the turbine location and this typically includes limits on certain parameters such as turbulence intensity and wind shear. The data used to create the measured power curve is filtered to eliminate data points that do not conform to the warranted conditions. The estimated AEP is therefore highly dependent on the filters applied during the test. Thus, the estimated AEP provides a means for comparing the effects of different filtering strategies. A recent study employing this technique reported on the comparative effects of filtering on TI, atmospheric stability and different methods for measuring wind speed (St. Martin et al., 2016). The results showed that AEP calculated using the sales power curve with no filters led to a higher figure than with filters applied. This is to be expected given the generic nature of the sales power curve and the restricted range for which any power curve may be deemed valid. Results also showed statistical difference between wind regimes defined by partitioning the data into three categories on each of the two parameters of interest. The largest AEP estimate was seen in the case of medium TI and unstable atmospheric conditions. The study concluded that site-specific power curves could be used to represent different combinations of parameters rather than applying filters to reject all but a narrow range of data points. The study did not, however, make any claims about which of the various AEP estimates was the most accurate. This points to a limitation on the use of the sales power curve for this purpose, and on the use of AEP in general as a comparative measure. Without taking site-specific conditions into account, the sales power curve can only provide an approximate benchmark. In addition, the manufacturer has a theoretical interest in providing an optimistic picture of a turbine's performance since the purpose of the sales power curve is to attract customers. In contrast, the manufacturer's best interests are served by applying conservative limitations on the turbine's performance in the warranted power curve. Thus, the sales power curve may overestimate actual production while the warranted power curve may underestimate it (Albers, 2012). While an objective benchmark for AEP may not therefore exist, an examination of the differences in AEP estimates can provide insight into the comparative performance of different data filtering strategies as shown by St Martin (2016).

From a statistical point of view, the optimal AEP estimate will be the one which minimises the unexplained variance in the data (Janssens et al., 2016). Since the variance in the data appears as scatter in the measured power curve, a filtering strategy which minimised the scatter will be preferred in this project.

2.2.4 IEC2017 process overview

At a high level, the PPT procedure set out in IEC 61400-12-1 is a simple one, consisting of preparation, measurement and analysis phases while site selection is assumed to have already taken place. The main phases can be further broken down as follows:

1. Preparation
    - Selection of test turbine(s)
    - Determination of the free-stream sector(s)
    - Location of the meteorological mast (met mast)
    - Determination of flow distortion effects and associated uncertainties
    - Traceable calibration of test instruments (ISO, 2005)
    - Site calibration
2. Measurement
    - Accumulation of data over contiguous ten-minute periods
    - Rejection of data that deviates from agreed constraints for the test
3. Analysis
    - Production of measured power curves
    - Calculation of AEP
    - Calculation of power coefficient
    - Calculation of measurement uncertainties
    - Extrapolation from test turbine result to the whole wind installation

There are five normalisation procedures included in IEC2017:

- Mast flow distortion correction
- Flow correction from site calibration
- Rotor equivalent wind speed (REWS)
- Air density correction
- Turbulence normalisation

Power curves and AEP are presented for both sea-level and site-specific air density. The reference sea-level density is the ISO standard atmosphere of 1.225 kg/m^3 while the site-specific value is simply the mean measured density over the course of a measurement campaign. Descriptions of the actual procedures used and the results of the PPT are presented in a standard test report which also includes estimated measurement uncertainty. The following concepts are central to the procedure.

Measurement sector

Wind flows are distorted when they interact with obstacles and this can include a reduction in velocity through blockage effects (Tindal et al., 2008), an increase in mechanical turbulence due to wake effects (Barthelmie et al., 2011) or changes in velocity and direction as the wind flows around the turbine nacelle (Dahlberg et al., 1999). In the first two cases, the general solution is to eliminate records where the wind is flowing from a direction in which there are known obstacles (including turbines and met masts) leaving a *measurement* or *free-stream* sector. To avoid the third issue, IEC2017 requires measurement instruments to be mounted on a met mast at a distance of at least two rotor diameters from the turbine.

Site calibration

During a power curve test, the data collected at the met mast are assumed to be representative of conditions at the turbine site. In flat, homogeneous terrain with no obstacles, this may be true, but often turbines may be sited close to forests, settlements or orographic features which can introduce systematic distortions into the air flow. The purpose of site calibration is to identify and correct for predictable distortions. IEC2017 provides limits on the slope and surface height variation shown in Table 1 to define *flat terrain*. *Complex terrain* encompasses any terrain that deviates from these conditions. In Table 1, L is the distance from the foot of the turbine to the wind measurement equipment, H is the turbine hub height and D is the rotor diameter. A site calibration is required where the terrain is assessed as complex, and may be performed in other situations as agreed by the parties to the PPT contract.

Table 1: Conditions for flat terrain

Distance	**Sector**	**Max. slope (%)**	**Max. variation from plane**
< 2L	360°	< 3	< 1/3 (H – 0.5D)
>= 2L and < 4L	Measurement sector	< 5	< 2/3 (H – 0.5D)
>= 2L and < 4L	Outside measurement sector	< 10	Not applicable
>= 4L and < 8L	Measurement sector	< 10	< (H – 0.5D)
>= 8L and < 16L	Measurement sector	< 10	Not applicable

Site calibration is a stage of the PPT process that takes place in advance of the installation of the turbine to be tested. A second met mast is installed at the turbine site (the *turbine mast*) where data is collected and compared with data from the permanent met mast (the *reference mast*). The data from both masts is divided into wind direction bins of 10° and wind shear bins of 0.05, and a slope and offset are calculated for each bin. During the test itself, flow distortion corrections are applied to the measured data by multiplying by the slope and adding the offset identified for each bin. Slope values are usually close to one, and offset values are usually close to zero. IEC2017 mandates a minimum quantity of data that must be collected per bin for the site calibration to be valid.

Site calibration represents a significant expense for developers. Not only is the cost of a second met mast significant; the PPT process is also extended, possibly by several months. This incurs additional professional fees as well as ongoing equipment overheads.

Ten-minute averages

The data required for PPT is typically sampled at 1 Hz and reduced to statistical quantities by aggregation over periods of ten minutes. Each period is then represented by its minimum, maximum, mean and standard deviation. The spectral gap identified by van der Hoven (1957) shows that high-frequency fluctuations corresponding to turbulence occur above 10 cycles per hour, or 1 cycle every six minutes, peaking at just below 60 cycles per hour. The choice of ten minutes as the averaging period is therefore justified since it captures all frequencies above the spectral gap (Christensen et al., 1986). However, Wächter et al. (2012) point out that as one-point statistics, the mean and standard deviation do not capture the dynamic information within the averaging period. Given that the response time of a wind turbine is of the order of 1s, fast variations such as wind gusts will have an effect on the turbine machinery which is not reflected in the standard statistics. Some authors have suggested that a characteristic averaging time should be associated with each type of turbine based on its characteristics (Morales et al., 2012). While this idea is not pursued in the current work, the alternative of employing alternative statistical measures that preserve information about the dynamic behaviour is investigated. Two-point statistics such as structure functions would be suitable for this purpose, and are discussed in §2.3.4.

Method of bins

IEC2017 employs the method of bins (Atkins, 1978) for aggregating data into ten-minute averages (TMA). The procedure is to divide the range of one parameter (typically wind speed) into a set of subranges or *bins* of equal size. The whole dataset is then partitioned according to the binned parameter, and ensemble averages of the other parameters are computed for each partition. To mitigate the effect of outliers, the median value is occasionally used in preference to the mean (Grachev et al., 2005; Türk & Emeis, 2010).

The method of bins is integral to the IEC standard for PPT (IEC, 2005) where it is used to calculate the measured power curve of a turbine and also the relationship between wind at the reference mast and wind at the turbine site during the site calibration phase. In the first case, the data is grouped by wind speed into bins of width 0.5 ms^{-1}, and in the second case, data are grouped by direction into 10° bins, and by shear into bins corresponding to increments of 0.05 in the value of the wind shear exponent, α.

When dividing data into bins, a logical requirement is that the bin intervals are closed at one end and open at the other. A scheme in which the intervals are closed at both ends would risk some data items being double-counted, and using open intervals would risk some data items being missed completely if their values happen to fall on a bin boundary. Although IEC2017 is silent on the interval to be used when binning data for PPT purposes, MEASNET recommends using a left-closed interval.

Measurement configuration

The standard allows four combinations of met mast and measurement instrumentation:

1. Met mast to hub height and remote sensing to all heights
2. Met mast below hub height and remote sensing to all heights
3. Met mast above hub height
4. Met mast to hub height

The use of remote sensing devices such as sodar and lidar was introduced into the standard with the new edition, and there has not yet been sufficient time to gather data about their use in real PPT contracts. A typical installation continues to involve a met mast that reaches up to the turbine hub height with at least one anemometer and one wind vane at that level and the same configuration lower down. Temperature, humidity and pressure are typically measured at a minimum of one level. Sonic anemometers capable of 3D measurements are permitted in place of mechanical instruments. However, concerns over costs often mean that the installation only satisfies the minimum requirement (Henke & Clive, 2017; Sumner & Masson, 2006a). All instruments must be professionally calibrated at a MEASNET-approved facility. In all configurations, power measurements are provided by the turbine's supervisory control and data acquisition (SCADA) system.

Data logging

Data is recorded using a data logger at 1 – 20 Hz, and a script on the logger aggregates the data into ten-minute records including the mean, standard deviation, minimum and maximum value for each period. The power output from the turbine is measured and aggregated in a similar fashion. The scripting capabilities of data loggers are quite powerful which has led some authors to suggest other statistics that could be collected as a matter of course. While the standard values listed above are all one-point statistics, it has been suggested that two point statistics such as transience might capture more detail of the actual meteorological conditions (Clive, 2012). So far however this idea has not been taken up.

Data rejection

The standard PPT procedure tests the operation of a turbine under an ideal set of conditions, only some of which can be defined using deterministic procedures. In the current work, these are referred to as *quality* filters because they are applied simply to safeguard the quality of the data. As part of a PPT contract additional filters are negotiated that reflect the capabilities of the turbine, the limits of applicability of the power curve and the expected conditions at the site. These *contractual* filters can be more or less restrictive depending on the concerns of the negotiating parties. IEC2017 specifies the following reasons for data rejection:

> a) external conditions other than wind speed are out of the operating range of the wind turbine
> b) the wind turbine cannot operate because of a wind turbine fault condition
> c) the wind turbine is manually shut down or in a test or maintenance operating mode
> d) failure or degradation (e.g. due to icing) of measurement equipment;
> e) wind direction outside the measurement sector(s) […];
> f) wind directions outside valid […] site calibration sectors;
> g) any special atmospheric condition filtered during the site calibration shall also be filtered during the power curve test
>
> (IEC, 2017)

Conditions b), c) and d) are technical requirements that have no relationship to the meteorological conditions. A common situation that falls under condition c) is where the output of the turbine is constrained by the supervisory control system to a certain level. This operational mode, known as *curtailment*, introduces artificial relationships into the data which appear as horizontal trends in the power curve at the curtailment level.

The detection of icing and the elimination of affected records is mandated by the standard, but no specific methods are recommended. MEASET provides a clarification which states that icing is likely where the measured temperature is below 2ºC and the relative humidity is above 80% (MEASNET, 2009).

Conditions e) and f) refer to the definition of the free-stream sector. Only records where the wind direction is deemed valid in that sense are permitted.

The conditions discussed so far can all be used to define quality filters as defined above. Conditions a) and g) in contrast are open to interpretation and to negotiation and give rise to the contractual filters for a particular PPT project. Contractual filters vary considerably from one project to another depending on the manufacturer's assessment of the site and primarily define limitations on turbulence intensity, shear and occasionally other parameters such as wind veer, inflow angle, temperature and air density. Any TMA records where the relevant parameter falls outside the agreed range is normally excluded from the analysis. However, the PCWG has agreed in principle that instead of distinguishing between valid and invalid records, it would be more appropriate to distinguish between an inner range and an outer range of parameter values. The inner range would define a set of conditions under which 100% of warranted AEP could be expected whereas a lower performance could be defined for the outer range (PCWG, 2013). However, this suggestion has not yet been taken up by the industry. To provide an illustration of a contractual filter, the valid range of TI might be specified as $0.05 < TI < 0.15$. Alternatively, a more complex filter might be defined such the example below taken from the warranty conditions for a real PPT project. The complexity in the upper bound arises from the tendency for higher wind speeds to suppress turbulence (Ernst & Seume, 2012; K. Y. Lee et al., 2017).

$$0.05 < TI < 0.1 * (1.25 * U_h + 6)/U_h$$

Reporting

The power curve test defined in IEC2017 requires the reporting of the measured power curve, AEP and the turbine power coefficient in tabular and graphical format. Wind speeds are normalised separately to sea-level and to the site-mean air density and both calculations are presented.

2.2.5 Uncertainty in IEC2017

Uncertainties are calculated for each wind speed bin using formulae based on the ISO Guide to the Expression of Uncertainty in Measurement (GUM) (JCGM, 2008). GUM distinguishes between category A uncertainties which are estimated with reference to the statistical distribution of measured values, and category B uncertainties which are estimated from other data. The uncertainty in the power curve and in the predicted AEP is estimated by combining the bin uncertainties.

IEC2017 provides a list of more than 60 sources of uncertainty of which only two are classified as category A. They are the statistical variation in site calibration and the variability of electrical power. The standard uncertainty in the normalised mean power, $s_{P,i}$, in bin i is given by

$$s_{P,i} = \frac{\sigma_{P,i}}{\sqrt{N_i}} \tag{4}$$

where

N_i	=	number of TMA power values in bin i
$\sigma_{P,i}$	=	standard deviation of TMA power values in bin i

Category B uncertainties arise from the resolution of the measurement instruments, the data acquisition (DAQ) system, the topological characteristics of the site, the prevailing wind conditions and the mathematical nature of any methods that are applied to the raw data. In cases where the uncertainty is expressed as a limit, (i.e. $\pm\delta$), as is the case with instrument specifications, and a rectangular probability distribution is assumed, the standard uncertainty, s, is estimated by Eq. 5.

$$s = \frac{\delta}{\sqrt{3}} \tag{5}$$

Each category B uncertainty is related to the power by a sensitivity parameter. For example, the sensitivity parameter for wind speed is defined by the slope of the power curve in the relevant bin. Many category B uncertainties are fixed quantities that do not change from one wind speed bin to another. Others are calculated as a percentage of the mean value in each bin.

Category B uncertainties are assumed to be uncorrelated, and are therefore summed quadratically. That is, each value is squared, the squares are added together and the combined uncertainty is the square root of the total.

2.2.6 Costs of PPT

The costs associated with a PPT project come in two kinds, direct and indirect. The direct costs are those concerned with

- setting up and maintaining the measurement equipment
- performing a site calibration if necessary
- monitoring the data collection
- analysing data
- writing reports
- decommissioning measurement equipment not needed in the long term

Because of the climatic conditions in temperate regions where many wind developments take place, the summer period is often critical for the overall construction schedule. It is common, for example, to carry out foundation work in one summer season, and to install the turbines themselves the following year. Foundation work includes geological surveys, construction of access roads and turbine hardstands and the installation of met masts. This means that there is a window of around six months in which to complete the site calibration after the installation of the masts and before turbine construction is due to begin. If the data collection required for the site calibration takes longer than expected, it will then start to impact the overall constructions schedule which leads to indirect costs. These can include, for example, the cost of cranes required for turbine installation. Continued use of such equipment can incur costs of around £250K per additional day (Wood Clean Energy, personal communication, 24 July 2019).

Independent engineers usually cost a PPT project assuming a three-month duration per measurement campaign which could refer either to the site calibration or to the test period itself. The actual details of a particular project will depend strongly on how the costs are accounted for by the various parties to the contract. Given this common practice though and assuming 30.4 days per month, an additional day would add approximately an extra 1% to the direct cost of the campaign:

$$100 \times \frac{1}{3 \times 30.4} \cong 1\%$$

However, this only accounts for the management and operational responsibility for the campaign itself. It does not include equipment maintenance costs, or any indirect costs that result from over-runs (Wood Clean Energy, personal communication, 24 July 2019).

2.3 Meteorological variation

2.3.1 Introduction

As intimated in §2.1.4, the meteorological context in which wind turbines operate is complex with highly inter-dependent and non-linear parameters, some of which are accommodated in the IEC2017 PPT procedure while others are not. Research on wind turbine performance tends to be selective, focussing on specific combinations of parameters. A common approach is to partition the data according to a parameter of interest and estimate AEP for high and low values. St. Martin et al. (2016), for example, examined the effect of turbulence on the AEP of a 1.5MW onshore turbine by partitioning the data into three categories corresponding to low ($TI < 0.15$), medium ($0.15 < TI < 0.2$) and high ($TI > 0.2$) turbulence intensity (TI). Their results showed that the AEP for low TI was reduced by 15% compared to the AEP for the medium category, and the AEP for high TI was reduced even further by about 32%.

Montes et al. (2009) examined the impact of different values of the wind shear exponent on the AEP calculated for three sites in Spain. The data was collected and analysed in accordance with IEC2005, and a similar pattern was found across all three sites. The whole database was partitioned into three shear classes, and high shear ($\alpha > 0.17$) was found to significantly reduce the performance of the turbine at low wind speeds. However, a high overall wind speed was shown to reduce the effect of shear. Elsewhere, very high shears where the shear exponent exceeds 0.35 have been shown to decrease power output of a turbine by up to 42% (Wagner et al., 2009). Other studies have demonstrated performance impacts of air density (Pandit et al., 2019), wind veer (Walter et al., 2009), inflow angle (Pedersen, 2004), atmospheric stability (Sumner &

Masson, 2006b; Wharton & Lundquist, 2010) and intermittency (non-Gaussian wind statistics) (Schottler et al., 2016).

Some studies go beyond the direct analysis of a single parameter. Kwon (2010), for example, examines the combined influence of air density, wind speed and distribution and the surface roughness exponent. Bulaevskaya et al. (2015) investigate wind speed at multiple heights, wind veer and air density while Lee et al. (2015) consider wind speed, wind direction, air density, humidity, turbulence, and wind shear. By selecting a small set of promising parameters to examine these examples improve on single-parameter studies, but still do not account for the influence of excluded parameters or interactions between parameters.

A further limitation of existing research in this area is the reliance on traditional measures of certain meteorological parameters. For example, turbulence is usually represented by the coefficient of variation of horizontal wind speed, referred to as turbulence intensity (TI) even though other measures have the potential to retain more information about turbulent structures and their behaviours. Turbulence kinetic energy, for example, incorporates information about turbulent variation in the vertical dimension as well as the horizontal (St. Martin et al., 2016) while structure functions retain information about temporal variations (Clive, 2012; Davidson, 2004, p. 90).

This section reviews meteorological parameters with a theoretical impact on turbine power production based on work in micrometeorology as well as wind energy. Where parameters are addressed in IEC2017, the means for accommodating them is described and alternative measures are discussed where appropriate. Through this exercise, candidate parameters are identified for further investigation in the current work. The intention is to avoid an over-reliance on those parameters and measures which are traditionally used, and to open up the possibility of identifying novel parameters or alternative representations of traditional parameters which could be incorporated into an improved PPT process.

2.3.2 Temperature

Generally speaking, the temperature of the air decreases with increasing height due to the dissipation of energy received at the surface via solar warming. In the absence of any other effects, the rate of decrease is 9.8 K km^{-1} (Wallace & Hobbs, 2006, p. 77) which is known as the dry adiabatic lapse rate, Γ_d. There are two major influences on the vertical temperature profile. The first of these is the decrease in pressure with height above the surface which results in air parcels of equal mass and enthalpy exhibiting different temperatures as predicted by the ideal gas law:

$$PV = nRT \tag{6}$$

where

P	=	pressure (Pa)
V	=	volume (m^3)
n	=	number of moles of gas
R	=	universal gas constant = 8.3144598 J mol^{-1} K^{-1}
T	=	absolute temperature (K)

To accommodate height-related pressure effects, a correction can be applied which leads to a theoretical quantity known as the *potential temperature*, θ, which represents the temperature that a parcel of air would have if it were brought adiabatically to a height of zero metres above ground level (Stull, 2015, p. 61). Potential temperature has the advantage of being a conserved quantity with changes in height.

The second factor that affects apparent temperature is the moisture content of the air. Because the gas constant for dry air is smaller than that for water vapour, moist air has a lower density than dry air under equal temperature and pressure (Jacobson, 2005, p. 33). For a dry air parcel to have the same density as a moist air parcel under equal pressure, its temperature would need to be higher and another correction can be applied to the measured temperature to correct for the degree of humidity. This yields the *virtual temperature*, T_v, defined as the temperature of dry air with the same density and pressure as moist air. The virtual temperature of a parcel of moist air is larger than its actual temperature. Temperature values measured with a sonic anemometer are very close to the virtual temperature because of the effect of moisture on the speed of sound (Schotanus et al., 1983) to the extent that the two can be treated as the same with negligible loss of accuracy (Kaimal & Gaynor, 1991). Where the actual temperature is required, a correction must be made to values from a sonic instrument.

The *potential virtual temperature*, θ_v, is the result of correcting for both height and humidity, and can be calculated from the virtual (sonic) temperature using Eq. 7:

$$\theta_v = T_v \left(\frac{1000}{B}\right)^{0.286} \tag{7}$$

where
T_v =virtual temperature (K) ≅ sonic temperature, T_s
B = barometric pressure (mbar)

Temperature variations in the ABL occur slowly and over relatively large distances. Differences in temperature over the vertical extent of a wind turbine rotor and within a ten-minute averaging period or between periods are likely to be very small. However, temperature is essential for the estimation of several other parameters including air density in particular. It has been shown that models that include temperature alongside wind speed and direction better describe the performance of wind turbines for performance monitoring (Schlechtingen et al., 2013).

2.3.3 Air density

The amount of energy in the wind available for extraction depends on the mass flow. Air density, defined as a function of temperature, pressure and relative humidity, is therefore an important parameter. IEC2017 provides Eq. 8 for the estimation of air density.

$$\rho = \frac{1}{T}\left[\frac{B}{R_0} - \phi P_w\left(\frac{1}{R_d} - \frac{1}{R_w}\right)\right] \tag{8}$$

where
B = barometric pressure (Pa)
ϕ = relative humidity (%)
R_d = gas constant for dry air
R_w = gas constant for water vapour
P_w = vapour pressure given by

$$P_w = 2.05 \times 10^{-5} \mathrm{e}^{0.0631846\,\mathrm{T}}$$

Using virtual (sonic) temperature, the humidity correction is not necessary and a simpler formula can be used:

$$\rho = \frac{B}{R_0 T_v} \tag{9}$$

The measured atmospheric pressure can be normalised to a particular height above sea level using the hypsometric equation (Stull, 2015, p. 17) as shown in Eq. 10. This can be useful, for example, in estimating sea-level pressure from values measured at another altitude.

$$B_2 = B_1 e^{\left[\frac{g(z_1 - z_2)}{R_d \overline{T_v}}\right]} \tag{10}$$

where
B_i =barometric pressure measured at height z_i (mbar)
g =acceleration due to gravity (ms^{-2})
R_d =gas constant for dry air (2.8704 m^3 hPa kg^{-1} K^{-1})

In order to allow comparison with the warranted power curve, an air density correction is applied to the measured wind speed values in IEC2017 using Eq. 11. The standard requires two sets of results to be presented – one where the data has been normalised to standard sea-level density of 1.225 kgm^{-3} and the second that uses the site-specific air density. This is simply the mean density calculated over the whole dataset.

$$U_n = U\left(\frac{\rho}{\rho_0}\right)^{1/3} \tag{11}$$

where
U_n = normalised wind speed (ms^{-1})
U = TMA value for mean horizontal wind speed (ms^{-1})
ρ = TMA value for density (kg m^{-3})
ρ_0 = reference density (kg m^{-3})

2.3.4 Turbulence

Turbulence is a high-frequency, three-dimensional chaotic component superimposed onto the mean direction of fluid flow (Davidson, 2004). The two main sources of turbulence are interactions with surface features and convection due to solar warming (Burton et al., 2011). Surface interactions create circular eddies primarily because of the pressure differential introduced into a smooth flow by viscous forces as the laminar flow passes over or around an obstacle. In fluid dynamics, viscous forces tend to damp the motion of a fluid while inertial forces act to maintain its motion and the ratio of inertial forces to viscous forces is represented by the dimensionless Reynolds number.

Turbulent eddies break down over time as kinetic energy is passed down from large scale structures – which can be similar in size to the ABL itself (Jacobson, 2005) – to smaller scales. During this energy cascade vortices become smaller and their kinetic energy eventually dissipates as heat at the Kolmogorov microscale around one or two millimetres when viscous forces start to dominate (Davidson, 2004; Jacobson, 2005). Because eddy formation and dissipation are not coherent, atmospheric turbulence consists of many superimposed eddies at different scales moving in different directions.

This complexity means that turbulent phenomena are resistant to a deterministic explanation and must be described in statistical terms (Davidson, 2004).

Traditionally, turbulent air flow is described in terms of its intensity, TI, defined as the coefficient of variation of wind speed given by Eq. 12.

$$TI = {}^{\sigma}/_{U} \tag{12}$$

where
σ = standard deviation of wind speed (ms^{-1})

Turbulence intensity is expressed as a percentage and is calculated over ten-minute intervals. This makes it a convenient measure which is simple to calculate and to interpret (Roy, 2014). However, since both the mean and standard deviation are one-point statistics, information about the temporal structure of the wind speed variation is lost. In addition, TI contains no information about variation in the vertical dimension. Mathematically, the coefficient of variation, V, has been criticised among other things for being sensitive to outliers and to changes in the mean. Kvålseth (2017) proposes a second-order coefficient of variation, V_2, defined as the standard deviation divided by the root mean sum of squares:

$$V_2 = \frac{\sigma}{\sqrt{\frac{1}{n}\sum_1^n x^2}} \tag{13}$$

Kvålseth argues that the resulting statistic resolves the issues mentioned above, and in addition is more amenable to physical interpretation. Taking values strictly between 0 and 1 it can be interpreted as a percentage representation of the variation in a set of data. In contrast, V can take values greater than 1 which are less intuitive.

Within a small enough averaging period, the distribution of deviations from the mean of a time series can be approximated by a Gaussian. Based on this observation, IEC2017 defines an analytical normalisation procedure that can be carried out using standard measurements (Albers, 2010; Clifton & Wagner, 2014). The stated purpose of the method is to correct for distortions to the power curve caused by the original averaging operation. A 3-step procedure – of which the second step is iterative – is provided for determining the zero-turbulence power curve based on characteristics of the measured power curve. The central concept is the calculation of a simulated power output, P_{sim}, using Eq. 14 which is adjusted until it converges with the measured values at key points in their distribution.

$$\overline{P_{sim}(u)} = \int_{v=0}^{\infty} P_{I=0}(u) \cdot f(u) du \tag{14}$$

where

$P_{sim}(u)$	=	simulated power output for a given 10-minute period (kW)
$P_{I=0}(u)$	=	zero turbulence power curve
$f(u)$	=	Gaussian distribution of wind speed within the 10-minute period

The power output at a reference turbulence intensity can be calculated using Eq. 15:

$$\overline{P_{Iref}(u)} = \overline{P(u)} - \overline{P_{sim,I}(u)} + \overline{P_{sim,Iref}(u)} \tag{15}$$

where

$P_{Iref}(u)$	=	power output normalised to reference turbulence intensity I_{ref}
$P(u)$	=	power output measured according to IEC2005
$P_{sim,I}(u)$	=	simulated power output for measured turbulence intensity
$P_{sim,Iref}(u)$	=	simulated power output for the reference turbulence intensity

The turbulence normalisation method offers the possibility of directly comparing measurements from a turbine under real conditions with the warranted power curve as long as the latter is associated with a specific turbulence intensity as in Fig. 2. With its various limitations however, turbulence intensity is a crude measure of high-frequency variation of wind velocity. Nevertheless, it often appears as the default measure in wind energy research with no justification or consideration of alternatives. This is the case in IEC2017 where the terms *turbulence* and *turbulence intensity* are used synonymously. The micrometeorology literature describes several other representations of atmospheric turbulence, however, and a review is warranted.

Turbulent variations can be described by making a distinction between a deterministic component of flow velocity represented by an average value and a stochastic component. Reynolds averaging is one such method which splits a time dependent variable such as wind speed into a mean value and associated perturbations as shown by Eq. 16.

$$u = \bar{u} + u' \tag{16}$$

where
$\bar{u}$ = mean wind speed (ms^{-1})
u' = wind speed perturbation (ms^{-1})

The perturbations form a series with a mean of zero over the averaging period. Reynolds decomposition can be performed separately on measurements in three dimensions. Multiplying the perturbation values together and then averaging produce covariances which represent the flux of momentum in different directions. Turbulent kinetic energy (TKE) is calculated as half of the sum of the wind speed variance in all three dimensions (Stull, 1988, p. 45). In Eq. 17, the variance is represented as the mean of the squared perturbations within a given averaging period. By convention, an Eulerian reference frame is assumed that is aligned with the cardinal geographic directions. The *zonal* direction is west-to-east and the *meridional* direction is south-to-north. TKE has the advantage over TI that information about variation in the vertical dimension is retained.

$$TKE = \frac{\overline{u'u'} + \overline{v'v'} + \overline{w'w'}}{2} \quad (17)$$

where
u' = perturbation of zonal wind speed
v' = perturbation of meridional wind speed
w' = perturbation of vertical wind speed

Turbulence has a characteristic length scale of the order of the diameter of the largest eddies and is calculated by integrating over the radii of all eddies (Pope, 2000, p. 569). While it is not practically possible to do this directly, the integral time scale (turnover time) of the eddies can be found by integrating the autocorrelation function of horizontal velocity. The integration may be approximated by the sum of the autocorrelation sequence for lags from 0 to n-1 (where n is the number of values in the series) divided by the sampling frequency (Pope, 2000, p. 197). The autocorrelation function r for a lag k is given by Eq. 18. Mathematically, it is the autocovariance of the sequence at the given time lag divided by the variance. Because the autocovariance describes the variation in the series at two different time steps, some of the information about the temporal structure of the series is preserved.

$$r_k = \frac{\sum_{i=1}^{N-k}(y_i - \bar{y})\,(y_{i+k} - \bar{y})}{\sum_{i=1}^{N}(y_i - \bar{y})^2} \quad (18)$$

where
N = number of values in the time series
y_i = series value at time step i
$\bar{y}$ = mean of the time series

The associated length scale can be found by invoking Taylor's frozen turbulence hypothesis (Burton et al., 2011, p. 227; Taylor, 1935) which simply involves multiplying the time scale by the mean wind speed. Since Taylor's hypothesis depends on the assumption of homogeneity, the magnitude of the turbulence intensity must be small compared to the mean horizontal wind speed (Stull, 1988, p. 7).

A great deal of work on atmospheric turbulence is based on Kolmogorov's three hypotheses (Kolmogorov, 1941). The first is the hypothesis of local isotropy which states that any turbulent flow is locally isotropic given a small enough spatial domain and a high enough Reynolds number. To be locally isotropic, the flow must first be locally homogeneous in the sense that it has the same quantitative structure in all parts of the flow field, and in addition it must be invariant to reflections and rotations of the coordinate axes (Kolmogorov, 1941; Pope, 2000, p. 190). Simply put, this means that the velocity fluctuations have no dominant directional features. A test for isotropy is to compare the square of the velocity perturbations (variance) in the longitudinal and vertical dimensions (Davidson, 2004, p. 89) where equality indicates isotropy. A great deal of work on turbulence is based on wind tunnel experiments where turbulence is created by passing the air flow through a wire grid which yields a good approximation of isotropic turbulence. However, although the definition of isotropic turbulence allows for the existence of a uniform but non-zero mean velocity gradient (Pope, 2000, p. 76), it is rarely achieved in natural flows. This can undermine generally-accepted assumptions as demonstrated by Stiperski (2018) who demonstrated that different similarity scaling relations can be identified for different degrees of isotropy.

The other two hypotheses, known as the first and second similarity hypotheses, concern the rate at which turbulent energy dissipates as heat. Fully-developed turbulence tends to dissipate at a constant characteristic rate, ϵ, as large eddies break down into smaller ones until they are overwhelmed by viscous forces at the Kolmogorov microscale (Davidson, 2004, p. 17). The first similarity hypothesis states that for isotropic turbulence the probability density function of differences in wind speed at different points within the restricted domain is defined solely by the dissipation rate and the viscosity. The second states that viscosity can be ignored as long as the distances between the measurement points are large relative to the Kolmogorov microscale. The dissipation rate can be estimated based on the second-order structure function of the wind speed which is a two-point statistic based on differences in speed. While dynamic information is lost when single point statistics are used, two-point statistics such as structure functions do not have this deficiency (Davidson, 2004, p. 90). The general formula for a structure function S of order p is given by Eq. 19. Clive (2012) has argued for the use of S_2, which Clive calls transience, as an alternative to the variance in turbulence and fatigue loading contexts. The dissipation rate ϵ is given by Eq. 20.

$$S_p = \langle [\Delta v(r)]^p \rangle \tag{19}$$

where
$\Delta v(r)$ = velocity increment of a lag time r
and the angle brackets signify expectation.

$$\epsilon = \frac{s}{U}\left[\frac{S_2}{C_K}\right]^{3/2} \tag{20}$$

where
s = sampling frequency (Hz)
C_K = Kolmogorov constant ≅ 2 (Muñoz-Esparza et al., 2017)

A further feature of atmospheric turbulence is its intermittent nature. An intermittent wind is characterised by frequent gusts caused by the presence of coherent structures which are known to affect the turbine loading and could reduce performance. The intermittency is visible in the probability density distribution of wind speed increments, especially at low time lags, where the tails of the distribution are fatter than they are in a Gaussian distribution as shown in Fig. 6 (Boettcher et al., 2003).

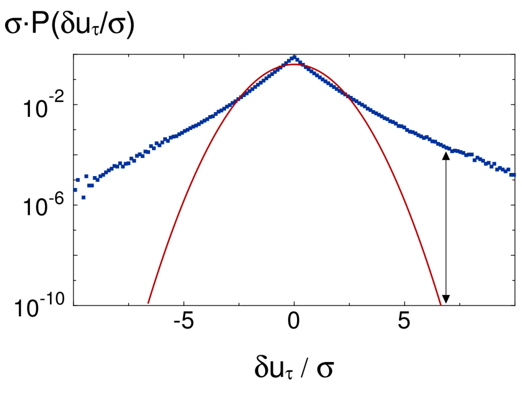

Figure 6: Frequency distribution of wind speed increments (Boettcher et al., 2003)

Assuming a Gaussian distribution would underestimate the likelihood of extreme events (Wächter et al., 2012), and the effect is stronger as Reynolds number increases (Hayot & Jayaprakash, 1999).

An indication of the intermittency of a data series may be obtained by calculating the excess kurtosis of the data increments (Mücke et al., 2011). Given that the kurtosis of a Gaussian distribution is 3, excess kurtosis, γ_2, is calculated from the kurtosis of wind speed increments at lag 1 by Eq. 21. The closer this value is to zero, the more homogenous the turbulent fluctuations.

$$\gamma_2 = K - 3 \tag{21}$$

where
K = kurtosis

In summary, turbulence is an extremely difficult phenomenon to describe mathematically. The traditional approach of using TI fails to account for certain aspects which might be supposed to have an effect on wind turbine power production. In particular, the following measures have been identified:

- Coefficient of variation (turbulence intensity, TI)
- Second-order coefficient of variation
- Turbulence kinetic energy (TKE)
- Turbulence length scale
- Isotropy
- Second-order structure function (transience)
- Turbulence dissipation rate
- Excess kurtosis of wind speed increments

Only TI is included in IEC2017 and the impact on power production of the other items in the list above has rarely been investigated.

2.3.5 Shear

The tendency of wind speed to increase with height affects the performance of a wind turbine as a result of the variation in angle of attack seen by a particular point on a rotor blade at different heights. Wind shear can be modelled with the logarithmic formula

$$u_z = \frac{u_*}{\kappa} ln \frac{z}{z_0} + \Psi_m \tag{22}$$

where
u_z = wind speed at height z (ms^{-1})
u_* = friction velocity (ms^{-1})
κ = von Kármán constant (≈ 0.4)
z_0 = roughness length which takes values such as those in Table 2 (m)
Ψ_m = stability correction
(Burton et al., 2011, p. 17)

Table 2: Surface roughness lengths

Type of terrain	Roughness length z_0 (m)
Cities, forests	0.7
Suburbs, wooded countryside	0.3
Villages, countryside with trees and hedges	0.1
Open farmland, few trees and buildings	0.03
Flat grassy plains	0.01
Flat desert, rough sea	0.001

The log law is often approximated by the power law:

$$u_z = u_{ref} \left(\frac{z}{z_{ref}}\right)^{\alpha} \tag{23}$$

where
α = empirically derived constant
u_{ref} = wind speed at reference height, z_{ref}

The power law is often used for its simplicity and because the shear exponent, α, is a more sensitive parameter than surface roughness (Kubik et al., 2011). A further advantage of the power law is that z_{ref} can be taken as any reference height for which a wind speed measurement exists. It therefore provides a convenient means for estimating the wind speed at a target height z with respect to the measured reference wind speed $u(z_{ref})$ and rearranging Eq. 23 provides a convenient method for calculating α directly (MEASNET, 2009):

$$\alpha = \frac{\log\left({}^{U_2}/{U_1}\right)}{\log\left({}^{z_2}/{z_1}\right)} \tag{24}$$

where
U_i =mean wind speed measured at height z_i (ms^{-1})

However, α is actually dependent on the stability of the atmosphere (Kubik et al., 2011) and ideally a different value of α should be chosen according to the height range over which the power law is applied (Burton et al., 2011, p. 17). This has led some authors to suggest that the power law is of limited usefulness (Petersen et al., 1998). Both laws assume that wind speed increases with height and if that is not the case they may become mathematically undefined (Elkinton et al., 2006). Despite these criticisms, the power law is used in IEC2017 as the standard means to extrapolate wind speeds above the top measurement height.

The wind speed ratio α_{eq} (equivalent alpha) is an alternative measure of shear for use specifically with wind turbines. It involves taking the ratio of the mean wind speed at the top of the rotor to that at the bottom (Colls, 2014). One of the benefits claimed for this measure is that it facilitates comparisons between turbines with different geometries.

With the publication of IEC2017, a new method for accommodating shear into the PPT process is introduced. The rotor equivalent wind speed (REWS) offers a means of deriving a single representative wind speed based on wind speed measurement from at least three heights spanning the whole vertical extent of the rotor where such measurements are available. REWS draws on the concept of the *driving wind* first introduced by Christensen et al. (1986) which is a virtual wind speed distinct from the measured wind speed, but which is more representative of the input to the turbine.

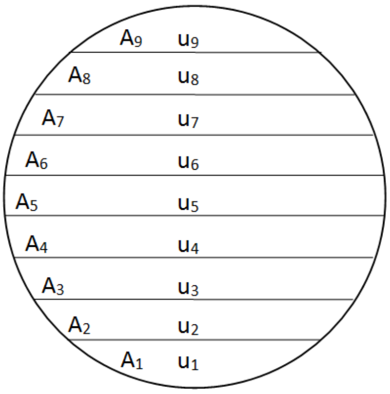

Figure 7: Division of the turbine rotor into segments A_1 - A_9 for the purposes of calculating the rotor equivalent wind speed *(Wagner et al., 2011)*

REWS divides the rotor into a series of n horizontal segments as shown in Fig. 7 and requires a separate representative wind speed measurement, U_i, for each segment (Wagner et al., 2009, 2011). REWS is calculated by summing the cube of the segment wind speeds weighted by their area, A_i, as a proportion of the total rotor disc area, A, and then taking the cube root as shown in Eq. 25.

$$U_{eq} = \left(\sum_{i=1}^{n} U_i{}^3 \frac{A_i}{A}\right)^{1/3} \tag{25}$$

where

U_{eq} = rotor equivalent wind speed (REWS) (ms^{-1})

U_i = wind speed corresponding to the i th segment (ms^{-1})

A = total swept area of the rotor (m^2)

A_i = area of the i th segment (m^2)

REWS is designed to represent the hub height wind speed corresponding to the kinetic energy flux through the rotor disk (IEC, 2017). While REWS has been shown to reduce the scatter in the measured power curve (Eecen et al., 2011), this is not always the case. An evaluation of REWS showed the anticipated improvement in only two out of eight test datasets (Wagner et al., 2014).

2.3.6 Veer

While the major driver of atmospheric wind is the meridional pressure gradient induced by solar warming, the Coriolis effect causes the flow of air to turn in the direction of the Earth's rotation which means clockwise in the northern hemisphere (Wallace & Hobbs, 2006, p. 276). As a result, wind direction changes with height causing further variation in the angle of attack seen by a point on a rotor blade as it rotates. In IEC2017, veer is usually represented simply as an additional source of uncertainty. Where appropriate measurements are available, however, veer can be accommodated into the calculation of REWS by multiplying the wind speed in each segment by the cosine of the angle difference φ_i between the wind direction in segment i and the wind direction at hub height as shown in Eq. 26.

$$U_{eq} = \left(\sum_{i=1}^{n} (U_i \cos \varphi_i)^3 \frac{A_i}{A}\right)^{1/3} \tag{26}$$

where
U_{eq} = rotor equivalent wind speed (REWS) (ms^{-1})
U_i = wind speed corresponding to the i th segment (ms^{-1})
A = total swept area of the rotor (m^2)
A_i = area of the i th segment (m^2)

While the approach taken in Eq. 26 is purely local – i.e. relative to the wind direction at the hub height of the turbine in question – there are more objective ways that it can be represented. One such method is to assume that the effect is linear, and to characterise veer in degrees per 100 m (Markowski & Richardson, 2006). Alternatively, the wind direction at a particular height can be compared to the direction of the geostrophic wind, G. The horizontal components of the surface geostrophic wind can be estimated from

$$G_{sz} = \frac{-\Delta P_m}{\rho f}$$
$$G_{sm} = \frac{\Delta P_z}{\rho f} \tag{27}$$

where

G_{sz}, G_{sm}	=	zonal and meridional components of the geostrophic wind
$\Delta P_z, \Delta P_m$	=	zonal and meridional pressure gradients

A mean horizontal temperature gradient induces a shear in the geostrophic wind known as the thermal wind effect. The wind conditions at the top of the ABL are predicted by the geostrophic wind formulae plus an increment due to the thermal wind effect which is given by Eq. 28 (Stull, 2015, p. 345).

$$G_{tz} = -\frac{gh\,\Delta T_{vm}}{T_v\,f}$$
$$G_{tm} = \frac{gh\,\Delta T_{vz}}{T_v\,f} \tag{28}$$

where

G_{tz}, G_{tm}	=	zonal and meridional components of the thermal wind
$\Delta T_{vz}, \Delta T_{vm}$	=	zonal and meridional gradients of virtual temperature
T_v	=	virtual (sonic) temperature (K)

With the passage of synoptic scale weather systems, the transient temperature gradients can exaggerate the effect of the Coriolis force, or counteract it, sometimes to the extent that the wind actually turns anticlockwise with increasing height in the northern hemisphere. This is known as *backing*, while the more usual clockwise rotation is known as *veering*. Evidence of veering or backing can be seen in the difference between the measured wind direction and the predicted direction of the geostrophic wind at the ABL top. Since the geostrophic wind tends to flow parallel to the isobars on a weather chart, this difference in direction is known as the cross-isobar angle, α_0, and can be calculated with a simple angular difference. That is, the cross-isobar angle is calculated at a given measurement height as the difference between the measured wind direction and the derived geostrophic wind direction. Negative values represent a clockwise rotation of the wind with increasing height as expected in the northern hemisphere.

2.3.7 Inflow angle

A wind turbine is designed to respond to the horizontal wind; however, when the turbine is situated on sloping terrain, or in stable or unstable conditions there is a mean vertical component to the flow. In these cases, the mean flow of air enters the rotor disc at some non-zero angle to the horizontal and such off-axis flow has been demonstrated to reduce performance (Tindal et al., 2008). The inflow angle, ϕ, is calculated as the inverse tangent of the vertical wind speed w divided by the mean horizontal wind speed U:

$$\phi = \tan^{-1}\left(\frac{w}{U}\right) \tag{29}$$

2.3.8 Stability

The diurnal cycle of warming and cooling gives rise to a predictable structure of the ABL which is illustrated in Fig. 8. During daylight hours, the surface is warmed by solar radiation and heat is transmitted to the air in the surface layer by conduction which becomes warmer than the air above. This condition in which a parcel of air will continue to rise if displaced from its original position is known as an unstable atmospheric regime. The surface and Ekman layers together constitute the ABL which grows over the course of the day by entrainment at its upper boundary through the action of turbulence (Stull, 1988, p. 11). During the night, the source of thermal eddies is absent and the residual layer is the result of the gradual decay of turbulent eddies created during the day. At the same time, a stable layer of cooler, denser air develops at the bottom of the ABL as heat energy is absorbed by the surface. In stable conditions, a displaced parcel of air tends to return to its original altitude. A neutral regime also exists either as a transition between stable and unstable atmospheres, or during overcast conditions where solar warming of the surface is suppressed (Emeis, 2011, p. 11).

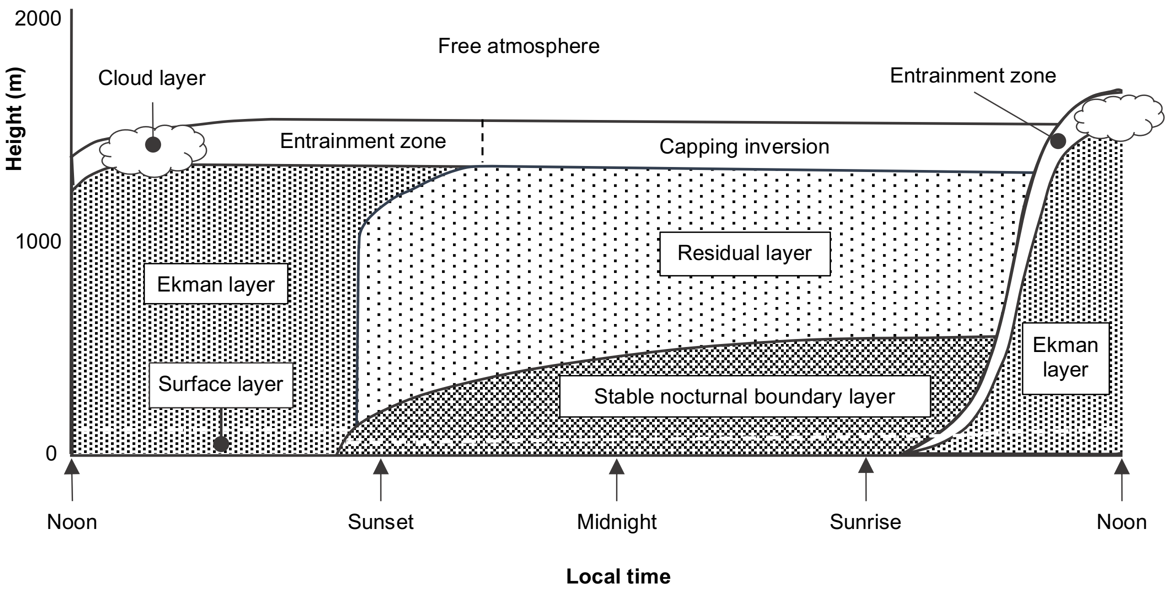

Figure 8: Diurnal evolution of the atmospheric boundary layer *(Stull, 1988, p. 11)*

The literature contains many methods for representing atmospheric stability ranging from those that require high-frequency measurements of temperature and wind velocity in three dimensions to very broad indicators such as the time of day. Table 3 illustrates this abundance and provides indictive references.

Table 3: Stability indicators used in the literature

Method/metric	Used by
Pasquill–Gifford–Turner classification (PGT)	(Ashrafi & Hoshyaripour, 2010; Gualtieri & Secci, 2011)
Temperature lapse rate	(Eecen et al., 2011; Eecen, 2009; Jacobson, 2005, p.55)
Obukhov length (L) by eddy covariance	(Argyle & Watson, 2012; Bartholy & Radics, 2005; Coelingh et al., 1996; Lange et al., 2004; Newman et al., 2015; Sumner & Masson, 2006b; Van Den Berg, 2008)
h/L (h = height of ABL)	(Donda, 2015)
Shear exponent	(Vanderwende & Lundquist, 2012; Wharton & Lundquist, 2012)
Wind speed ratio	(Tambke et al., 2006)
Shear + turbulence intensity	(Bleeg et al., 2015; Dörenkämper et al., 2014; Hayes et al., 2012)
Gradient Richardson number	(Krogsæter & Reuder, 2015; Newman & Klein, 2014; Newman et al., 2015)
Bulk Richardson number	(Alblas et al., 2012; Chambers et al., 2016; Donda, 2015; K. S. Hansen et al., 2012; Holtslag et al., 2014; Optis, 2015; Sathe et al., 2011; Tambke et al., 2006; Vanderwende & Lundquist, 2012)
Brunt–Väisälä frequency	(Jacobson, 2005, p. 56; S. S. Zilitinkevich & Esau, 2005)
Shear capacity	(van Hooijdonk et al., 2015)
Variance of vertical wind speed	(Contini et al., 2009; Hunter, 2012)
Turbulence kinetic energy (TKE)	(Wharton & Lundquist, 2011; Wilson & Venayagamoorthy, 2015)
Wind direction standard deviation	(Barrios et al., 2008; Slade, 1968; USEPA, 2000)
Time of day	(Ashrafi & Hoshyaripour, 2010; Bailey, 1981; Bleeg et al., 2015; Istchenko & Turner, 2009)

With 3-dimensional measurements taken at frequencies at or above 1 Hz with a sonic anemometer, vertical fluxes of horizontal momentum and sensible heat can be obtained as a direct indication of atmospheric stability through the use of the eddy covariance technique (Burba, 2013). Such data is not commonly available during measurement campaigns for resource estimation or power performance assessment which typically rely on cup anemometers and data averaged over ten-minute periods (Newman & Klein, 2014). Mathematically, the covariance of the vertical wind velocity and the concentration of a quantity of interest provides a measure of vertical flux (Burba, 2013, p.17). Because the change in air density over small vertical distances is negligible, fluxes can be expressed in kinematic form by dividing by the density of air and by any other constant term (Stull, 1988, p.48). This is convenient because the fluxes can then be measured directly since they have the same units as quantities such as temperature and wind speed. Positive flux (i.e. away from the surface) indicates unstable conditions and a negative flux indicates stable conditions. Common terms in flux studies are

$\overline{u'w'}$ covariance of longitudinal (along-wind) velocity with vertical velocity

$\overline{v'w'}$ covariance of lateral (across-wind) velocity with vertical velocity

$\overline{\theta_v{}'w'}$ covariance of potential virtual temperature with vertical velocity

The covariances of horizontal and vertical velocities represent the two components of the vertical kinematic flux of horizontal momentum, F. Likewise, the covariance of temperature and vertical velocity represents the vertical kinematic flux of sensible heat, Q. Studies have shown that to capture flux-carrying wavelengths in stable conditions requires an averaging period of only 5.6 minutes for momentum flux (Biltoft, 2003b). However, this requirement rises in unstable conditions to 27.8 minutes for momentum flux and to 16.6 minutes for sensible heat flux. Standard practice in eddy-covariance studies is to calculate flux values over consecutive averaging periods of 30 minutes (Finnigan et al., 2003; Mauder & Foken, 2006).

Measurements from sonic anemometers must be adjusted to compensate for the fact that these instruments cannot be levelled exactly (Burba, 2013). The procedure requires the coordinate frame to be rotated such that the x-axis is aligned with the mean wind flow, and the vertical and lateral means are minimised. This can either be done directly using trigonometric operations (Foken, 2008, p. 109), or by fitting the measurements to a plane in 3-dimensional space, and there is little practical difference in the results of these two approaches (Mahrt el al, 2000). The planar fit method takes advantage of the fact that the mean wind vector can be used to define a plane as the wind direction changes. As a first step, the best-fit plane may be calculated by least-squares regression using the algorithm of Wilczak (2001). Secondly, unit vectors in the rotated coordinate frame may be derived using the approach of Lee et al. (2004). Finally, the new flux vectors are determined by projecting the original vectors onto the new frame of reference by matrix transformation (X. Lee et al., 2004, p. 62).

When using sonic instruments, a further correction must also be applied to the values of vertical flux of sensible heat because sonic temperature is sensitive to humidity. The method of Schotanus (1983) whose canonical form is given by Eq. 30 can be used for this purpose.

$$\overline{w'T_s'} = \overline{w'T'}\left(1 + \frac{0.51\bar{T}C_p}{\lambda\beta}\right) - 2\frac{\bar{T}\bar{U}}{\overline{c^2}}\overline{u'w'} \tag{30}$$

where

c	=	speed of sound (ms^{-1})
λ	=	latent heat of condensation for water (2.5×10^6 J kg^{-1})
β	=	Bowen ratio (ratio of heat flux to moisture flux)
$\overline{w'T_s'}$	=	sensible heat flux calculated using the sonic temperature T_s
$\overline{C_p}$	=	specific heat of air at constant pressure (1012 J kg^{-1} K^{-1})

Since the moisture term is relatively small the Schotanus method assumes a value of 0.4 for grassland. Eq. 30 can then be rearranged to find the corrected sensible heat flux.

In a rotated coordinate frame where the lateral wind velocity component is minimised, the vertical kinematic flux of horizontal momentum, F, may are estimated using Eq. 31.

$$F = \overline{u'w'} \tag{31}$$

The lowest 10% of the ABL is the atmospheric surface layer (ASL) in which vertical fluxes of momentum and sensible heat are approximately constant. In this region, several parameters can be described by self-similar relationships. Two phenomena are mathematically similar if the numerical description of one can be applied to the other through a simple transformation such as a change of unit of measurement (Barenblatt, 1996). In self-similar phenomena, the ratio of values at different heights is constant. This simplification facilitates *dimensional analysis* in which terms are combined so that the dimensions associated with them cancel out leaving a dimensionless quantity whose value is independent of the measurement scale. The main benefit of similarity theory is to reduce the number of independent parameters in a mathematical model by combining fundamental parameters into dimensionless groups and establishing the value of the resulting dimensionless parameter by experiment. Within the ASL, Monin-

Obukhov similarity theory (Monin & Obukhov, 1954) defines the Obukhov length, L, which can be interpreted as the height at which buoyant parameters start to dominate shear-driven turbulent production (Stull, 1988, p. 182) given by

$$L = \frac{-{u_*}^3\, \theta_0}{\kappa g\, \overline{w'\theta_0'}} \tag{32}$$

where
u_* = friction velocity
κ = von Karman constant $\cong 0.4$
θ_0 = potential virtual temperature at the surface (K)

The covariance of θ_0 with the vertical wind speed in the denominator represents sensible heat flux. L is positive in stable conditions and negative in unstable conditions and tends to infinity in neutral conditions. It is therefore more usual to use the Obukhov stability parameter, ζ, defined as the ratio z/L where z is the measurement height as an indicator of stability. While a value of zero nominally indicates neutrality, a small range of values is usually used to define a near-neutral band. The customary height for making ASL measurements is 10 m above ground level.

The friction velocity, u_*, is a generalised velocity scale related to the shearing stress in a turbulent air flow (Foken, 2008, p. 31) and defined by Eq. 33.

$$u_* = \left[\left(\overline{u'w'}\right)^2 + \left(\overline{v'w'}\right)^2\right]^{1/4} \tag{33}$$

Because the cross-wind flow is close to zero in a rotated coordinate frame, this definition can be simplified to

$$u_* = \sqrt{\left(\overline{u'w'}\right)} \tag{34}$$

Other estimates of stability are based on standard measurements of wind speed and temperature, and provide approximate representative values over some height range. The bulk Richardson number, Ri_b, is one of a family of related dimensionless numbers which also include the gradient Richardson number based on the temperature gradient at a particular height, and the flux Richardson number which is calculated based on the vertical fluxes of sensible heat and horizontal momentum. As with the Obukhov stability parameter, all variants of the Richardson number are negative in stable conditions, positive in unstable conditions and zero in neutral conditions.

The bulk Richardson number, given by Eq. 35, is essentially the ratio of buoyant turbulence production, represented by the difference in potential virtual temperature, $\Delta\theta_v$, between the surface and the top measurement height, z, to the mechanical production of turbulence represented by the square of the wind speed, U_z, measured at the same height.

$$Ri_b = \frac{g}{\overline{\theta_v}} \frac{\Delta\theta_v \, z}{U_z^2} \tag{35}$$

where
$\overline{\theta_v}$ =average potential virtual temperature of the layer

The literature contains many examples of schemes to divide atmospheric stability into a set of classes. However, there is little agreement over the precise number of classes and the threshold values. Mohan and Siddiqui (1998), for example, define seven classes with thresholds based on the bulk Richardson number, while Wharton and Lundquist (2010) define only five classes based on the Obukhov length as illustrated in Table 4.

Table 4: Stability class thresholds

Stability class (Mohan & Siddiqui, 1998)	**Ri_b**	**L (m)**	**Stability class** (Wharton & Lundquist, 2010)
Extremely stable, low wind	$0.084 \le Ri_b$	$0 < L < 50$	**Strongly stable**
Extremely stable	$0.042 \le Ri_b < 0.084$	–	–
Moderately stable	$0.0072 \le Ri_b < 0.042$	$50 < L < 200$	**Stable**
Neutral	$-0.0036 \le Ri_b < 0.0072$	$L > 200$ or $L < -300$	**Neutral**
Slightly unstable	$-0.011 \le Ri_b < -0.0036$	$-300 < L < -15$	**Convective**
Moderately unstable	$-0.023 \le Ri_b < -0.011$	–	–
Highly unstable	$Ri_b < -0.023$	$-15 < L < 0$	**Strongly convective**

These and other similar schemes can be criticised for the arbitrary nature of some of the divisions; however, several authors (Nieuwstadt, 1984; Van de Wiel, Moene, & Jonker, 2012; Vogelezang & Holtslag, 1996) identify a physical transition in the stable regime which separates conditions in which continuous turbulence is maintained by higher wind speed at a characteristic height from those in which turbulence is intermittent. Vogelezang and Holtslag (1996) identify the wind speed at 40 m (U_{40}) as the appropriate height. Adopting this approach would lead to a scheme which defines unstable and neutral classes and which divides stable regimes into strongly and weakly stable depending on the mean wind speed. Thus, the two schemes shown in Table 4 can be reconciled as shown in Table 5.

Table 5: Four-level stability classification

Class	**Obukhov length range**	**Bulk Richardson number range**	**Other conditions**
Strongly stable	$0 < L < 200$	$Rib > 0.0072$	$U_{40} < 5$m/s
Weakly stable	$0 < L < 200$	$Rib > 0.0072$	$U_{40} >= 5$m/s
Neutral	$-300 > L$ or $L > 200$	$-0.0036 < Rib <= 0.0072$	
Unstable	$0 > L > -300$	$Rib < -0.0036$	

While the main cycle of atmospheric stability is driven by diurnal variations, it is also affected by seasonal effects in temperate latitudes. Solar irradiation is greater in the summer because the tilt of the Earth's axis induces a longer day length with a greater *solar elevation*, β, or the angle between the sun and the horizon, at noon. Seasonality can be represented directly by the *solar declination*, δ, which is the angle between the sun and the plane of the equator. The time of day can also be defined with reference to solar geometry. The *hour angle* is the direction of the sun as an angular offset from 0 at solar noon, or the moment when the sun is at its highest. Using solar geometry to represent these time-related parameters has the benefit of accuracy with respect to physical processes rather than to the essentially arbitrary system of clock time. The Pasquill–Gifford–Turner classification (PGT) makes use of solar elevation and cloud cover to classify stability regimes (Ashrafi & Hoshyaripour, 2010; Gualtieri & Secci, 2011).

2.3.9 ABL height

The height, h, of the ABL is a potentially important scaling length given that it defines the limit on the size of turbulent eddies. Changes in h are driven by the solar cycle of heating and cooling and it can be estimated in a number of ways including direct measurements of temperature changes and the presence of clouds at the capping inversion (Stull, 1988, p. 9). Remote sensing methods are also available including radiosonde, ceilometer, light detection and ranging (lidar) and sound detection and ranging (sodar) (Contini et al., 2009). The value of h can be estimated using surface measurements by relying on theoretical scaling relationships; however, Monin-Obukhov similarity theory breaks down above the surface layer (Optis et al., 2016) which implies that modifications or alternatives are needed. Some success in extrapolating wind speeds and estimating h has been achieved using a three-layer model (Gryning et al., 2007). Recently, Holtslag et al. (2017) achieved a good correlation between measured and predicted values for h using the formula of Rossby and Montgomery (1935):

$$h = C_{RM} \frac{u_*}{f} \tag{36}$$

where
f = Coriolis parameter
C_{RM} = Rossby-Montgomery coefficient
u_* = friction velocity (ms^{-1})

Previously, there was no general consensus on the value of C_{RM} with values in the range 0.1 – 0.5 being found in the literature (See for example Kinoshita & Niino, 1990; Kraus, 2008; Peña et al., 2010; Rossby & Montgomery, 1935). Many authors note that a constant value for the Rossby-Montgomery coefficient is not realistic since the height of the boundary layer is clearly dependent on atmospheric stability. Holtslag et al (2017) present modified formulae for C_{RM}, shown as Eqs. 37, based on the Obukhov length, thus accommodating atmospheric stability into the estimate of h. A limitation of Holtslag's approach is that the empirical coefficients are derived from data from an offshore site and may not be ideally suited to onshore locations.

Stable $$C_{RM} = 0.04 + 0.05\left(1 + 2\frac{100}{L}\right)^{-1} \tag{37}$$

Unstable $$C_{RM} = 0.17 - 0.08\left(1 - 0.5\frac{100}{L}\right)^{-3}$$

2.3.10 Normality

When averaging a series of values over time, it is common to use the mean and standard deviation of the aggregation to characterise the whole sample. While applicable to any distribution, this approach implicitly suggests that the data is normally (Gaussian) distributed. This can be misleading as illustrated by the plots in Fig. 9 which all have the same mean and standard deviation, but very different coverage.

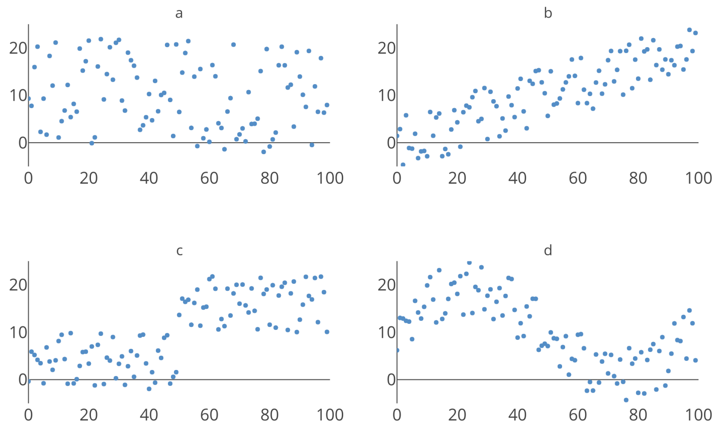

Figure 9: Data distributions with the same mean and standard deviation

Within a short enough averaging period an assumption of normality may be adequate; however, violation of this assumption could lead to unwanted variation in the results of calculations. Procedures for filtering turbulence data based on their deviation from an assumed Gaussian distribution have been developed (Hojstrup, 1993); however, the purpose in the current work is not to eliminate such data but to provide a measure of normality. A normal distribution has a skewness of 0, which is to say that it is symmetric about the mean, and a kurtosis of 3. The Jarque-Bera test (JB) uses these benchmark values to calculate a test statistic under the null hypothesis that the data is Gaussian distributed (Bera & Jarque, 1981). Thus, a probability value (p-value) smaller than 0.05 gives 95% confidence that the data is not normally distributed. The JB statistics is calculated as

$$JB = N\left(\frac{S^2}{6} + \frac{(K-3)^2}{24}\right) \tag{38}$$

where

S	=	skew
K	=	kurtosis
N	=	number of data points

2.3.11 Stationarity

If there are no systematic changes in the mean and variance of a time series, and there are no periodic variations, then it is said to be *stationary* (Chatfield, 2004). Effectively, this means that a sample from any point in the time series is representative of the whole. Often there is an assumption that the data under study represents a steady state; in reality however, meteorological parameters are constantly changing, some faster than others. In a strictly stationary time series, the mean is constant and a term in the series can be described by:

$$y_t = \mu + \epsilon \tag{40}$$

where
y_t = term at time step t
μ = constant mean value
ϵ = random noise with a constant variance

These types of series are simple to work with but this definition is too restrictive for many applications. Weaker forms of stationarity have been defined that accommodate more realistic situations. Trend stationarity, for example, allows the mean of the series to evolve over time through the introduction of a linear function of the time step as described in Eq. 41. A trend stationary series can be transformed into a strictly stationary series by removal of the deterministic trend.

$$y_t = \beta t + \epsilon \tag{41}$$

where
β = constant representing the linear trend

When the linear function is replaced by an additive reference to the previous value in the series, the trend is said to be stochastic. This type of series can be transformed into a strictly stationary series by taking the difference between successive terms and is described as *difference stationary* on account of this property. A series of this kind is also known as a random walk with drift and is defined by Eq. 42.

$$y_t = \beta + y_{t-1} + \epsilon \tag{42}$$

Realisations of trend and difference stationary series can appear quite similar at first glance. However, their differing behaviour becomes clear if several realisations are shown together. Fig. 10 shows 20 realisations of each type of series demonstrating the tendency of a trend stationary series with a deterministic mean to vary around a straight line. A difference stationary series with a stochastic mean, on the other hand, drifts away from the deterministic line over time.

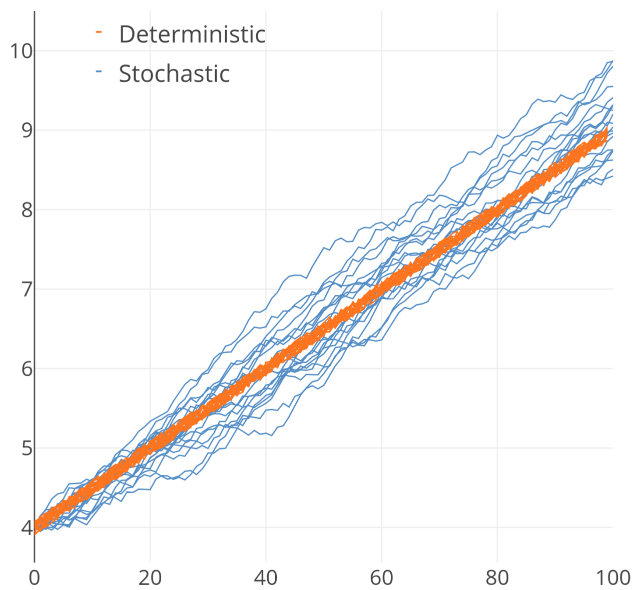

Figure 10: Deterministic and stochastic trends

Stationarity is often assumed either implicitly or explicitly in order to simplify real phenomena under study. Monin-Obukhov similarity theory, for example, is technically only valid in stationary flow conditions (Lange et al., 2004). In certain cases, such as studies involving the calculation of atmospheric fluxes, non-stationarity can significantly affect the results and data therefore has to be filtered (Foken & Wichura, 1996; Morales & Peinke, 2012). Other authors have found that filtering TMA records for stationarity can reduce the scatter in resulting plots (Lange et al., 2004).

Stationarity can be identified locally by directly comparing the values over a short series of time steps (Lange et al., 2004; Peña & Floors, 2014). For larger data samples, statistical tests such as the augmented Dickey-Fuller test (ADF) are available. ADF checks for a unit root to the characteristic polynomial of the first-order autoregressive model which best fits the time series (Chamorro et al., 2015; Dickey & Fuller, 1979). The test statistic is calculated by optimising the modified Akaike information criterion (MAIC) over a range of time lags. The null hypothesis is that a unit root exists, and therefore a p-value below 0.05 indicates a 95% probability that the data is either strict stationary or difference stationary. The Kwiatkowski-Phillips-Schmidt-Shin test (KPSS) checks for stationarity around a linear trend without reference to the existence of a unit root (Kwiatkowski et al., 1992). The two tests are therefore complementary and used together they can differentiate between the different types of stationarity. The null hypothesis in KPSS is that the data is stationary and a p-value below 0.05 indicates a 95% probability of non-stationarity. Table 6 clarifies how the combined results should be interpreted.

Table 6: Interpreting stationarity indicators

ADF	KPSS	Interpretation
$p < 0.05$	$p > 0.05$	Strict stationary
$p > 0.05$	$p > 0.05$	Trend stationary
$p < 0.05$	$p < 0.05$	Difference stationary
$p > 0.05$	$p < 0.05$	Non-stationary

2.3.12 Summary

The complexity of the ABL is illustrated by the large number of micrometeorology studies which investigate interdependence between parameters. Van de Wiel et al. (2012), for example, explore the minimum mean wind speed required for sustained turbulence, while van Hooijdonk et al. (2015) were concerned with the minimum wind shear. The relationship between shear and stability represented by the Obukhov length was investigated by Tambke et al. (2006), while Newman and Klein (2014) suggest separate power-law extrapolations of wind speed for different stability classes. Mahrt et al. (2015) suggest a dependence of turbulence intensity on both wind speed and stratification with similar findings by Vogelezang and Holtslag (1996). Rodrigues et al. (2010) treat both turbulence intensity and shear as functions of mean wind speed, while Wilson and Venayagamoorthy (2015) show a systematic relationship between turbulence and shear directly.

The foregoing discussions identify a large number of meteorological parameters that have either been shown to influence wind turbine power output, or which have a theoretical potential to do so. In current practice, direct measurements are aggregated over a standard averaging period to produce a set of meaningful statistics. Some of these have been discussed above in relations to specific meteorological influences; however, current practice is selective in the way statistical measures are used. For example, the coefficient of variation is applied to the horizontal wind speed as an indicator of turbulence, but not to any other measured parameter. A more comprehensive and agnostic approach would be to apply all statistics equally to all measured parameters when seeking to reveal additional influences on power production. The parameters that can be directly measured are referred to as *base parameters*, and are listed in Table 7.

Table 7: Meteorological base parameters

Parameter
Wind speed
Temperature
Pressure
Relative humidity

Table 8: Statistical measures

Statistic
Mean
Standard deviation
Minimum
Maximum
Skew
Kurtosis
Coefficient of variation
Second-order coefficient of variation
Stationarity
Normality

Base parameters can all be measured at different heights to provide information about variation in the vertical dimension. If wind speed and temperature are measured using a sonic anemometer, then wind speed measurements are available in three dimensions and the sampling frequency can be large enough to support flux calculations. Adopting an averaging period of ten minutes, the standard statistics listed in Table 8 can be produced for each of the base parameters. The first four entries in Table 8 are already included in current practice. Skew and kurtosis are added to complete the set of standard moments, while the coefficients of variation are included for all parameters by analogy with their specific importance in the characterisation of turbulence. The stationarity of each parameter, indicated by the ADF and KPSS tests, provides information about variation within the averaging period as does the normality as indicated by the JB test.

In addition to the base parameters and their statistical characteristics, a number of derived parameters have also been identified, and those not already covered by the contents of Tables 7 and 8 are listed in Table 9. Sunrise and sunset times for a specific location may be looked up from appropriate reference sources for use in the derivation of solar parameters. In addition to local measurements, the estimation of geostrophic wind speed requires knowledge of the local horizontal gradients of temperature and pressure which can be readily obtained from ground-based weather stations nearby.

Table 9: Derived parameters

Category	Parameter
General	Air density
	ABL height
	Rotor equivalent wind speed
	Geostrophic wind speed
	Inflow angle
Turbulence	Turbulent kinetic energy
	Turbulence length scale
	Isotropy
	Second-order structure function (transience)
	Turbulence dissipation rate
	Excess kurtosis of wind speed increments
Wind shear	Wind shear exponent
	Wind speed ratio
Wind veer	Degrees per 100 m
	Cross-isobar angle
Stability	Obukhov length
	Obukhov stability parameter
	Bulk Richardson number
	Vertical flux of horizontal momentum
	Vertical flux of sensible heat
	Environmental lapse rate
Solar geometry	Declination
	Elevation
	Hour angle

Assuming wind measurements in three dimensions and three measurement heights (hub-height, rotor-bottom and rotor-top) a minimum of 83 parameters can be defined based on the content of Tables 7 – 9. Other variations could also be introduced such as the evaluation of measures of turbulence in three dimensions rather than just one, calculation of shear indicators over the lower and upper parts of the rotor in addition to the whole, the calculation of different measures of temperature and the estimation of parameters such as stability at multiple heights. Applying such variations takes the total number of potential parameters to around 140. The actual number of parameters available in a particular case would depend on the measurement configuration at the turbine location. It is clear that consideration of a comparable range of parameters would lead to a more complete picture of the meteorological influence on power production compared to the approach in IEC2017. In addition, Tables 7 – 9 define the requirements for an appropriate dataset that could support such an investigation as detailed in Table 10.

Table 10: Dataset requirements

Requirement
Measurements of all base parameters
Multiple measurement heights spanning the vertical extent of the rotor
Wind speed in three dimensions
High-frequency wind speed and temperature measurements
Availability of nearby weather station data

A further data requirement is for turbine SCADA data so that the power output may be synchronised with the meteorological measurements. Access to SCADA data also provides a means of cross-checking some of the parameters derived from meteorological data and opens up the possibility of investigating the value of mechanical parameters as predictors of power output (Janssens et al., 2016; Mckay et al., 2013; Pelletier et al., 2016).

2.4 Wind turbine modelling

2.4.1 Types of model

A model is a simplified mathematical representation of a physical system which can be used to predict the output of the system given a particular set of inputs (Cukier et al., 1978; Jacobson, 2005, p. 7). Two primary types of model can be distinguished. *Parametric* models predict the value of the output variable based on a bounded set of input parameters which may or may not have physical counterparts. For example, the wind speed values in the power curve represent the speed of the physical wind which can be measured, whereas the shape and scale parameters in the Weibull model of wind speed distribution are mathematical constructs. In contrast, *non-parametric* models are the result of fitting mathematical expressions to available data. This process can proceed to an arbitrary level of detail with a potentially unbounded set of parameters. Fitting power curve data with a polynomial expression, for example, may include as many terms as deemed necessary. In general, parametric models are simpler to apply but lack accuracy, while non-parametric models have greater accuracy but lack explanatory power since they are black-box approaches with no direct relationship with observable quantities (Sohoni et al., 2016; Sprenger, 2009; Thapar et al., 2011).

As a simple parametric model, the power curve has poor explanatory power. Its primary input parameter is a single characteristic wind speed which is usually taken as the mean measured horizontal component of the hub-height wind. With the application of REWS, the driving wind is a virtual quantity that represents the mean energy flux through the rotor (Christensen et al., 1986; IEC, 2017). Other parameters are used in PPT either to make similar adjustments to the data values as is the case with the turbulence normalisation method, or to identify invalid records that may be rejected through filtering. Many other potential influences are ignored, and the simplifications applied in the model result in a significant degree of uncertainty in the results which appears as unwanted dispersion in the power curve scatter plot.

More complex parametric approaches include blade-element/momentum (BEM) and computational fluid dynamics (CFD) models. BEM theory treats a rotor blade as a series of thin slices with an aerofoil cross-section. Each element sweeps out an anulus within the rotor disk, and it is assumed that the lift and drag forces arising from the air flow over the aerofoils not only induce rotation of the blades, but also a rotation in the wake. Integrating over all blade elements yields values for mechanical power, thrust and blade root bending moment (M. O. L. Hansen, 2008). These modifications account for phenomena such as the pressure drop in the wake and this greater physical fidelity can be used to predict power output (Arramach et al., 2017; D. A. Johnson et al., 2012).

CFD uses the Reynolds-averaged Navier-Stokes (RANS) equations for fluid flow to deliver a very fine level of detail in the examination of fluid flows. The model domain is split into a large number of cells, each of which is small enough that the dynamic activity within it can be approximated by linear relationships. Initial conditions are provided to the model, and calculations are performed for each cell individually with outputs being propagated to its neighbours. The process is iterative and computationally expensive, however, and even for a small model turbine in a wind tunnel over a million cells and 500 iterations may be required to reach a result (Kalvig et al., 2014). Both BEM and CFD require knowledge of the precise aerodynamic profile of the blades which is often proprietary information. Additionally, the detailed knowledge of the wind field inflow that they require would make their use in PPT infeasible.

Non-parametric approaches to wind turbine performance modelling draw on techniques from data science and machine learning including data mining, data clustering and artificial neural networks (Lydia et al., 2014; Sohoni et al., 2016). Of the available techniques, artificial neural networks (ANNs) have been shown to be particularly accurate (Li et al., 2002; Pelletier et al., 2016; Sohoni et al., 2016). However, a disadvantage of all parametric models is the requirement for them to be trained on existing data (Ghahramani, 2013) which ties the model to a very specific context. In this way a very accurate representation of the site-specific performance of a particular turbine could be created, but it would not be transferable to another turbine in a different location. The site-specific nature of non-parametric models is an advantage however in the context of ongoing performance and condition monitoring (Janssens et al., 2016).

The ability of an analytical parametric model to relate power output to measurable physical inputs is desirable because of its explanatory power and its ease of use. Such a model has a bounded set of input parameters which necessarily involve the use of simplified expressions to approximate physical phenomena and consequently there exists a significant error term. The residual error in a non-parametric model, on the other hand, can be reduced to insignificance by extending the fitting process to an arbitrary level, the trade-off being that the resulting model is not generalisable. Each approach thus has its advantages and disadvantages. A strategy for resolving the dichotomy is to examine the sensitivity of a non-parametric model to different input parameters. By identifying those with the most significant impact on the output, a more representative set of input parameters can be proposed for use in a parametric model. The remainder of this section discusses the use of an ANN for creating an accurate representation of a physical system, and the identification of parameters of significance using correlation analysis and variance-based sensitivity analysis.

2.4.2 Artificial neural networks

An ANN is a computational model that is trained to recognise patterns in sample data and which can subsequently be used to identify those same patterns in unseen data, or predict outputs based on unseen data (Rojas, 1996). It is composed of a set of computational units called neurons arranged in layers of which there are three types, input, output and hidden layers. Neurons in one layer are connected to those in the next as shown in Fig. 11 which shows two generic types of ANN each with four input parameters. The first, network a, has three maximally-connected layers with several output neurons. This is a typical configuration for a classifier whose purpose is to assign an input vector to a class represented by one of the output nodes. Network b, on the other hand, only has a single output node. This is the typical configuration for a regressor whose purpose is to predict the value of a dependent variable based on the independent variables supplied in the input vector.

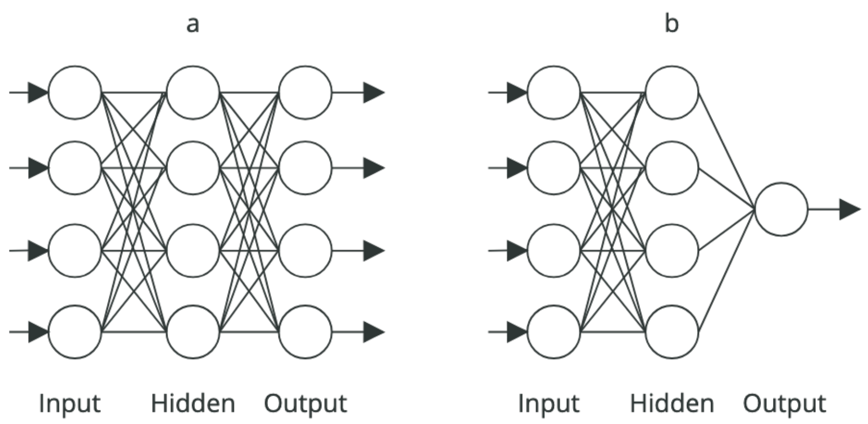

Figure 11: Artificial neural network configurations. a: classifier; b: regressor

The connections between neurons have weights associated with them that are modified by the training input, and the nodes themselves have bias values that determine the significance of their contribution to the overall communication of data through the network. Biases are also modified during training which involves the simultaneous presentation of sample input and expected output. Error feedback is propagated through the network and the values of the weights and biases are modified until the network converges on a stable configuration. Each node has an integration function, g, which reduces its inputs to a single value, and an activation function, f, which determines the node's output based on the aggregate input. This arrangement can be visualised schematically in Fig. 12 for a node with three inputs, $x1$, $x2$ and $x3$. In order to successfully model non-linear systems, it is important that the activation function is also non-linear.

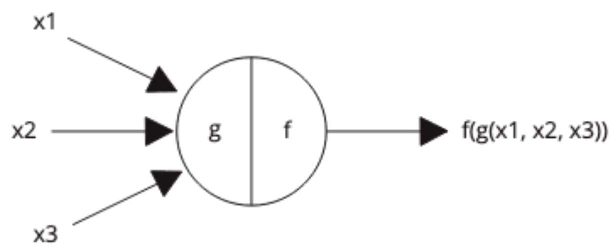

Figure 12: ANN node with three inputs.

The output is the result of applying the activation function, f, to the aggregate input determined by the integration function, g. (Rojas, 1996, p. 31)

Neural networks have been shown to be capable of approximating any function (Hornik et al., 1989). However, there is a risk of overfitting the training data leading to poor generalisation on later tasks. A simple method to avoid overfitting known as the early stopping strategy is to monitor the error between the current prediction and the target value, and to terminate the training when no further improvement is observed (Caruana & Lawrence, 2001). Although many numerical schemes have been proposed for determining the optimum ANN structure for a given problem and the number of nodes in each hidden layer, there are no definitive methods (Sheela & Deepa, 2014). Trial and error approaches are therefore commonly used to develop a working configuration. The *constructive* strategy starts with a small number of nodes and increases the number until a successful result is achieved, while the *pruning* approach starts with a large number of nodes and successively decreases the number until a degradation in the result is seen (Sheela & Deepa, 2014). It has been observed that a larger number of hidden nodes can provide a better fit where in domains where there is significant non-linearity (Caruana & Lawrence, 2001).

It has been shown that an ANN can be used to model wind turbine power performance with greater accuracy that standard methods. Manobel et al. (2018), for example, demonstrate that an ANN with only two inputs, hub height wind speed and direction, performs better that several other techniques. Using the root mean square error (RMSE) the authors show that the ANN approach leads to a smaller spread of output values than four other methods including the IEC standard for nacelle anemometry (IEC, 2013). Li et al. (2002) take a similar approach to demonstrate better performance than standard regression using RMSE. Pelletier et al. (2016) demonstrate that ANNs can be trained to model a power curve with smaller mean absolute error (MAE) than alternatives including IEC2005. Their model is based on data from the turbine's SCADA system and includes nacelle wind speed, air density, turbulence intensity, wind shear, wind direction, and yaw error as input parameters. Using SCADA data presents no problems since an ANN is a universal function approximator and can therefore accommodate the flow disturbance around the nacelle during the training process. The six input parameters are selected from an initial set of 50 on the basis of correlation plots, but the authors provide no information about the rejected parameters.

2.4.3 Feature selection

Feature selection is the general term used to describe a process in which the number of features (parameters) initially found in a dataset is reduced to a subset which retains enough information to provide a good approximation to the whole (Bolón-Canedo et al., 2015). It was developed in the context of big data to extract useful information in fields such as image classification, financial transactions and computational biology. In such areas, there can be thousands of dimensions leading to the *curse of dimensionality*, the apparent failure of traditional methods for searching and generalising from high-dimensional spaces (Donoho, 2000).

When using machine learning to build a non-parametric regression model, the system is trained by presenting training data in the form of input vectors and associated output values. In the ideal case, the set of input parameters is optimal for the task in the sense that all parameters are relevant, and the set contains no redundant parameters (Yu & Liu, 2004). Relevance may be judged by the degree to which a parameter is correlated with the expected output. This criterion has been used successfully to select parameters from those available in turbine SCADA data for predicting power output (Morshedizadeh et al., 2017). In a high-dimensional dataset, the problem of *multicollinearity* can arise in which input parameters are highly correlated with each other because of causal relationships between the phenomena they represent, the way that the original data was collected, or because the parameters share a derivation (Verhoef & Leendertse, 2001). The existence of a hidden common factor between parameters can lead to errors in standard regression analysis (Kalnins, 2018), and in terms of predictive power, the introduction of a new parameter that is correlated with an existing one adds no new information. There is no gain in accuracy in output predictions, and the new parameter is redundant in an information theoretical sense (Dormann et al., 2013; Hall & Smith, 1997). Where redundancy is identified, the input vector can be simplified by removing one of the correlated parameters. This reduces the complexity of the model, the training time and the amount of training data required (Kowshalya et al., 2019; Morshedizadeh et al., 2017).

Various deterministic procedures based on correlation analysis have been proposed for the elimination of irrelevant and redundant parameters (Bolón-Canedo et al., 2015). A fully automatic procedure, however, does not allow for the inclusion of domain-specific knowledge (Foresti et al., 2011; Morshedizadeh et al., 2017; Pelletier et al., 2016; Yu & Liu, 2004) or the application of other non-statistical criteria (Bolón-Canedo et al., 2015, p. 117). A simple solution is to construct a pairwise correlation matrix for all parameters and to apply judgements based on domain-specific knowledge in combination with the statistical information to select appropriate features (Bolón-Canedo et al., 2015, p. 126; Pelletier et al., 2016).

2.4.4 Sensitivity analysis

The output of a mathematical model is determined by the value of its input parameters; however, some of them may have a more significant effect than others. The objective of sensitivity analysis (SA) is to provide a relative measure of this variation (Saltelli et al., 1999). Local SA examines the immediate effect of varying a parameter value in a specific case while holding other parameters constant (Saltelli et al., 1999). Methods can be as simple as selecting a small set of values that span the range of the input parameter and running the model in order to reveal the effect on the output (See for example Peña et al., 2014; Wagner et al., 2009). Alternatively, data can be partitioned according to a particular parameter in order to isolate its effects (eg. Kubik et al., 2011). The local approach is limited by the choices of parameter and the specific values selected for examination. For linear models, this may be sufficient since values elsewhere in the model can be determined by simple extrapolation (Saltelli et al., 2008, p. 11). For nonlinear models with uncertain inputs, a global approach is required which explores the entire space defined by the input parameters and including interactions between them. The global approach has the advantage that it can reveal unexpected interactions between parameters since it is not restricted by a subjective choice of test values (Cukier et al., 1978).

Tian (2013) identifies four different approaches to global SA which differ in their characteristics and applicability to different types of model. Regression models are fast and easy to compute but are restricted to linear models. Screening methods proceed by fixing the value of one parameter and examining the effect on the model output. They are also fast to compute, but do not support the evaluation of significance of a parameter compared to the total variation. Variance-based methods decompose the total variance in the model and apportion it to parameters in the form of main and total effects. The main effect is the direct contribution of the parameter to the variance of the output, while the total effects include interactions with other parameters. This is the method advocated by Saltelli et al. who recommend the Fourier Amplitude Sensitivity Test (FAST) as its most elegant implementation (Saltelli et al., 1999). Tian also mentions meta-models which combine a first step based on regression with a refinement step which uses variance-based methods or other non-parametric fitting techniques. The remainder of this section will concentrate on the variance-based approach and the FAST method in particular.

Describing or predicting the behaviour of a physical system often involves building a mathematical model that relates the combined effect of a series of input parameters on the model's output values. A general model can be represented by

$$Y = f(X_1, X_2 \dots X_n) \tag{43}$$

where

X_i	=	set of parameters, $i \in [1..n]$
$f(\cdot)$	=	some function
Y	=	model output

Throughout this section, uppercase letters are used to represent parameters, and lowercase letters are used to refer to parameter values. The sensitivity of the model to parameter X_i can be described in terms of a first-order sensitivity index, S_i, defined by

$$S_i = \frac{V[E(Y|X_i)]}{V(Y)} \tag{44}$$

In Eq. 44, $V(Y)$ represents the total variance in the model output, while $V[E(Y|X_i)]$ is the conditional variance of parameter X_i. This is interpreted as the variance in the output when X_i is fixed to a particular value, averaged over all possible fixed values of X_i. The conditional variance is independent of any subjectively-chosen value, and S_i takes values strictly in the range 0 – 1. Interactions between parameters can be captured along with their main effects by calculating total effects terms, S_{Ti}. This involves finding the expected variance in the model when all parameters except X_i are fixed as expressed in Eq. 45.

$$S_{Ti} = \frac{E[V(Y|X_{\sim i})]}{V(Y)} \tag{45}$$

Saltelli et al. demonstrate that a parameter whose total effects term is zero has no influence on the model at all and may be removed (Saltelli et al., 2008, p. 32). Thus, SA can be useful in simplifying models.

2.4.5 Fourier Amplitude Sensitivity Test

The spectrum produced by applying a Fourier transform to coherent data can be interpreted as equivalent to the statistical analysis of variance or ANOVA (Emerson, 1983). Taking advantage of this relationship, the Fourier Amplitude Sensitivity Test (FAST) can be used to implement variance-based sensitivity tests of the type discussed above (Cukier et al., 1978). Given a model with n parameters, each parameter is represented by an oscillating signal at a characteristic frequency, ω. Coherence is ensured by driving the variation of each signal by a common variable, s, which takes regularly-spaced values over the range $[-\pi, \pi]$. The input signal for the i^{th} parameter is generated using Eq. 46 (Saltelli et al., 1999). This equation defines a search curve that ideally fills the available parameter space.

$$x_i = \frac{1}{2} + \frac{\sin^{-1}(\sin \omega_i s)}{\pi} \tag{46}$$

Applying a Fourier transform to the model output results in a set of peaks corresponding to the frequencies chosen for the input parameters, and the amplitude of the peaks corresponds to their contribution to the overall variance. The *partial variance* of each parameter can be calculated by dividing the amplitude of each peak by the total energy in the Fourier spectrum. To avoid aliasing, the number of samples, N_s, in the input sequence must exceed the Nyquist frequency and is given by:

$$N_s = 2M\omega_{max} + 1 \tag{47}$$

where

M	=	number of harmonics to be included, often taken as 4
ω_{max}	=	highest frequency in the set

To avoid interference between parameters, the input frequencies need to be carefully chosen to be *incommensurate*. That is to say, no frequency may be an integer multiple of another up to the threshold multiple, M, and no frequency may be the sum of any subset of frequencies.

The calculation of total effects terms is achieved by using one frequency, ω_i, for the i^{th} parameter, and a second frequency, $\omega_{\sim i}$, for all other parameters. This time, the peak at $\omega_{\sim i}$ represents the variance for all terms and interactions not involving the i^{th} parameter, while all other peaks must theoretically be attributable to the i^{th} parameter either directly or by interaction. The total effects term for the i^{th} parameter is therefore found by subtracting the amplitude of the peak at $\omega_{\sim i}$ from the total energy in the spectrum. This last step by Saltelli et al. (1999) who refer to it as the extended FAST, or eFAST, and claim that it is computationally efficient and robust at small sample sizes.

Kusiak and Zhang (2010) used the eFAST method to investigate sources of vibration in wind turbines. They selected a set of three input parameters, torque, wind speed and blade pitch angle, from those available from the turbine SCADA system based on their domain knowledge and existing literature. Three derived parameters, wind deviation, torque rate and blade pitch rate were added to the set. The authors' key innovation was to represent the turbine response using a trained ANN. The oscillating signals were passed into the ANN and the Fourier transform applied to its output. McKay et al. (2013) also used an ANN with eFAST to rank eight input parameters in terms of their level of influence on wind turbine power output. The parameters were chosen according to three general rules of thumb and with a focus on comparing wake and non-wake behaviour. The parameters were yaw angle, rotor speed, blade pitch angle, wind speed, ambient temperature, main bearing temperature, wind speed standard deviation and yaw angle standard deviation, all collected from the turbine's SCADA system. The importance of density was discussed, but since the majority of the variation in density is due to temperature fluctuations, it was not included directly. The focus of the study was on turbine structural health monitoring which is reflected in the parameter selection. The authors mention the possibility of using the same approach to improve power performance, but do not follow this up explicitly.

2.5 Conclusions from literature review

All stakeholders in the wind energy industry rely on IEC2017 for verifying the performance of installed turbines, and the power curve is fundamental to the procedure. As a simple relationship between wind speed and power, however, the power curve fails to accommodate the full complexity of the meteorological influences on a turbine. Non-parametric models offer a way to identify those excluded parameters which have the most impact on uncertainty in the power curve. From the foregoing discussion, the following particular conclusions can be drawn:

- The range of parameters accommodated by IEC2017 is limited

  The base parameters defined in Table 7 are all referenced in the IEC2017 model; however, statistical measures are used selectively, many derived parameters are not considered, and some parameters such as turbulence intensity are typically only used as validity thresholds. In particular, there is no direct reference to atmospheric stability in the standard.

- The explanatory power of IEC2017 is poor

  Because of the small range of parameters used, the variance observed in the measured power curve is simply treated as stochastic uncertainty. While the REWS and turbulence normalisation methods address the issue of data validity in a pragmatic way, they are data-driven and do not provide any further explanation for the remaining scatter in the power curve.

- The measures used to represent parameters in IEC2017 have limitations

  The shortcomings of using the coefficient of variation (TI) to represent turbulence are discussed in §2.3.4. Other measures of turbulence are available that preserve more information about the high-frequency variations of wind speed. These alternatives can be evaluated for their ability to better predict power output along with alternative measures of shear, veer and stability.

- Non-parametric models can represent physical systems to an arbitrary level of accuracy

  A non-parametric model can be trained to model a single dataset very closely. This can be exploited to evaluate the sensitivity of the model to different parameters. Artificial neural networks have been shown to represent wind turbine data well, and would be a good choice for this purpose.

- Conditioning data on a significant parameter should reduce the dispersion in the power curve scatter plot

  The appearance of unexplained variation as excessive dispersion in the power curve scatter plot can be exploited to evaluate the significance of potentially influential parameters. If the dispersion can be reduced by partitioning the data based on a given parameter, then it can be concluded that the parameter has a non-negligible impact on the power output. It can then be considered a candidate for inclusion in the model used for PPT.

- A dataset with particular characteristics is needed to support investigation into the influence of an appropriate range of parameters on power production

  Certain parameters can only be derived using high-frequency raw data, measurements from multiple heights or using data not usually collected in PPT. Table 10 lists these desirable dataset characteristics, and can be used to select appropriate data sources.

Together, the conclusions summarised here map out a strategy for identifying potentially influential parameters and evaluating them with reference to dispersion in the measured power curve. The next chapter provides details on how this will be done.

3 Methodology

3.1 Overview

The aim of this project is to investigate the potential of alternative data filtering strategies with respect to data loss, AEP estimates and the dispersion of points in the power curve scatter plot. By doing this, improvements to the established PPT process can be motivated through the isolation of influences not currently accounted for, or by identifying better measures of known influences. Using a more representative set of parameters in the PPT process should mitigate the need for restrictive contractual filters, thereby reducing the time required to collect PPT data and consequently reduce the associated costs. This chapter develops a three-stage process for achieving the intended outcome based on the conclusions from the literature review. The main stages are described below and are summarised in Figure 13.

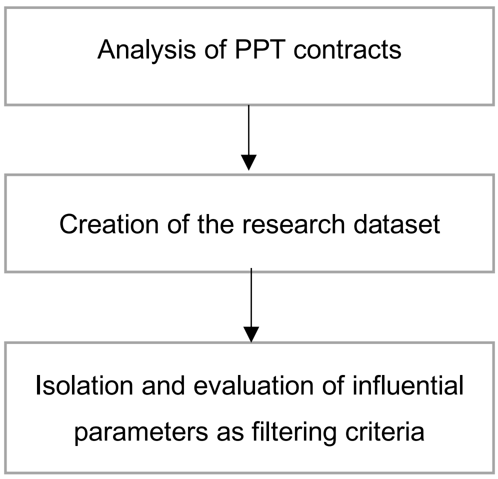

Figure 13: Methodology overview

As an initial step, an analysis of real PPT contracts is undertaken in order to explore the range and severity of the problem of data loss and to evaluate the effect of contractual filters on the measurement campaign duration. The purpose of this step is to provide the justification for the current project based on recent data rather than relying solely on reports from previous publications. The results of this exercise are novel in that they provide greater detail than previous works while protecting the anonymity of individual projects. They are also visualised in a way that highlights the contribution of contractual filters to data loss compared to quality filters. Because of these features, the results of this exercise constitute a novel research contribution from the current project.

The characteristics of a dataset suitable for investigating an appropriate range of parameters are identified in §2.4.10. In the absence of a readily-available dataset with the necessary features, a new dataset is created as the second stage. Its major components come from a well-instrumented research turbine operated by the University of Minnesota. Anomalies are first eliminated from the data through a series of quality checks and filters. Thereafter, the data is reduced to ten-minute aggregated values and a number of statistical quantities are calculated in the process. Further derived quantities and complementary data from other sources are added to the dataset so that the final result provides a rich platform for analysis. As a new resource capable of supporting a wide range of possible analyses beyond the aim of the current work, this dataset constitutes a novel contribution to current research.

In the third stage, the methods reviewed in §2.4 are applied to the research dataset to identify the parameters with the most impact on instantaneous power output. In preparation for testing these parameters as the basis for filtering criteria, a baseline power curve is created from the data using the IEC2017 procedure and filtering criteria based on the real PPT examples reviewed in the first stage. The theoretically influential parameters are used to define experimental filtering criteria whose effects are compared to the baseline in terms of data loss, the degree of dispersion in the point cloud and the estimated AEP. The results from the last two stages constitute the main novel contribution of the current work.

Throughout the project, data analysis is carried out using original software built using the python language. Python is an appropriate choice because of its wide support for numerical operations[7], statistical processing[8], digital signal processing[9], data science[10] and machine learning[11]. Example code is provided in Appendices C and E, and the entire codebase can be accessed at https://bitbucket.org/coillarach/phd.

3.2 Analysis of PPT contracts

The aim of this stage of the process is to develop a clearer appreciation of

a) The variation in contractual conditions applied in different PPT projects
b) The quantity of data that is lost as a result of different types of filter
c) The effect of filters on the overall duration of PPT projects and hence on the associated costs

The next few sections describe the source of the data used in the analysis and the analytical steps that are applied. Results appear in Chapter 4.

3.2.1 Source of data

The sample consists of data from 42 turbines from 15 independent PPT projects in both simple and complex terrain. All the tests were carried out by Wood Clean Energy[12] between June 2014 and May 2018. Because of the sensitivity of this data, no identifying details are provided on the PPT projects that are included. In each case, the data comes directly from the documentation for the PPT project without manipulation of any kind.

3.2.2 Minimum and expected campaign duration

In the ideal situation, all the required data would be collected within a contiguous time period with no loss of data. Since the minimum requirement in IEC2017 is for 180

---

7 http://www.numpy.org/
8 https://www.statsmodels.org/
9 https://docs.scipy.org/doc/scipy/reference/signal.html
10 https://pandas.pydata.org/
11 https://www.tensorflow.org/
12 https://www.woodplc.com

hours of data, or 1080 ten-minute samples and there are 144 ten-minute periods in one day, the minimum possible campaign duration is 1080 / 144 = 7.5 days. In cases where a proportion of the data is lost through filtering, the minimum duration can be found using Eq. 49.

$$D_{min} = \frac{7.5}{(1 - f_{loss})} \tag{49}$$

where

D_{min} = minimum campaign duration (days)

f_{loss} = fraction of data lost through filtering

However, the result of this calculation takes no account of practical issues such as instrumentation faults, data quality, calibration issues, etc. For this reason, it is considerably shorter than the usual three-month period allocated for a PPT measurement campaign (Wood Clean Energy, personal communication, 24 July 2019). Applying Eq. 49 yields the relationship shown by the red trace in Fig. 14.

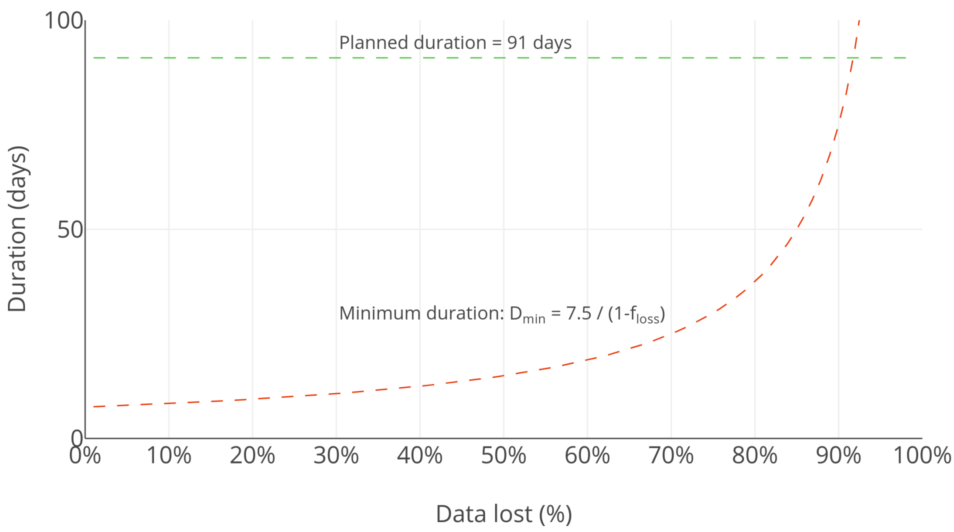

Figure 14: Minimum and planned campaign duration as a function of data loss fraction

3.2.3 Effective duration and turbine selection

To evaluate the effect of data filtering on the duration of measurement campaigns, it is important to identify and control for extraneous factors. This section describes three such quality measures that are applied to the campaign data.

The first issue is simple to identify and to remedy since it concerns measurement campaigns that are curtailed before the measurement database is complete. In this situation, the duration of the campaign is artificially short and does not accurately reflect the effect of filtering. All records related to turbines with fewer than 180 hours of data by the end of the campaign are therefore excluded.

Practical considerations may extend the duration in a way that has nothing to do with filtering and any distortions of this kind need to be eliminated. Measurements may not be available for the entire elapsed time for a number of practical reasons such as faults with the measurement instruments, calibration issues, errors that required the data collection to be restarted, etc. Although the dataset contains no direct information about such situations, the actual duration of the data collection can be inferred from the number of TMA records before filters are applied. Since there are 144 ten-minute periods in a day, dividing the number of TMA records by 144 gives the *effective duration* of the measurement campaign in days.

Plotting the elapsed and effective durations of real projects against data loss fraction and superimposing the limits in Fig. 14 would reveal those that incurred additional costs by comparing their elapsed durations to the standard period of 91 days. The same plot can be used to infer the priority attached to the end of data collection based on the time between the minimum effective duration and the actual effective duration for a project. Where the effective duration appears close to the theoretical minimum, data collection was terminated as soon as the required amount of data was available. This would be expected in cases where the measurement campaign was over-running and incurring additional costs. Where the effective duration appeared further from the minimum line the termination of data collection was not such a high priority. This would be the expected situation where the elapsed time was under three months because this would not incur additional costs.

Where several turbines are measured as part of the same project they may share a met mast. In this situation, it is likely that the measurement campaign will continue until sufficient data has been collected for every turbine. It is a matter of convenience for the consultant organisation performing the test to cease logging data for all turbines at the same time. Such instances can be recognised where the campaign end dates are the same for several turbines in a group. This implies that surplus data is collected for some turbines while completing the measurement database for others. Only the turbine with the shortest effective campaign duration in such cases is therefore be used.

There are other reasons why campaign durations may be longer than expected, such as the need to repeat part of the measurement process or to collect data for other purposes, or because it is convenient to terminate the campaign at a later date. These additional reasons cannot be inferred from the data available.

3.2.4 Analysis

Four main categories of information are drawn from the project documentation:

- The contractual filter conditions applied to the data
- The overall duration of each of the measurement campaigns
- The proportion of measured data lost through filtering
- The terrain type at the turbine site

The details of the contractual filters are compared to provide an understanding of the typical range for each type of filter and the variation

First, the conditions applied on turbulence intensity, wind shear exponent and temperature on different projects are gathered together and compared. This provides insight into the variation in conditions across projects. Results are presented in graphical form in order to highlight this variation.

Because quality filters are applied before contractual filters, the number of data records that are rejected as a result of each category can be evaluated. In the second step, the proportion of records eliminated by quality and contractual filters is calculated by combining the effects of filters in each category by project, and presenting the results in graphical form. Results are arranged in descending order of the proportion of data remaining after all filters are applied. The intention is to determine whether the extreme cases of up to 90% data loss reported in the literature (Mellinghoff, 2012; Rareshide et al., 2009) are isolated cases or whether such losses are relatively common.

To assess whether terrain type is a major factor in the duration of measurement campaigns, sites with flat terrain are compared to those with complex terrain. A histogram of campaign durations is presented colour-coded by terrain type. An uneven spread of durations in which projects with complex terrain last longer in general than those with flat terrain would suggest that terrain is a major factor. Although statistical tests such a Student's t test are designed to differentiate between sample from different populations, the small number of instances available in this case is insufficient to justify their use. The simple graphical approach is therefore used instead.

Finally, the elapsed and effective durations of the remaining campaigns are plotted against data loss rate. Effective durations are expected to fall close to the minimum effective duration line in cases where there is commercial pressure to terminate the campaign, and to vary between the minimum theoretical duration and the standard three-month planned duration in other cases.

3.2.5 Limitations

The set of PPT projects used here constitute a convenience sample from a single consultant organisation. It can be argued therefore that they may not be representative of PPT projects across the industry. Mathematically, this is true and the same exercise could be performed with a larger set of projects from multiple consultants to provide more representative results; however, the purpose of IEC2017 and the certification scheme operated by MEANET are both designed to ensure the consistency of the assessment process across different consultants. This increases the degree of confidence in the sample used here.

Some projects contribute data from multiple turbines to the sample used here which potentially introduces bias into the results since the filtering criteria applied to the turbines within a single project are likely to be the same. However, even if such effects are present, it is likely that they will simply to introduce redundancy into the data. The range of durations will still be evident, and as a precaution, related turbines will be identified in the results so that any such duplication can be considered when interpreting the results.

3.3 Compilation of the research dataset

3.3.1 Introduction

The analyses envisaged for the current work require a dataset with the characteristics listed in Table 10. Datasets collected as part of PPT projects are therefore unsuitable since they consist solely of TMA records that are aggregated by the data logger. Storage of raw data files would increase the costs for the consultant organisation beyond acceptable commercial limits. In addition, customers are often unwilling to allow the collection of data over and above the minimum needed to complete the test. Finally, PPT data collection rarely includes measurements of meteorological parameters above hub height.

Publicly-available open-access datasets are available, but none with the appropriate characteristics. Some research projects such as CASES-99 publish their data for verification and reanalysis[13]; however, all of those investigated for the current work were deficient in some respect. CASES-99, for example, provides high-frequency wind data, but is not associated with a wind turbine because of the micrometeorological nature of

[13] https://www.eol.ucar.edu/content/integrated-surface-flux-facility-during-cases99

the research (Poulos et al., 2002). The same problem exists for research stations such as Cabauw in the Netherlands where detailed wind data is available[14] but cannot be related to turbine output (Bosveld, 2017). A brief analysis of the data available from winddata.com[15], a repository of wind-related data maintained by the Danish Technical University (DTU) revealed that only four sites out of 60 contained data on output power. Of these, one provided high-frequency wind speed data in three dimensions but did not offer pressure or relative humidity and was also lacking measurements above hub height. For the analysis of the datasets available at winddata.com, please refer to Appendix D.

An adequate dataset could theoretically be obtained from a turbine manufacturer; however, close cooperation mediated by a non-disclosure agreement is generally required because of the commercial sensitivity of the data. The current project did not benefit from this type of relationship, and even if it did, there would be considerable restrictions on the detail that could be made public.

For all of the reasons above, no extant dataset is available to support the type of research activity proposed here. The creation of such a dataset is therefore an essential element of the current work. By virtue of its generic structure, including many statistical characteristics of the base parameters and a wide range of derived parameters, the envisaged dataset is capable of supporting a wide range of comparative analyses beyond those required for the current work. For this reason, it also constitutes an important contribution to knowledge in its own right.

The following sections outline the methods used to create the research dataset and to assure its quality. The practical details of the process application including the specific sources used, issues encountered, results and limitations are reported in Chapter 5.

---

[14] http://www.cesar-database.nl/

[15] http://www.winddata.com/

3.3.2 Requirements

The majority of analyses required for the current work call for the use of synchronised meteorological and SCADA data aggregated over ten-minute periods. The primary result will therefore be a single file of TMA records indexed by timestamp with parameters represented as columns. The parameters required include the statistical variations listed in Table 8 for each of the base parameters listed in Table 7 along with the derived parameters listed in Table 9.

Further, the characteristics listed in Table 10 must be ensured:

- Measurements of all base parameters

  Mirroring the IEC2017 procedure, meteorological data must be available from instruments mounted on an appropriate met mast and not from the turbine SCADA. This avoids the flow distortion around the turbine nacelle.

- Multiple measurement heights spanning the vertical extent of the rotor

  This allows the capture of variation in the vertical dimension, and specifically facilitates the calculation of REWS as long as a minimum of three wind speed measurement heights are present at the rotor top and bottom and at hub height.

- Wind speed in three dimensions

  Measurements in three dimensions in order to facilitate the estimation of flux-, turbulence- and stability-related parameters. Sonic anemometers would be ideal for this purpose.

- High-frequency wind speed and temperature measurements

  High-frequency measurements facilitate the estimation of flux-, turbulence- and stability-related parameters. Sonic anemometers would be ideal for this purpose.

- Availability of nearby weather station data

  Estimation of the geostrophic wind speed requires knowledge of the local horizontal gradients of temperature and pressure which can be calculated from data from at least three weather stations in the vicinity of the turbine site.

Each of the requirements above calls for a source of measured data from meteorological instruments, turbine SCADA or surface weather stations. Solar elevation, declination and hour angle may be added into the set based on standard mathematical expressions. The data from a particular source is referred to here as a *component* of the final dataset.

3.3.3 Process overview

The process of conflating the components to create the research dataset is summarised in Fig. 15, and important considerations are discussed in the sections below.

3.3.3.1 Selection of data sources

The main meteorological and SCADA data used here is provided by the Eolos Wind Research Station operated by the University of Minnesota[16]. Weather data is obtained from the Automated Surface Observing Systems (ASOS) network of meteorological measurement stations maintained by US government agencies[17]. Solar parameters are calculated based on local sunrise and sunset times from timeanddate.com[18]. Further details of these sources are provided in Chapter 5.

3.3.3.2 Size and format of data files

Files from different sources tend to be divided into time periods of different size. To facilitate later processing, data is arranged into files of one day in length. Automated and manual checks are performed to ensure that records at the start and end of each day are correctly located in the appropriate file. In addition, file headers are reduced to a single row of column headings. At this point, file metadata is recorded independently of the data files to inform later operations.

---

16 http://eolos.umn.edu/facilities/eolos-wind-research-station

17 http://mesonet.agron.iastate.edu/ASOS/

18 https://www.timeanddate.com/sun/usa/minneapolis

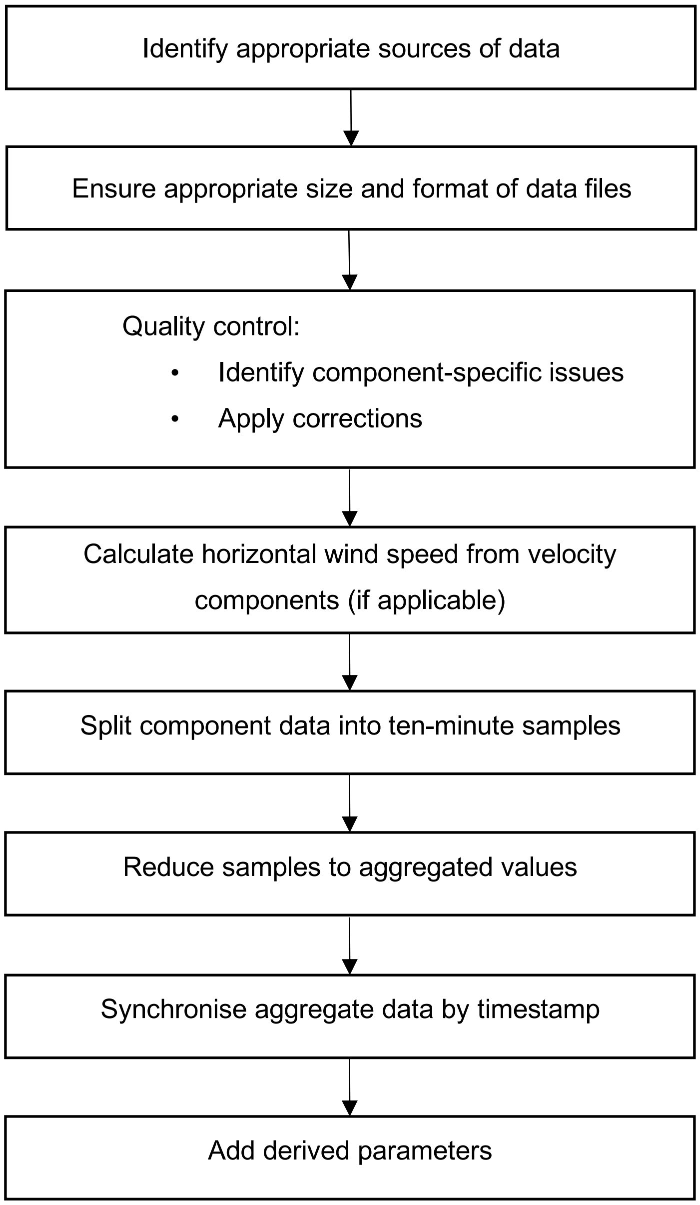

Figure 15: Overview of the research dataset creation process

3.3.3.3 Quality control

Before carrying out any manipulation of the data it is checked for erroneous values or other issues. Documentary information about the data is employed in addition to procedural checks based on the data values themselves. In particular, in the case of sonic anemometer and turbine faults the entire affected set of values is replaced by null values. Power values are also suppressed where the reported curtailment level is not null.

Please refer to §3.4.4 for further methodological detail on quality assurance, and §5.1.3 for details related to the practical application of quality control in constructing the research dataset.

3.3.3.4 Calculation of horizontal wind speed

The horizontal wind speed is calculated as the magnitude of the vector sum of the horizontal wind velocity components in advance of reducing the data to TMA values. It is done at this point so that the relevant statistics such as mean and standard deviation can be calculated easily at the same time as for the base parameters. The opportunity is also taken to calculate the full range of statistics for the horizontal wind speed as listed in Table 8.

3.3.3.5 Division into ten-minute samples

This step allows the raw data related to a particular TMA record to be preserved for easy access should further inspection be required. This might be needed, for example, to investigate a value soft-flagged during quality control.

3.3.3.6 Reduction to TMA values

In this step, the raw data for each of the base parameters and horizontal wind speed is processed independently to derive the statistics listed in Table 8. Where the parameter is a direction, mean and standard deviation are estimated using the approximation of Yamartino (1984) but no other statistical parameters are stored. The resulting TMA values are accumulated into daily files for each component. TMA values are indexed by their starting time so that the index 2017-01-01 00:00 indicates the interval [2017-01-01 00:00 - 2017-01-01 00:10).

Perturbations from the mean and their products are calculated for wind speed, wind velocity components and sonic temperature. The mean of the perturbation products are the covariances that represent atmospheric fluxes. While the averaging period normally used in the eddy-covariance method is 30 minutes, ten minutes is used here to match the standard practice in PPT. The use of a shorter averaging period here introduces some uncertainty into the flux values calculated during unstable conditions.

As part of the reduction step, several diagnostic values are recorded for each parameter including:

- The number of points in the sample
- The number of points removed by the despiking algorithm
- The number of points removed by the relevant absolute limit condition

These are used as quality filtering criteria during analyses.

3.3.3.7 Synchronisation

The daily files resulting from the reduction process are synchronised on their timestamps. The output from this stage is one file for each day of the year containing data from all components.

3.3.3.8 Addition of derived parameters

Derived parameters are added in two steps. The parameters added in the first step only reference other parameters within the same ten-minute period. Those added in the second step depend on the rotation of the measured flux values into a Lagrangian reference frame so that the x-axis is aligned with the mean horizontal wind direction. In particular, the planar fit of wind speeds to determine the vertical unit vector relies on the fact that the resultant wind vectors from successive averaging periods trace out a plane as the azimuth changes over time (Finnigan, 2004). Once the vertical unit vector is derived, the other two orthogonal unit vectors can be calculated and the coordinate frame for flux values can be rotated (X. Lee et al., 2004). Tables 11 and 12 summarise the derived parameters added in steps 1 and 2 respectively along with a reference to the relevant python function in the list provided in Appendix E. The tables also indicate whether a parameter is evaluated for all measurement heights.

Table 11: Derived parameters added in step 1

Parameter	All heights	Python function
Air density		airDensityFromSonic
Bulk Richardson number		richardsonBulk
Horizontal wind speed	Y	windSpeedFromComponents
Inflow angle	Y	inflowAngle
Lapse rate of potential virtual temperature		lapseRate
Lapse rate of temperature		lapseRate
Potential virtual temperature	Y	potentialVirtualTemperature
Richardson number stability class		stabilityClass
Rotor equivalent wind speed		rotorEquivalentWindSpeed
Sea-level pressure		pressureNormalised
Specific humidity		specificHumidity
Surface potential virtual temperature		extrapolate
Turbulence kinetic energy	Y	turbulenceKineticEnergy
Wind direction	Y	windDirectionFromComponents
Wind shear exponent		windShearExponentTwoHeights
Wind shear exponent (lower half of rotor)		windShearExponentTwoHeights
Wind shear exponent (upper half of rotor)		windShearExponentTwoHeights
Wind speed ratio		windSpeedRatio

There is a further issue related to the introduction of derived values and the parameters used in their calculation. If one of the input parameters is later identified to be invalid according to some filtering criterion, it is also important to suppress any derived values that rely on it. To address this requirement, a reference list of dependencies is maintained. Dependencies are checked during any filtering operation during an analysis, and for any values that fail the filtering criterion, dependent derived values are also suppressed. The list of dependencies is provided in Appendix G.

Table 12: Derived parameters added in step 2

Parameter	All heights	Python function
Boundary layer height		boundaryLayerHeightRM
Cross-isobar angle	Y	signedAngle
Friction velocity		frictionVelocity
Geostrophic wind components		surfaceGeostrophicU surfaceGeostrophicV
Geostrophic wind direction		windDirectionFromComponents
Geostrophic wind speed		windSpeedFromComponents
Humidity-corrected heat flux	Y	schotanusFluxCorrection
Momentum flux components	Y	rotateTensor
Obukhov length		obukhovLength
Obukhov stability parameter		obukhovStabilityParameter
Obukhov stability class		stabilityClassObukhov
Rossby-Montgomery coefficient		rossbyMontgomeryCoefficientStable rossbyMontgomeryCoefficientUnstable
Sensible heat flux components	Y	rotateScalar
Thermal wind components		thermalU thermalV
Wind veer		signedAngle

3.3.4 Quality assurance

The purpose of any dataset created on the basis of direct measurement is to represent as faithfully as possible the underlying phenomena of interest. However, the process of measurement is subject to a range of unwanted variations that can obscure the phenomena of interest including

- Equipment faults
- Incorrect instrument calibration
- Electromagnetic disturbances
- Physical interference with sensors (due to precipitation, for example)

(Foken et al., 2005; Starkenburg et al., 2016)

The result of these variations can be missing data points, or data points which are in some way incorrect and must be removed in order to avoid unrepresentative bias in the dataset. *Quality control* (QC) is the identification of missing or erroneous data and the possible application of corrections to mitigate their effects (Zahumenský, 2004) while *quality assurance* (QA) is the wider framework of activities used to safeguard confidence in the data.

In the current work, the research dataset is intended as a generic resource capable of supporting a wide range of analyses, some of which are not defined at the time of its creation. For this reason, the strategy of removing entire records with missing data values is not followed since doing so would remove valid data in the remaining columns. Instead, individual erroneous or suspect values are replaced by null values. The final TMA dataset is therefore expected to have data gaps which will be handled by individual analyses.

As shown in Fig. 15, QC is applied to each of the components before combination and the specific checks and actions are dependent on the nature of the data. The current work relies on data from existing sources with no influence over the way that data is collected, or over the measurement instruments themselves. Therefore, these details are simply noted as limitations on the research dataset. Because weather station data is typically aggregated to hourly means before it is published, the current work must assume that appropriate QC has already been applied. Confidence in this assumption can be increased where the data is collected by scientific agencies according to published standards.

Estimations of atmospheric fluxes are particularly sensitive to certain types of data error, and more stringent quality control is recommended than for other types of meteorological data (Foken et al., 2005). Vickers and Mahrt (1997) provide several tests for identifying instrumentation issues, flux sampling problems, and situations where erroneous data may appear physically plausible. Their process involves marking data with either a *hard flag* which identifies a clear error such as an instrument fault, or a *soft flag* which indicates unusual values that may optionally be filtered out in certain cases. Hard flags are implemented by sonic anemometers, SCADA systems and logger scripts which provide diagnostic information in the form of integer values in the data. The following tests advocated by Vickers and Mahrt (1997) are implemented in the current work and result in the suppression of individual data values before the data is reduced to TMA values:

- Identification and elimination of spikes

  Spikes are data values which are significantly different from neighbouring points as to be considered anomalous outliers. As such, they can bias the results of calculation if they are not removed. Spikes can have various causes including power supply fluctuations, water droplets on the sensor and physical disturbances. Because of their origin, it is likely that spikes will be correlated across several data channels. This can be particularly important when using data from sonic anemometers to estimate heat and momentum flux (Foken et al., 2005). Please refer to §3.4.8 for further discussion and details of the despiking method used here.

- Absolute limits

  Certain physical parameters are bounded by upper and lower limits which define the range of physically plausible values. These can be used to identify and eliminate a particular class of data error. The ranges shown in Table 13 are applied in the current work, and values that fall outside these ranges are replaced by null values in the component data before its reduction to TMA records.

Table 13: Absolute limits applied to component data

Parameter	Lower limit	Upper limit
Wind direction (°)	0	360
Horizontal wind speed (ms^{-1})	0	30
Horizontal wind speed component (ms^{-1})	-30	30
Vertical wind speed component (ms^{-1})	-10	10
Temperature (°C)	-40	40

- Visual inspection

  Vickers and Mahrt (1997) state that the final quality assurance step should be a visual examination of records that have been identified as suspect by automated checks. While this rule is not adhered to comprehensively here simply because of the quantity of data involved, the data sample associated with each TMA record is retained in a separate data file so that it is available for inspection if needed. Where TMA records are discovered to have data issues which are not detected by the automated tests, they are added to a black list which is excluded from all analyses.

In addition, two further recommendations are incorporated into the research dataset as soft flags which provide information about the TMA records:

- Higher-moment statistics

  Vickers and Mahrt (1997) use skewness and kurtosis of wind speed components to identify deviations from the mean that exceed normal expectations. These statistics are calculated for all base parameters in the current work and are therefore available as filtering criteria if required.

- Non-stationarity of the horizontal wind

  Stationarity is calculated for all base parameters, and may therefore also be used to filter the data during analysis.

In addition to the data-driven tests recommended by Vickers and Mahrt (1997), manual inspection of each component is performed as part of QC and any related information about the component is also used to determine any corrective actions required. Vickers and Mahrt (1997) further recommend that TMA values are rejected where more than 1% of the sample data is identified as spikes, but also acknowledge that the value is "somewhat arbitrary". A number of other quality criteria shown in Table 14 are also recommended. Records that fail on these criteria are not suppressed in the stored dataset to allow for flexibility when running analyses. Retaining the TMA values allows a criterion to be relaxed if it is thought appropriate. Please refer to §5.3.2 for the practical application of QC, the issues found and the specific actions taken.

Table 14: Quality filters

Criterion	Description
Point count	A value must be based on at least 90% of the expected number of raw data points.
Spike count	The number of spikes in the sample must be less than 1% of the expected number of points (Foken et al., 2005, p. 185; Vickers & Mahrt, 1997).
Free-stream sector	Wind directions are excluded to avoid the turbine wake.
Positive flux	Friction velocity and Obukhov length require a negative value for momentum flux despite calculated values appearing feasible (Biltoft, 2003a). Values for these parameters are therefore suppressed when momentum flux is positive.
Precipitation	Data is suppressed where relative humidity is 99% or above (X. Lee et al., 2004, p. 47) to avoid problems with the sonic instruments.

3.3.5 Despiking

Vickers and Mahrt (1997) identify despiking as the first quality control check to be done on data recorded for flux calculations, and the only one which involves changing the original data. A common approach to spike identification is to select points whose deviation from the mean of the signal is greater than a certain multiple of the standard deviation (Hojstrup, 1993). There is no agreed standard threshold, however, and multiples of 3.5 to 5.5 are found (Mauder et al., 2013). Median absolute deviation (MAD) is a related technique for identifying spikes which selects any points whose absolute deviation from the median exceeds a multiple of the median (Mauder et al., 2013). Both of these approaches essentially operate as a band pass filter and points are eliminated if they fall beyond the band limits. Fig. 16 illustrates the effect of applying a threshold of four times the standard deviation to an example ten-minute wind speed record with obvious spikes.

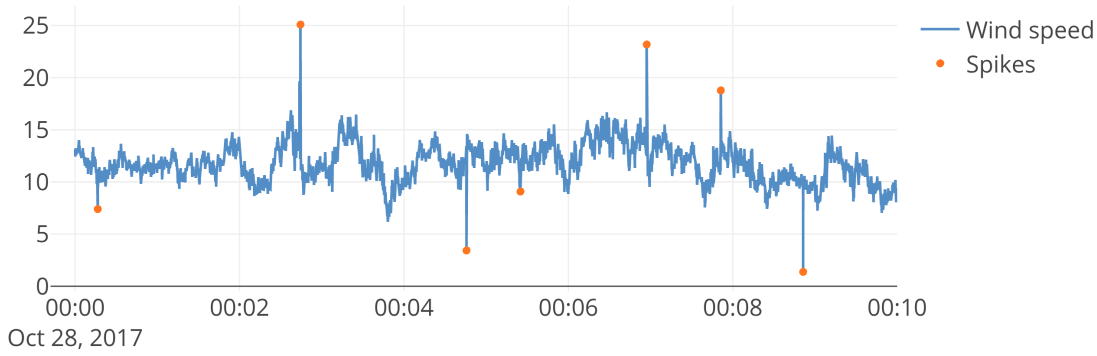

Figure 16: Using 4 x standard deviation as a despiking threshold

The algorithm can become too aggressive if the threshold is poorly chosen in relation to the data. For illustrative purpose, Fig. 17 shows the effect of using 2.5 times the standard deviation instead of 4. The pass band starts to become clearly visible, and real data is starting to be lost.

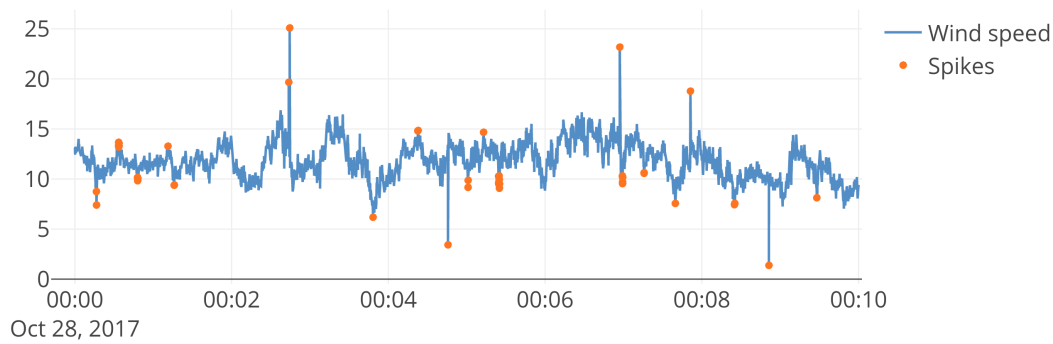

Figure 17: Using 2.5 x standard deviation as a despiking threshold

Brock (1986) defines a more robust method for identifying spikes based on a median filter. In a first step, a histogram is produced of differences between the raw signal and a median filtered version. Valid values tend to cluster in the centre while outliers are separated from the central population by a gap. The location of the gap is then used to define a local threshold for spike identification that is dependent only on the size of the data selection window. Applying the median filter approach to the data sample shown in Fig. 16 identifies the same six points as spikes. The implementation here uses a third-order median filter as recommended by Starkenburg et al. (2016) with a data selection window of 60 s.

3.4 Accounting for variation in the power curve

3.4.1 Introduction

The aim of this project is to investigate the potential of alternative data filtering strategies with respect to data loss, AEP estimates and the dispersion of points in the power curve scatter plot. This section describes the methods used to do this based on the research dataset. Candidate parameters are identified using sensitivity and correlation analysis. They are then evaluated against comparator power curves also derived from the research dataset. The performance of a filter is determined on the basis of the dispersion evident in the power curve scatter plot and on the quantity of data lost through the application of the filter. The ideal filter is the one which minimises both measures while producing an AEP estimate comparable to that obtained using traditional filters such as those for TI and wind shear. The main stages of the approach are shown in Figure 18.

The research dataset provides a rich array of parameters that can be evaluated for their influence on instantaneous power output. However, not all of the parameters represented by columns in the data file are relevant – some provide diagnostic information only while others provide information on turbine characteristics rather than meteorological phenomena. The process therefore begins with the manual selection of candidate parameters based on the nature of the columns in the data file and on expectations drawn from the material covered in the literature review.

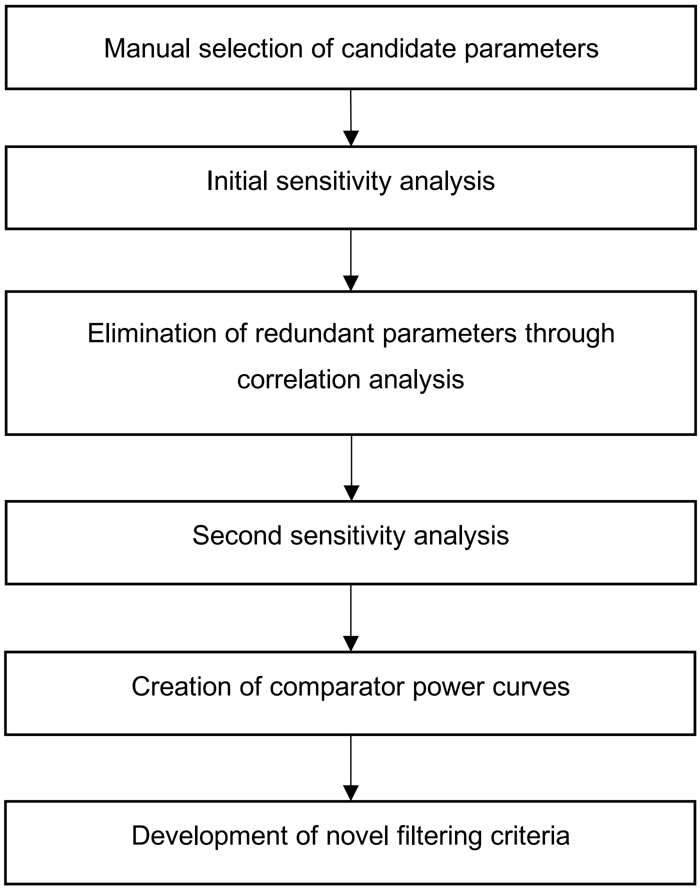

Figure 18: Overview of methodology

3.4.2 Quantifying dispersion

In linear regression studies, the goodness-of-fit is typically quantified by measures such as the mean error (MA), mean absolute error (MAE) or the root mean squared error (RMSE) whose formula is shown as Eq. 50. Of these the RMSE offers a larger range and gives more weight to large errors than do the other measures, and is therefore adopted here. For a series of length N, the squared differences between the values x_i

and the expected values $\hat{x}_i$ are summed and divided by N to yield the mean squared deviation. Solutions to regression problems are found by minimising the RMSE which is found by taking the square root.

$$RMSE = \sqrt{\frac{1}{N}\sum_{i=1}^{N}(\hat{x}_i - x_i)^2} \tag{50}$$

Although turbine power output is a non-linear function of wind speed, residual values can be calculated if the expected values are taken as those predicted by the reference or measured power curves. The binned power curve is first interpolated to provide appropriate resolution of the data values, taken here to be three decimal places. This ensures the existence of an expected value for every data point and the RMSE can then be calculated using the standard formula. The result is a positive integer whose magnitude is a relative indication of the dispersion of the data. The lower the RMSE value, the more tightly grouped the data is around the expected values.

3.4.3 Sensitivity analysis

The eFAST method described in §2.6.2 represents the input parameters to a model with a series of oscillating signals at incommensurate frequencies. After the synthetic input is run through the model implemented as a trained ANN, a Fourier transform of the output reveals the model's sensitivity to the different parameters in the amplitude of the peaks in the frequency spectrum. Each pass through the eFAST algorithm includes the following steps:

1. Create and train the ANN
2. Synthesise a signal for each parameter using its assigned frequency
3. Feed the synthesised data into the ANN to produce a predicted power output
4. Calculate and report the variance of the simulated power signal
5. Apply a fast Fourier transform to the simulated power signal to create a spectrum

Schaibly and Shuler (1973) provide tabulated lists of suitable frequencies ranging from 5 to 19 in length that were prepared through trial and error. Since these are unlikely to be sufficient to represent the number of frequencies required for the present task, three python routines were created. The first recursively checks a value against a list to determine whether it is the sum of a subset of the list values. The second routine checks that no integer multiple of a value is within ± 5 of any other, and the third takes a maximum starting frequency and explores the range of numbers towards zero for compatible values which once found are added to the generated set. This approach yields a compact set of incommensurate frequencies with a narrower range that those of Schaibly and Shuler. The code for the python functions is provided in Appendix C.

Once the maximum frequency is known, the number of required records is calculated using Eq. 47 and a synthetic dataset is generated using the transformation defined by Eq. 46. The resulting synthetic signal is detrended before applying a Fourier transform. In order to accommodate the natural variation in the training of the ANN, the entire process is repeated 10 times and average power densities are calculated for each of the parameters. Following McKay et al. (2013), any output above the highest frequency used is discarded on the assumption that any energy at higher frequencies are the result of imperfections in the structure of the ANN.

In a second stage, total effects are calculated using only two frequencies instead of the full set. The frequencies 139 Hz and 202 Hz were selected for this purpose. Each parameter in turn is set to the higher frequency (202 Hz) while all other parameters were assigned the lower frequency (139 Hz). Thus, the peak at 139 Hz in the resulting spectrum comprises the main effects of all parameters other than the one assigned to 202 Hz, and any other variance is due to the main effect of the selected parameter and its second and higher order interactions. In order to minimise the noise in the spectrum, frequencies above 207 Hz are discarded. This makes the total effects values more precise, but it means that the amplitude of the spectral peaks is not directly comparable with the main effects calculated in the previous stage; however, the difference between the two figures is a reasonable indication of a parameter's interaction with others.

Once the process is complete, a suitable threshold is identified based on the total effects of the parameters and those which fall below the threshold are eliminated.

3.4.4 Model building with ANN

The python library TensorFlow[19] provides a packaged implementation of a wide range of functionality for building, training and testing ANNs although the precise structure of a particular network is left to the user. Decisions therefore need to be made about the number of layers and the number of nodes in each hidden layer. While there is no shortage of advice on possible structures, there are no deterministic methods for choosing an optimal structure, and a certain amount of experimentation is required (Sarle, 2001). Adopting a principle of simplicity, a constructive approach is applied in which smaller structures are tested for adequacy first, adding structure when a deficiency is identified. In all cases, the ANN is trained using the early stopping strategy to avoid over-fitting. In advance of each run, the initial dataset is randomly split and 20% set aside for testing. Of the 80% used during training, 20% is used for validation.

The type of network required here is a regressor, and the output layer therefore consists of a single node representing the estimated power output. The number of nodes in the input layer is also fixed by the number of input parameters. Most examples in the literature have a smaller number of input parameters than is likely to be required here (Mckay et al., 2013; Pelletier et al., 2016). Typical examples also make use of two hidden layers with a relatively small number of nodes although the rationale for using two hidden layers is rarely justified. Given that it has been shown that a single input layer can approximate any measurable function to an arbitrary degree of accuracy with a sufficient number of hidden nodes (Hornik et al., 1989), the initial configuration is one hidden layer and 8 nodes. The performance of the trained ANN can be evaluated using the RMSE to compare predicted and observed power values.

[19] https://www.tensorflow.org/

3.4.5 Correlation analysis

Parameters may be correlated in the research dataset either because the quantities they measure are physically related, or for the more mundane reason that their mathematical derivations follow a similar path. This is especially true for the derived parameters in the dataset which share a common set of measured parameters and where correlations may be spurious (Baas et al., 2006; Kim, 1999). Whatever the source of a correlation, including both variables in a model is redundant, and it can be simplified by eliminating one of them (L. Lee et al., 2017, p. 6). The Pearson correlation coefficient, r^2, is calculated for all pairs of parameters in a set, and for those pairs with a resulting value greater than or equal to a threshold value of 0.7, one parameter is eliminated. In deciding which parameter in a pair to eliminate, the following simplicity criteria are applied:

1. Where one parameter is derived and the other is measured, the measured one is retained
2. Where one parameter is a traditionally-collected value and the other is speculative, the traditional one is retained
3. Where one parameter requires three-dimensional wind data and the other does not, the one requiring two-dimensional data is retained

3.4.6 Creation of comparator power curves

To provide a benchmark for comparison, two power curves are created. The first, referred to here as the *baseline* power curve, only has quality filters applied, while the second, referred to here as the *contractual* power curve is also subject to artificial filters based on those used in real PPT projects. These filters are also referred to as *contractual* filters to distinguish them from the experimental filters that are to be tested. The baseline curve provides a common point of reference for the contractual curve and for those created using the experimental filters. This is useful in comparing the effects on data loss, measurement campaign duration and dispersion; however, because of the established value of current filters, the AEP estimate used as a benchmark will be the one from the contractual curve.

The comparator curves are created according to the methodology defined in IEC2017 including rules for data selection, data aggregation and uncertainty analysis. IEC2017 requires two sets of results to be presented, one normalised to standard sea level pressure of 1.225 kg m^{-3} and the second normalised to the mean density measured at the site. The site-specific values are used as benchmarks in the current work.

3.4.7 Development of novel filtering criteria

The purpose of a filter is to set limits on the validity of the data based on the value of the parameter in question, and to exclude values that fall outside those limits. A *symmetrical* filter is one in which both upper and lower bounds define a pass band and both lower and higher values are excluded. An *asymmetric* filter is one which defines only a single bound beyond which values are excluded. An asymmetric filter would be appropriate, for example, where the value of a parameter is typically close to zero, but in rare circumstances is much higher. A filter would define an upper bound to exclude the abnormal cases.

An ideal filter for use with a power curve would exclude a relatively small proportion of records, say around 10%, at the extremes of its range. Because the values of a parameter are not necessarily Gaussian distributed, a Pearson type III distribution is used to fit the data and the 5^{th} and 95^{th} percentiles are used as the lower and upper bounds. If the parameter is asymmetric, zero is used as the lower bound.

With its bounds defined and appropriate benchmarks available, the effects of a new filter can be observed. In the ideal case, the 10% of data excluded by the filter would be entirely located in the periphery of the power curve point cloud, thus reducing the overall dispersion. It would also produce an AEP estimate similar to that of the contractual power curve.

4 Analysis of PPT contracts

Previous studies have reported significant loss of data during power curve measurement projects as a result of filtering out records that do not conform to the warranted conditions (Mellinghoff, 2012; Rareshide et al., 2009). This chapter presents the results of applying the methods described in §3.3 to data from 15 PPT projects carried out by Wood Clean Energy from January 2014 to November 2018 inclusive. Both the analysis itself and the graphical presentation of the results are novel contributions of this project. While the limitations of wind turbine warranties have been discussed (Albers, 2012), this is the first attempt to quantify the impacts of filtering strategies. The results therefore inform the rest of the current project and provide insights into a significant source of variation across PPT projects.

4.1 Contractual filter criteria

The three most common filters in PPT contracts place limits on TI, wind shear and temperature for which the turbine performance is guaranteed by the manufacturer. Of the 15 projects covered by the present dataset, 12 defined a temperature filter, and 11 defined both TI and shear filters. While the existence of contractual filters demonstrates the importance of the associated meteorological phenomena for turbine performance, the range of limits applied in different projects has not previously received attention.

Fig. 19 contrasts the different restrictions imposed on the data for temperature, turbulence intensity and shear for each of the 15 projects labelled A – O. The grey bars indicate that the relevant project did not define a filter for that particular quantity. The variation is quite wide for all three quantities with some projects imposing much tighter restrictions than others. The temperature range specified by project J, for example, was 2 – 25 °C while the valid range for project O was -40 – 50 °C which more or less includes the full range of temperatures in temperate regions where the majority of wind turbines are located. Projects K – N are very restrictive in terms of turbulence intensity and only allow values in the range 0.06 – 0.12. In addition to the three types of filter illustrated in the figure, three of the projects excluded records where the inflow angle exceeded a threshold of either ±2° or ±4°, two projects excluded records where the veer exceeded ± 10 degrees per 100 m, and one project required the air density to be greater than 1.13 kgm^{-3}.

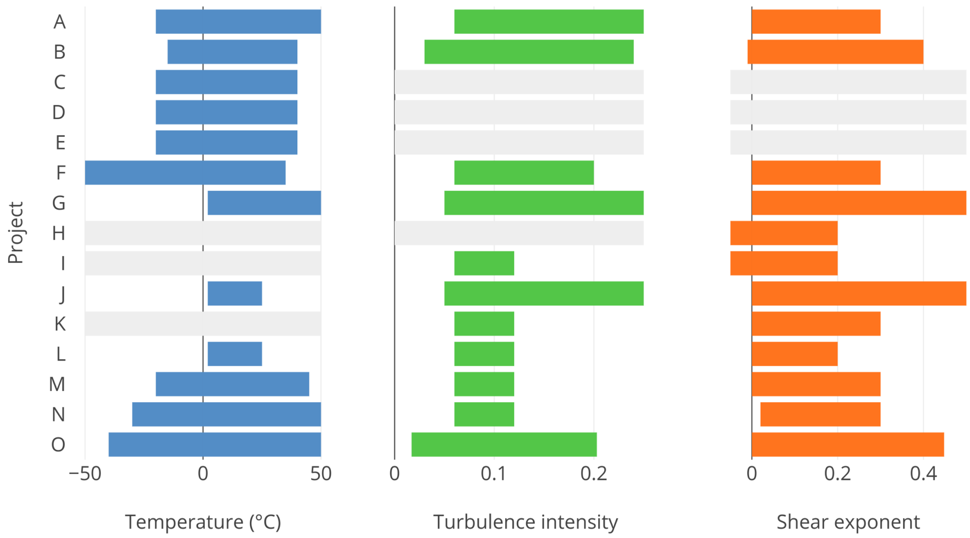

Figure 19: Comparison of filter criteria by project

The more restrictive the filters applied to a measurement campaign, the longer it will take to accumulate the required amount of data. Such disparities across projects create problems for project planning and costing, since for the more restrictive cases, it is likely that the elapsed duration will exceed the customary three-month period. The patterns in the data in Fig. 19 suggest that there are commonly-used ranges for all three filters, but there is no dominant range in any of the three cases. It could be proposed that a standard range be adopted for each filter criterion; however, that would restrict the ability of a PPT contract to reflect site-specific conditions and would almost certainly be unacceptable to manufacturers and developers alike. Alternative filters that target more specific aspects of the wind regime could help avoid the sort of tight restrictions seen here.

4.2 Data loss

Ranking the turbines according to the proportion of data remaining reveals which type of filter is mainly responsible for data loss. In Fig. 20, the series labelled *IEC* represents the minimum filtering requirements defined in the standard. For the most part, losses due to these filters are fairly modest with some notable exceptions. The IEC losses related to turbine O2, for example, are mainly the result of the turbine operating with active curtailment, and those related to turbine J1 are caused by an intermittent grid connection. The large losses related to turbine B3 are reportedly due to turbine unavailability and those related to turbine F1 are the result of a combination of turbine unavailability and blade icing. Apart from those individual cases, the majority of losses are due to the contractual filters. In the best case of turbine C3, 10% of data is lost because of technical availability, and a further 6% because of extreme temperatures. Temperature losses in this case are most likely due to measurement issues such as spikes since the valid range is defined as -20 – 40 °C and the expected range of temperatures at the turbine location is -3 – 34 °C. It is notable though that no filters for turbulence intensity or shear were defined for turbine C3 or for the next three turbines in sequence in Fig. 20. At the other end of the scale, most of the data losses related to turbine M1 are a result of the very restrictive turbulence intensity filter identified previously. Excluding turbine F1 with its technical availability issues, the six turbines at the right-hand end of Fig. 20 all have the same restriction.

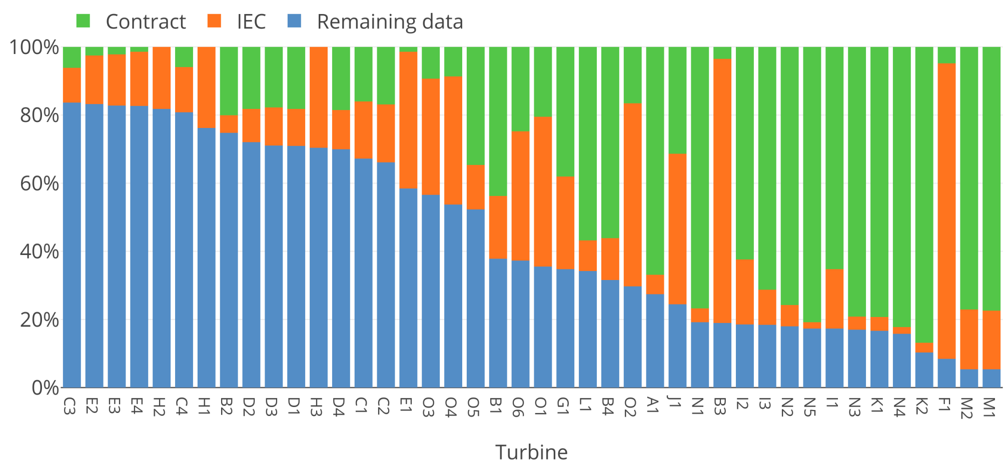

Figure 20: Quantity of data lost through mandatory and contractual filters by turbine

This small sample of PPT results shows that the extreme data losses of up to 90% reported in the literature are not isolated instances. The two turbines at the low end of the scale in Fig. 20 retain only 5% of the measured data, mainly due to a very restrictive condition on turbulence intensity. Both turbines are part of the same project, but there are a further 12 turbines out of 42 which retain less than 20% of the measured data mainly due to contractual restrictions. The measurement campaigns for these 12 turbines range from 99 to 308 days, and all are sited in simple terrain.

4.3 Controlling for terrain effects

Local topology can disturb the flow of air and IEC2017 differentiates between flat and complex terrain for this reason. Flat terrain is relatively homogeneous, while complex terrain can include forestry, obstacles or significant variations in local topography such as abrupt changes in height or steep inclines. It could be hypothesised that PPT data collection for turbines in complex terrain would take longer because of the greater variation in inflow conditions. If that were the case, the impact of filtering strategies on measurement campaign duration would potentially be less significant. The terrain type for each project is recorded in the PPT reports, and is used to categorise the effective duration of each valid measurement campaign in Fig. 21. Applying the quality criteria defined in §3.3.4 to the original 42 turbines in the dataset, 30 were excluded leaving 12.

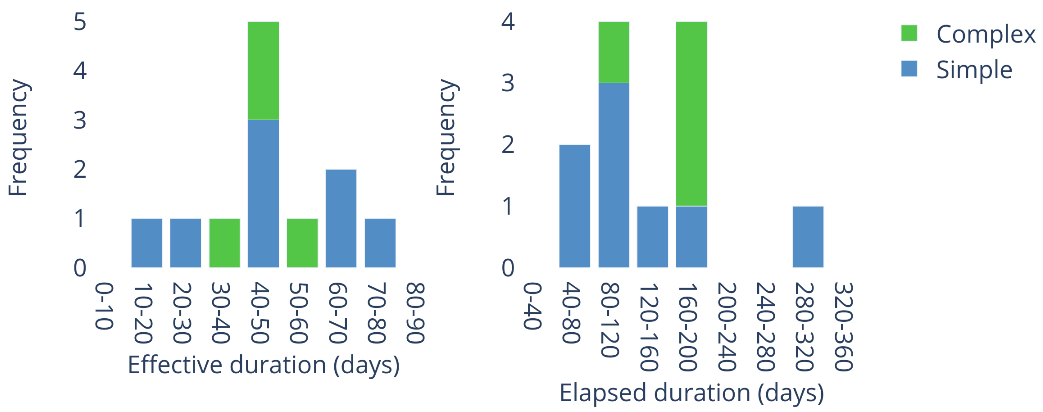

Figure 21: Campaign durations by terrain type

The two sets of effective durations are clearly coincident and the two highest durations are for sites with flat terrain. Apart from one outlying case, the plot of elapsed duration is clearly skewed with projects in complex terrain typically taking longer to complete than those in flat terrain. While the terrain clearly has an impact, using the measure of effective duration removes the bias in the data and makes comparison across projects meaningful. It must always be borne in mind using this measure that it is a theoretical quantity that is always shorter than the elapsed duration.

4.4 Impact of data loss on project duration

A premise of the current work is that PPT measurement campaigns of long duration are undesirable. Theoretically, there are three types of financial benefit that follow from a short PPT process. The first concerns the control of direct costs by terminating the PPT project at the earliest opportunity, and thereby moving the development project onto the next stage. The other types of benefit on successful conclusion of the test are that final contractual payments between parties can be completed and valuable resources assigned to the project can be released. Because information about specific project costs are commercially sensitive, it is not possible to report on them directly; however, if it can be shown that PPT projects are indeed terminated as soon as possible then it can be inferred that fast completion is a priority for the project client. This would further imply that it is financially valuable since it forms part of a commercial activity.

The elapsed and effective durations of each valid measurement campaign are plotted in Fig. 22 against the proportion of data remaining after filtering. Five out of the 12 values for effective duration lie very close to the minimum duration limit. Measurement in these cases ceased as soon as the required quantity of data had been accumulated which implies is that a fast completion was a priority for the project client. In four of the cases, the elapsed duration is far above the planned duration suggesting that there were considerable financial reasons to terminate the measurement campaign as soon as possible.

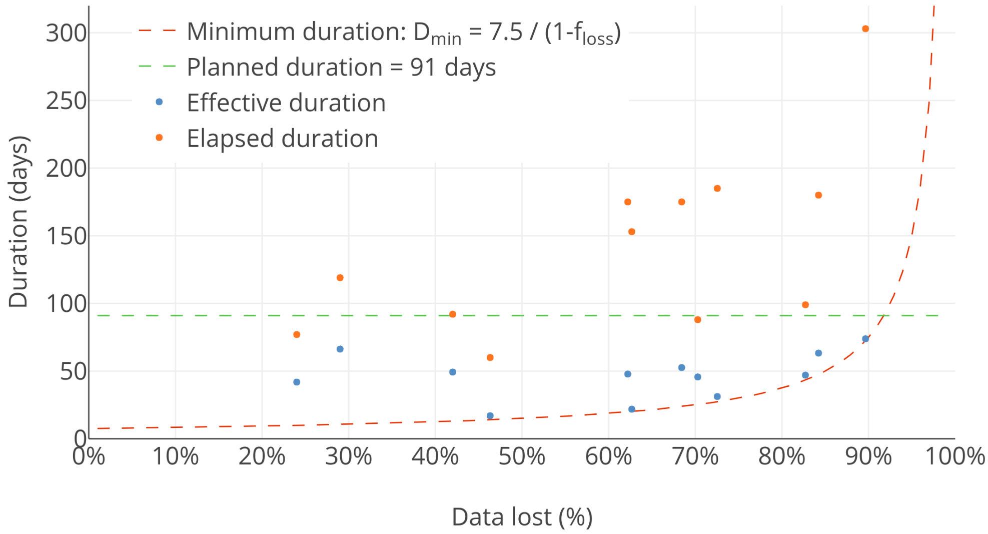

Figure 22: Effective campaign durations

The points are related in the vertical dimension: an orange point represents the same project as the blue point directly below it.

There is a clear trend in Fig. 22 for projects with greater percentage data loss to have longer elapsed durations. Two thirds of the measurement campaigns exceeded the standard three-month duration with the most extreme case lasting three times as long as expected. The direct financial implications of these delays are summarised in Table 15; however, the indirect costs are not so easily quantifiable. Where a measurement campaign takes nine months rather than three, the consequences for the overall project schedule could be severe to the extent of adding an additional year to the construction if the window of good weather in the summer is overshot. Even assuming no such major extension, such an overshoot on a site calibration campaign could incur considerable costs because of the need to retain heavy-duty construction equipment and vehicles. Assuming a rate of around £250K per day, a six-month overshoot could add an additional £45.6M to construction. In Table 15, the cost is shown as a percentage of the planned cost assuming an additional 1% of the planned cost per extra day and the results are presented in order of cost/duration.

Table 15: Direct campaign costs

Campaign	Elapsed duration	Percentage cost
H1	77	100
O2	88	100
O4	60	100
E1	92	101
I1	99	108
D1	119	128
O6	153	162
B1	175	184
B4	175	184
N4	180	189
A1	185	194
K2	303	312

4.5 Conclusions from the project analysis

The foregoing discussion can be summarised as follows:

- Contractual filter criteria vary considerably between projects and can be very restrictive

  Although there appear to be commonly-used ranges for typical filters, none are dominant across projects. The introduction of standard reference ranges is unlikely to be acceptable for commercial and practical reasons.

- Large data losses through contractual filters are not exceptional

  In the small sample of projects examined, an even spread of data losses from 10% to 95% is observed. This confirms the results of previous studies reporting losses of up to 90%, and suggests that large losses are quite common.

- Terrain type is a major factor on elapsed duration

  As expected, measurement campaigns in complex terrain typically take longer than those in flat terrain. However, the relationship is not deterministic, and the project with the longest elapsed duration in this sample was in flat terrain.

- The concept of effective duration allows comparison across projects

  The effective duration is calculated from the valid data that is collected before filters are applied. It provides an indication of the priority attached to the termination of the campaign through a comparison with the minimum theoretical duration.

- The pressure to terminate data collection increases with the rate of data loss

  It is observed that as the elapsed duration of a campaign increases, the effective duration tends to be minimised. This provides evidence that there is a financial imperative to control the duration of campaigns.

- Direct campaign costs often exceed the original budget by up to twice the planned amount

  Two thirds of the valid projects reviewed exceeded the standard three-month period, some by a small amount and others by over 200%. This shows that the issue of controlling the duration of a campaign is significant.

- Indirect costs can theoretically add tens of millions to the overall construction project

  Although it is difficult to be specific because of the commercial sensitivity of costs, it is possible to examine campaign costs in proportional terms. In addition, every project will have its own specific characteristics that determine its actual costs. Nevertheless, the rough estimates presented here show that both direct and indirect costs resulting from long campaign durations can be significant.

There are obvious limitations to the investigation carried out here. Firstly, the data come only from one consulting organisation. To ensure generality of the results, a wider review would need to take in data from several organisation to ensure there are no organisational or operational factors at play.

Secondly, the sample of projects is small and consequently the results presented here must be considered indicative rather than generally applicable. However, the results are supported by industry experts, and confirm previously reported observations about the extent of data losses. These factors increase the confidence in the conclusions drawn here.

Thirdly, limited information was available concerning the reasons for the low rate of accumulation of data during each campaign leading to the difference between elapsed and effective duration. Greater knowledge of these factors could provide additional insights into how campaign duration could be better controlled. However, the focus in the current work is on the data itself, and the patterns observed above appear to be internally consistent.

5 Compilation of research dataset

5.1 Introduction

The range of parameters having a potential impact on instantaneous power output requires a dataset with particular characteristics summarised in Table 10 and explained in greater detail in §3.3. No extant dataset was found to satisfy the requirements, and a new dataset is therefore constructed from original sources using the methods described in §3.3. The result of this exercise is a general resource capable of supporting comparative research beyond the current aims, and therefore constitutes a core contribution from the current work. Its main element is a single file of TMA values which contains 727 columns including the timestamp. In addition, the raw data sample used to derive each TMA record is preserved for more detailed investigation if required.

This chapter provides details of the practical implementation of the methods set out in §3.3 with particular focus on the sources of data, and the process of constructing the final dataset including

- data quality control
- removal of spurious data
- the conflation of data from different sources
- the reduction of raw data to ten-minute averages
- the addition of derived parameters

Wind speed and direction values are calculated from wind velocity components measured using sonic anemometers. As a simple validation of the process, the calculated hub-height wind speed and direction are compared to measurements from the turbine SCADA and are found to agree within expected limits. A description of the format of the TMA file is provided in Appendix F along with a data excerpt; however, because of the dimensions of the data, the excerpt is necessarily abbreviated. The entire dataset is available via the University of Minnesota Digital Conservancy (Davison, 2019).

5.2 Sources

5.2.1 Eolos research turbine

The Eolos Wind Energy Research Field Station is operated by the University of Minnesota, and is located at 44.73N, -93.05E, approximately 30km south-east of the centre of Minneapolis. A 2.5 MW Clipper Liberty C96 turbine, commissioned in 2011, with a rotor diameter of 96 m and a hub height of 80 m is paired with a meteorological mast (met mast) located 160 m to the south. The relative positions of the turbine and met mast are shown as red circles in Fig. 23.

Figure 23: Turbine location showing excluded sector

The immediate vicinity of the turbine is rolling farmland with no more than a 3 m change in elevation in a 2 km radius with respect to the turbine base (Howard & Guala, 2016). Within the same area there are some small wooded areas and two-storey buildings which introduce localised changes in surface roughness. The sector indicated by the arc is excluded to avoid disturbance from the turbine wake and flow distortion due to the met mast.

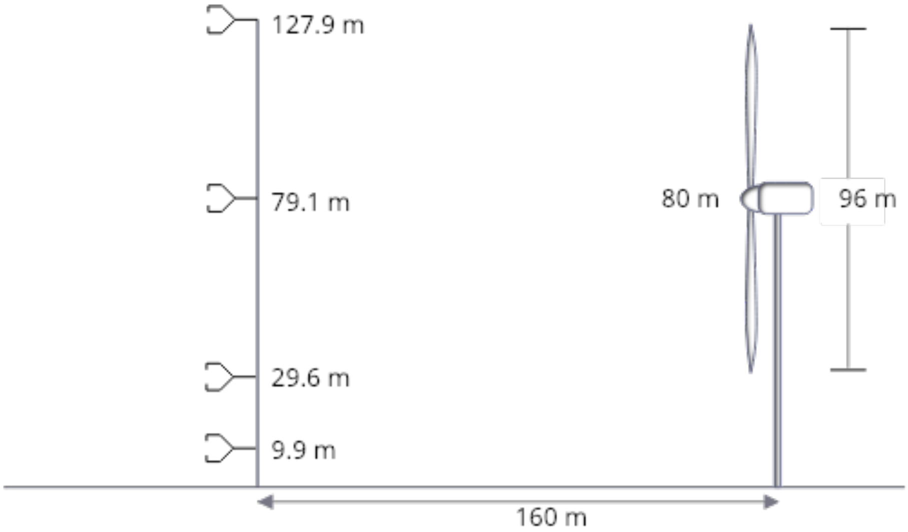

Figure 24: Eolos turbine dimensions and instrumentation

The mast is equipped with sonic anemometers at four elevations as shown in Fig. 24 which sample temperature and wind speed in three dimensions at a frequency of 20 Hz. Data sample at 1 Hz is provided for pressure and relative humidity measured at hub height, and temperature measured at six heights. SCADA data is also sampled at 1 Hz and includes measurements of a number of meteorological and turbine parameters including active power.

In a commercial PPT, the manufacturer usually provides a site-specific power curve with associated limits of validity which forms the basis of the turbine warranty and the benchmark for the test itself (Albers, 2012). Here the sales power curve is used, and the data has been recovered from an online database[20]. The reference power curve is shown in graphical form in Fig. 25 which is based on the table in Appendix A.

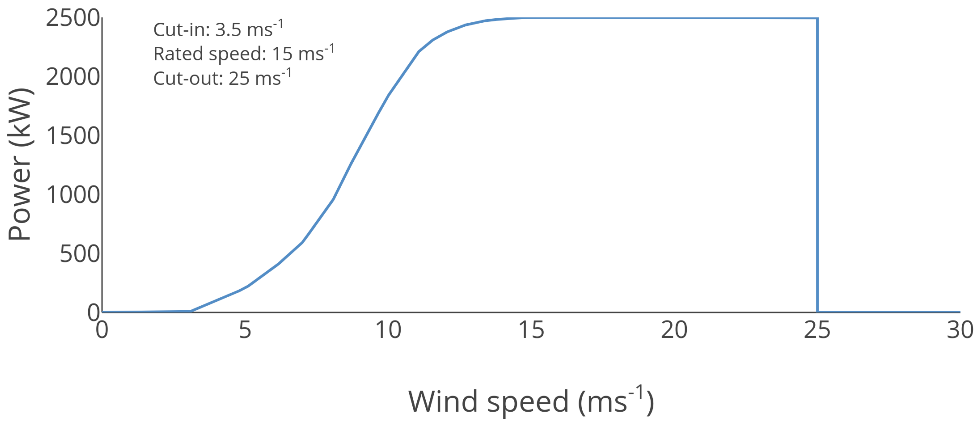

Figure 25: Clipper Liberty C96 reference power curve

Since data is collected using several data loggers, the Eolos data is supplied in parts which are summarised in Table 16.

Table 16: Data sources from the Eolos research turbine

Identifier	Data	Levels	Sampling frequency
MetA	Sonic anemometer data	79.1 m, 127.9 m	20 Hz
MetB	Sonic anemometer data	9.9 m, 29.6 m	20 Hz
RH	Pressure and relative humidity	80 m	1 Hz
Temp	Temperature	7.3 m, 27.1 m, 51.5 m, 76.7 m, 101.5 m, 125.9 m	1 Hz
SCADA	Data from instruments on board the turbine including power	80 m	1 Hz

[20] https://www.thewindpower.net/turbine_en_296_clipper_liberty-c96.php

5.2.2 *ASOS weather observation stations*

Surface measurements at several locations in the vicinity of the turbine in order to calculate the local gradients of pressure and temperature. These are needed for the rotation of the flux vectors as described in §3.3.3.8. The Automated Surface Observing Systems (ASOS) network is a system of meteorological measurement stations maintained by the US National Weather Service, the Federal Aviation Administration, and the Department of Defence. Surface temperature and pressure are measured in accordance with the procedures set out by the US Office of the Federal Coordinator for Meteorological Services and Supporting Research (OFCM, 2017) at hourly intervals.

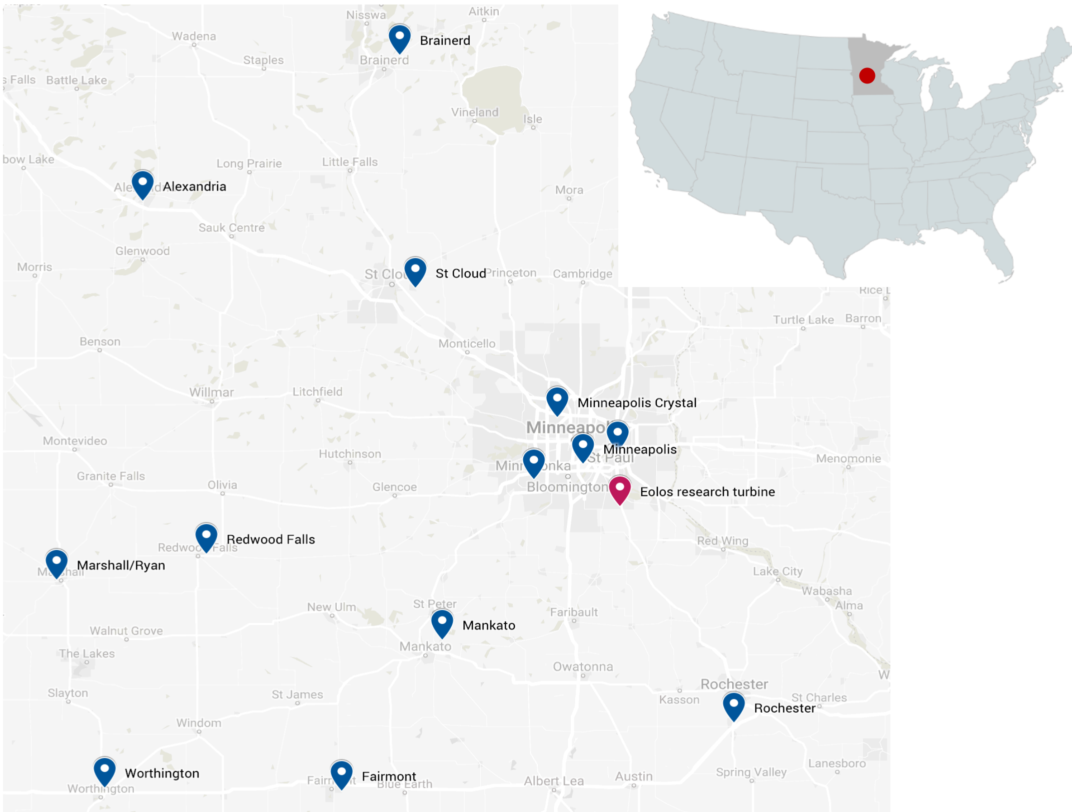

Figure 26: Network of weather stations in Minnesota. The location of the Eolos turbine is highlighted in red

Data is freely available via the aggregation site operated by Iowa State University. Although there are 106 ASOS stations in the state of Minnesota, some are a long way north of the Eolos turbine site, and could exaggerate the local temperature gradient if they were included in the calculation. In addition, not all stations were able to provide a complete record of pressure for 2017. Eventually, 13 stations within a 240 km radius of the turbine site were selected as shown in Fig. 26.

5.2.3 Solar data

Basic solar data including sunrise and sunset times and azimuths was obtained for the whole of 2017 from the Internet site timeanddate.com. On the basis of this initial data and the julian day number, hour angle, elevation and declination can be calculated using standard formulae whose implementation can be found in Appendix E.

5.2.4 Wind regime

This section describes the wind regime at the Eolos turbine location based on the content of the research dataset. Meteorological characteristics are described primarily with reference to standard hub-height parameters.

5.2.4.1 Stability

The state of Minnesota is characterised by its flat terrain and continental climate. The average high temperature for July is 28.6º and the average low in January is -4.6º (US Climate Data, n.d.). This is reflected in the distribution of stability classes throughout the year as shown in Fig. 27 where the proportion of unstable conditions peaks in June. The figure uses stability classes based on the Obukhov length, L, based on the limits in Table 5.

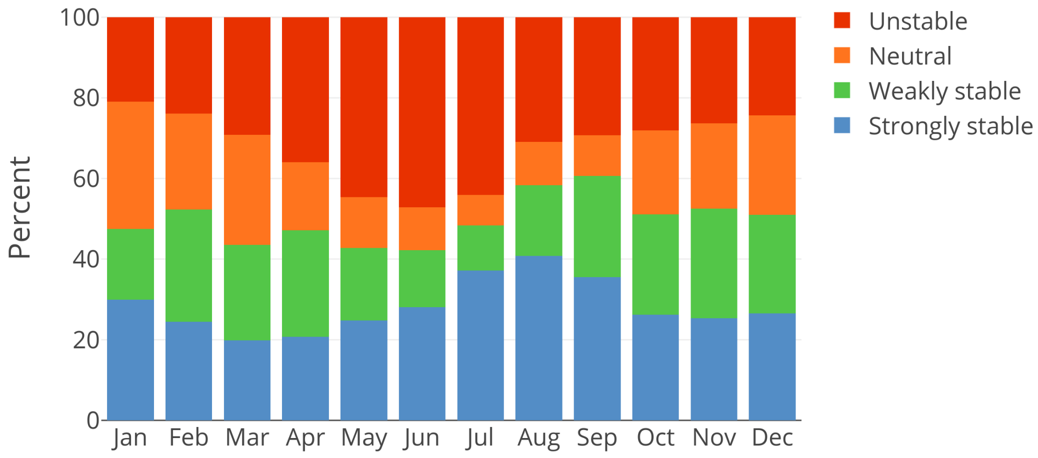

Figure 27: Distribution of stability classes during 2017

5.2.4.2 *Wind direction*

The prevailing wind direction has previously been reported as southerly (Chamorro et al., 2015). The wind rose of the hub height wind in Fig. 28 however shows that in 2017 the predominant direction was approximately 300º.

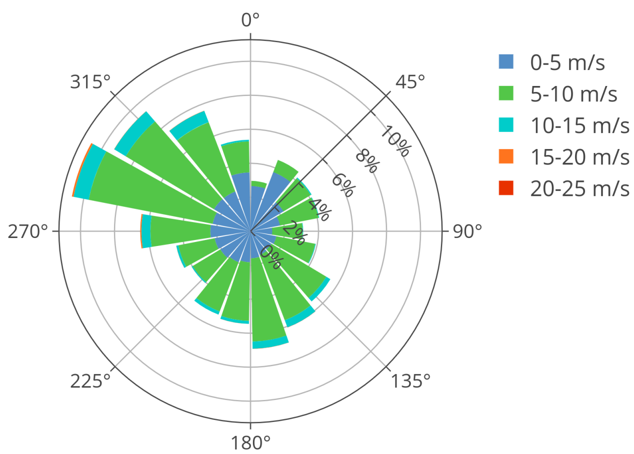

Figure 28: Wind rose for 2017

Breaking the wind direction down by stability class as shown in Fig. 29 reveals a greater spread of directions in strongly stable conditions when wind speeds are low compared to other classes.

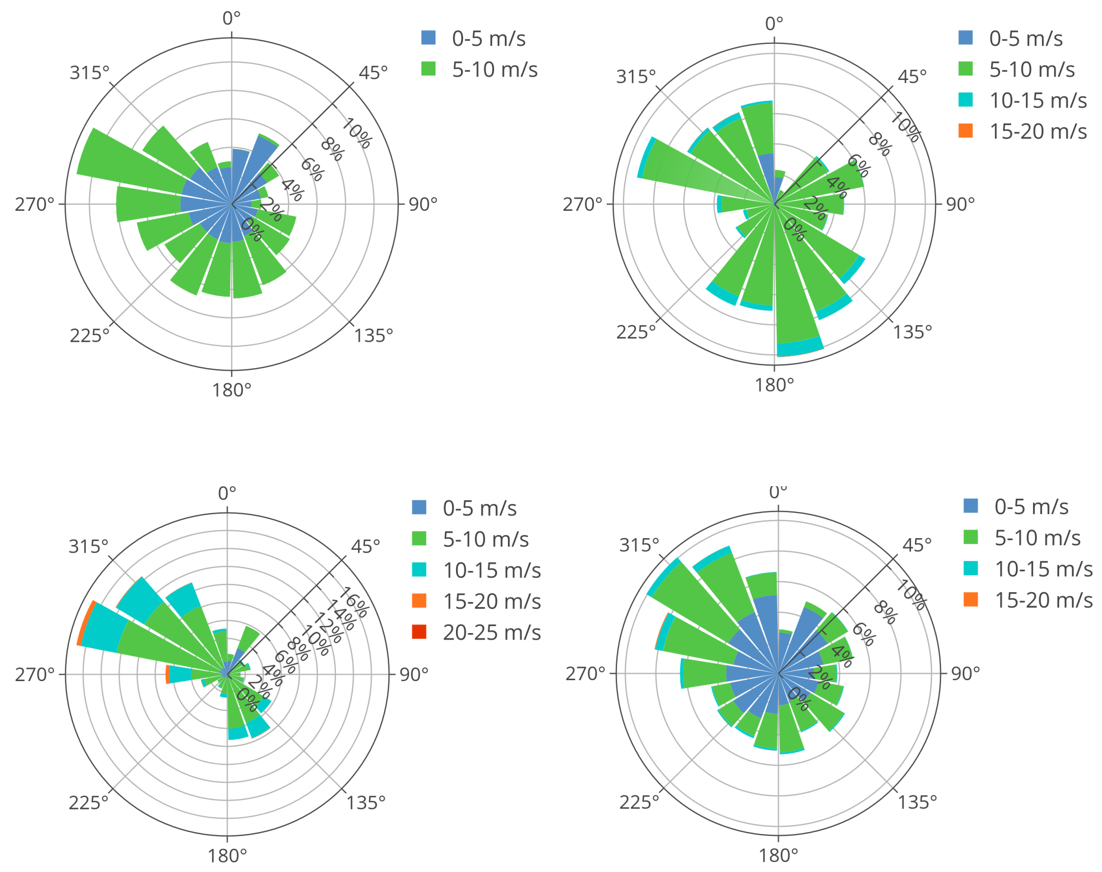

Figure 29: Wind roses for 2017 broken down by stability class.
Top-left: strongly stable (28902 records); top-right: weakly stable (8844 records); bottom-left: neutral (3750 records); bottom-right: unstable (9202 records).

Wind direction shows a small dependence on time of day as shown in Fig. 30. There is a consistent tendency for the wind direction to veer shortly after solar noon by around 20° and to back by a similar amount towards evening. This observation is congruent with the content of the wind roses in Fig. 29 where the wind from the north west is stronger in neutral and unstable conditions. During the night when stable conditions dominate, the wind direction is more likely to be from the south. Also evident in Fig. 30 is the tendency for stronger wind veer during stable conditions. This can be illustrated more clearly by plotting veer in degrees per 100 m against hour angle as in Fig. 31.

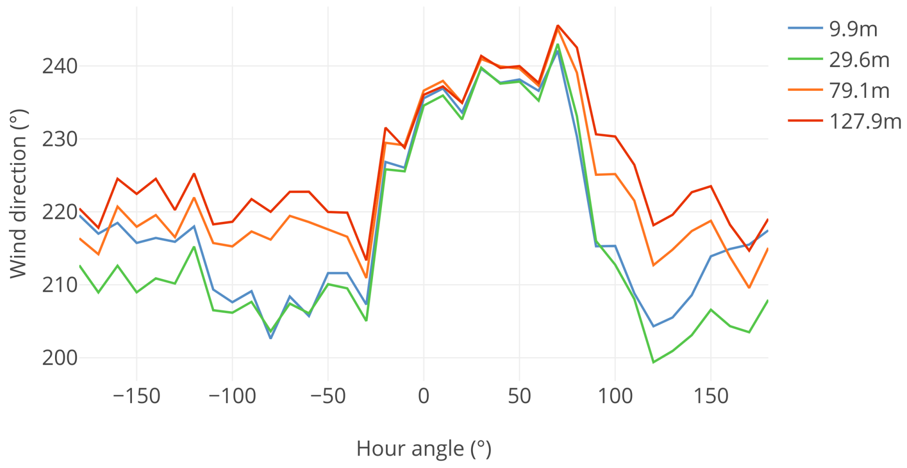

Figure 30: Wind direction by time of day represented by the hour angle

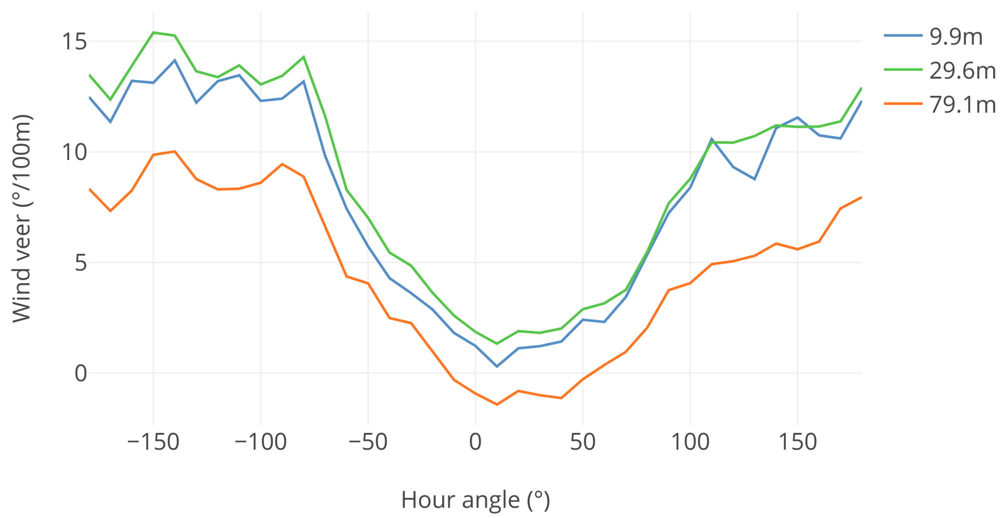

Figure 31: Wind veer by time of day represented by the hour angle

5.2.4.3 *Wind speed distribution*

Overall the site is characterised by moderate winds with a hub height mean of 5.79 ms^{-1} for the year and a standard deviation of 2.57 ms^{-1}. The turbine's rated speed of 15 ms^{-1} is rarely achieved implying that the turbine operates predominantly in region II of the power curve. Fitting a Weibull distribution to the wind speed histogram as required for the IEC AEP calculation results in a shape parameter of 2.39 and a scale parameter of 6.53 as shown in Fig. 32.

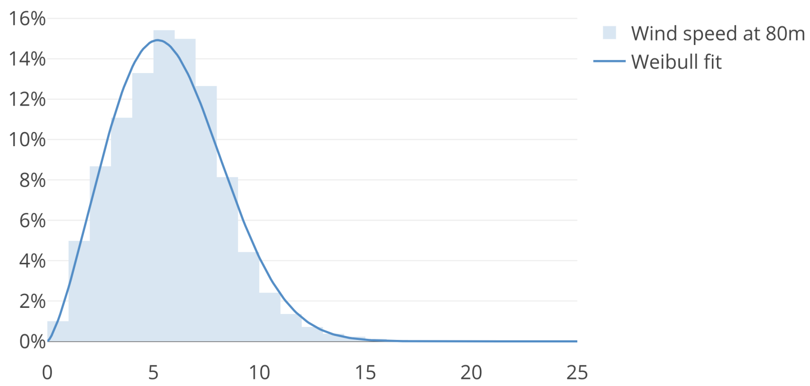

Figure 32: Hub-height wind speed histogram and Weibull fit for 2017

Fitting a Weibull distribution to the data from the four available measurement heights shows the expected evolution of wind speed with both the mean and standard deviation increasing with height.

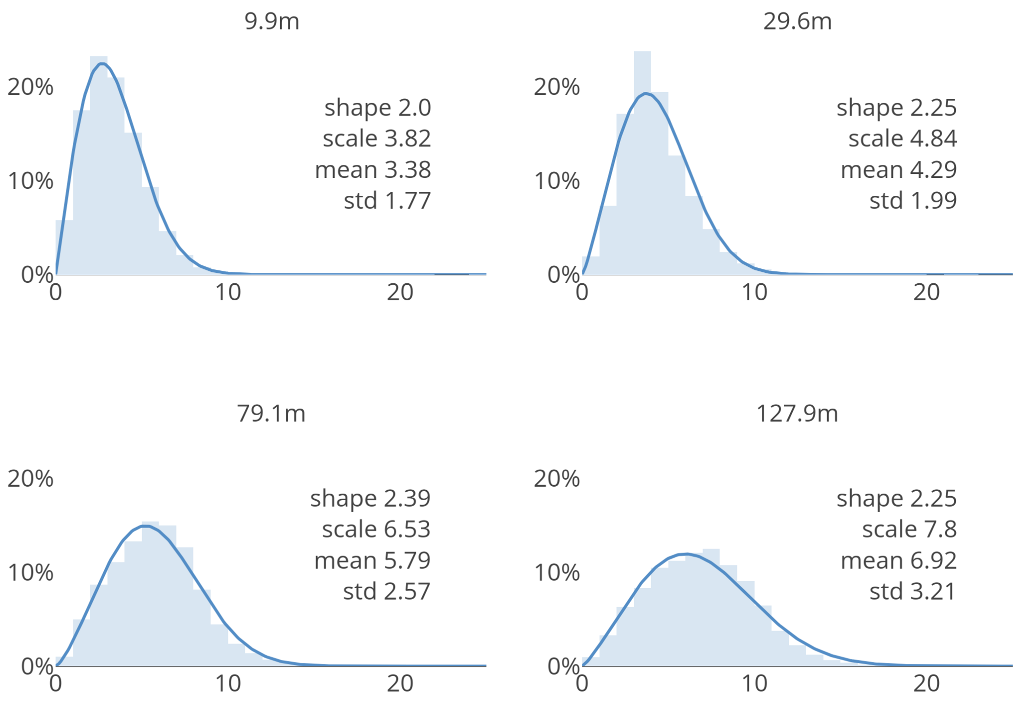

Figure 33: Wind speed histograms from four heights with Weibull fits for 2017

The variation in conditions across the year can be demonstrated by fitting a Weibull distribution to the hub height wind speed for each successive quarter. Although the standard deviation does not vary significantly, there is a 1.26 ms^{-1} difference in the mean between the third and fourth period. While not very large in absolute terms, this represents a 25% increase in average wind speed given the overall moderate regime. The implication for PPT is that the timing of the campaign could be a significant parameter in the final AEP calculation. Since the period from September to November is the preferred time for carrying out a site calibration, there is a risk that wind speeds measured during that time might not be representative of the whole year.

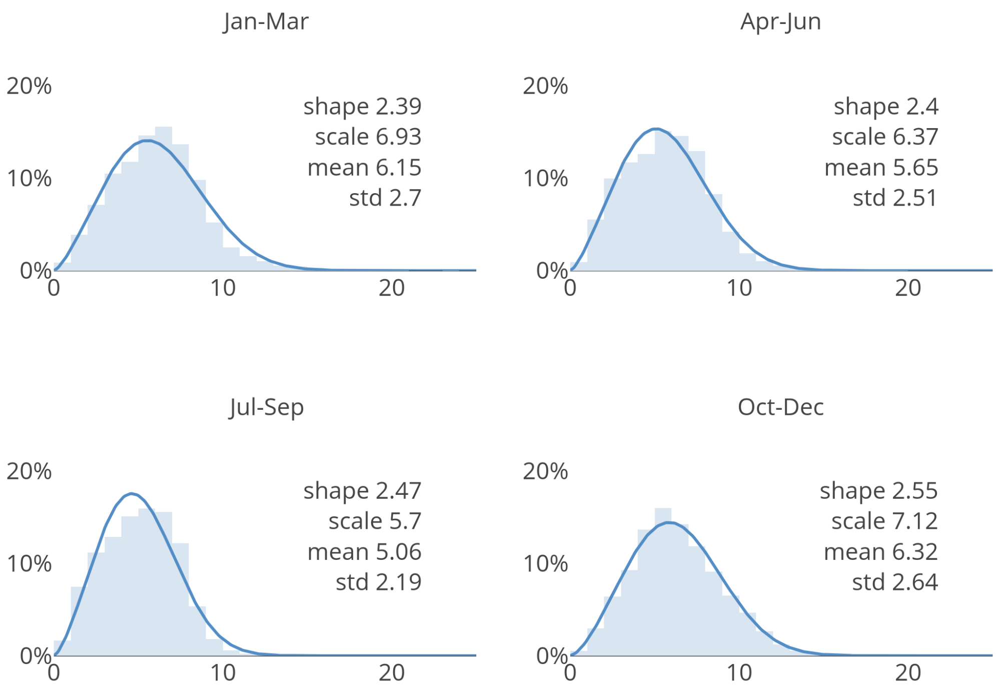

Figure 34: Hub-height wind speed histogram and Weibull fits by season

The description of the Eolos wind regime exhibits expected patterns of behaviour, and to that extent confirms that the measurements have no anomalous features. The distribution of wind direction contrasts with that previously reported and could be an indication of incorrect processing of the sonic anemometer data. However, comparison with the turbine's SCADA system in Fig. 39 confirms that the wind directions have been correctly calculated. The anomaly therefore remains unexplained. The Eolos site is characterised by a low mean wind speed and modest turbulence, to the extent that the rated wind speed of the Clipper Liberty C96 turbine of 15 ms^{-1} is rarely achieved. This is most clearly appreciated with reference to the velocity exceedance curve in Fig. 35.

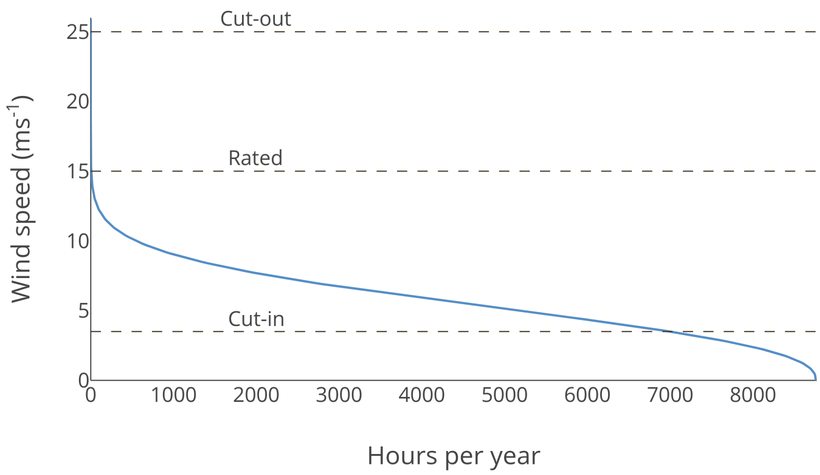

Figure 35: Velocity exceedance curve

5.2.4.4 *Turbulence and shear*

Plotting hub height turbulence intensity and wind shear exponent against time of day represented by the hour angle as in Fig. 36 shows the expected pattern of variation. During the stable conditions that prevail during the night, turbulence intensity is low and shear is high and the opposite is true in unstable conditions.

Examining the turbulence intensity binned by wind direction provides a verification of the definition of the free-stream sector, and also facilitates the identification of any other surface roughness influences that need to be eliminated. The higher proportion of values above 0.25 in the sector 340-20° due to the turbine wake is clearly visible in Fig. 37. The excluded sector was calculated as 320-40° using the IEC recommendations, and disturbances due to the turbine are therefore eliminated from analyses. In all other sectors, the spread of values is fairly even in proportion to the number of data points revealing no major disturbances due to the turbine's immediate surroundings.

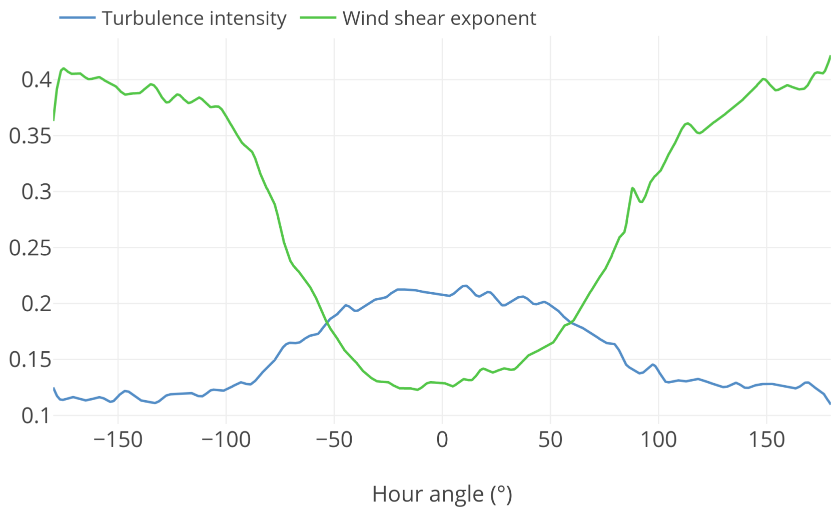

Figure 36: Turbulence intensity and wind shear exponent by time of day represented by the hour angle

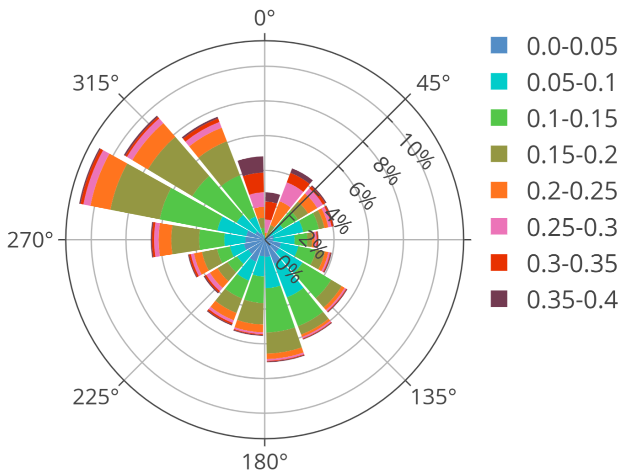

Figure 37: Turbulence rose for 2017

5.3 Data preparation process

This section reports on the application of the methods described in §3.3.3 – 3.3.5. Minor variations to the planned methods were required to accommodate practical issues during the data preparation process, and they are also described here.

5.3.1 Quality control

The characteristics of each original source of data were examined to identify any limitations or corrective actions that need to be applied. Table 17 summarises the issues found. Appropriate action is then taken to resolve or work around these issues.

Table 17: data issues

	Dataset	Issue	Description
1	MetA, MetB	Calibration	There is no evidence that recalibration has been carried out since installation in June 2013
2	MetA, MetB	Sample consistency	The 5-minute samples provided do not have consistent length or boundary
3	MetA, MetB	Anemometer faults	A significant minority of records show an anemometer fault code
4	MetA, MetB	Coordinate frame	The sonic wind speed components are recorded using a left-handed coordinate frame in which north to south is taken as positive in contrast to the usual convention (Stull, 2015, p. 2)
5	MetA	Misalignment	Sonic anemometer at 79.1 m requires a correction of -12.8 degrees (Information provided by the University of Minnesota)
6	MetB	Misalignment	Sonic anemometer at 29.6 m requires a correction of -6.4 degrees (Information provided by the University of Minnesota)
7	SCADA	Turbine faults	A significant minority of records show a turbine fault code
8	SCADA	Curtailment	A significant number of records show that the turbine output is curtailed
9	ASOS	Sampling frequency	The sampling frequency is lower that the target frequency of the final dataset

Most instruments require recalibration within one to two years of installation which helps to guard against drift. Since there is no information about any recalibrations since installation (1), some inaccuracy in pressure and relative humidity readings is expected. The Campbell Scientific CSAT3 sonic anemometers should not require field calibration (Campbell Scientific, 1998); however, see the discussion regarding temperature readings below.

The sampling problem (2) is resolved by partitioning the data by day rather than by periods of five minutes. This resolves most of the anomalies leaving only a small number of cases where records from one day appear in the file corresponding to a different day. These last few anomalies are resolved manually.

The CSAT3 sonic anemometer provides a diagnostic signal to help filter out invalid readings. It appears in the instrument output as an integer value which indicates an error condition if its value is 61440 or greater. The fault issue (3) is resolved by filtering out data where a fault code greater than or equal to 61440 is reported. The filtering code suppresses values from the relevant anemometer only. Because data from two separate anemometers occur in each of the MetA and MetB files, removing an entire record when a fault code appears would risk removing valid data from the second instrument.

To simplify the application of existing meteorological formulae (4), the coordinate frame was changed from left-handed to right-handed by flipping the sign of the meridional (south-north) readings.

The misalignment issues (5 & 6) are resolved by explicitly correcting the data. To perform the correction, the resultant wind vector is calculated and rotated by the relevant angle. The corrected vector is then decomposed back into zonal (west-east) and meridional (south-north) components.

The turbine fault issue (7) is similar to that related to anemometer faults in that it relies on reported values in the data. Valid SCADA records were identified by a turbine state value of *Run* (corresponding to internal code 8), and a fault code of either *0 (no fault)* or *920 (feather check warning)* (Stone, 2015). Records showing any other fault codes are suppressed.

Curtailment (8) refers to the situation where the power output of the turbine is deliberately constrained to a particular level. Records that correspond to a period of operation where output was curtailed can introduce misleading biases into any analyses. 27.5M SCADA records out of 28.5M (96%) reported a curtailment level below 2,500 kW. However, only 16.8M (59%) of records reported a curtailment level below 2,300 kW. According to the published power curve, a hub height wind speed of 11.5 m/s is required to produce 2,300 kW. A later examination of the TMA data revealed that this wind speed was only exceeded during 1048 periods out of 51,050 (2%). The risk of distortion associated with such a small proportion of the data was considered minimal, and all records with a curtailment level of 2,300 kW were retained.

The low ASOS sampling frequency (9) implies gaps in the data at the point it is synchronised at 0.00167 Hz (ten-minute intervals) with data from other sources. The solution is to upsample the data in advance of synchronisation, and to fill the resulting gaps using a second order spline interpolation.

5.3.2 *Despiking*

The value of visual inspection is illustrated by the sample shown in Fig. 38 where an apparent failure of the despiking routine demonstrates the need for manual exclusion of certain TMA records. The discontinuity seen at 12:59 actually represents the sonic anemometer recovering from an error condition which was not flagged by the instrument's fault code.

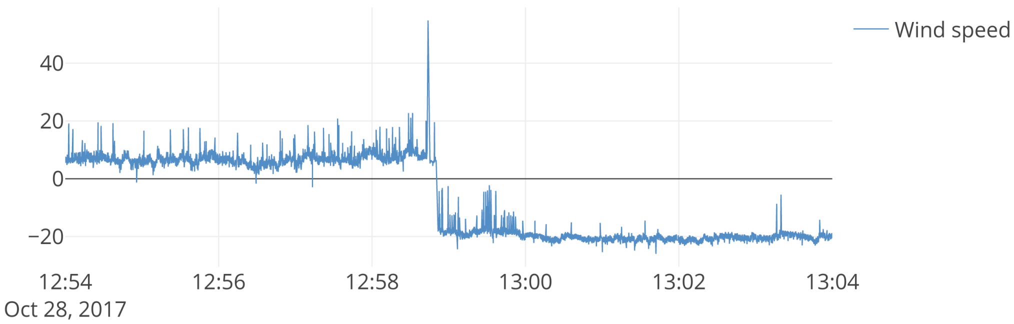

Figure 38: Example of a data anomaly not identified by the anemometer fault code

5.3.3 Data reduction

Cross comparison between the hub height wind speed and direction calculated from the sonic instruments and those on board the turbine shows good agreement, and therefore supports the conclusion that no errors have been made in handling the sonic data. The correlations shown in Fig. 39 are not expected to be perfect because of the flow disturbance around the turbine nacelle. This is particularly evident in the wind speed plot at low wind speeds. The truncation of the direction plot at 40° and at 320° is the result of including only the free-stream sector.

During data reduction there was an issue with the calculation of the coefficient of variation for temperature parameters. In most cases, temperatures are recorded in degrees Celsius, and consequently the coefficient of variation becomes undefined at 0°C. However, because temperature varies only slowly, changes within a ten-minute averaging period are assumed to be unimportant for present purposes. This issue could have been avoided by converting all temperatures to Kelvin before performing the calculation. Coefficients of variation for temperature parameters do not appear in the final dataset.

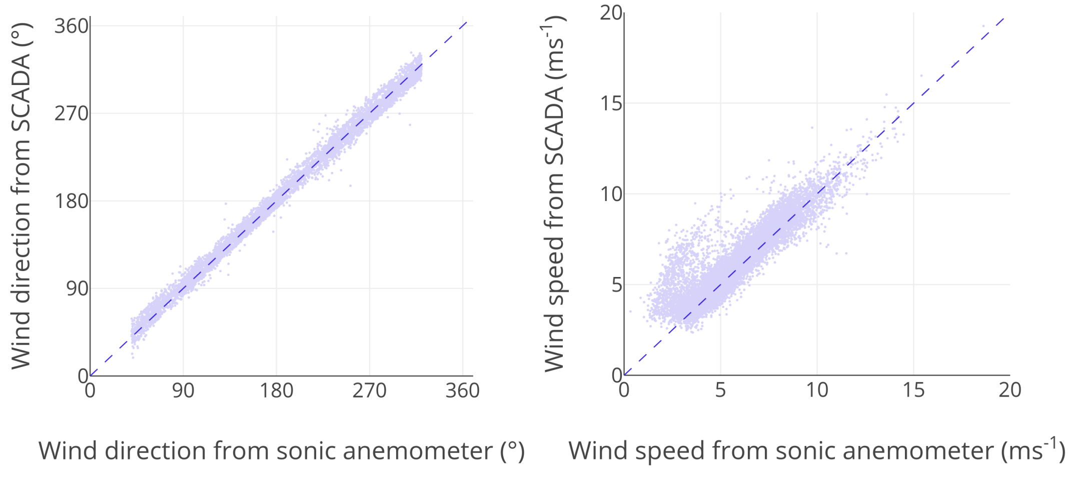

Figure 39: Comparison between wind direction and speed from the hub-height sonic anemometer and the turbine SCADA

5.3.4 Addition of derived parameters

The calculation of air density is based on the sonic temperature and therefore differs from the formula given in IEC2017 which assumes that the temperature is measured with a PT100 temperature probe. The IEC formula includes a correction for humidity which is not needed with sonic measurements. The calculation used here is based on Eq. 9.

The Eolos dataset provides a wind speed measurement at hub height and at the two vertical extremes of the rotor. This is the minimum number of measurements for REWS to be applied. However, please see the note in §5.4 regarding the quantity of data.

Because Monin-Obukhov similarity theory is only valid within the atmospheric surface layer (Optis et al., 2016), the flux values measured at the lowest level of 9.9m are used to derive L.

When deriving the zero-turbulence power curve during turbulence normalisation, the iterative step involves simulating the cut-in wind speed, maximum power coefficient and the rated power. When these three values converge on the reference values, the iteration terminates. Because the site is dominated by moderate wind speeds, rated power output is not reached at any point. This makes it impossible to use the turbulence normalisation procedure since the convergence with the rated power cannot be achieved. Turbulence normalisation therefore cannot be applied here, and its limitations are clear.

5.4 Quantity of data

The TMA file contains a total of 727 columns including the minimum requirements listed in Tables 7 – 9, diagnostic values such as spike count added during data reduction, intermediate values produced during certain calculations and parameters related to the SCADA data other than active power. The latter values are included for completeness, but are not relevant to the current work. A full description of the columns is provided in Appendix F.

The TMA file contains a total of 52,560 records; however, not all of the columns are fully populated either because of instrument faults or for other reasons. In the first half of the year, for example, the turbine was either operating with a curtailment level lower than 2,300 kW, or not operating at all. Consequently, only 12,628 records have power values. When all of the relevant quality filters are applied, this number falls further. As discussed in §3.5.1, TMA values for wind speed and power are suppressed if they are based on fewer than 90% the expected number of raw data points, and where more than 1% of the sample has been removed because of spikes. In addition, the data needs to be filtered by direction to include only the free-stream sector. The result is a final dataset of around 8,000 records which is just 15% of the possible total.

Table 18: Quantity of wind speed data lost through quality filtering and number of records remaining

Height (m)	Physically implausible values (0-30 ms^{-1})	Less than 90% of expected points	More than 1% spikes	Remaining	
127.9	410	17,794	4,327	30,029	57%
79.1	15	1,069	454	51,022	97%
29.6	2	710	232	51,616	98%
9.9	17	261	41	52,241	99%

Table 18 summarises the data lost when the dataset is filtered for validity of the mean wind speed values at the four measurement heights and the number of records remaining after the filters are applied. While a high proportion of data remains for the lower three instruments, a lot of data is lost at the top tip height because of instrument issues. This constrains the possible analyses that rely on measurements across the full rotor diameter including the use of the rotor equivalent wind speed (REWS). When applying filters to limit the dataset to only those TMA records containing the data required for REWS, the number of records is reduced to 2,818 or 5.4% of the possible total.

5.5 Summary and limitations

The main result from the data preparation process is a single file of coordinated ten-minute average (TMA) values drawn from the various sources and synchronised on their timestamps. In contrast to current practice, the data contains a wider range of statistics that have the potential to provide insight into the behaviour of the measured values within each averaging period. Care is taken to eliminate data that could bias the results of analyses unduly, and additional quality indicators have been added which characterise the ten-minute data samples from which each TMA value is derived.

In addition to the TMA data, the preparation process preserves all ten-minute samples from the various sources which are used to create a TMA record. In this way, the original data is available for further examination should any interesting or anomalous features be identified. This not only provides a means of providing further evidence for any apparent effects; it also helps to eliminate false positive situations in which an effect appears to be present, but which is in fact the result of poor data quality, calculation errors or other oversights.

The following limitations on the final dataset have been identified:

- No recent instrument calibrations have been performed

  The measurement instruments were already installed and there was no opportunity to perform calibrations. There was also no information about calibration activity since their installation in 2011. The results presented here must therefore assume that adequate equipment maintenance has been performed.

- The low-wind location means that rated power is not achieved

  Although it is the behaviour of the turbine in region II of the power curve that is of most interest, the low mean wind speed limits the analyses that can be performed. One very specific limitation is that the turbulence normalisation procedure cannot be used since it requires a point of reference at rated speed. Likewise, no observation of other behaviour related to high-speed wind regimes is possible. This limits the observations that can be made, for example, regarding the interaction of wind speed with other meteorological phenomena.

- The dataset has a large number of missing values

  The dataset nominally covers an entire calendar year; however, there are many missing values related to instrument failure and turbine curtailment. Nevertheless, the remaining data is still substantial at around 7000 – 8000 records depending on the filters applied, and also has the desirable feature of spanning the seasons.

- A number of SCADA parameters are not included in the final TMA file

  The focus of the current work is on meteorological impacts on power production, and therefore meteorological parameters are prioritised. The exclusion of some SCADA parameters does not impact the current work, but might limit future analyses that can be performed on the research dataset.

- A small number of TMA records are affected by curtailment

  A pragmatic decision was taken to retain records with a curtailment level of 2,300 kW to avoid eliminating a large number of records. Checks indicated that a very small number of records would be affected by the curtailment because of the low mean wind speed. However, it is expected that a small number of points will appear as a horizontal anomaly in the power curve scatter plot at 2,300 kW. The effect of this small set of data points is thought to be negligible with respect to data analyses.

- Visual inspection of all samples was not possible due to the quantity of data

  Some anomalies such as the one illustrated in Fig. 38 were identified and eliminated; however, other such issues may still exist undetected in the data. Because no obvious anomalies have been observed in the TMA records, however, there is a reasonable level of confidence that even if such issues do exist, the reduction process used to produce the TMA records has largely mitigated their effects.

- Wind speed and direction are based solely on sonic measurements

  One aspect of the Eolos data that was not explored was the incorporation of the wind speed measurements taken with cup anemometers. This decision was mainly taken to control the quantity of data that needed to be processed, and to avoid issues related to the combination of data from different types of instrument. This does not pose any problems for the current work, but again limits future analyses based on the research dataset.

- Flux calculations use a ten-minute averaging period rather than the standard 30 minutes

  A ten-minute averaging period is used here so that flux values can easily be calculated along with other derived parameters. This potentially introduces uncertainty into flux values calculated for unstable conditions as discussed in §3.4.3.6.

6 Accounting for variation in the power curve

This chapter reports on the results of applying the methods described in §3.5 to the research dataset. Candidate parameters are selected from those available and evaluated for their relationship with power performance through a sensitivity analysis using the eFAST method applied to an ANN trained on the Eolos data. Parameters with relatively low total effects are excluded and correlation analysis is used to eliminate redundancy. The aim is to drive the identification of a set of experimental filters from the data in order to eliminate subjective decisions as far as possible. There are two types of subjective decision which cannot be avoided, however. The first is the initial selection of candidate parameters which is mitigated by the deliberate inclusion of parameters not currently used in PPT and alternative measures for traditional phenomena such as turbulence and shear. The second type of subjective decision is related to the thresholds for retaining parameters following sensitivity and correlation analysis. As far as possible, thresholds are selected based on the form of the data, and this is discussed in the appropriate places below.

6.1 Initial parameter selection

With over 700 parameters, the research dataset can support a huge array of possible analyses and the first step must be to identify those parameters that are most relevant to a particular case. For the current work, all diagnostic parameters are eliminated as are all SCADA parameters except active power. Hub-height parameters are used for comparison with existing methods and the majority of parameters relating to other measurement heights are therefore excluded. Table 19 lists the base parameters included in the analysis along with the measurement height and statistical or derived variations where relevant.

Table 19: Initial set of selected parameters

Base parameter	Height	Variations
Horizontal wind speed	79.1m	Basic moments (mean, standard deviation, skew, kurtosis) Stationarity (ADF, KPSS) Turbulence (V, V_2, dissipation, length scale) Intermittency (β_2) Normality (jb) Structure (transience)
Vertical wind speed	79.1m	As above
Air density	80 m	
Temperature	76.7m	Basic moments (mean, standard deviation, skew, kurtosis) Stationarity (ADF, KPSS) Normality (jb) Structure (transience)
Relative humidity	80m	As above
Pressure	80m	As above
Flux	79.1m	Vertical flux of horizontal momentum Vertical flux of sensible heat Turbulence kinetic energy (TKE)
Cross-isobar angle	79.1m	
Inflow angle	79.1m	
Potential virtual temperature	79.1m	
Wind veer	79.1m	
Obukhov stability parameter	9.9m	
Bulk Richardson number		
Wind shear exponent		Lower half of rotor Upper half of rotor Whole rotor
Wind speed ratio		
Lapse rate		Measured temperature Potential virtual temperature
Solar declination		
Solar elevation		
Hour angle		
Geostrophic wind speed		
REWS		
Specific humidity		
Sea-level pressure		
ABL height		

6.2 First-stage application of eFAST

The dataset was first prepared by excluding parameters other than those in Table 19 and by applying quality filters related to the following list of directly-measured quantities:

- Power
- Vertical wind speed at hub height
- Temperature, relative humidity and pressure at hub height
- Wind direction at hub height and rotor top
- Horizontal wind speed measurements at rotor bottom, hub height and rotor top

In addition, the data was quality filtered for the Obukhov stability parameter which is dependent on the measured fluxes of momentum and sensible heat. These criteria are more stringent than would normally be applied, but are needed to ensure that parameters such as REWS and the shear in the top half of the rotor cab calculated for all TMA records. This produced a maximally-populated grid of data values containing 2,818 TMA records with 74 columns representing the selected parameters. A set of 74 incommensurate frequencies was generated using the code in Appendix C. The eFAST method was applied as described in §3.5.3

6.2.1 ANN configuration

Through training the network following the procedure outlined in §3.4 and plotting the correlation between predicted and actual output values, it was found that the initial configuration of only eight hidden nodes was not capable of modelling the full range of output values. Incrementally increasing the number of nodes by a small amount was found to increase the coverage as illustrated in the correlation plots in Fig. 40.

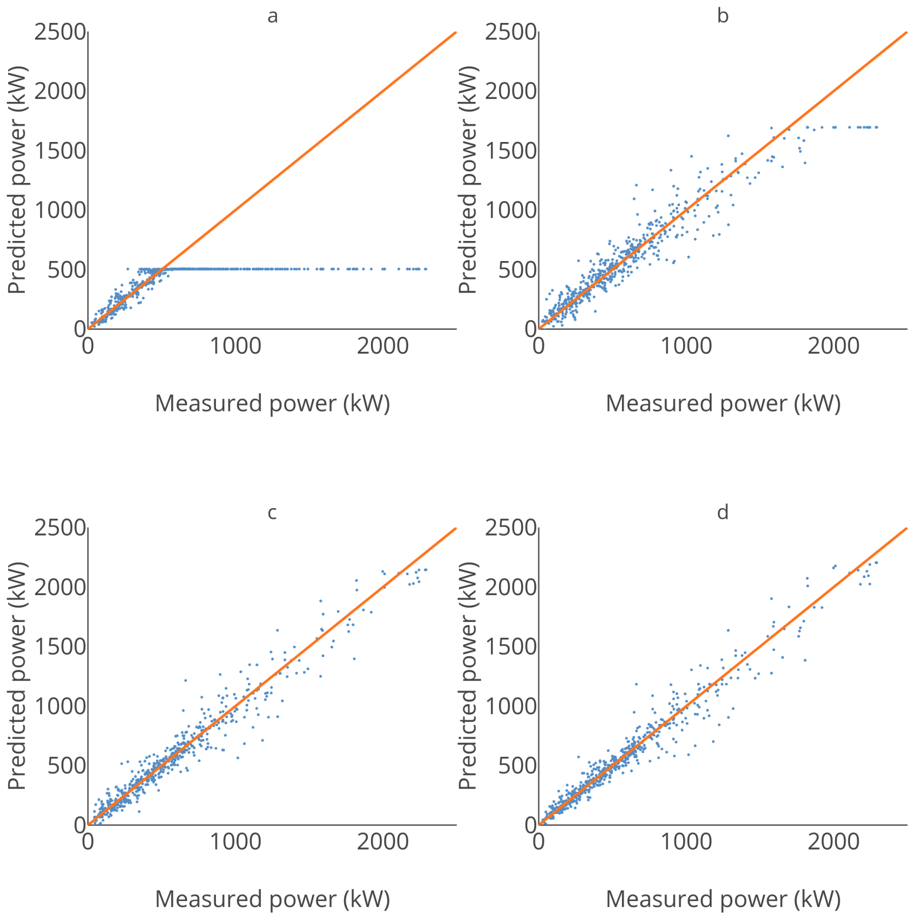

Figure 40: Truncation of the output from the ANN with too few training records. a: 8 nodes, b: 38, c: 128, d: 218

Examining the RMSE in the power output predicted by the ANN compared to the observed values, it was clear that after a large improvement in performance the accuracy gain above 120 nodes was marginal. On the other hand, it was observed that the required number of training epochs reached a local minimum at 218 nodes peaking again at around 300 nodes before falling at higher numbers. On the basis of these figures, shown in Fig. 41, the number of hidden nodes was set to 218.

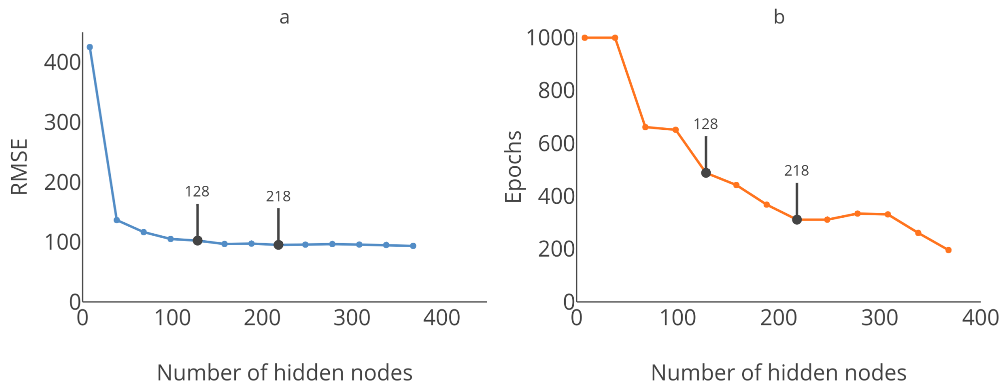

Figure 41: Performance and time to convergence of the ANN with different numbers of hidden nodes

6.2.2 *Initial results*

The spectrum of main parameter effects shown in the upper plot in Fig. 42 has the expected format. Parameters expected to make a large contribution to the variance in the power output have higher peaks than others. This is particularly true for the two highest peaks which correspond to the measured hub-height wind speed and REWS; however, this also illustrates the problem with multicollinearity. These parameters are highly correlated since REWS is calculated from the measured wind speed. That is to say, they represent the same physical phenomenon. In an optimum set of parameters, only one of the them would appear, ideally the one which explains the largest proportion of variance in the output. The other would be considered redundant from a mathematical point of view. The multicollinearity appears as unwanted interaction effects make up the difference between the main effect and the total effect of each parameter in the lower plot in Fig. 42.

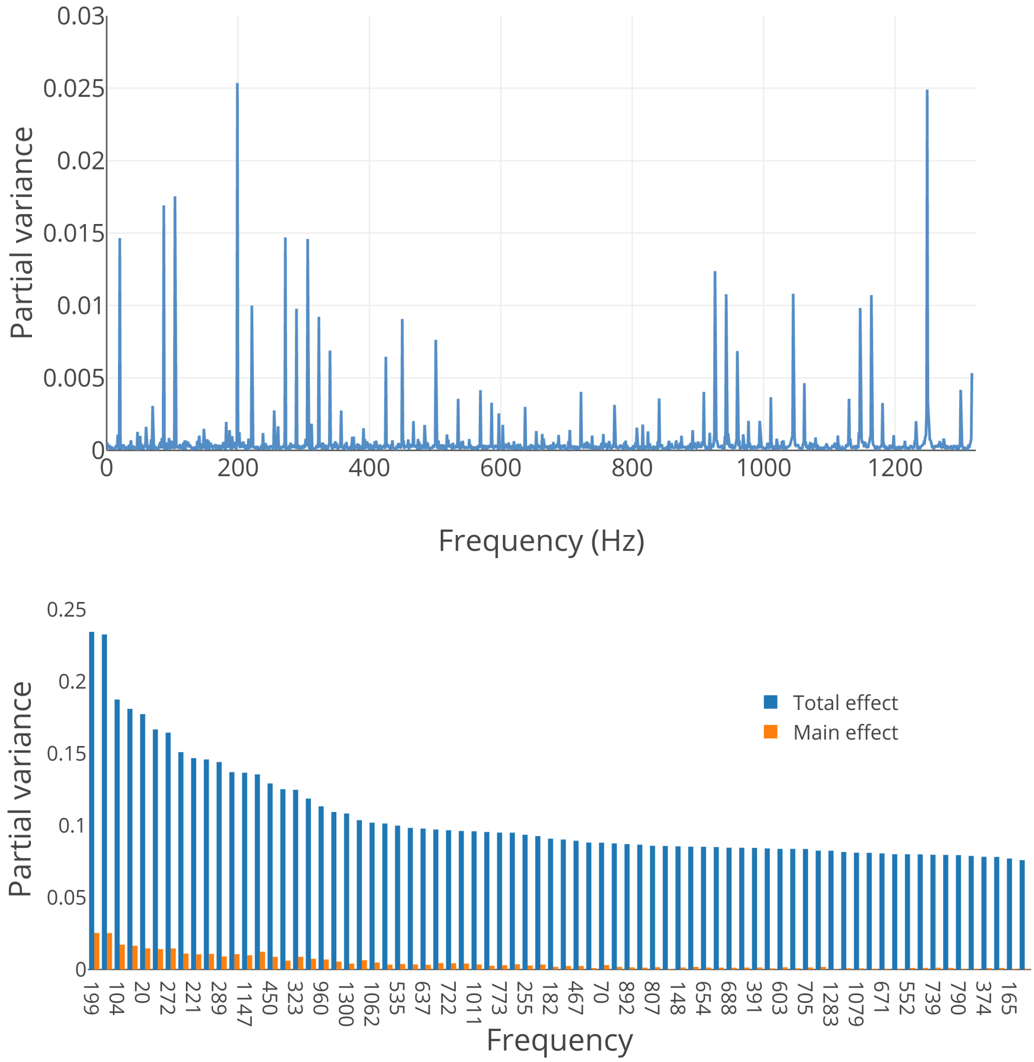

Figure 42: Main (top) and total (bottom) effects of initial set of 74 parameters

The partial variance due to a particular phenomenon is not apportioned linearly to parameters that are correlated. This can be seen in the upper plot in Fig. 43 which is the result of repeating the first trial but omitting REWS. The peak related to the measured hub-height horizontal wind has increased from approximately 0.024 to 0.041 while the sum of the partial variances due to the two wind speeds was approximately 0.049. Some of the other peaks in the spectrum also show a slight difference in amplitude which can be attributed to interactions with REWS in the first trial.

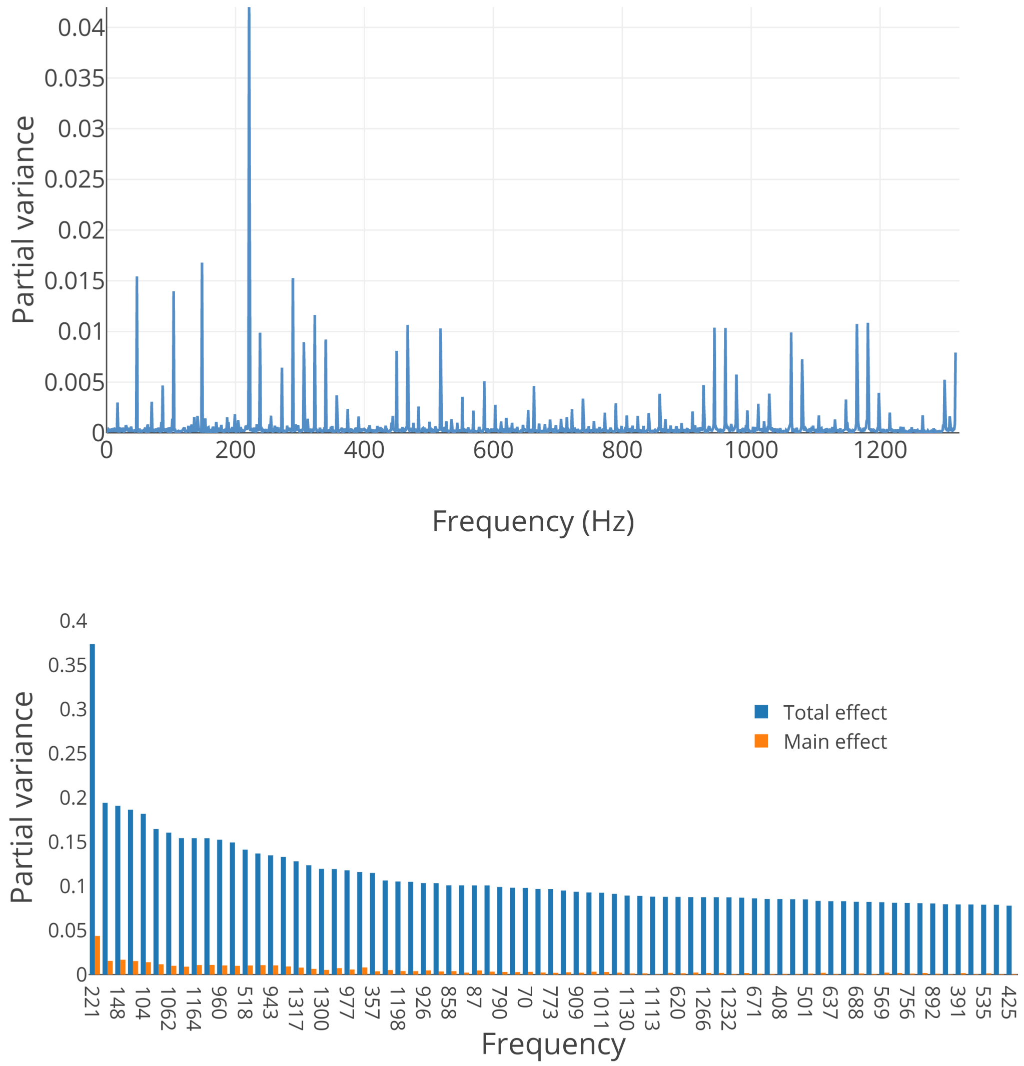

Figure 43: Main (top) and total (bottom) effects of initial set of parameters except REWS

The specific frequency values are different because of the exclusion of one of the input parameters

One approach to eliminating redundant parameters is to calculate a comprehensive set of pairwise correlations and where the correlation coefficient exceeds a certain threshold to eliminate one of the pair. This has the advantage of being a procedure amenable to automation, but is does not allow for the application of domain knowledge.

Table 20: Initial parameter set grouped by meteorological phenomenon

Phenomenon	Parameter
Horizontal wind speed	Mean measured hub-height wind speed, U Normalised hub-height wind speed REWS
Turbulence	Standard deviation of hub-height wind speed Coefficient of variation of U (turbulence intensity) 2nd order coefficient of variation of U Transience of U Intermittency of U Turbulence dissipation rate Turbulence length scale Turbulence kinetic energy (TKE)
Shear	Wind shear exponent (whole rotor) Wind shear exponent (lower half of rotor) Wind shear exponent (upper half of rotor) Wind speed ratio Horizontal wind speed at rotor top and bottom
Stability	Bulk Richardson number Obukhov stability parameter Lapse rate of measured temperature Lapse rate of potential virtual temperature Vertical flux of horizontal momentum Vertical flux of sensible heat
	Inflow angle
	ABL height
	Solar elevation
	Hour angle
Wind veer	Veer in degree per 100 m Cross-isobar angle
Mass flux	Air density Site-specific air density Pressure + temperature + relative humidity (means)
Seasonality	Solar declination

Most of the parameters in the initial set are intended as proxies for recognised meteorological phenomena such as turbulence or shear. Others such as the stationarity of relative humidity are more speculative and do not necessarily have a predetermined interpretation. An alternative approach would be to group the parameters according to their relationship with real phenomena and to define a minimal parameter set as one which contains one proxy measure from each group except the speculative inclusions. The approach is complicated for derived parameters such as REWS which is primarily a measure of horizontal wind speed, but which also incorporates shear and veer. The main issue, however, is the number of possible combinations of parameters that would need to be evaluated. Despite the fact that one parameter might be related to more than one phenomenon, Table 20 shows a rough grouping which would lead to 7,200 possible parameter subsets. A more pragmatic strategy is therefore needed.

6.3 Reducing the number of parameters

Examining Figs. 41 and 42, it is clear that there is a proportion of the parameter set that contribute relatively little to the variance in the output in terms of both main and total effects. With reference to the plots in Fig. 41 for example there are 21 parameters whose partial variance for their main effect is less than or equal to 0.001. At the other end of the scale, there are also 21 parameters with a partial variance of 0.005 or greater. The lower plot shows that the total effects for the top 21 parameters falls off relatively steeply while the total effects values for the bottom 21 parameters are all of a similar value. Simply dividing the parameter set in half according to their total effects retains those displaying a proportionally larger effect than the rest while allowing a wide tolerance to allow for slight variations in ordering between the main and total effects calculations. An interesting result of this approach is that all three variations of the wind shear exponent (whole-rotor, lower-half-rotor and upper-half-rotor) are excluded while the wind speed ratio is retained. Although more direct comparisons would be required for confirmation, this suggests that the wind speed ratio is more representative of the turbine inflow conditions than the simplified measure of the overall state of the ABL provided by the wind shear exponent. A maximal set of pairwise correlations is then generated for the remaining parameters which can be found in Appendix H. Highly correlated parameters ($|r^2| \geq 0.7$) are examined to decide which can be eliminated.

As a result of these steps, the 17 pairs of highly correlated parameters shown in Table 21 were identified. It is clear that several of the correlations arise because the parameters are alternative indicators of the same meteorological phenomenon. The parameters in rows 3 – 7 and 14 for example are all related to atmospheric stability, while rows 8 – 13 and 15 are related to turbulence. The parameters in rows 1, 2 and 17 are highly correlated because the potential virtual temperature and density are calculated from the measured temperature. REWS is similarly a modification of the measured wind speed which accounts for row 16; however, REWS is a special case since it also includes information about shear and veer. In all cases, there is clearly significant multicollinearity and the several of the parameters can be eliminated.

Table 21: Highly-correlated parameters in the reduced set

	Parameter 1	Parameter 2	r^2
1	Potential virtual temperature	Density	-1.00
2	Measured temperature	Density	-0.99
3	Turbulence kinetic energy	Momentum flux	-0.92
4	Wind speed standard deviation	Momentum flux	-0.87
5	Transience of vertical wind speed	Momentum flux	-0.78
6	Lapse rate of potential virtual temperature	Bulk Richardson number	-0.75
7	Lapse rate of measured temperature	Bulk Richardson number	-0.71
8	Transience of horizontal wind speed	Transience of vertical wind speed	0.70
9	Wind speed standard deviation	Turbulence length scale	0.71
10	Wind speed standard deviation	Transience of vertical wind speed	0.80
11	Transience of vertical wind speed	Turbulence kinetic energy	0.86
12	Transience of horizontal wind speed	Turbulence dissipation rate	0.92
13	Wind speed standard deviation	Turbulence kinetic energy	0.94
14	Lapse rate of potential virtual temperature	Lapse rate of measured temperature	0.96
15	Coeff. of variation of vertical wind speed	Vertical turbulence dissipation rate	0.98
16	Measured wind speed	REWS	0.99
17	Measured temperature	Potential virtual temperature	1.00

In general, the simpler parameter is retained. For example, measured parameters are preferred over derived ones and parameters based on one-dimensional measurements are preferred to those that require three-dimensional measurements. Table 22 lists the parameters retained in this exercise as well as those excluded. An interesting case concerns the air density which is excluded from the set of parameters. This is not to suggest that density is not significant in terms of the physical operation of the turbine; rather, it reflects the fact that temperature is the most significant element in the calculation of density (Pandit et al., 2019) and that therefore variations in temperature cause parallel fluctuations in density. Only one of these parameters is therefore required from a mathematical point of view to explain the corresponding variation in the power output.

Table 22: Parameters retained and excluded after correlation analysis

Retained	Excluded
Measured temperature	Potential virtual temperature
Lapse rate of measured temperature	Lapse rate of potential virtual temperature
Measured wind speed	Turbulence dissipation rate
Wind speed standard deviation	Turbulence length scale
Transience of horizontal wind speed	Transience of vertical wind speed
Coeff. of variation of vertical wind speed	Vertical turbulence dissipation rate
	Turbulence kinetic energy
	Momentum flux
	Bulk Richardson number
	Density

The correlation analysis did not show a high correlation between the coefficient of variation of vertical wind speed and the corresponding second-order coefficient of variation even though this might have been expected. The poor correlation stems from the behaviour of the coefficient of variation at low values. Since it becomes undefined when vertical wind speed is zero, there are extremely large spikes in value when the vertical wind speed is between -1 and 1. The behaviour of the second-order coefficient of variation on the other hand is much more stable as shown in Fig. 44 although it saturates at its maximum value of 1. While not relevant in most other cases, this nevertheless demonstrates the value of using the second-order coefficient, and the coefficient of variation of vertical wind speed is therefore excluded.

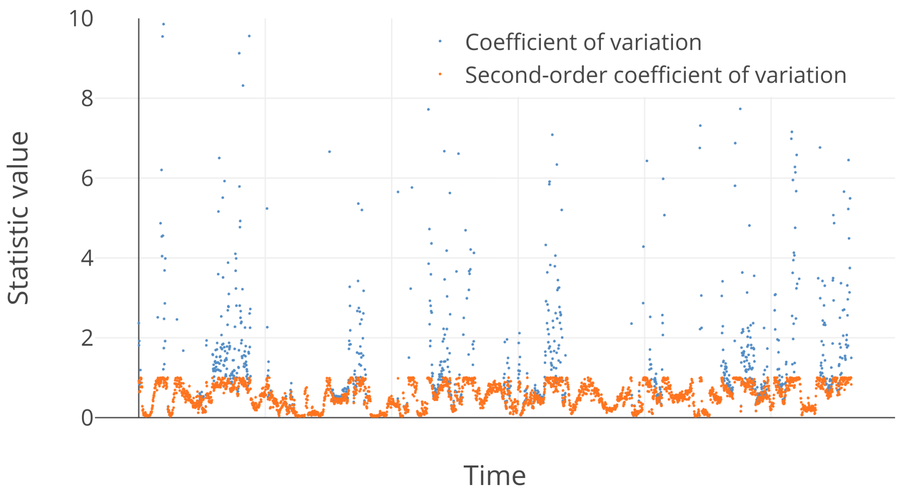

Figure 44: First- (blue) and second-order (orange) coefficients of variation of vertical wind speed

Although some other parameters are known to be correlated (Belu & Koracin, 2012; Eecen et al., 2011), the correlation analysis performed here shows that their correlation coefficients are less than 0.7 and they are therefore retained in the parameter set. Thus, not all multicollinearity is eliminated and it is expected that the total effects will still be considerably larger than the main effects with the reduced set of parameters. However, the lower values of the correlation coefficients show that the remaining parameters all contribute to the variance in the output power in their own right. The remaining parameters, listed in Table 23, are examined again using the eFAST method to reveal those having the most significant effect on the variance of the output power. The exercise is carried out first using the measured wind speed and a second time using REWS.

Table 23: Remaining 27 parameters after correlation analysis

Base parameter	Parameter
Horizontal hub-height wind speed	Mean
	Standard deviation
	Intermittency
	Transience
	Stationarity (ADF)
	Normality
Vertical hub-height wind speed	Mean
	2^{nd} order coeff. of variation
	Intermittency
	Stationarity (ADF)
	Normality
Temperature	Mean
	Transience
	Stationarity (KPSS)
	Normality
	Lapse rate
Pressure	Transience
	Normality
Relative humidity	Mean
	Transience
Solar declination	
Vertical flux of sensible heat	
Wind speed ratio	
Wind veer at hub height	
ABL height	
Obukhov stability parameter	
REWS	

6.4 Second-stage application of eFAST

The eFAST algorithm was applied to the reduced parameters set excluding REWS, and then again including REWS but excluding the measured wind speed. The results in Fig. 45 are consistent across the two cases with the same parameters showing prominent peaks. Those whose amplitude exceeds 0.01 are labelled in the figure. The only major difference between the two plots concerns the standard deviation of measured wind speed which drops below 0.01 in the REWS plot. Although standard deviation of wind speed is usually considered an indicator of turbulence, and is integral to the calculation of turbulence intensity, the much larger peak related to the transience of wind speed suggests that it may be a better measure. However, when total effects are considered, the standard deviation of wind speed remains significant due to its interactions.

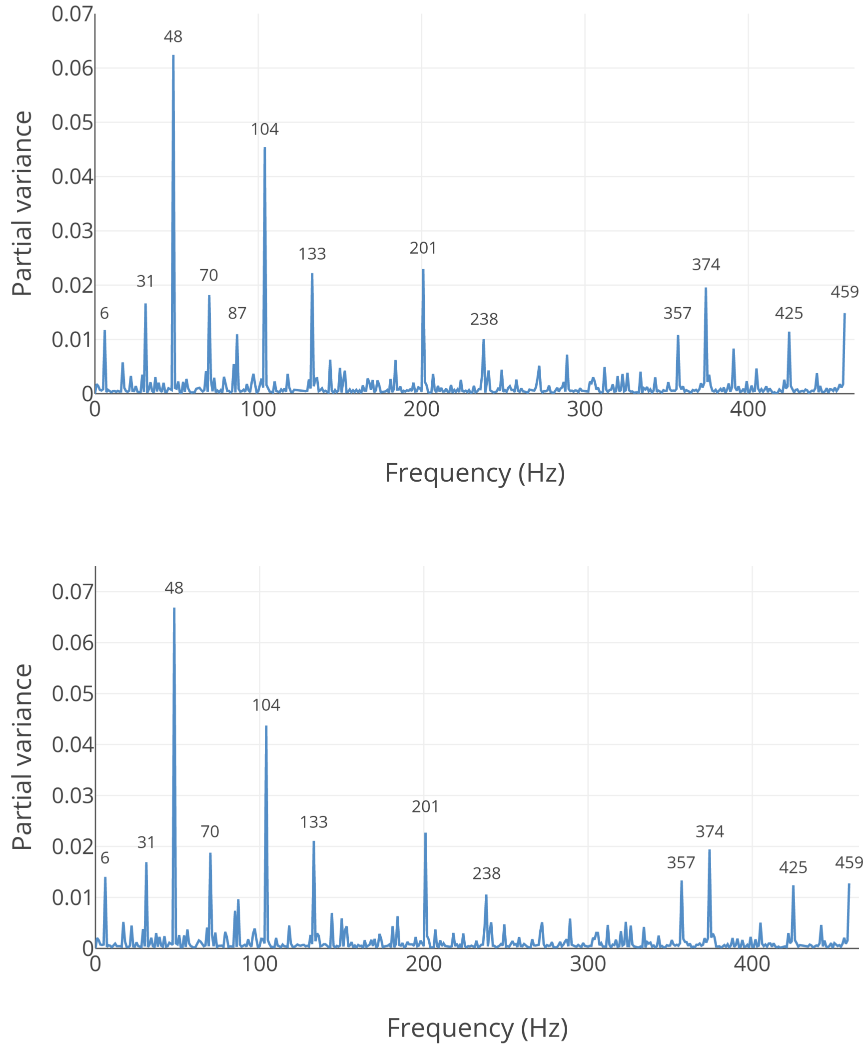

Figure 45: Main effects of reduced set of parameters using the measured wind speed (top) and REWS (bottom) Labelled frequencies are 6: stationarity of wind speed, 31: intermittency of wind speed, 48: wind speed, 70: normality of wind speed, 87: standard deviation of wind speed, 104: transience of wind speed, 133: stationarity of vertical wind speed, 201: normality of vertical wind speed, 238: temperature, 357: sensible heat flux, 374: Obukhov stability parameter, 425: environmental lapse rate, 459: ABL height

Taking 0.01 as the threshold yields a set of 11 parameters other than wind speed which appear to have a significant impact on the variance of the power output. These are shown in bold and in descending order of main effect in Table 24.

Table 24: Reduced set of parameters in descending order of main effect.

Frequency	Parameter	Main effect	Total effect
48	**Mean horizontal wind speed/REWS**	**0.0669**	**0.4434**
104	**Transience of horizontal wind speed**	**0.0437**	**0.3456**
201	**Normality of vertical wind speed**	**0.0227**	**0.2836**
133	**Stationarity of vertical wind speed (ADF)**	**0.0211**	**0.2721**
374	**Obukhov stability parameter**	**0.0194**	**0.2519**
70	**Normality of horizontal wind speed**	**0.0188**	**0.2463**
31	**Intermittency of horizontal wind speed**	**0.0169**	**0.2394**
6	**Stationarity of horizontal wind speed (ADF)**	**0.0140**	**0.2343**
357	**Sensible heat flux**	**0.0133**	**0.2184**
459	**ABL height**	**0.0128**	**0.2170**
425	**Environmental lapse rate**	**0.0124**	**0.1981**
238	**Mean temperature**	**0.0106**	**0.1906**
87	Standard deviation of horizontal wind speed	0.0097	0.1983
184	Mean vertical wind speed	0.0063	0.1804
150	Coefficient of variation of vertical wind speed	0.0059	0.1754
289	Normality of pressure	0.0059	0.1803
323	Mean relative humidity	0.0052	0.1812
272	Transience of temperature	0.0051	0.1828
442	Solar declination	0.0046	0.1713
218	Stationarity of temperature (KPSS)	0.0030	0.1719
306	Transience of pressure	0.0030	0.1775
391	Wind speed ratio	0.0019	0.1679
408	Wind veer	0.0008	0.1624
167	Intermittency of vertical wind speed	0.0007	0.1609
255	Normality of temperature	0.0007	0.1707
340	Transience of relative humidity	0.0006	0.1636

Direct measures of wind shear are conspicuously absent from the final set of parameters that result from the second sensitivity analysis. However, the list does include a major indicator of atmospheric stability. Since shear is greatly affected by stability, it is possible that the information normally present in the wind shear exponent is carried here by the Obukhov stability parameter. The list also contains various characteristics of the vertical wind speed which could also account for some of the information content of the wind shear exponent. Establishing the validity of these conjectures would require additional investigation.

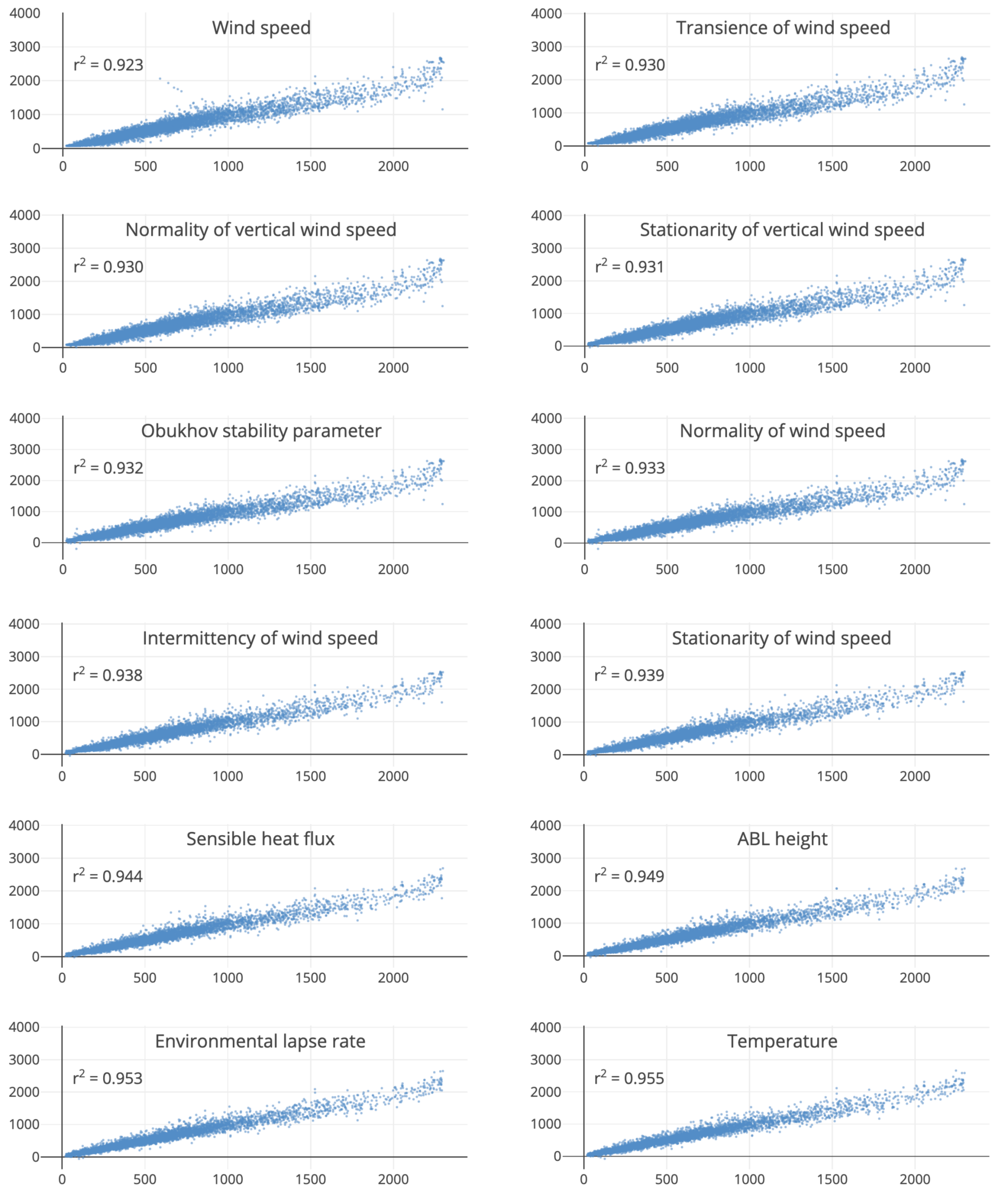

Figure 46: Third-order polynomial regression on a progressively larger set of parameters
The plots are cumulative so that moving from left to right and downwards, the title indicates the next parameter to be added. E.g. The top-right plot includes both wind speed and transience of wind speed

The adequacy of the set of selected parameters was tested by performing a multivariate third-order polynomial regression on a progressively larger subset starting with just the mean horizontal wind speed. The results in Fig. 46 show the coefficient of variation increasing from 0.923 to 0.955 as each additional parameter is included. The regression exercise is a verification exercise only. With 12 parameter including wind speed, a third order polynomial requires 1,820 coefficients which would make such a model impractical to use.

6.5 Comparator power curves

Two comparator power curves are created as described in §3.5.6. The *baseline power curve* has only quality filters applied while the *contractual power curve* is also filtered for TI and shear. The curves are created according to the methodology defined in IEC2017 using values normalised to site-specific density which is found to be 1.188 kg m^{-3}. Data for sea-level normalisation and additional detail as might be produced in a PPT report are provided in Appendix A.

6.5.1 Data selection

To replicate the contractual filters in a commercial PPT process, the following limits were adopted for turbulence intensity, TI, and wind shear, α:

$$0.06 < TI < 0.2$$

$$0 < \alpha < 0.3$$

Table 25 summarises the quality and contractual filters applied and the resulting number of records lost. It is common practice to rely solely on the anemometer fault code to identify and remove spikes from measured data. Here, the more stringent approach of applying a median filter is employed, along with the requirement that no more than 1% of the expected data may be removed. On the other hand, a TMA value is accepted as valid if it is based on 90% or more of the expected raw data points. This is less strict than the usual practice in PPT which requires 100%. However, it is used here to preserve a greater number of TMA records for analysis. The invalid power values are primarily the result of curtailment. The counts shown are cumulative and are dependent on the order in which the filters were applied.

Table 25: Data lost through application of quality and contractual filters

Filter type	Filter	Excluded	Remaining
Quality	Valid power values	39932	12628
Quality	Power count > 90%	1461	11167
Quality	Power spikes < 1%	1106	10061
Quality	Valid temperature values	1	10060
Quality	Temperature count > 90%	138	9922
Quality	Temperature spikes < 1%	35	9887
Quality	Valid pressure values	1	9886
Quality	Pressure count > 90%	25	9861
Quality	Pressure spikes < 1%	19	9842
Quality	Excluded sector	1889	7953
Quality	Icing	605	7348
Contractual	Turbulence intensity	2569	4779
Contractual	Shear exponent	2034	2745

After application of the quality filters, 7,348 records remain out of a possible 52,560 which equates to 14%. The majority of this data loss is due to curtailment of the turbine. Of the remaining valid data, only 2,745 records remain after application of the contractual filters which equates to 37% or in other words, a loss of 63%.

6.5.2 Quantity of data

Due to the moderate winds at the site, rated wind speed of 15 ms^{-1} is exceeded by only four TMA records. The maximum power output of 2361 kW achieved in 2017 is considerably lower than the rated value of 2,500 kW. According to the standard, the database should consist of 180 hours of data in total (1080 TMA records), and each wind speed bin must contain at least 30 minutes (three TMA values). The collected data should cover the whole wind speed range either up to 1.5 times the wind speed value at

85% of rated power, or until the measured AEP is greater than or equal to 95% of the AEP extrapolated from the highest measured wind speed bin up to cut-out. The procedure allows for one incomplete bin to be interpolated from the values on either side. For the Eolos turbine, this means that all bins should be complete from 3 ms^{-1} (0.5 ms^{-1} below cut-in) up to 16.5 ms^{-1}. In fact, the data only covers bins up to 14.5 ms^{-1}. Calculated AEP values are therefore likely to be lower than might be expected for a 2.5 MW turbine.

The PPT results reviewed in Chapter 3 include several examples of databases that are incomplete according to the standard. This can happen, for example, when the warranty period expires before sufficient data has been collected. In such cases, the parties involved negotiate a way forward. For example, a more relaxed set of filters can be agreed which allow data to be included which would normally be rejected. An incomplete database therefore does not in practice prevent a test from being completed.

6.5.3 Uncertainty analysis

Uncertainties are calculated for each wind speed bin based on the recommendations in IEC2017. Table 26 summarises the category B uncertainties that need to be considered with respect to the Eolos turbine. Where insufficient data is available to identify a precise value, one has been estimated with reference to similar installations in real PPT projects.

Table 26: Uncertainty calculations

Source of uncertainty	Value	Sensitivity
Electrical power output		
Current/voltage transformers	$0.004 * P_i/\sqrt{3}$	1
Power transducer	$0.005 * P_{rated}/\sqrt{3}$	
DAQ	$0.001 * P_{rated}/\sqrt{3}$	
Wind speed (sonic)		
Calibration	$0.005/\sqrt{3}$	For power curve: $\frac{1}{2}\left(\frac{(P_{i+1}-P_i)}{(U_{i+1}-U_i)}+\frac{(P_i-P_{i-1})}{(U_i-U_{i-1})}\right)$
Mounting effects (side mounted)	$0.015 * U_i/\sqrt{3}$	
DAQ	$0.001 * U_{range}/\sqrt{3}$ U_{range} = 131 ms^{-1}	For AEP: $\frac{(P_i-P_{i-1})}{(U_i-U_{i-1})}$
REWS		
Wind shear measurement		As for wind speed
Wind veer measurement		
Air temperature		
Sensor	$0.15°C/\sqrt{3}$	$-\frac{c_{Ui}U_i}{3\rho_i}\left(\frac{\rho_i}{T_i}+\frac{\phi_i}{T_i}\left(\frac{1}{R_0}-\frac{1}{R_w}\right)a.\exp(bT_i)\right)$
Radiation shielding	$2°C/\sqrt{3}$	
Mounting effects	$0.3°C/\sqrt{3}$	
DAQ	$0.001 * T_{range}/\sqrt{3}$ T_{range} = 80ºC	$a = 0.0000205$ $b = 0.0631846$ c_{Ui} = wind speed sensitivity ϕ_i = relative humidity
Air pressure		
Sensor	$3\ hPa/\sqrt{3}$	$\frac{c_{Ui}U_i}{3\rho_i T_i R_0}$
DAQ	$0.1\ hPa/\sqrt{3}$	
Relative humidity		
Sensor	$0.02 * RH/\sqrt{3}$	$-\frac{c_{Ui}U_i}{3\rho_i T_i}\left(\frac{1}{R_0}-\frac{1}{R_w}\right)a.\exp(bT_i)$
Mounting effects	$0.0015 * RH/\sqrt{3}$	
DAQ	$0.001 * RH_{range}/\sqrt{3}$	$a = 0.0000205$ $b = 0.0631846$
Flow distortion (no site calibration)	$0.02 * U_i/\sqrt{3}$	As for wind speed
Method		
Air density correction	$abs(\rho-\rho_{corr})/2$	As for wind speed
Inflow angle	$0.001 * U_i/\sqrt{3}$	
Missing turbulence normalisation	$2\sigma_i/\sqrt{3}$	
Seasonal effects	$0.007 * U_i/\sqrt{3}$	

6.5.4 *Measured power curves*

The baseline power curve and power coefficient presented in the top panel of Fig. 47 are based on the data in Table 27. The contractual power curve and power coefficient presented in the bottom panel of Fig. 47 are based on the data in Table 28. In the filtered data, the 13 ms^{-1} wind speed bin has only two TMA records and is therefore interpolated.

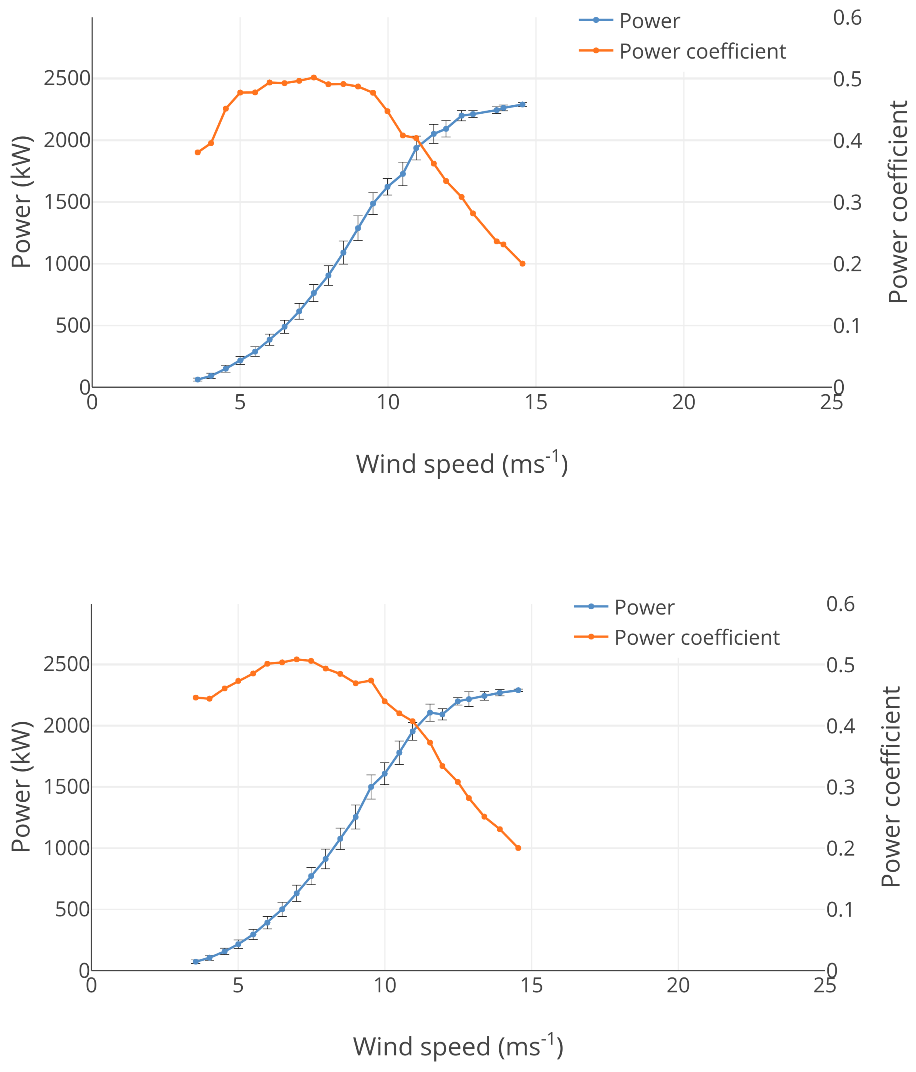

Figure 47: Measured baseline (top) and contractual (bottom) power curves and power coefficients

Table 27: Baseline power curve data

Wind speed (ms-1)	Active power (kW)	Power coefficient	Records per bin	Category A uncertainty (kW)	Category B uncertainty (kW)	Combined uncertainty (kW)
3.58	62.77	0.39	162	2.89	12.15	12.49
4.02	98.57	0.43	377	2.42	21.97	22.10
4.51	154.01	0.47	616	1.99	28.65	28.72
5.01	223.81	0.50	715	2.45	33.56	33.65
5.51	298.85	0.50	811	2.27	39.72	39.78
5.99	396.63	0.52	871	2.85	47.28	47.36
6.50	504.25	0.51	924	3.09	55.30	55.38
7.00	635.98	0.52	758	4.28	65.46	65.60
7.49	781.82	0.52	641	5.75	70.84	71.07
7.98	930.24	0.51	464	7.88	83.26	83.63
8.48	1122.91	0.51	344	10.50	96.46	97.03
8.98	1321.74	0.51	219	16.42	96.76	98.14
9.49	1510.84	0.49	145	21.09	85.88	88.43
9.98	1658.20	0.46	91	23.24	68.31	72.15
10.49	1777.32	0.43	73	36.83	81.30	89.25
10.95	1947.05	0.41	37	48.29	66.39	82.09
11.54	2022.46	0.36	28	62.50	64.64	89.91
12.04	2196.15	0.35	13	20.01	52.96	56.62
12.54	2208.60	0.31	14	20.80	19.17	28.29
12.80	2173.10	0.29	6	43.38	10.74	44.69
13.61	2244.78	0.25	7	11.64	24.57	27.19
13.92	2270.82	0.23	5	17.00	20.91	26.95
14.48	2286.65	0.21	5	1.04	12.19	12.23

Table 28: Contractual power curve data

Wind speed (ms-1)	Active power (kW)	Power coefficient	Records per bin	Category A uncertainty (kW)	Category B uncertainty (kW)	Combined uncertainty (kW)
3.56	72.31	0.45	18	6.48	11.93	13.57
4.02	104.57	0.44	97	3.66	19.34	19.68
4.54	156.29	0.46	206	3.14	25.18	25.37
5	215.09	0.47	253	3.95	32.4	32.64
5.51	294.17	0.49	282	3.87	40.46	40.64
5.99	390.47	0.5	296	5.31	47.16	47.46
6.5	499.6	0.5	299	5.86	55.28	55.59
6.99	629.92	0.51	238	8.22	62.72	63.26
7.49	770.08	0.51	244	9.97	68.18	68.9
7.98	910.52	0.49	194	11.79	75.54	76.45
8.48	1074.52	0.49	143	15.62	80.3	81.81
9	1251.78	0.47	133	20.1	101.51	103.48
9.53	1496.96	0.47	90	25.22	88.56	92.08
9.99	1604.85	0.44	79	25.01	76.75	80.72
10.49	1776.45	0.42	55	30.2	98.49	103.02
10.94	1950.1	0.41	42	33.96	85.95	92.42
11.54	2102.91	0.37	22	30.48	33.91	45.59
11.96	2088.99	0.33	16	49.05	25.68	55.37
12.49	2195.21	0.31	12	22.28	36.76	42.98
12.86	2212.93	0.28	10	26.83	15.25	30.86
13.39	2238.91	0.25	2	23	16.57	28.35
13.92	2264.9	0.23	5	15.37	15.1	21.55
14.55	2285.46	0.2	5	1.39	13.13	13.2

6.5.5 *Annual Energy Production*

Estimates of AEP are presented in Table 29 for the baseline power curve and in Table 30 for the contractual power curve. The final row in each table shows the site-specific AEP calculated using the Weibull shape and scale parameters found in §6.1.5 and this is the value that is used later for comparison with experimental filters. The value for the site-specific measured AEP for the filtered data represents 95.49% of the theoretical figure of 4677 MWh/year obtained using the reference power curve and the Weibull parameters from §6.1.5. The turbine would therefore pass the IEC performance test.

Table 29: Calculated AEP for the baseline power curve

Wind speed (Rayleigh) (ms^{-1})	AEP measured (MWh/year)	Standard uncertainty in AEP (MWh/year)	Standard uncertainty in AEP %	AEP extrapolated (MWh/year)	Status
4	1753	17	0.97	1753	Complete
5	3287	24	0.73	3313	Complete
6	4914	29	0.59	5112	Complete
7	6247	34	0.54	6921	Incomplete
8	7105	36	0.51	8588	Incomplete
9	7504	37	0.49	10031	Incomplete
10	7554	37	0.49	11207	Incomplete
11	7371	35	0.47	12095	Incomplete
Weibull	4425	30	0.41	4448	Complete

Table 30: Calculated AEP for the filtered power curve

Wind speed (Rayleigh) (ms^{-1})	AEP measured (MWh/year)	Standard uncertainty in AEP (MWh/year)	Standard uncertainty in AEP (%)	AEP extrapolated (MWh/year)	Status
4	1787	18	1.01	1787	
5	3324	25	0.75	3350	
6	4955	29	0.59	5153	
7	6291	32	0.51	6964	Incomplete
8	7150	34	0.48	8633	Incomplete
9	7550	33	0.44	10077	Incomplete
10	7599	32	0.42	11252	Incomplete
11	7414	31	0.42	12138	Incomplete
Weibull	4466	31	0.42	4488	

6.5.6 Dispersion

The root mean square error (RMSE) is calculated to reflect the dispersion in the power curve point cloud as described in §3.4.2. This provides the final characteristic on which the power curves are to be compared along with the AEP estimate, data loss and consequent minimum duration. The results summarised in Table 31 show that although the uncertainty calculated using the IEC2017 methodology is practically the same in the baseline and filtered cases, the data dispersion represented by the RMSE actually increases when the filters are applied. In addition, over half of the data is excluded by the filters which nearly triples the minimum duration calculated using Eq. 49.

Table 31: Results for baseline and contractual power curves

Case	Data loss	Duration (days)	AEP estimate	Uncertainty	RMSE
Baseline	0%	7.5	4425	30	119.8
Filtered	63%	20.3	4466	31	130.3
TI only	32%	11.0	4454	30	116.4
Shear only	50%	15.0	4553	30	132.3

The table also includes the results of applying the TI and shear filters in isolation. Both remove significant data and increase the minimum duration of the test. Both also increase the estimate of AEP compared to the baseline and in combination the increase is slightly larger again. Although without a reliable benchmark it is not possible to say with certainty whether a higher or lower AEP estimate is the more accurate, the value related to the contractual power curve will be used in the following sections for comparison with alternative filtering strategies. This is based on the premise that the filters currently used in PPT projects have been shown through experience to yield more accurate results than unfiltered data.

On its own, the TI filter reduces the dispersion in the power curve by a small amount, but the shear filter increases it by over 10%. There are clearly compensatory effects at work when the two are used in combination. The two filters target TMA records with opposing characteristics as demonstrated in Fig. 48 which colour-codes the points by atmospheric stability and wind speed. The points in the shaded area in each plot are excluded by the combination of both filters leaving only those within the rectangular area at the bottom left. Thus, unstable conditions and higher wind speeds are over-represented in the filtered data. Because higher wind speeds tend to suppress other meteorological phenomena (Bunse & Mellinghoff, 2008; Deola, 2010; Ernst & Seume, 2012; K. Y. Lee et al., 2017), the shear filter suppresses considerable variation in other parameters; however, in this respect it is a blunt tool. A more discerning approach that defined filters based on other parameters might be able to target specific variations more precisely which could lead to less data being excluded.

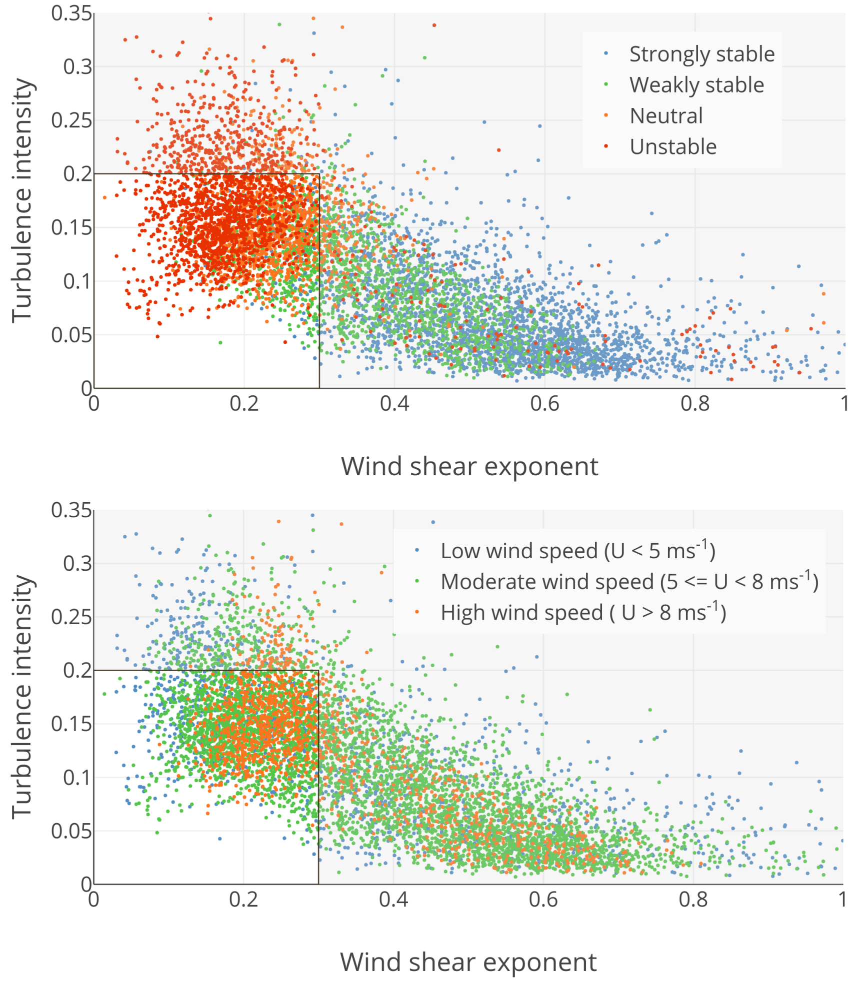

Figure 48: Data excluded by the combined effect of TI and shear filters coloured by atmospheric stability (top and wind speed (bottom)

The tendency of the TI filter to reduce the dispersion can be partly explained with reference to the disposition of the rejected points in the power curve scatter plot. As shown in Fig. 49, the TI filter rejects points towards the periphery of the point cloud while the shear filter rejects points closer to the centre. The ideal filter would operate only on the periphery, leaving the points closest to the measured power curve line in place.

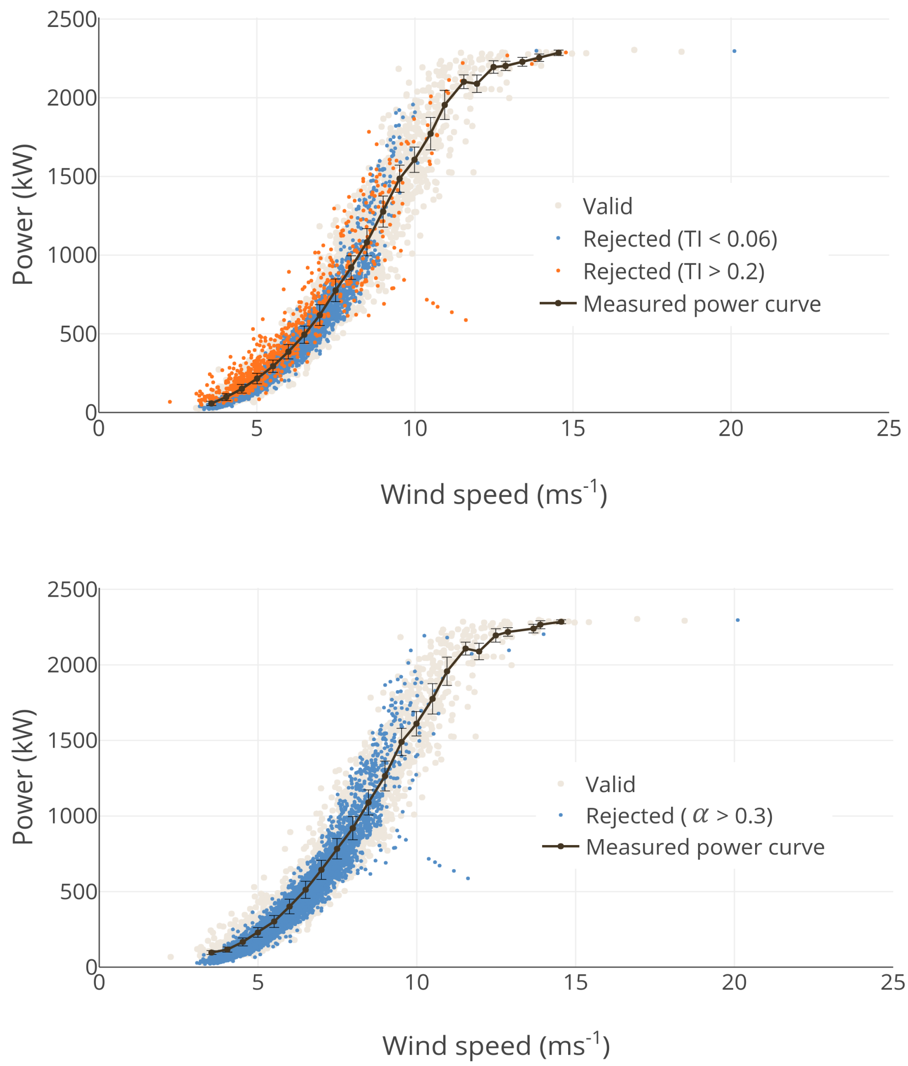

Figure 49: Disposition in the power curve of the points rejected by the TI (top) and shear (bottom) filters

6.5.7 Comment on IEC2017

The updated standard for power performance testing inherits methods from the earlier edition to compensate for differences in air density and for flow distortion caused by complex local topography. The new rotor equivalent wind speed method compensates for wind shear and veer, and the turbulence normalisation procedure corrects distortions introduced into the measured power curve by bin averaging. The exercise in this chapter has illustrated some of the limitations of the standard and its component methods. Turbulence normalisation for example was not possible since rated wind speed was not achieved in the measured dataset. This could be dismissed as a mismatch between the turbine and the location: a turbine with a taller tower would have benefitted from higher mean wind speeds and would therefore have reached rated power output more often. Similarly, a turbine with a lower rated power and wind speed could have been placed at the same height and reached maximum output even in the modest wind regime prevalent in Minnesota. Such arguments do not, however, detract from the observation that there are circumstances in which the turbulence normalisation technique cannot be used.

REWS promises a more reliable accommodation of shear and veer. Essentially a finite-element approach, the more vertical measurements there are available, the more accurate the approximation of the total energy flux becomes. A disadvantage of the technique is the increase in complexity with respect to the estimation of uncertainty in the measured power curve and AEP. The set of uncertainties applicable to the Eolos case shown in Table 26 illustrates some of that complexity. In IEC2017, Annex E which defines the approach to the estimation of uncertainty runs to 40 pages out of 262, up from 10 out of 90 in the previous version. That constitutes an absolute increase of 300% and a relative increase of 4% (15% of the total number of pages compared to 11% in the earlier edition). Of the additional pages, more than 18 are related to the category B uncertainties around the application of REWS as listed below. Although the number of pages is a crude measure at best, the increase in complexity is clear.

- §E.7: Remote sensing devices (RSD): ~4 pages
- §E.8: REWS: ~2 pages
- §E.11.2.2.3: Evaluation of shear across the whole rotor: ~0.5 pages
- §E11.2.3.4: Evaluation of veer across the whole rotor: ~0.5 pages
- §E.12.3: Wind direction measured by RSD: ~1 page
- §E.13.5: Wind speed measurement by RSD: ~0.5 pages
- §E.13.6: Wind speed measurement by REWS: ~ 10 pages

Because of the complexity of the calculations involved in the standard, a common interpretation cannot be taken for granted. For example, MEASNET pointed out an ambiguity with respect to the calculation of measured AEP in 2014 and the same wording persists in the new edition (MEASNET, 2014). Recent round robin trials conducted by the Power Curve Working Group (PCWG) have also revealed discrepancies in the results obtained by different organisations when applying the new edition of the standard to the same test datasets (Parkhe, 2016; Simmons, 2016; Stuart, 2013). In addition, while the standard mandates that incomplete bins are reported in the AEP results, there is no guidance on how this should be interpreted.

6.6 Evaluation of novel filtering strategies

IEC2017 provides detailed guidelines for calculating the uncertainty in the power curve and AEP. However, the method does not account for the full range of dispersion evident in the cloud of data points that make up the power curve. Fig. 50 makes this clear by comparing the calculated uncertainty in the filtered power curve described in §6.5 with the actual spread of data represented by the interquartile range.

Despite having been filtered for TI and shear, there are clearly other influences affecting the variance of the power output. Some of the apparent variance will be due to stochastic variations in the meteorological input to the turbine, the mechanical operation of the turbine components and turbine electronics. However, it is also possible that there exist systematic dependencies other than those already captured by IEC2017 that affect the dispersion of the power output values. The sensitivity analysis conducted in §6.4 provides a set of 11 parameters that are candidates for filter criteria. This section reports on the application of the methods described in §3.5.6 and §3.5.7.

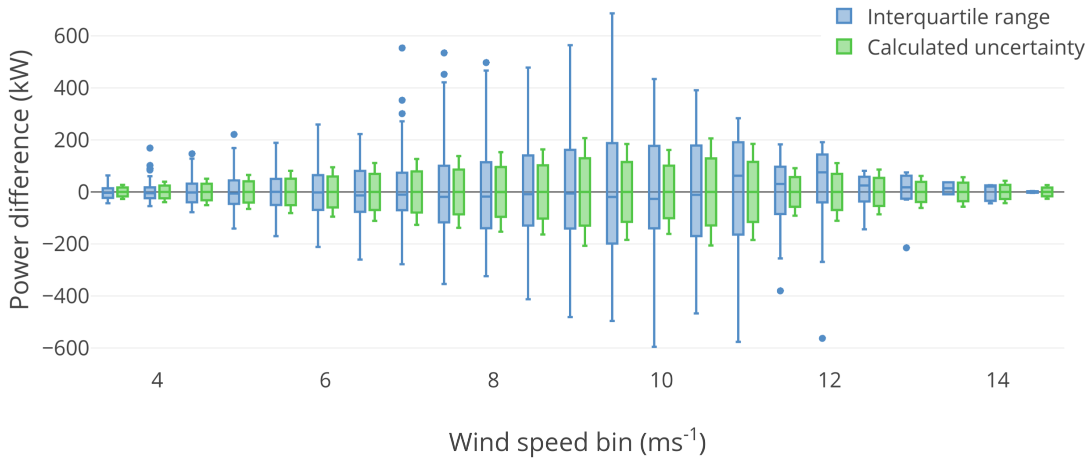

Figure 50: Comparison between the calculated uncertainty in the power curve and the actual spread of the data

6.6.1 *Filter definition*

Following the methods described in §3.5.7, the first step in creating experimental filters from the parameters identified in §6.4 is to fit a Pearson type III distribution to the data to identify appropriate lower and upper bounds. The results of this exercise are shown in Fig. 51 with the data presented in Table 32 in descending order of total effect.

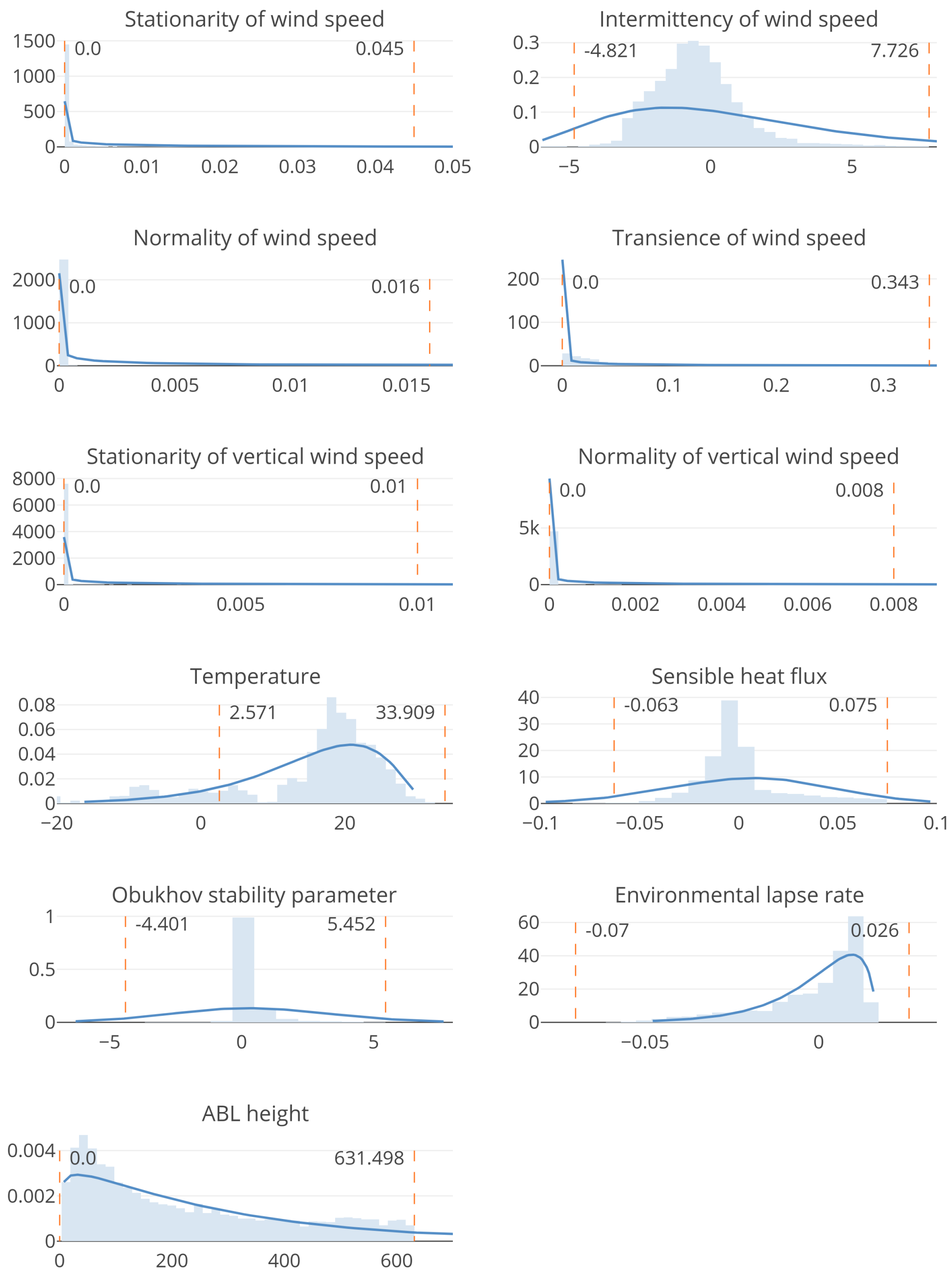

Figure 51: Pearson type III fits for the 11 parameters

The upper and lower limits of the related filters calculated from the 5th and 95th percentiles of the distribution are shown as vertical dashed orange lines labelled with their numerical values.

Table 32: Initial filter specifications

Name	Symbol	Total effect	Lower bound	Upper bound
Transience of wind speed (m^2s^{-2})	τ_U^2	0.3456	0.000	0.343
Normality of vertical wind speed	n_z	0.2836	0.000	0.008
Stationarity of vertical wind speed	a_z	0.2721	0.000	0.010
Obukhov stability parameter	ζ	0.2519	-4.401	5.452
Normality of wind speed	n_U	0.2463	0.000	0.016
Intermittency of wind speed	i_U	0.2394	-4.821	7.726
Stationarity of wind speed	a_U	0.2343	0.000	0.045
Sensible heat flux ($W\ m^{-2}$)	Q	0.2184	-0.063	0.075
ABL height (m)	h	0.2170	0.000	631.498
Environmental lapse rate ($K\ m^{-1}$)	Γ_e	0.1981	-0.017	0.026
Temperature (°C)	T	0.1906	2.571	33.909

6.6.2 Comparison with the baseline and contractual power curves

Each filter can be compared to the baseline and to the contractual filters by applying it to the data in isolation. The desired effect is to increase the AEP estimate towards that produced by the contractual filters (4466 MWh) while reducing data loss and RMSE. The results shown in Table 33 reveal a range of behaviours. Four of the filters reduce the RMSE by a small fraction compared to the baseline for a very small loss of data, but they do not come close to the difference of 3.39 kW between the contractual TI filter and the baseline. Of these four filters, two increase the AEP estimate by a small amount with the largest difference exhibited by the stationarity of the vertical wind speed, a_z, represented by the p-value of the Augmented Dickey-Fuller test. The AEP estimate for the other two filters either remains the same or falls. The remaining filters all increase the AEP estimate, with the increase associated with the stationarity of the horizontal wind speed, a_U, coming very close to that achieved with the contractual filters. However, they also increase the RMSE value, some such as a_U by a small amount but others by more than 2 kW.

Table 33: Results from initial filters applied in isolation compared to baseline and contractual filters

Case	Data loss (%)	Min. duration (days)	AEP estimate (MWh)	Uncertainty (kW)	RMSE (kW)
Baseline	0.0	7.5	4425	30	119.81
Contractual	62.64	20.1	4466	31	130.29
TI	35.0	11.5	4454	30	116.42
Shear	49.9	16.29	4553	30	132.25
$\boldsymbol{\tau_U^2}$	1.4	7.6	4447	29	119.94
$\boldsymbol{n_z}$	2.5	7.7	4425	30	119.69
$\boldsymbol{a_z}$	3.3	7.8	4443	30	119.73
$\boldsymbol{\zeta}$	1.4	7.6	4432	30	119.86
$\boldsymbol{n_U}$	1.9	7.6	4421	30	119.69
$\boldsymbol{i_U}$	1.3	7.6	4429	30	119.67
$\boldsymbol{a_U}$	8.3	8.2	4460	30	119.95
$\boldsymbol{Q}$	6.5	8.0	4435	29	119.93
$\boldsymbol{h}$	11.7	8.5	4337	35	121.92
$\boldsymbol{\Gamma_e}$	15.5	8.9	4444	30	120.14
$\boldsymbol{T}$	15.5	8.9	4379	37	121.60

Because the ideal filter should remove around 10% of the data at the periphery of the point cloud, the filters which remove very small proportions of the data have the potential to be refined by reducing their range. However, it was found that even in cases where a smaller range moved the AEP estimate closer to the target figure, the RMSE increased. The original filter bounds are therefore retained.

A further option is to examine the effects of applying several filters in succession and Table 34 provides the results of one particular combination. The values shown are cumulative and the leftmost column shows the parameter most recently added to the set. Thus, for example, the second row implies that the data is filtered on both the transience of horizontal wind speed and normality of vertical wind speed in that order. Although the final RMSE value is marginally larger than for the baseline (119.81 kW) it is significantly smaller than the figure for the contractual filters (130.29 kW). The AEP estimate is comparable with that produced by the contractual filters (4466 MWh) while the data loss is considerably smaller (11.1% compared to 62.6%).

Table 34: Cumulative effects of experimental filters

Case	Data loss (%)	Min. duration (days)	AEP estimate (MWh)	Uncertainty (kW)	RMSE (kW)
$\boldsymbol{\tau_U^2}$	1.4	7.6	4447	29	119.94
$\boldsymbol{n_z}$	4.0	7.8	4445	29	119.88
$\boldsymbol{a_z}$	7.2	8.1	4459	29	119.92
$\boldsymbol{\zeta}$	8.2	8.2	4463	29	119.94
$\boldsymbol{n_U}$	10.1	8.3	4458	29	119.89
$\boldsymbol{i_U}$	11.1	8.4	4458	29	119.86

The difference between the cumulative effect of the experimental filters in Table 34 and the contractual filters can be appreciated qualitatively by comparing the power curve scatter plots in Fig. 52 which superimpose the points rejected by the filters onto the retained point cloud. A clear feature of the experimental filter plot is that the rejected points rejected are asymmetrically distributed about the line of the measured power curve. In contrast, the points rejected by the contractual filters appear to be more evenly distributed. Both cases eliminate a certain number of outlying points that the other does not. The apparent massing of rejected points at low wind speeds in both cases probably has two main causes. The first is the tendency of high wind speeds to mitigate other meteorological effects (Bunse & Mellinghoff, 2008; Deola, 2010; Ernst & Seume, 2012; K. Y. Lee et al., 2017), and the second is the moderate mean wind speed at the Eolos site which means that there are simply more points in the lower part of the curve.

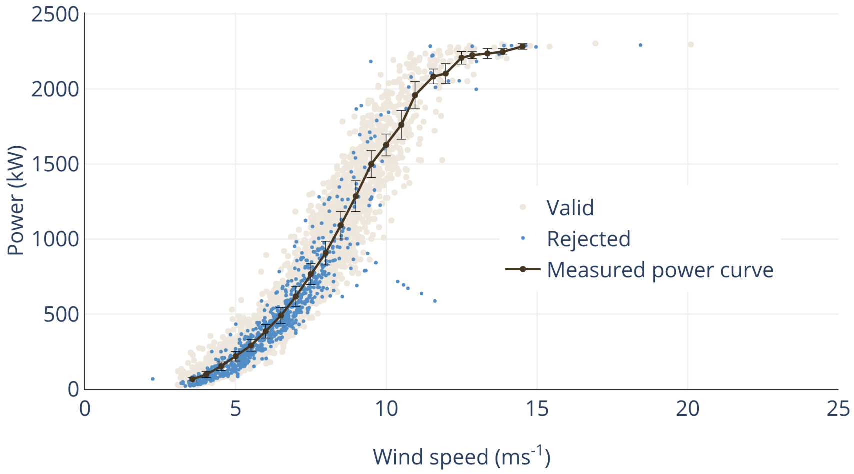

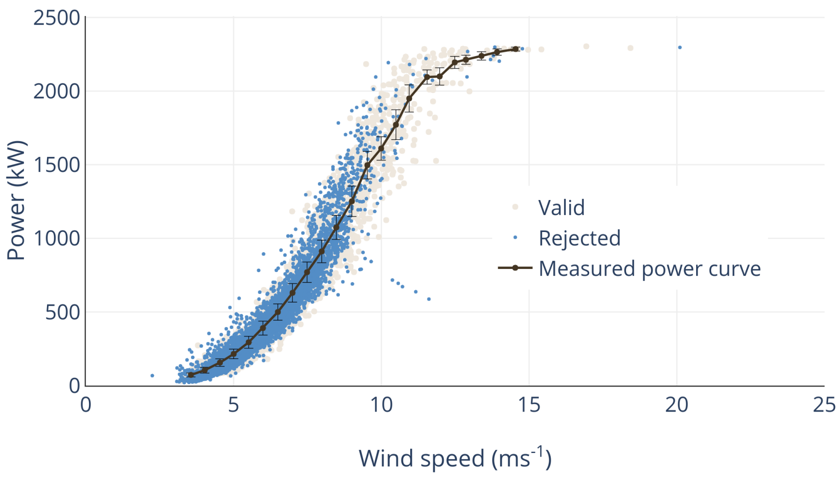

Figure 52: Data points rejected by combined experimental filters (top) and contractual filters (bottom)

6.6.3 Discussion

Normal practice in PPT is to filter the data primarily for turbulence represented by TI and for wind shear represented by the wind shear exponent. It was shown in the literature review, however, that there is significant interaction between parameters, and that turbulence and shear in particular are closely related to atmospheric stability (Bleeg et al., 2015; Dörenkämper et al., 2014; Hayes et al., 2012). Wind speed is also known to reduce the variation in other meteorological phenomena (Bunse & Mellinghoff, 2008; Deola, 2010; Ernst & Seume, 2012; K. Y. Lee et al., 2017). Filtering the data by these two parameters therefore, while convenient, runs the risk of obscuring more fine-grained variation due to other parameters. The success of the TI and shear filters could be the result of excluding the finer-grained variation along with a large proportion of valid data. Certainly, the comparisons performed here show that applying typical limits for TI eliminates a third of the data. In the case of a standard shear filter, half of the data is lost, and in combination more than 60% of the measured data is deemed invalid. A novel contribution of the current work is the addition of information about the dispersion of the data in the power curve point cloud. On this measure, the TI filter performs well reducing the RMSE value by 3.39 kW (2.8%) compared to the baseline. This is the best performance overall, and suggests that TI may be preferable to other measures of turbulence although the large data loss remains a concern. The shear filter, on the other hand, performs worst overall on the dispersion measure, increasing the RMSE value by 12.44 kW (10.4%) compared to the baseline. This is attributed to the exclusion of a large proportion of points close to the centre of the point cloud whereas the ideal filter would remove points from the periphery. When these two filters are used in combination, the RMSE value is almost as high as using the shear filter on its own suggesting that although there are some compensatory effects, the shear filter dominates in terms of the disposition of points in the scatter plot.

The novel parameters tested here are selected as a result of patterns in the research dataset and thus reflect real observed variation rather than theoretical deduction. Tested in isolation, several of them show desirable behaviour as filtering criteria. In particular, the normality of the vertical wind speed appears to reduce dispersion by a small amount while not affecting the AEP estimate. The stationarity of the vertical wind speed and the intermittency of the horizontal wind speed appear to reduce dispersion and produce a small increase in the AEP estimate. In all three cases, the quantity of data lost is very small in comparison to the TI and shear filters and much less than the target data loss of around 10%. The possibility therefore exists that small number of points excluded by these filters are also excluded by the TI and shear filters along with other data which does not make much difference to the outcome of the AEP calculation.

A further possibility is that the experimental filters are complementary and that taken in combination might have a cumulative effect that performs even better on the chosen metrics. Six of the experimental filters removed 3.3% of the data or less in isolation, and when tested in combination the dispersion increased only slightly in comparison to the baseline, data loss was just over the target at 11.1% and the AEP estimate approached that produced by the contractual power curve (4458 MWh compared to 4466 MWh up from 4425 MWh for the unfiltered data). An examination of the disposition of the rejected points in the point cloud showed that the cumulative experimental filters targeted points in the same region as the TI filter.

The isolated and cumulative results suggest that the approach followed here has merit based on the evaluation criteria used. The main limitation on any conclusions, though, is the lack of a definitive benchmark for the AEP estimate. The benchmark used here is the value produced from the contractual power curve on the assumption that the TI and shear filters will produce a good estimate because of their fundamental place in current PPT practice. An appropriate way to follow up on the work carried out her would be to conduct a similar exercise in controlled conditions where the AEP could be estimated in a more rigorous fashion. Alternatively, some of the variation with regard to the AEP estimate could be eliminated by conditioning the data on wind speed bin. Any interactions with wind speed would thus be eliminated. Again, performing this test under controlled conditions would increase the reliability further. A third possibility could be to abandon the AEP metric altogether and to use a different criterion for calculating the expected power output. This would probably be a statistical measure based on the distribution of power values within the ten-minute averaging period. As previously, partitioning the data on wind speed and conducting the study under controlled conditions could yield more reliable results.

It is noticeable from the results presented here that none of the experimental filters produce the ideal behaviour of removing points exclusively from the periphery of the point cloud. While some asymmetry is observed in the disposition of points, they still tend to cluster close to the line of the measured power curve. This could suggest that there exist still other parameters that account for more of the variance in the power output values. On the other hand, the more mundane possibility is that some of the outlying points really are the result of stochastic variation. This could also be investigated further using the methods suggested in the previous paragraph.

Regarding the cost implications of applying alternative filtering strategies, the reduction in data collection time would be considerable if the data loss rate could be reduced from around 60% to around 10%. Such a small data loss was not achieved by any of the projects reviewed in Chapter 4, and would almost guarantee that a measurement campaign could be completed within the standard period of three months. However, this would depend entirely on the ability to show that the AEP estimate produced using the filters was as accurate as current practice which remains to be shown.

6.7 Conclusions from the investigation of novel filters

The investigations and results reported in this chapter have successfully revealed a set of parameters that appear to account for the majority of the variance in the instantaneous power output of the Eolos turbine. During parameter selection, strict conditions were applied to the research dataset to allow the calculation of parameters such as REWS that require data across the vertical extent of the rotor. The working sample used for this purpose thus consists of a maximally-populated set of 2,818 TMA records. During the later stages, the data set does not need to be maximally-populated and looser conditions based only on the defined quality filters need to be applied. This leads to a working data sample of 7,348 records.

It is demonstrated that filtering the data on certain of those parameters can reduce the observed scatter in the power curve point cloud with little data loss while yielding good AEP estimates. Within limitations, then, the exercise has been successful. In particular the following conclusions can be drawn:

- Traditional measures of turbulence and shear are not necessarily the best way to capture impacts on instantaneous power output

  Neither the coefficient of variation of horizontal wind speed (TI) or the wind shear exponent survived the elimination of parameters through correlation analysis. The standard deviation of horizontal wind speed which is a major component of the TI calculation was retained at this stage. In contrast, though, the second order structure function of horizontal wind speed (transience) was found to be the most influential parameter after mean wind speed. In the case of wind shear, the wind speed ratio was retained by the correlation analysis although it too was eliminated later on. Both of these cases bring into question the continued reliance on TI and the wind shear exponent. Given their ubiquity however, a significant quantity of confirmatory evidence would be required to make a definitive claim in either regard. The provision of such evidence is beyond the scope of the current work which has simply broached the question.

- As a two-point statistic, transience appears to be a good way to represent turbulence

  Structure functions are a fundamental method for describing turbulent flows in many areas of science (Davidson, 2004, p. 90; Kolmogorov, 1941). Because they are based on differences in flow conditions at two points in the flow, they can capture dynamic variation that is missed by single-point statistics such as the standard deviation. Transience has already been proposed as a way of estimating turbine loads and can be captured by a standard data logger (Clive, 2012). The large comparative significance of the second-order structure function of wind speed (transience) seen here suggests that these dynamics are important for explaining a proportion of the variance in the instantaneous power output.

- Direct measures of wind shear may not be necessary

  Surprisingly, direct measures of wind shear were not prominent in the results of either sensitivity analysis. Instead, indicators of atmospheric stability and vertical motions were present. This suggests that wind shear may best be treated as a consequence of other phenomena rather than a fundamental phenomenon in its own right. As another controversial observation on the basis of the results presented here, significant confirmatory evidence beyond the scope of the current work would be required for this notion to be accepted.

- The characteristics of the wind behaviour within the ten-minute averaging period appear to be significant

  The instantaneous power output appears to be sensitive to the degree to which the distribution of horizontal and vertical wind speed within the ten-minute averaging period deviates from Gaussian. Likewise, the stationarity of the vertical wind speed and the intermittency of the horizontal wind speed appear significant. The usual practice of relying on one-point statistics obscures such details.

- Some procedures in IEC2017 cannot be used in certain circumstances

  REWS has the obvious limitation that wind speed measurements are required from the top of the rotor. This requirement had a minor impact on the analyses carried out here in that it reduced the number of data points available during the parameter selection. However, it also became clear that the turbulence normalisation procedure could not be used when rated speed was not achieved.

- Characteristics of the vertical wind speed appear to be significant

  Standard practice is to measure only the horizontal component of the wind velocity using cup anemometers. The recognition that characteristics of the vertical component are also significant raises the question of whether this is adequate. Although sonic instruments will continue to be an expensive and therefore undesirable option for PPT, the use of scanning lidar is now permitted by IEC2017 for measuring horizontal wind speed under certain circumstances. If further evidence confirms the importance of vertical motions, lidar could provide a relatively inexpensive method for measuring them.

- Filters can be designed which improve the form of the data for very little data loss

  Several of the experimental filters evaluated here showed the desirable properties of producing an AEP estimate similar to that delivered by more conventional filters while reducing data dispersion and loss. The greatest strength of the filters explored here was the reduction in lost data. On the other hand, dispersion was not reduced below that associated with the unfiltered data in contrast to the standard TI filter. Further experimentation would be necessary to further optimise the filter definitions to improve performance in this aspect.

- The cumulative effect of data filters needs to be considered

  It was shown that the conventional shear filter used in isolation removed 50% of the data and increased the dispersion of the data by over 10% in comparison the baseline. The dispersion was slightly mitigated when used in combination with the TI filter, while the data loss increased to over 60%. The use of several of the experimental filters in combination showed similar compounding and compensatory effects as the RMSE values increased or decreased with the addiction of successive parameters. The ideal combination of filters would have a monotonic effect on the quality measures, and further work in this area would be needed to develop complementary filter definitions.

- A major barrier to definitive conclusions in this area is the lack of a reliable AEP benchmark

  For various reasons, none of the AEP estimates used here can be considered definitive, and this is true for any similar exercise including PPT. Ostensibly, the contract warranty conditions are adapted to reflect the wind regime at the site, and may therefore be considered an objective benchmark. However, these conditions may be subject to deliberate or accidental bias (Albers, 2012). The solution in the context of the current work was to use an internally consistent model by synthesising a benchmark estimate using artificial contractual filters inspired by real PPT projects. More concrete conclusions would depend on a more reliable AEP benchmark. Some potential ways forward are discussed in §6.6.3.

7 Conclusions

Power performance testing (PPT) is a necessary part of a commercial wind energy project but the warranty conditions applied from one project to another exhibit considerable variation. As a consequence, the process duration is difficult to predict and control, and there is a significant risk of project delays and additional costs. This risk can be traced to the loss of data through the application of filters whose purpose is to exclude operating conditions that might adversely affect the operation of the wind turbine. Conventional filters centre on a small set of parameters such as turbulence intensity (TI) and wind shear. Using conventional filters, losses of up to 90% have been reported in the literature (Bunse & Mellinghoff, 2008; Rareshide et al., 2009). The question therefore arises as to whether data loss can be reduced by using alternative filtering strategies based either on different meteorological parameters entirely, or on alternative measures of the same meteorological phenomena.

The aim of the current work is to investigate the potential of alternative data filtering strategies with respect to data loss, AEP estimates and the dispersion of points in the power curve scatter plot with particular interest in relationships not accounted for in the current power performance testing standard. An appropriate range of candidate parameters was identified during the literature review, and these were the starting point for the methodology described in Chapter 3. The investigation was carried out in three main stages which are the subjects of Chapters 4 – 6 and which also have a direct relationship to the three objectives defined in Chapter 1. These objectives are recapped below along with a summary of the findings and main contributions.

7.1 Review of PPT contracts

The relevant project objective was to

> **explore and quantify the loss of data through filtering in real PPT contracts with an emphasis on the requirements of the standard, the associated costs and the potential for savings.**

A sample of measurement campaigns related to 42 turbines from 15 different PPT projects was examined in Chapter 4. It was shown that contractual filter criteria vary considerably between projects and can be very restrictive leading to the conclusion that large data losses through contractual filters are not exceptional. In the small sample of projects examined, an even spread of data losses from 10% to 95% was observed. In the most extreme case, the measurement campaign took over nine months to complete which is more than three times the duration usually planned and costed.

As expected, projects in complex terrain have a higher rate of data loss; however, the relationship between terrain type and elapsed duration is not deterministic, and the project with the longest elapsed duration in this sample was in flat terrain. The concept of *effective duration* was introduced to allow comparison across projects. The effective duration is calculated from the quantity of valid data that is collected before filters are applied based on the simple fact that there are six ten-minute sampling periods in each hour. It can be used to provide an indication of the priority attached to the termination of a measurement campaign through a comparison with the minimum theoretical duration. Using this relationship, it was observed that as the elapsed duration of a campaign increases, the effective duration tends to be minimised. Thus, the pressure to terminate data collection increases with the rate of data loss.

A mathematical relationship provided by Wood Clean Energy calculates that a delay of one day on a three-month project incurs direct costs of around 1% of the original budget. Using this formula, it was shown that direct campaign costs can reach more than three times the planned amount when the majority of data is lost through restrictive filtering. In addition, the indirect costs related to such delays can add tens of millions of pounds to the overall construction project. Major indirect factors include the need to carry out major construction works during fair weather windows which typically occur during the summer months in temperate regions, and the need to retain expensive construction equipment longer than planned.

Although it is difficult to be specific for reasons of commercial sensitivity, campaign costs have been examined in proportional terms. The estimates presented here show that both direct and indirect costs resulting from long campaign durations can be significant. The main limitations on these results are

1. The data comes only from one consulting organisation.

   A future project might undertake a wider review including data from several consultants to eliminate any organisational bias.

2. The sample of projects used here is small.

   From a statistical point of view, the results presented here must be considered indicative rather than generally applicable. On the other hand, the results are supported by industry experts, and confirm previously reported observations about the extent of data losses. A future project could explore a more extensive set of cases to confirm the results of the current work.

3. Information concerning the reasons for the low rate of accumulation of data during each campaign was limited.

   Greater knowledge of such factors could provide additional insights into how campaign duration could be better controlled. A future project could focus specifically on these prior factors to explore ways of controlling campaign duration and cost that are not related to filtering the data.

The impact of data filtering strategies on campaign durations and costs has not previously been reported in the literature to the level of detail show here. Previous works have provided headline figures for data loss in extreme cases, but have not offered insight into the range of impacts, or the likely occurrence of large losses. The results presented here fill this gap and are therefore considered a major contribution of the current work. In addition, the novel concept of effective campaign duration is introduced to allow comparison across projects, and the minimum theoretical campaign duration given a particular rate of data loss is characterised.

7.2 The research dataset

The relevant project objective is

> **to compile a new, high-fidelity dataset corresponding to the wind regime impacting on turbine performance which incorporates a wide range of parameters that is not constrained by the assumptions embodied in the current PPT standard.**

No extant datasets were found that satisfy the needs of this project which required a demanding range of features. Existing datasets provided some of these features but were deficient in others, and a new dataset was therefore required. Data from a well-instrumented research turbine operated by the University of Minnesota was synchronised with data from other sources to create a composite dataset spanning the whole of 2017. The main element of the final output is a file of 52,560 records, one for each ten-minute period during the year. Each record consists of 727 values (including the timestamp) made up of statistical descriptions of measured parameters, as well as additional parameters derived on the basis of recognised formulae covered in the literature review. Recommended quality controls were applied during the creation of the dataset to ensure that the eventual content was as robust as possible.

As it is based on real measured data, the final version of the dataset has some limitations:

1. No recent instrument calibrations have been performed

   This constraint increases the uncertainty in the individual measurements; however, the instruments are in constant use by researchers and may therefore be assumed to be well-maintained.

2. High wind speeds are poorly represented

   The mean wind speed at the turbine location is low, and wind speed above the turbine rated speed of 15 ms^{-1} are rarely achieved. This limits the range of future analyses that the dataset can support.

3. There is a large number of missing values

   The dataset nominally covers an entire calendar year; however, there are many missing values related to instrument failure. A particular issue was found with the topmost sonic anemometer which meant that certain derived parameters such as the rotor equivalent wind speed could only be calculated for a small proportion of the overall data. Appropriate quality filters therefore need to be applied in advance of any future analysis.

4. The number of SCADA parameters is limited

   Any future analysis that requires knowledge of turbine characteristics such as nacelle direction or yaw error would need to source such data independently.

5. A small number of TMA records are affected by curtailment

   A pragmatic decision was taken to retain records with a curtailment level of 2,300 kW to avoid eliminating a large number of records. Checks indicated that a very small number of records would be affected by the curtailment because of the low mean wind speed. However, it is expected that a small number of points will appear as a horizontal anomaly in the power curve scatter plot at 2,300 kW. The effect of this small set of data points is thought to be negligible with respect to data analyses performed here.

6. Visual inspection of all samples was not possible due to the quantity of data

   Future analyses should be prepared to investigate unexpected behaviour with reference to the raw data samples.

7. Wind speed and direction are based solely on sonic measurements

   Any future analysis that requires wind speed measurements from the cup anemometers and wind vanes would need to source such data independently.

8. Flux calculations use a ten-minute averaging period rather than the standard 30 minutes

   This constraint introduces some additional uncertainty into the flux values especially for momentum flux during unstable conditions.

The dataset was compiled with the intention of supporting a wider range of analyses than needed for the current work. It is thus a general resource available to future wind energy projects and is a major contribution of the current work in its own right. The dataset is available from the University of Minnesota Digital Conservancy (Davison, 2019) and the python code used to prepare it is available at https://bitbucket.org/coillarach/phd.

7.3 Evaluation of novel filtering criteria

The relevant project objective is

> **to evaluate traditional and novel filtering strategies in terms of data loss, dispersion in the power curve and estimated AEP.**

The results in Chapter 6 demonstrate that filtering the data on certain novel parameters can reduce the observed scatter in the power curve point cloud with little data loss while yielding good AEP estimates. They also show that the current reliance on filters on turbulence intensity (TI) and wind shear may not be optimal. For example, sensitivity analysis showed that power output was more sensitive to the second-order structure function (transience) of horizontal wind speed than to TI. A second controversial result was that direct measures of wind shear were not required to account for the majority of variance in the power output. Instead, indicators of atmospheric stability and vertical motion were prominent. Both of these observations represent major departures from current practice, and would require considerable confirmatory evidence before they could be completely accepted.

Several characteristics of the wind flow within the standard ten-minute averaging period were found to be related to the instantaneous power output. In particular, measures of stationarity in both the horizontal and vertical dimensions had an effect, as did departures from a Gaussian distribution of wind speed values. Intermittency was also observed to account for a proportion of the variance in the power output. These observations suggest that the conventional model based on one-point statistics may not be adequate, and the vertical wind speeds also need to be taken into account.

In carrying out the analysis, it was observed that some of the procedures in the current version of the PPT standard have limited applicability. As well as the rotor equivalent wind speed (REWS) method relying on wind speed measurements spanning the vertical extent of the rotor, the turbulence normalisation method cannot be used when the turbine rated wind speed is not achieved.

It was shown that using artificial filters for TI and shear based on values used in real PPT projects led to data losses of over 60%. While the effect of the TI filter reduced the dispersion in the point cloud by around 3%, the effect of the shear filter was to increase it by over 10%. The experimental filters examined here did not manage to reduce the dispersion of points in the power curve scatter plot significantly below that seen in the unfiltered data; however, they were successful in producing AEP estimates similar to those based on conventional filters for much smaller data losses of around 11%. Although further experimentation would be necessary to further optimise the filter definitions, these results suggest that the approach has merit and the topic of alternative filters could be productively pursued. The cumulative effect of filters was also shown to be significant with respect to both the conventional and experimental filters examined.

The major limitation identified for the results presented here and for any other study based on AEP is the lack of a reliable AEP benchmark. The usual approach in the literature is to examine the sensitivity of AEP to a particular parameter. However, that approach cannot draw any conclusions about the accuracy of the AEP estimates, such as whether a higher or lower estimate is the more correct. The approach taken here was to define a self-referential benchmark based on the IEC2017 using a set of artificial filters, and that was successful within the stated limitations. Several approaches were discussed for enhancing the reliability of AEP estimates were discussed which could be taken up by future projects to extend the work carried out here including:

- Conducting similar analyses to those presented here in controlled conditions
- Conditioning the data on wind speed bin to reduce interaction effects
- Abandon the AEP metric altogether and to use a different criterion for calculating the expected power output

7.4 General conclusion and suggestions for future work

The results presented here demonstrate that alternative data filtering strategies have the potential to reduce data loss by a significant amount. In the example of the Eolos turbine, over 60% of data was lost using conventional filters, while a combination of experimental filters produced a comparable AEP estimate with only an 11% data loss. On the proviso that the AEP estimate could be shown to be reliable, this reduction in data loss would make it much more likely that a measurement campaign could be completed within the standard three-month period. This would reduce the risk for wind energy projects by eliminating the uncertainty around campaign durations and thereby avoiding additional direct and indirect costs amounting potentially to tens of millions of pounds.

In addition to the points made with respect to the three main objectives of the current work, a number of other questions might be addressed by future research:

- **Why do conventional filters for TI and shear remove more points from the centre of the power curve scatter plot than from the periphery?**

  Reducing the dispersion of the power curve point cloud has been identified as a desirable (Bandi & Apt, 2016; Eecen et al., 2011; Wagner et al., 2014). It is therefore odd that the two major filters currently used either reduce the dispersion by a very small amount, or actually increase it. The results presented here suggest that a large proportion of the rejected data may have no distorting effect on the power curve, and may therefore be retained without problems. A future project could investigate the physical phenomena at play.

- **How should the results of the sensitivity analysis be further interpreted?**

  The eFAST method reveals relationships between the variance in the input parameters and the variance in the instantaneous power output. While it can quantify a parameter's main and total effects, its mathematical limitations mean that it cannot specify precisely which parameters interact together. A future project could investigate such parameter interactions to discover which are significant and which are not. An examination of parameter interactions would require the testing of different combinations of parameters which would provide further insights into their individual and combined importance.

- **Can a trained neural network be used as a multivariate reference for turbine power performance?**

  As a non-parametric model, the artificial neural network (ANN) used here captures the behaviour of the Eolos turbine well. This ability has also been used to provide a self-referential benchmark for performance monitoring (Janssens et al., 2016; Mckay et al., 2013; Morshedizadeh et al., 2017). An ANN trained on a set of reference data predicts expected performance based on a much wider range of inputs than just wind speed. It therefore offers a multivariate alternative to the power curve. A future project could investigate the feasibility of this approach including such issues as the availability of appropriate reference data and the expected range of variability in output under boundary conditions.

References

Albers, A. (2010). Turbulence normalization of power curve data. In *European Wind Energy Conference* (pp. 0–6).

Albers, A. (2012). Critical Limitations of Wind Turbine Power Curve Warranties. In *European Wind Energy Conference & Exhibition 2012*.

Alblas, L., Bierbooms, W., & Veldkamp, D. (2012). Power output of offshore wind farms in relation to atmospheric stability. In *The Science of Making Torque from Wind*. http://doi.org/10.1088/1742-6596/555/1/012004

Allaei, D. (2012). Using CFD to Predict the Performance of Innovative Wind Power Generators. In *Proceedings of the 2012 COMCOL Conference*. Boston.

Argyle, P., & Watson, S. (2012). A Study of the Surface Layer Atmospheric Stability at Two UK Offshore Sites. In *European Wind Energy Conference*.

Arramach, J., Boutammachte, N., Bouatem, A., & Al Mers, A. (2017). Prediction of the Wind Turbine Performance by Using a Modified BEM Theory with an Advanced Brake State Model. *Energy Procedia*, *118*, 149–157. http://doi.org/10.1016/j.egypro.2017.07.033

Ashrafi, K., & Hoshyaripour, G. A. (2010). A Model to Determine Atmospheric Stability and its Correlation with CO Concentration. *International Journal of Civil and Environmental Engineering*, *2*(2), 83–88.

Atkins, R. E. (1978). Performance evaluation of wind energy conversion systems using the method of bins - current status. Sandia Laboratories.

Baas, P., Steeneveld, G. J., de Wiel, B. J. H. V, & Holtslag, A. A. M. (2006). Exploring self-correlation in flux-gradient relationships for stably stratified conditions. *Journal of the Atmospheric Sciences*, *63*(11), 3045–3054. http://doi.org/10.1175/JAS3778.1

Bailey, B. H. (1981). Predicting vertical wind profiles as a function of time of the day and surface wind speed. In *Proceedings of an International Colloquium on Wind Energy*. Brighton: BWEA.

Bandi, M., & Apt, J. (2016). Variability of the Wind Turbine Power Curve. *Applied Sciences*, *6*(9), 262. http://doi.org/10.3390/app6090262

Barenblatt, G. I. (1996). *Scaling, self-similarity, and intermediate asymptotics*. Cambridge University Press.

Barrios, A., Zubiaur, R., & Cordón, R. (2008). Advanced Numerical Site Calibration Using Commercial Software. In *European Wind Energy Conference and Exhibition* (pp. 1–3).

Barthelmie, R. J., Frandsen, S. T., Rathmann, O., Hansen, K., Politis, E. S., Prospathopoulos, J., … Heath, M. (2011). *Flow and wakes in large wind farms : Final report for UpWind.*

Bartholy, J., & Radics, K. (2005). Wind profile analyses and atmospheric stability over a complex terrain in southwestern part of Hungary. *Physics and Chemistry of the Earth*, *30*(1-3 SPEC. ISS.), 195–200. http://doi.org/10.1016/j.pce.2004.08.013

Belu, R., & Koracin, D. (2012). Effects of complex wind regimes and meteorological parameters on wind turbine performances. In *IEEE Energytech*. Cleveland, OH: IEEE. Retrieved from http://ieeexplore.ieee.org/stamp/stamp.jsp?tp=&arnumber=6304638&isnumber=6304622

Bera, A. K., & Jarque, C. M. (1981). Efficient tests for normality, homoscedasticity and serial independence of regression residuals. Monte Carlo Evidence. *Economics Letters*, *7*(4), 313–318. http://doi.org/10.1016/0165-1765(81)90035-5

Biltoft, C. (2003a). Momentum flux: gross, scalar, alongwind or net. Adiabat Meteorological Services. Retrieved from http://www.apptech.com/wp-content/uploads/2016/04/fluxnote0303.pdf

Biltoft, C. (2003b). Some thoughts on in-situ flux measurements in the atmospheric surface layer. Adiabat Meteorological Services. Retrieved from http://www.apptech.com/wp-content/uploads/2016/04/fluxnote.pdf

Bleeg, J., Digraskar, D., Woodcock, J., & Corbett, J.-F. (2015). Modeling stable thermal stratification and its impact on wind flow over topography. *Wind Energy*, *18*, 369–383. http://doi.org/10.1002/we.1692

Boettcher, F., Renner, C., Waldl, H. P., & Peinke, J. (2003). On the statistics of wind gusts. *Boundary-Layer Meteorology*, *108*(1), 163–173. http://doi.org/10.1023/A:1023009722736

Bolón-Canedo, V., Sánchez-Maroño, N., & Alonso-Betanzos, A. (2015). *Feature Selection for High-Dimensional Data*. Springer. http://doi.org/10.1007/978-3-319-21858-8

Bosveld, F. C. (2017). Cabauw In-situ Observational Program 2000 – Now : Instruments , Calibrations and Set-up. Retrieved from http://projects.knmi.nl/cabauw/insitu/observations/documentation/Cabauw_TR/Cabauw_TR.pdf

Brand, A. J., Peinke, J., & Mann, J. (2011). Turbulence and Wind Turbines. In *13th European Turbulence Conference*. Warsaw.

Brock, F. V. (1986). A Nonlinear Filter to Remove Impulse Noise from Meteorological Data. *Journal of Atmospheric and Oceanic Technology*, *3*(1), 51–58. http://doi.org/10.1175/1520-0426(1986)003<0051:ANFTRI>2.0.CO;2

Bulaevskaya, V., Wharton, S., Irons, Z., Qualley, G., Clifton, A., Qualley, G., & Miller, W. O. (2015). Wind power curve modeling in complex terrain using statistical models. *Journal of Renewable and Sustainable Energy*, *7*(1). http://doi.org/10.1063/1.4904430

Bunse, U., & Mellinghoff, H. (2008). Influences of vertical wind profiles on power performance measurements. In *German Wind Energy Conference DEWEK* (pp. 1–5). Wilhelmshaven.

Burba, G. (2013). *Eddy Covariance Method for Scientific, Industrial, Agricultural and Regulatory Applications*. Lincoln, Nebraska: LI-COR® Biosciences. http://doi.org/10.1016/j.infsof.2008.09.005

Burton, T., Jenkins, N., Sharpe, D., & Bossanyi, E. (2011). *Wind Energy Handbook*. Wiley.

Campbell Scientific. (1998). Csat3 Three Dimensional Sonic Anemometer Instruction Manual, (c), 1996–1998.

Caruana, R., & Lawrence, S. (2001). Overfitting in Neural Nets: Backpropagation, Conjugate Gradient, and Early Stopping. *Advances in Neural Information Processing Systems.*, 402–408. Retrieved from https://papers.nips.cc/paper/1895-overfitting-in-neural-nets-backpropagation-conjugate-gradient-and-early-stopping.pdf

Castellani, F., & Garinei, A. (2013). On the way to harness high-altitude wind power: Defining the operational asset for an airship wind generator. *Applied Energy*, *112*, 592–600. http://doi.org/10.1016/j.apenergy.2013.01.019

Celik, A. N., Makkawi, A., & Muneer, T. (2010). Critical evaluation of wind speed frequency distribution functions. *Journal of Renewable and Sustainable Energy*, *2*(1), 013102. http://doi.org/10.1063/1.3294127

Chambers, S. D., Galeriu, D., Williams, A. G., Melintescu, A., Griffiths, A. D., Crawford, J., … Zorila, B. (2016). Atmospheric stability effects on potential radiological releases at a nuclear research facility in Romania: Characterising the atmospheric mixing state. *Journal of Environmental Radioactivity*, *154*, 68–82. http://doi.org/10.1016/j.jenvrad.2016.01.010

Chamorro, L. P., S-J.Lee, Olsen, D., C.Milliren, J.Marr, Arndt, R. E. A., & Sotiropoulos, F. (2015). Turbulence effects on a full-scale 2.5 MW horizontal-axis wind turbine under neutrally stratified conditions. *Wind Energy*, *18*, 339–349. http://doi.org/10.1002/we.1700

Chatfield, C. (2004). *The analysis of time series*. Boca Raton: CRC Press.

Chavan, D. S., Gaikwad, S., Singh, A., Himanshu, Parashar, D., Saahil, V., … Karandikar, P. B. (2017). Impact of vertical wind shear on wind turbine performance. In *Proceedings of IEEE International Conference on Circuit, Power and Computing Technologies, ICCPCT 2017*. http://doi.org/10.1109/ICCPCT.2017.8074395

Christensen, C. J., Dragt, J. B., Carlson, O., Derdelinkx, I. R., Hunter, R., Infield, D., … Paulsen, U. S. (1986). *Accuracy of Power Curve Measurements*. DTU Risø.

Clifton, A., & Wagner, R. (2014). Accounting for the effect of turbulence on wind turbine power curves. *Journal of Physics: Conference Series*, *524*(1), 012109. http://doi.org/10.1088/1742-6596/524/1/012109

Clive, P. J. M. (2012). Transience statistics for fatigue calculations. In *DEWEK 2012*.

Coelingh, J. P., Van Wijk, A. J. M., & Holtslag, A. A. M. (1996). Analysis of wind speed observations over the North Sea. *Journal of Wind Engineering and Industrial Aerodynamics*, *61*(1), 51–69. http://doi.org/10.1016/0167-6105(96)00043-8

Colls, M. (2014). Steps towards comparison of turbine performance across varying turbine geometries. In *Proceedings of the Power Curve Working Group*. Retrieved from http://www.pcwg.org/proceedings/2014-04-01/06-Steps-towards-comparison-of-turbine-performance-Matthew-Colls-Prevailing.pdf

Contini, D., Cava, D., Martano, P., Donateo, A., & Grasso, F. M. (2009). Comparison of indirect methods for the estimation of boundary layer height over flat-terrain in a coastal site. *Meteorologische Zeitschrift*, *18*(3), 309–320. http://doi.org/10.1127/0941-2948/2009/0381

Courtney, M., Borbon, F., & Dupont, E. (2011). *SafeWind: Measurements in flat terrain – Assessment*.

Cukier, R. I., Levine, H. B., & Shuler, K. E. (1978). Nonlinear sensitivity analysis of multiparameter model systems. *Journal of Computational Physics*, *26*(1), 1–42.

Dahlberg, J.-A., Frandsen, S., Madsen, H. A., Antoniou, I., Friis Pedersen, T., Hunter, R., & Klug, H. (1999). Is the nacelle-mounted anemometer an acceptable option in performance testing? In *EWEC 1999*. Nice.

Davidson, P. A. (2004). *Turbulence: An Introduction for Scientists and Engineers*. OUP Oxford.

Davison, B. (2019). Rich Data for Wind Turbine Power Performance Analysis. Minnesota: University of Minnesota. http://doi.org/10.13020/1etn-1q17

Deola, R. A. (2010). *Characterization of winds through the rotor plane using a phased array SODAR and recommendations for future work.*

Dickey, D. A., & Fuller, W. A. (1979). Distribution of the Estimators for Autoregressive Time Series with a Unit Root. *Journal of the American Stat. Association*, *74*(366).

Donda, J. (2015). *Collapse of turbulence in the nocturnal boundary layer*. Eindhoven University of Technology.

Donoho, D. L. (2000). High-Dimensional Data Analysis : The Curses and Blessings of Dimensionality. In *AMS conference on math challenges of the 21st century*. Los Angeles.

Dörenkämper, M., Tambke, J., Steinfeld, G., Heinemann, D., & Kühn, M. (2014). Atmospheric Impacts on Power Curves of Multi-Megawatt Offshore Wind Turbines. *Journal of Physics: Conference Series*, *555*(DECEMBER), 012029. http://doi.org/10.1088/1742-6596/555/1/012029

Dormann, C. F., Elith, J., Bacher, S., Buchmann, C., Carl, G., Carré, G., … Lautenbach, S. (2013). Collinearity: A review of methods to deal with it and a simulation study evaluating their performance. *Ecography*, *36*(1), 027–046. http://doi.org/10.1111/j.1600-0587.2012.07348.x

Eecen, P. J., Wagenaar, J. W., Stefanatos, N., Pedersen, T. F., Wagner, R., & Hansen, K. S. (2011). *Final report UpWind 1A2: Metrology.*

Elkinton, M. R., Rogers, A. L., & Mcgowan, J. G. (2006). An Investigation of Wind-shear Models and Experimental Data Trends for Different Terrains. *Wind Engineering*, *30*(4), 341–350.

Ellis, C. (2013). *Eolos Meteorological Tower and Associated Sensor System.* http://doi.org/10.1215/15476715-

Emeis, S. (2011). *Surface-Based Remote Sensing of the Atmospheric Boundary Layer*. Springer.

http://doi.org/10.1007/978-90-481-9340-0

Emerson, P. L. (1983). Analysis of variance with Fourier analysis of coherent data. *Behavior Research Methods & Instrumentation*, *15*(2), 242–250. http://doi.org/10.3758/BF03203555

Ernst, B., & Seume, J. R. (2012). Investigation of site-specific wind field parameters and their effect on loads of offshore wind turbines. *Energies*, *5*(10), 3835–3855. http://doi.org/10.3390/en5103835

Fine, S., D'Costa, P., & Kumaraswamy, K. (2017). Policies for Accommodating Higher Penetration of Variable Energy Resources (VERs)—U.S. Outlook and Perspectives. In L. E. Jones (Ed.), *Renewable Energy Integration Practical Management of Variability, Uncertainty, and Flexibility in Power Grids* (2nd ed.). http://doi.org/10.1016/B978-0-12-809592-8.00002-0

Finnigan, J. J. (2004). A re-evaluation of long-term flux measurement techniques part II: Coordinate systems. *Boundary-Layer Meteorology*, *113*(1), 1–41. http://doi.org/10.1023/B:BOUN.0000037348.64252.45

Finnigan, J. J., Clement, R., Malhi, Y., Leuning, R., & Cleugh, H. A. (2003). A re-evaluation of long-term flux measurement techniques, Part I: Averaging and coordinate rotation. *Boundary-Layer Meteorology*, *107*, 1–48.

Foken, T. (2008). *Micrometeorology*. Berlin Heidelberg: Springer.

Foken, T., Göckede, M., Mauder, M., Mahrt, L., Amiro, B., & Munger, W. (2005). Post-field data quality control. In X. Lee, W. Massman, & B. Law (Eds.), *Handbook of Micrometeorology*. Kluwer Academic Publishers.

Foken, T., & Wichura, B. (1996). Tools for quality assessment of surface-based flux measurements. *Agricultural and Forest Meteorology*, *78*, 83–105.

Foresti, L., Tuia, D., Kanevski, M., & Pozdnoukhov, A. (2011). Learning wind fields with multiple kernels. *Stochastic Environmental Research and Risk Assessment*, *25*(1), 51–66. http://doi.org/10.1007/s00477-010-0405-0

Ghahramani, Z. (2013). Bayesian non-parametrics and the probabilistic approach to modelling. *Philosophical Transactions. Series A, Mathematical, Physical, and Engineering Sciences*, *371*. http://doi.org/10.1098/rsta.2011.0553

Goldstein, L. (2013). Theoretical analysis of an airborne wind energy conversion system with a ground generator and fast motion transfer. *Energy*, *55*, 987–995. http://doi.org/10.1016/j.energy.2013.03.087

Grachev, A. A., Fairall, C. W., Persson, P. O. G., Andreas, E. L., & Guest, P. S. (2005). Stable boundary-layer scaling regimes: The SHEBA data. *Boundary-Layer Meteorology*, *116*(2), 201–235. http://doi.org/10.1007/s10546-004-2729-0

Gryning, S. E., Batchvarova, E., Brümmer, B., Jørgensen, H., & Larsen, S. (2007). *On the extension of the wind profile over homogeneous terrain beyond the surface boundary layer. Boundary-Layer Meteorology* (Vol. 124). http://doi.org/10.1007/s10546-007-9166-9

Gualtieri, G., & Secci, S. (2011). Comparing methods to calculate atmospheric stability-dependent wind speed profiles: A case study on coastal location. *Renewable Energy*, *36*(8), 2189–2204. http://doi.org/10.1016/j.renene.2011.01.023

Hall, M. A., & Smith, L. A. (1997). Feature subset selection: a correlation based filter approach. In *International Conference on Neural Information Processing and Intelligent Information Systems*. Springer.

Hansen, K. S., Barthelmie, R. J., Jensen, L. E., & Sommer, A. (2012). The impact of turbulence intensity and atmospheric stability on power deficits due to wind turbine wakes at Horns Rev wind farm. *Wind Energy*, *15*(1), 183–196. http://doi.org/10.1002/we.512

Hansen, M. O. L. (2008). *Aerodynamics of Wind Turbines* (2nd ed.). London: Earthscan.

Hayes, C., Tchou, J., Tanenhaus, S., Head, A., & Walter, K. (2012). Atmospheric stability and its effects on wind speed correlations. In *WindPower*. Atlanta. Retrieved from http://c3417655.r55.cf0.rackcdn.com/20049-0800px.png

Hayot, F., & Jayaprakash, C. (1999). Intermittency in Turbulence, 16.

http://doi.org/10.1016/0378-4371(93)90382-E

Hedevang, E. (2014). Wind turbine power curves incorporating turbulence intensity. *Wind Energy*, *17*(2), 173–195. http://doi.org/10.1002/we.1566

Henke, M., & Clive, P. J. M. (2017). Robust low cost offshore power curve tests with lidar. In *SUPERGEN Wind General Assembly*. Durham. Retrieved from https://www.supergen-wind.org.uk/files/GA April2017/Poster PC3.pdf

Hernandez, W., Méndez, A., Maldonado-Correa, J., & Balleteros, F. (2016). Modeling of a Robust Confidence Band for the Power Curve of a Wind Turbine. *Sensors*, *16*(12), 2080. http://doi.org/10.3390/s16122080

Hojstrup, J. (1993). A statistical data screening procedure. *Measurement Science and Technology*, *4*(2), 153–157. http://doi.org/10.1088/0957-0233/4/2/003

Holtslag, M. C., Bierbooms, W. A. A. M., & van Bussel, G. J. W. (2014). Estimating atmospheric stability from observations and correcting wind shear models accordingly. *Journal of Physics: Conference Series*, *555*(1), 12052. http://doi.org/10.1088/1742-6596/555/1/012052

Holtslag, M. C., Bierbooms, W. A. A. M., & van Bussel, G. J. W. (2017). Extending the diabatic surface layer wind shear profile for offshore wind energy. *Renewable Energy*, *101*, 96–110. http://doi.org/10.1016/j.renene.2016.08.031

Hornik, K., Stinchcombe, M., & Halbert, W. (1989). Multilayer Feedforward Networks are Universal Approximators. *Neural Networks*, *2*, 359–366.

Howard, K. B., & Guala, M. (2014). Characterizing the effects of inflow on a 2.5 MW research utility turbine. In *32nd SciTech, ASME Wind Energy Symposium*. Retrieved from http://arc.aiaa.org/doi/abs/10.2514/6.2014-1400

Howard, K. B., & Guala, M. (2016). Upwind preview to a horizontal axis wind turbine: a wind tunnel and field-scale study. *Wind Energy*, *19*, 1371–1389. http://doi.org/10.1002/we.1901

Hunter, C. H. (2012). *A Recommended Pasquill-Gifford Stability Classification Method for Safety Basis Atmospheric Dispersion Modeling at SRS*. Retrieved from https://digital.library.unt.edu/ark:/67531/metadc840628/m2/1/high_res_d/1037732.pdf

Hwangbo, H., Johnson, A. L., & Ding, Y. (2015). Power Curve Estimation : Functional Estimation Imposing the Regular Ultra Passum Law, (1965).

IEC. (2005). International standard IEC 61400-1 Wind turbines - Part 1: Design requirements. International Electrotechnical Commission.

IEC. (2013). International standard IEC 61400-12-2 Wind turbines - Part 12-2: Power performance of electricity-producing wind turbines based on nacelle anemometry. International Electrotechnical Commission.

IEC. (2017). International standard IEC 61400-12-1 Wind Turbines - Part 12-1: Power performance measurements of electricity producing wind turbines. International Electrotechnical Commission.

IRENA. (2018). *Power Generation Costs in 2017*. Abu Dhabi: International Renewable Energy Agency.

ISO/IEC. (2005). *General requirements for the competence of testing and calibration laboratories* (2nd ed., Vol. 2005). International Standards Organization/International Electrotechnical Commission. http://doi.org/10.1109/IEEESTD.2015.7106438

Istchenko, R., & Turner, B. (2009). Extrapolation of Wind Profiles Using Indirect Measures of Stability. *Wind Engineering*, *32*(5), 433–438. http://doi.org/10.1260/030952408786411967

Jacobson, M. Z. (2005). *Fundamentals of atmospheric modeling* (2nd ed.). Cambridge: Cambridge University Press.

Janssens, O., Noppe, N., Devriendt, C., Walle, R. Van de, & Hoecke, S. Van. (2016). Data-driven multivariate power curve modeling of offshore wind turbines. *Engineering Applications of Artificial Intelligence*, *55*, 331–338.

http://doi.org/10.1016/j.engappai.2016.08.003

JCGM. (2008). *Evaluation of measurement data — Guide to the expression of uncertainty in measurement*. Joint Committee for Guides in Metrology.

Johnson, D. A., Gu, M., & Gaunt, B. (2012). Wind Turbine Performance in Controlled Conditions: Experimental Results. *International Journal of Green Energy*, *2016*, null-null. http://doi.org/10.1080/15435075.2012.675799

Johnson, G. L. (2001). *Wind energy systems*. Retrieved from http://www.cd3wd.com/cd3wd_40/JF/JF_OTHER/BIG/Wind Energy - Johnson.pdf

Kaimal, J. C., & Gaynor, J. E. (1991). Another look at sonic thermometry. *Boundary-Layer Meteorology*, *56*(4), 401–410. http://doi.org/10.1007/BF00119215

Kalnins, A. (2018). Multicollinearity: How common factors cause Type 1 errors in multivariate regression. *Strategic Management Journal*, *39*(8), 2362–2385. http://doi.org/10.1002/smj.2783

Kalvig, S., Manger, E., & Hjertager, B. (2014). Comparing different CFD wind turbine modelling approaches with wind tunnel measurements. *Journal of Physics: Conference Series*, *555*(1). http://doi.org/10.1088/1742-6596/555/1/012056

Katic, I., Højstrup, J., & Jensen, N. O. (1986). A Simple Model for Cluster Efficiency. In *European Wind Energy Association Conference* (Vol. 1). Rome.

Katul, G. G., Parlange, M. B., & Chu, C. R. (1994). Intermittency, local isotropy, and non-Gaussian statistics in atmospheric surface layer turbulence. *Physics of Fluids*, *6*(7), 2480–2492. http://doi.org/10.1063/1.868196

Kelley, N. D., Jonkman, B. J., & Scott, G. N. (2005). The Impact of Coherent Turbulence on Wind Turbine Aeroelastic Response and Its Simulation.

Kim, J.-H. (1999). Spurious correlation between ratios with a common divisor. *Statistics & Probability Letters*, *44*, 383–386.

Kinoshita, N., & Niino, H. (1990). On the depth of the surface layer in the turbulent Ekman Layer. *Journal of the Meteorological Society of Japan*, *68*(6), 747–751.

Kolmogorov, A. (1941). The Local Structure of Turbulence in Incompressible Viscous Fluid for Very Large Reynolds Numbers. *Dokl. Akad. Nauk SSSR*, *30*, 299–303.

Kowshalya, A. M., Madhumathi, R., & Gopika, N. (2019). Correlation Based Feature Selection Algorithms for Varying Datasets of Different Dimensionality. *Wireless Personal Communications*, (0123456789). http://doi.org/10.1007/s11277-019-06504-w

Kraus, H. (2008). *Grundlagen der Grenzschicht-Meteorologie*. Springer Berlin Heidelberg.

Krogsæter, O., & Reuder, J. (2015). Validation of boundary layer parameterization schemes in the Weather Research and Forecasting (WRF) model under the aspect of offshore wind energy applications—part II: boundary layer height and atmospheric stability. *Wind Energy*, *18*, 1291–1302. http://doi.org/10.1002/we.1765

Kubik, M. L., Coker, P. J., & Hunt, C. (2011). Using meteorological wind data to estimate turbine generation output: a sensitivity analysis. In *World renewable energy congress 2011* (pp. 4074–4081). C. http://doi.org/10.3384/ecp110574074

Kusiak, A., & Zhang, Z. (2010). Analysis of Wind Turbine Vibrations Based on SCADA Data. *Journal of Solar Energy Engineering*, *132*(3), 031008. http://doi.org/10.1115/1.4001461

Kvålseth, T. O. (2017). Coefficient of variation: the second-order alternative. *Journal of Applied Statistics*, *44*(3), 402–415. http://doi.org/10.1080/02664763.2016.1174195

Kwiatkowski, D., Phillips, P. C. B., Schmidt, P., & Shin, Y. (1992). Testing the null hypothesis of stationarity against the alternative of a unit root. *Journal of Econometrics*, *54*, 159–178.

Kwon, S.-D. (2010). Wind energy uncertainty caused by wind characteristics.

Lange, B., Larsen, S., Hojstrup, J., & Barthelmie, R. J. (2004). Importance of thermal effects and sea surface roughness for offshore wind resource assessment. *Journal of Wind*

Engineering and Industrial Aerodynamics, *92*(11).

Lee, G., Ding, Y., Genton, M. G., & Xie, L. (2015). Power Curve Estimation With Multivariate Environmental Factors for Inland and Offshore Wind Farms. *Journal of the American Statistical Association*, *110*(509), 56–67. http://doi.org/10.1080/01621459.2014.977385

Lee, K. Y., Tsao, S. H., Tzeng, C. W., & Lin, H. J. (2017). Influence of the vertical wind and wind direction on the power output of a small vertical-axis wind turbine installed on the rooftop of a building. *Applied Energy*, *209*(August 2017), 383–391. http://doi.org/10.1016/j.apenergy.2017.08.185

Lee, L., Srivastava, P. K., & Petropoulos, G. P. (2017). Overview of Sensitivity Analysis Methods in Earth Observation Modeling. In G. P. Petropoulos & P. K. Srivastava (Eds.), *Sensitivity Analysis in Earth Observation Modelling*. Elsevier.

Lee, X., Massman, W., & Law, B. (2004). *Handbook of Micrometeorology*. Dordrecht: Kluwer Academic Publishers.

Li, S., Wunsch, D. C., O'Hair, E., & Giesselmann, M. G. (2002). Comparative Analysis of Regression and Artificial Neural Network Models for Wind Turbine Power Curve Estimation. *Journal of Solar Energy Engineering*, *123*(4), 327. http://doi.org/10.1115/1.1413216

Lydia, M., Kumar, S. S., Selvakumar, A. I., & Kumar, G. E. P. (2014). A comprehensive review on wind turbine power curve modeling techniques. *Renewable and Sustainable Energy Reviews*, *30*, 452–460. http://doi.org/10.1016/j.rser.2013.10.030

Mahrt, L., Sun, J., & Stauffer, D. (2015). Dependence of Turbulent Velocities on Wind Speed and Stratification. *Boundary-Layer Meteorology*, *155*(1), 55–71. http://doi.org/10.1007/s10546-014-9992-5

Manobel, B., Sehnke, F., Lazzús, J. A., Salfate, I., Felder, M., & Montecinos, S. (2018). Wind turbine power curve modeling based on Gaussian Processes and Artificial Neural Networks. *Renewable Energy*, *125*, 1015–1020.

http://doi.org/10.1016/j.renene.2018.02.081

Markowski, P., & Richardson, Y. (2006). On the Classification of Vertical Wind Shear as Directional Shear versus Speed Shear. *Weather and Forecasting*, *21*, 242–247.

Mauder, M., Cuntz, M., Drüe, C., Graf, A., Rebmann, C., Schmid, H. P., … Steinbrecher, R. (2013). A strategy for quality and uncertainty assessment of long-term eddy-covariance measurements. *Agricultural and Forest Meteorology*, *169*, 122–135. http://doi.org/10.1016/j.agrformet.2012.09.006

Mauder, M., & Foken, T. (2006). Impact of post-field data processing on eddy covariance flux estimates and energy balance closure. *Meteorologische Zeitschrift*, *15*(6), 597–609. http://doi.org/10.1127/0941-2948/2006/0167

Mckay, P. M., Carriveau, R., Ting, D. S.-K., & Johrendt, J. L. (2013). Global sensitivity analysis of wind turbine power output. *Wind Energy*, (April 2013). http://doi.org/10.1002/we.1614

MEASNET. (2009). *Power performance measurement Version 5*.

MEASNET. (2014). *Shortcomings of AEP calculation as defined in IEC61400-12-1*.

Mellinghoff, H. (2012). Development of Power Curve Measurement Standards. In *DEWEK 2012: Deutsche Windenergie-Konferenz*. Bremen.

Mohan, M., & Siddiqui, T. A. (1998). Analysis of various schemes for the estimation of atmospheric stability classification. *Atmospheric Environment*, *32*(21), 3775—3781.

Monin, A. S., & Obukhov, A. M. (1954). Basic laws of turbulent mixing in the surface layer of the atmosphere. *Contrib. Geophys. Inst. Acad. Sci. USSR*, *24*(151), 163–187.

Montes, E., Arnedo, A., Cordón, R., & Zubiaur, R. (2009). Influence of wind shear and seasonality on the power curve and annual energy production of wind turbines. *Ewec 2009*, (1), 7.

Morales, A., & Peinke, J. (2012). Assessment of turbulence by high-order statistics.

Offshore example. *European Wind Energy Conference & Exhibition 2012*, *126*, 38120. http://doi.org/10.1002/3.

Morales, A., Wachter, M., & Peinke, J. (2010). Advanced characterization of wind turbulence by higher order statistics. In *EWEC 2010*.

Morales, A., Wächter, M., & Peinke, J. (2012). Characterization of wind turbulence by higher-order statistics. *Wind Energy*, *15*, 391–406. http://doi.org/10.1002/we.478

Morshedizadeh, M., Kordestani, M., Carriveau, R., Ting, D. S.-K., & Saif, M. (2017). Improved power curve monitoring of wind turbines. *Wind Engineering*, 0309524X1770973. http://doi.org/10.1177/0309524X17709730

Mortensen, N. G., Nielsen, M., & Ejsing Jørgensen, H. (2015). Comparison of Resource and Energy Yield Assessment Procedures 2011-2015: What have we learned and what needs to be done? *Proceedings of the EWEA Annual Event and Exhibition 2015*, 10.

Motta, M., Barthelmie, R. J., & P. Vølund. (2005). The influence of non-logarithmic wind speed profiles on potential power output at danish offshore sites. *Wind Energy*, *8*(2), 219–236. http://doi.org/10.1002/we.146

Mücke, T., Kleinhans, D., & Peinke, J. (2011). Atmospheric turbulence and its influence on the alternating loads on wind turbines. *Wind Energy*, *14*, 301–316. http://doi.org/10.1002/we.422

Muñoz-Esparza, D., Sharman, R. D., & Lundquist, J. K. (2017). Turbulent dissipation rate in the atmospheric boundary layer: observations and WRF mesoscale modeling during the XPIA field campaign. *Monthly Weather Review*, MWR-D-17-0186.1. http://doi.org/10.1175/MWR-D-17-0186.1

Newman, J. F., & Klein, P. M. (2014). The Impacts of Atmospheric Stability on the Accuracy of Wind Speed Extrapolation Methods. *Resources*, *3*(1), 81–105. http://doi.org/10.3390/resources3010081

Newman, J. F., Klein, P. M., Wharton, S., Sathe, A., Bonin, T. A., Chilson, P. B., & Muschinski, A. (2015). Evaluation of three lidar scanning strategies for turbulence measurements. *Atmospheric Measurement Techniques*, *8*(11), 12329–12381. http://doi.org/10.5194/amtd-8-12329-2015

Niebsch, J. (2011). Determination of Rotor Imbalances. In R. Carriveau (Ed.), *Fundamental and Advanced Topics in Wind Power*. London: IntechOpen. http://doi.org/10.5772/731

Nieuwstadt, F. T. M. (1984). The Turbulent Structure of the Stable, Nocturnal Boundary Layer. *Journal of the Atmospheric Sciences*. http://doi.org/10.1175/1520-0469(1984)041<2202:TTSOTS>2.0.CO;2

OFCM. (2017). Federal Meteorological Handbook No . 1 Surface Weather Observations and Reports. Office of the Federal Coordinator for Meteorological Services and Supporting Research.

Optis, M. (2015). *The modelling of the wind profile under stable stratification at heights relevant to wind power: A comparison of models of varying complexity*. University of Victoria. http://doi.org/10.1017/CBO9781107415324.004

Optis, M., Monahan, A., & Bosveld, F. C. (2016). Limitations and breakdown of Monin–Obukhov similarity theory for wind profile extrapolation under stable stratification. *Wind Energy*, *19*(6), 1053–1072. http://doi.org/10.1002/we.1883

Paiva, L. T., Rodrigues, C. V., & Palma, J. M. L. M. (2013). Determining wind turbine power curves based on operating conditions. http://doi.org/10.1002/we

Pandit, R. K., Infield, D., & Carroll, J. (2019). Incorporating air density into a Gaussian process wind turbine power curve model for improving fitting accuracy. *Wind Energy*, *22*(2), 302–315. http://doi.org/10.1002/we.2285

Parkhe, V. (2016). IEA Task 32 Power Performance Uncertainty Round Robin. In *20th meeting of the Power Curve Working Group* (pp. 1–12). Minneapolis. Retrieved from https://pcwg.org/proceedings/2016-09-29/03 - IEA Task 32 Round Robin on 12-1 Ed. 2 Power Performance Measurement Uncertainty using Lidar, Vineet Parkhe (DNV GL).pdf

PCWG. (2013). Inner-Outer Range Proposal. Retrieved from http://www.pcwg.org/proposals/PCWG-Inner-Outer-Range-Proposal-Dec-2013.pdf

Pedersen, T. F. (2004). On wind turbine power performance measurements at inclined airflow. *Wind Energy*, *7*(3), 163–176. http://doi.org/10.1002/we.112

Pelletier, F., Masson, C., & Tahan, A. (2016). Wind turbine power curve modelling using artificial neural network. *Renewable Energy*, *89*, 207–214. http://doi.org/10.1016/j.renene.2015.11.065

Peña, A., & Floors, R. (2014). The Høvsøre Tall Wind-Profile Experiment : A Description of Wind Profile Observations in the Atmospheric Boundary Layer, 69–89. http://doi.org/10.1007/s10546-013-9856-4

Peña, A., Gryning, S. E., Mann, J., & Hasager, C. B. (2010). Length scales of the neutral wind profile over homogeneous terrain. *Journal of Applied Meteorology and Climatology*, *49*(4), 792–806. http://doi.org/10.1175/2009JAMC2148.1

Peña, A., Réthoré, P. E., & Rathmann, O. (2014). Modeling large offshore wind farms under different atmospheric stability regimes with the Park wake model. *Renewable Energy*, *70*, 164–171. http://doi.org/10.1016/j.renene.2014.02.019

Petersen, E. L., Mortensen, N. G., Landberg, L., Højstrup, J., & Frank, H. P. (1998). Wind power meteorology. Part I: climate and turbulence. *Wind Energy*, *1*(S1), 25–45.

Pope, S. B. (2000). *Turbulent flows*. Cambridge University Press. http://doi.org/10.1017/CBO9780511840531

Poulos, G. S., Blumen, W., Fritts, D. C., Lundquist, J. K., Sun, J., Burns, S. P., … Jensen, M. (2002). CASES-99: A comprehensive investigation of the stable nocturnal boundary layer. *Bulletin of the American Meteorological Society*, *83*(4), 555–581. http://doi.org/10.1175/1520-0477(2002)083<0555:CACIOT>2.3.CO;2

Rareshide, E., Tindal, A., Johnson, C., Graves, A., Simpson, E., Bleeg, J., … Schoborg, D. (2009). Effects of complex wind regimes on turbine performance. In *AWEA Windpower* (pp. 1–15).

Rodrigues, C. V., Matos, J. C., Paiva, L. T., & Palma, J. M. L. M. (2010). Analysis of the Similarity in Turbulence Intensity and Wind Shear as Function of the Wind Velocity : Field Measurements and Numerical Results. In *European Wind Energy Conference* (pp. 1–10). Warsaw.

Rojas, R. (1996). *Neural networks: A systematic introduction*. Berlin Heidelberg: Springer-Verlag.

Rossby, C.-G., & Montgomery, R. B. (1935). The layer of frictional influence in wind and ocean currents. *Papers in Physical Oceanography and Meteorology*, *3*(71), 1–101. http://doi.org/10.1575/1912/1157

Roy, S. (2012). Impact of Short Duration Wind Variations on Output of a Pitch Angle Controlled Turbine. *IEEE Transactions on Sustainable Energy*, *3*(3), 566–575.

Roy, S. (2014). Performance prediction of active pitch-regulated wind turbine with short duration variations in source wind. *Applied Energy*, *114*, 700–708. http://doi.org/10.1016/j.apenergy.2013.10.009

Sakagami, Y., Santos, P. A. A., Haas, R., Passos, J. C., & Taves, F. F. (2015). Effects of turbulence, wind shear, wind veer, and atmospheric stability on power performance : a case study in Brazil. In *EWEA 2015*. Paris.

Saltelli, A., Ratto, M., Andres, T., Campolongo, F., Cariboni, J., Gatelli, D., … Tarantola, S. (2008). *Global Sensitivity Analysis: The Primer*. Wiley-Blackwell.

Saltelli, A., Tarantola, S., & Chan, K. P. (1999). A Quantitative Model-Independent Method for Global Sensitivity Analysis of Model Output. *Technometrics*, *41*(1), 39–56. http://doi.org/10.1080/00401706.1999.10485594

Sarle, W. S. (2001). Generalization. Retrieved March 20, 2019, from http://www.faqs.org/faqs/ai-faq/neural-nets/part3/

Sathe, A. R., Gryning, S.-E., & Peña, A. (2011). Comparison of the atmospheric stability and wind profiles at two wind farm sites over a long marine fetch in the North Sea.

Wind Energy, *14*(6).

Schaibly, J. H., & Shuler, K. E. (1973). A study of the sensitivity of coupled reaction systems to uncertainties in rate coefficients II: Applications. *Journal of Chemical Physics*, *59*, 3879-3888.

Schlechtingen, M., Santos, I. F., & Achiche, S. (2013). Using Data-Mining Approaches for Wind Turbine Power Curve Monitoring: A Comparative Study. *IEEE Transactions on Sustainable Energy*, *4*(3), 671–679. http://doi.org/10.1109/TSTE.2013.2241797

Schotanus, P., Nieuwstadt, F. T. M., & De Bruin, H. A. R. (1983). Temperature measurement with a sonic anemometer and its application to heat and moisture fluxes. *Boundary-Layer Meteorology*, *26*, 81–93. Retrieved from http://search.jamas.or.jp/link/ui/1999062159

Schottler, J., Reinke, N., Hölling, A., Whale, J., Peinke, J., & Hölling, M. (2016). On the impact of non-Gaussian wind statistics on wind turbines - an experimental approach. *Wind Energy Science Discussions*, (2007), 1–21. http://doi.org/10.5194/wes-2016-24

Scottish Government. (2017). *Scottish Energy Strategy*. Retrieved from https://www.gov.scot/publications/scottish-energy-strategy-future-energy-scotland-9781788515276/

Sheela, K. G., & Deepa, S. N. (2014). Selection of number of hidden neurons in neural networks in renewable energy systems. *Journal of Scientific and Industrial Research*, *73*(10), 686–688.

Simmons, L. (2016). IEA Task 32 Power Performance Uncertainty Round Robin. In *21st meeting of the Power Curve Working Group*. Glasgow. Retrieved from https://pcwg.org/proceedings/2016-12-13/03 - IEC61400-12-1 Ed 2 Round Robin Results Overview, Luke J Simmons, DNV GL.pptx

Slade, D. H. (1968). *Meteorology and atomic energy*. U. S. Atomic Energy Commission Office of Information Services.

Sohoni, V., Gupta, S. C., & Nema, R. K. (2016). A critical review on wind turbine power curve modelling techniques and their applications in wind based energy systems. *Journal of Energy*, *2016*. http://doi.org/10.1155/2016/8519785

Sprenger, J. (2009). Science without (parametric) models: the case of bootstrap resampling. *Synthese*, *180*(1), 65–76. http://doi.org/10.1007/s11229-009-9567-z

St. Martin, C. M., Lundquist, J. K., Clifton, A., Poulos, G. S., & Schreck, S. J. (2016). Wind turbine power production and annual energy production depend on atmospheric stability and turbulence. *Wind Energy Science*, *1*, 1–37. http://doi.org/10.5194/wes-1-221-2016

Starkenburg, D., Metzger, S., Fochesatto, G. J., Alfieri, J. G., Gens, R., Prakash, A., & Cristóbal, J. (2016). Assessment of despiking methods for turbulence data in micrometeorology. *Journal of Atmospheric and Oceanic Technology*, *33*(9), 2001–2013. http://doi.org/10.1175/JTECH-D-15-0154.1

Stiperski, I. (2018). Dependence of near-surface similarity scaling on the anisotropy, (May 2017), 641–657. http://doi.org/10.1002/qj.3224

Stone, N. (2015). University of Minnesota EOLOS Educational Data Set : An Overview. Retrieved from http://eolos.umn.edu/sites/g/files/pua1541/f/general/eolos_educational_data_set.pdf

Stuart, P. (2013). Round Robin Results Overview. In *4th Meeting of the Power Curve Working Group*. Retrieved from https://pcwg.org/proceedings/2013-09-19/02-Round-Robin-Results-Overview-Peter-Stuart-RES.pdf

Stull, R. B. (1988). *An introduction to boundary-layer meteorology*. Kluwer Academic Publishers.

Stull, R. B. (2015). *Practical Meteorology: An Algebra-based Survey of Atmospheric Science*. Vancouver: University of British Columbia. Retrieved from https://www.eoas.ubc.ca/books/Practical_Meteorology/

Sumner, J., & Masson, C. (2006a). A Turbulence-based Model for Resolving Velocity and Temperature Profiles in the Atmospheric Surface Layer. *Wind Engineering*, *30*(4), 317–340.

Sumner, J., & Masson, C. (2006b). Influence of Atmospheric Stability on Wind Turbine Power Performance Curves. *Journal of Solar Energy Engineering*, *128*(4), 531. http://doi.org/10.1115/1.2347714

Sun, J., Lenschow, D. H., Mahrt, L., & Nappo, C. (2013). The Relationships among Wind, Horizontal Pressure Gradient, and Turbulent Momentum Transport during CASES-99. *Journal of the Atmospheric Sciences*, *70*(11), 3397–3414. http://doi.org/10.1175/jas-d-12-0233.1

Tambke, J., Claveri, L., Bye, J. A. T., Poppinga, C., Lange, B., Bremen, L. Von, … Wolff, J. (2006). Offshore Meteorology for Multi-Mega-Watt Turbines.

Taylor, G. I. (1935). Statistical Theory of Turbulence. *Proceedings of the Royal Society A: Mathematical, Physical and Engineering Sciences*, *151*(873), 421–444. http://doi.org/10.1098/rspa.1935.0158

Thapar, V., Agnihotri, G., & Sethi, V. K. (2011). Critical analysis of methods for mathematical modelling of wind turbines. *Renewable Energy*, *36*(11), 3166–3177. http://doi.org/10.1016/j.renene.2011.03.016

Tian, W. (2013). A review of sensitivity analysis methods in building energy analysis. *Renewable and Sustainable Energy Reviews*, *20*, 411–419. http://doi.org/10.1016/j.rser.2012.12.014

Tindal, A., Johnson, C., Leblanc, M., Harman, K., Rareshide, E., & Graves, A. (2008). Site-specific adjustments to wind turbine power curves. In *American Wind Energy Association WINDPOWER* (pp. 1–11).

Türk, M., & Emeis, S. (2010). The dependence of offshore turbulence intensity on wind speed. *Journal of Wind Engineering and Industrial Aerodynamics*, *98*(8–9), 466–471. http://doi.org/10.1016/j.jweia.2010.02.005

US Climate Data. (n.d.). US Climate Data. Retrieved January 24, 2019, from https://www.usclimatedata.com/climate/minneapolis/minnesota/united-states/usmn1524

USEPA. (2000). Meteorological Monitoring Guidance for Regulatory Modeling Applications. *Epa-454/R-99-005*. U.S. Environmental Protection Agency. Retrieved from http://www.epa.gov/scram001/guidance/met/mmgrma.pdf

Van de Wiel, B. J. H., Moene, A. F., & Jonker, H. J. J. (2012). The cessation of continuous turbulence as precursor of the very stable nocturnal boundary layer. *Journal of the Atmospheric Sciences*, *69*(11), 3097–3115. http://doi.org/10.1175/JAS-D-12-064.1

Van de Wiel, B. J. H., Moene, A. F., Jonker, H. J. J., Baas, P., Basu, S., Donda, J. M. M., … Holtslag, A. A. M. (2012). The Minimum Wind Speed for Sustainable Turbulence in the Nocturnal Boundary Layer. *Journal of the Atmospheric Sciences*, *69*(11), 3116–3127. http://doi.org/10.1175/JAS-D-12-0107.1

Van Den Berg, G. P. (2008). Wind turbine power and sound in relation to atmospheric stability. *Wind Energy*, *11*(2), 151–169. http://doi.org/10.1002/we.240

van der Hoven, I. (1957). Power Spectrum of Horizontal Wind Speed in the Frequency Range from 0.0007 to 900 Cycles Per Hour. *Journal of Atmospheric Sciences*, *14*(2). http://doi.org/10.1175/1520-0469(1957)014<0160:PSOHWS>2.0.CO;2

van Hooijdonk, I. G. S., Donda, J. M. M., Clercx, H. J. H., Bosveld, F. C., & van de Wiel, B. J. H. (2015). Shear Capacity as Prognostic for Nocturnal Boundary Layer Regimes. *Journal of the Atmospheric Sciences*, *72*(4), 1518–1532. http://doi.org/10.1175/JAS-D-14-0140.1

Vanderwende, B. J., & Lundquist, J. K. (2012). The modification of wind turbine performance by statistically distinct atmospheric regimes. *Environmental Research Letters*, *7*(3), 034035. http://doi.org/10.1088/1748-9326/7/3/034035

Verhoef, J. P., & Leendertse, G. P. (2001). *Identification of Variables for Site Calibration and Power Curve Assessment in Complex Terrain*. Energy research Centre of the Netherlands.

Vickers, D., & Mahrt, L. (1997). Quality control and flux sampling problems for tower and aircraft data. *Journal of Atmospheric and Oceanic Technology*, *14*(3), 512–526. http://doi.org/10.1175/1520-0426(1997)014<0512:QCAFSP>2.0.CO;2

Vogelezang, D. H. P., & Holtslag, A. A. M. (1996). Evaluation and model impacts of alternative boundary-layer height formulations. *Boundary-Layer Meteorology*, *81*(3–4), 245–269. http://doi.org/10.1007/BF02430331

Wächter, M., Heißelmann, H., Holling, M., Morales, A., Milan, P., Mucke, T., … Rinn, P. (2012). The turbulent nature of the atmospheric boundary layer and its impact on the wind energy conversion process. *Journal of Turbulence*, *13*(N26).

Wagenaar, J. W., & Eecen, P. J. (2009). *Measurements of Wind , Wave and Currents at the Offshore Wind Farm Egmond aan Zee*. Energy Research Centre of the Netherlands (ECN).

Wagner, R., Antoniou, I., Pedersen, S. M., Courtney, M. S., & Jørgensen, H. E. (2009). The influence of the wind speed profile on wind turbine performance measurements. *Wind Energy*, *12*(4), 348–362. http://doi.org/10.1002/we.297

Wagner, R., Cañadillas, B., Clifton, A., Feeney, S., Nygaard, N., Poodt, M., … Wagenaar, J. W. (2014). Rotor equivalent wind speed for power curve measurement – comparative exercise for IEA Wind Annex 32. *Journal of Physics: Conference Series*, *524*, 012108. http://doi.org/10.1088/1742-6596/524/1/012108

Wagner, R., Courtney, M., Gottschall, J., & Lindelöw-Marsden, P. (2011). Accounting for the speed shear in wind turbine power performance measurement. *Wind Energy*, *14*, 993–1004. http://doi.org/10.1002/we.509

Wallace, J. M., & Hobbs, P. V. (2006). *Atmospheric Science: An Introductory Survey* (2nd ed.). Elsevier.

Walter, K., Weiss, C. C., Swift, A. H. P., Chapman, J., & Kelley, N. D. (2009). Speed and Direction Shear in the Stable Nocturnal Boundary Layer. *Journal of Solar Energy Engineering*, *131*(1), 011013. http://doi.org/10.1115/1.3035818

Wharton, S., & Lundquist, J. (2011). Assessing atmospheric stability and the impacts on wind characteristics at an onshore wind farm. *Wind Energy*, *15*(4), 525–546.

Wharton, S., & Lundquist, J. K. (2010). Atmospheric Stability Impacts on Power Curves of Tall Wind Turbines - An Analysis of a West Coast North American Wind Farm.

Wharton, S., & Lundquist, J. K. (2012). Atmospheric stability affects wind turbine power collection. *Environmental Research Letters*, *7*(1), 014005. http://doi.org/10.1088/1748-9326/7/1/014005

Wilczak, J. M., Oncley, S. P., & Stage, S. A. (2001). Sonic anemometer tilt correction algorithms. *Boundary-Layer Meteorology*, *99*(1), 127–150. http://doi.org/10.1023/a:1018966204465

Wilson, J. M., & Venayagamoorthy, S. K. (2015). A Shear-Based Parameterization of Turbulent Mixing in the Stable Atmospheric Boundary Layer. *Journal of the Atmospheric Sciences*, *72*(5), 150210124617001. http://doi.org/10.1175/JAS-D-14-0241.1

Yamartino, R. J. (1984). A Comparison of Several "Single-Pass" Estimators of the Standard Deviation of Wind Direction. *Journal of Climate and Applied Meteorology*. http://doi.org/10.1175/1520-0450(1984)023<1362:ACOSPE>2.0.CO;2

Yu, L., & Liu, H. (2004). Efficient Feature Selection via Analysis of Relevance and Redundancy. *Journal of Machine Learning Research*, *5*, 1205–1224.

Zahumenský, I. (2004). Guidelines on Quality Control Procedures for Data from Automatic Weather Stations. *CBS/OPAG-IOS/ET AWS-3/Doc. 4(1)*. Geneva: World Meteorological Association. Retrieved from https://www.wmo.int/pages/prog/www/OSY/Meetings/ET-AWS3/Doc4(1).pdf

Zilitinkevich, S. S., & Esau, I. N. (2005). Resistance and heat-transfer laws for stable and neutral planetary boundary layers: Old theory advanced and re-evaluated. *Quarterly Journal of the Royal Meteorological Society*, *131*(609), 1863–1892. http://doi.org/10.1256/qj.04.143

Appendix A: Baseline power curve details

A.1 Reference power curve

Table 35 provides the details of both the reference power curve and the nominal wind distribution which is required to perform the AEP calculation.

Table 35: Reference power curve and nominal wind distribution at 1.225 kg m^{-3}

Wind speed	**Interval**		**Wind dist.**	**Power**	**Wind speed**	**Interval**		**Wind dist.**	**Power**
	Min	Max				Min	Max		
ms-1	ms-1	ms-1	Hours/year	kW	**ms-1**	ms-1	ms-1	Hours/year	kW
0.5	0	0.75	90	0	**13**	12.75	13.25	47	2468
1	0.75	1.25	234	0	**13.5**	13.25	13.75	30	2477
1.5	1.25	1.75	403	0	**14**	13.75	14.25	19	2486
2	1.75	2.25	583	0	**14.5**	14.25	14.75	12	2495
2.5	2.25	2.75	763	0	**15**	14.75	15.25	7	2500
3	2.75	3.25	931	0	**15.5**	15.25	15.75	4	2500
3.5	3.25	3.75	1076	49	**16**	15.75	16.25	2	2500
4	3.75	4.25	1190	99	**16.5**	16.25	16.75	1	2500
4.5	4.25	4.75	1267	152	**17**	16.75	17.25	1	2500
5	4.75	5.25	1304	205	**17.5**	17.25	17.75	0	2500
5.5	5.25	5.75	1301	290	**18**	17.75	18.25	0	2500
6	5.75	6.25	1259	374	**18.5**	18.25	18.75	0	2500
6.5	6.25	6.75	1185	484	**19**	18.75	19.25	0	2500
7	6.75	7.25	1084	593	**19.5**	19.25	19.75	0	2500
7.5	7.25	7.75	966	756	**20**	19.75	20.25	0	2500
8	7.75	8.25	838	918	**20.5**	20.25	20.75	0	2500
8.5	8.25	8.75	707	1162	**21**	20.75	21.25	0	2500
9	8.75	9.25	582	1405	**21.5**	21.25	21.75	0	2500
9.5	9.25	9.75	466	1621	**22**	21.75	22.25	0	2500
10	9.75	10.25	364	1836	**22.5**	22.25	22.75	0	2500
10.5	10.25	10.75	276	2016	**23**	22.75	23.25	0	2500
11	10.75	11.25	204	2196	**23.5**	23.25	23.75	0	2500
11.5	11.25	11.75	147	2300	**24**	23.75	24.25	0	2500
12	11.75	12.25	103	2370	**24.5**	24.25	24.75	0	2500
12.5	12.25	12.75	70	2425	**25**	24.75	25.25	0	2500

Under normal circumstances, the wind distribution would be extrapolated from independent measurements; in this case, it is based on the Weibull parameters derived in §6.5 (shape = 2.39, scale = 6.53). The power values correspond to standard sea-level pressure of 1.225 kgm^{-3}.

A.2 Test equipment

Table 36 lists the relevant instruments with their respective uncertainty limits. In the case of the power transducer, the uncertainty limit was not available from the documentation and has therefore been estimated based on similar configurations.

Table 36: Test equipment

Sensor	Model	Height (m)	Uncertainty limit
Sonic anemometer	Campbell Scientific CSAT3 3D	127.9	0.04 ms^{-1} / 0.002°C
Sonic anemometer	Campbell Scientific CSAT3 3D	79.1	0.04 ms^{-1} / 0.002°C
Sonic anemometer	Campbell Scientific CSAT3 3D	29.6	0.04 ms^{-1} / 0.002°C
Sonic anemometer	Campbell Scientific CSAT3 3D	9.9	0.04 ms^{-1} / 0.002°C
Relative Humidity Sensor	Met One 038E/593A	80	2%
Pressure Sensor	Met One 092	80	0.75 hPa
Power sensor	Turbine SCADA		0.5 kW
Data logger	Campbell Scientific CR3000		

IEC2017 requires anemometers to be calibrated in MEASNET approved testing facilities, and the definition of a procedure to ensure the calibration of the instruments throughout the measurement campaign. (IEC, 2017 §10). The results of the calibration tests are used to apply corrections to the measured data values, and in the calculation of uncertainty. However, no information was available on the calibration of the instruments used in this study. This is somewhat mitigated by the use of Campbell Scientific CSAT3 sonic anemometers which are designed not to require field calibration (Campbell Scientific, 1998). There was also no opportunity to perform an in-situ comparison as described in Annex K of IEC2017 since none of the instruments are sited at the same elevation.

A.3 Turbine generating status

As discussed earlier, the output of the turbine was frequently constrained through supervisory curtailment. It is common in PPT to exclude TMA values which are derived from less than 100% of the expected data points. Where a turbine has been curtailed for part of a ten-minute period, for example, that record is discarded regardless of the size of the deficit. In order to maximise the number of TMA records available for analysis, a looser requirement of 90% is applied here. Records were also excluded where the SCADA fault code indicated a state other than *Run* or *Feather check*.

A.4 Quantity of data

Table 37 contains record counts by wind speed bin and by reference density. The counts in the baseline column refer to the baseline power curve and are the result of applying the quality filters but not the contractual filters. The counts in the filtered column have had both types of filter applied. Bins with fewer than 3 records have been omitted except for the 13.5 ms^{-1} bin in the case of the filtered data. The value for this bin is interpolated as mandated by IEC2017.

A.5 Data normalisation

The booms on the Eolos met mast are mounted at 210º, and the anemometers are in the wake of the mast when the wind direction is around 30º. Since this direction falls within the sector already excluded because of the turbine wake, mast flow distortion correction is not required. Likewise, flow distortion corrections due to topology are not necessary since no site calibration is required and no significant obstacles were identified.

REWS is calculated and recorded during the dataset preparation. Given the loss of data at 127.9 m through quality filtering, however, the measured hub height wind speed is used in the measured power curve.

It is not possible to apply specific calibration correction to the data from the various instruments because that information is not available.

The wind speed data from the sonic anemometers is normalised to sea-level density of 1.225 kgm^{-3} and also to a mean site density of 1.188 kgm^{-3}.

Table 37: Power curve database for site-mean air density

Wind speed bin (ms^{-1})			Baseline		Filtered	
Centre	Min	Max	TMA records at 1.225 kg m^{-3}	TMA records at 1.188 kg m^{-3}	TMA records at 1.225 kg m^{-3}	TMA records at 1.188 kg m^{-3}
3.5	3.25	3.75	172	146	24	18
4	3.75	4.25	410	399	101	97
4.5	4.25	4.75	679	653	218	206
5	4.75	5.25	811	781	259	253
5.5	5.25	5.75	890	880	291	282
6	5.75	6.25	962	953	300	296
6.5	6.25	6.75	979	967	288	299
7	6.75	7.25	811	827	251	238
7.5	7.25	7.75	698	713	240	244
8	7.75	8.25	482	513	182	194
8.5	8.25	8.75	355	370	140	143
9	8.75	9.25	227	247	119	133
9.5	9.25	9.75	157	162	99	90
10	9.75	10.25	102	117	73	79
10.5	10.25	10.75	75	72	57	55
11	10.75	11.25	41	52	32	42
11.5	11.25	11.75	28	26	24	22
12	11.75	12.25	15	18	13	16
12.5	12.25	12.75	14	12	14	12
13	12.75	13.25	6	12	4	10
13.5	13.25	13.75	7	3	4	2
14	13.75	14.25	5	8	4	5
14.5	14.25	14.75	5	5	4	5
Total			**7931**	**7936**	**2741**	**2741**

A.6 Measured power curve at standard air density (1.225 kg m-3)

The standard plot of minimum, maximum, mean and standard deviation of the TMA values is shown in Fig. 66 The four series have the expected distribution except that the highest mean values fall somewhat short of the rated value of 2.5 MW which should be achieved at 15 ms^{-1}. As noted previously, however, the number of data points available above about 14 ms^{-1} is very limited. In addition, data with a curtailment level of 2,300 kW was retained in the dataset in order to maximise the overall quantity of data available. This would account for the behaviour of the mean values which level out at 2,300 kW above 14 ms^{-1}. This is more clearly shown in Fig. 67 where only the plot of mean power output is shown as a function of hub height wind speed.

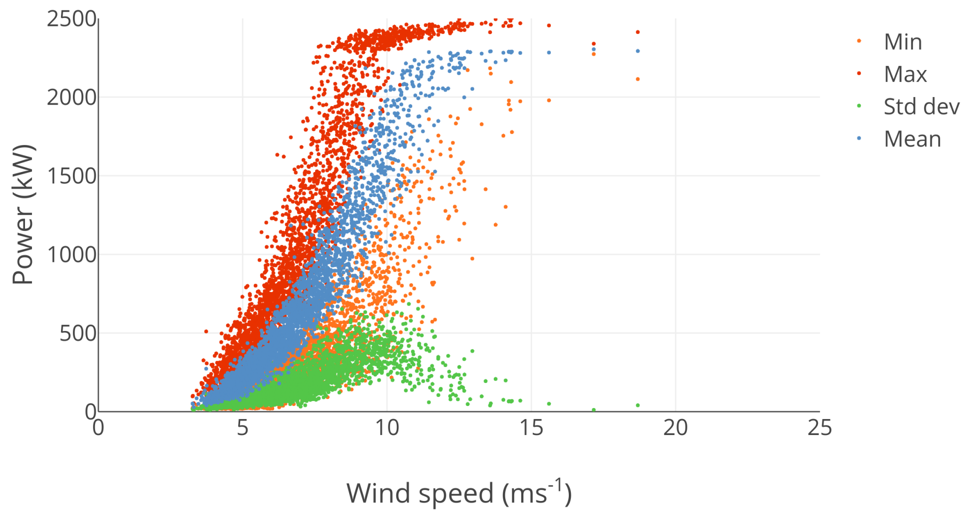

Figure 53: Summary statistics plot

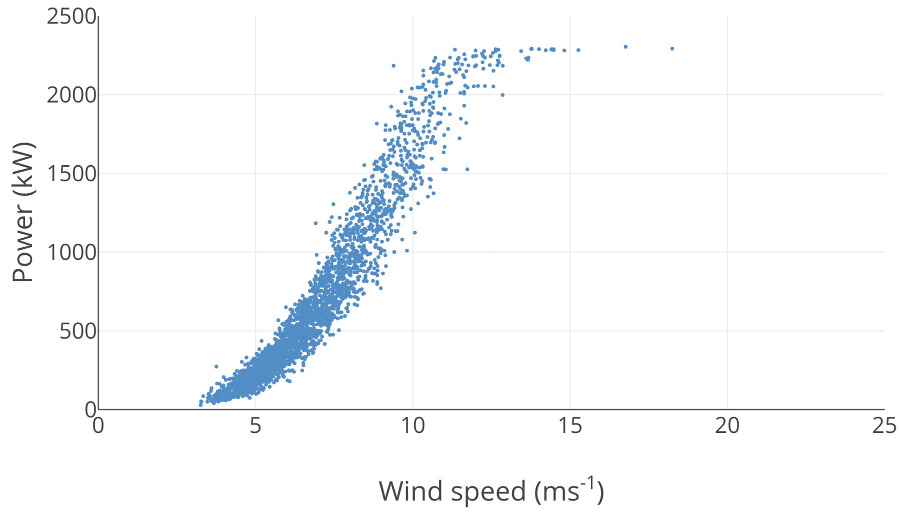

Figure 54: Sea-level density scatterplot

The measured power curve and the plot of power coefficient as a function of wind speed are presented in Fig. 68 with the calculated uncertainty shown as vertical error bars. The source data for the power curve plot is presented in Table 38.

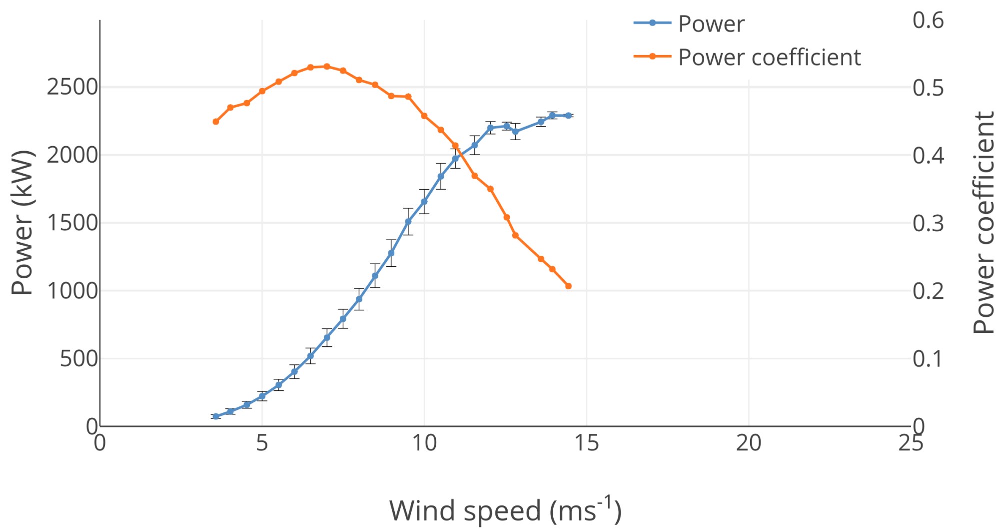

Figure 55: Measured power curve and power coefficient for sea-level air density

Table 38: Sea-level uncertainty results

Wind speed (ms^{-1})	Active power (kW)	Power coefficient	Records per bin	Category A uncertainty (kW)	Category B uncertainty (kW)	Combined uncertainty (kW)
3.57	73.09	0.45	24	5.01	13.48	14.38
4.02	109.36	0.47	101	3.68	20.32	20.65
4.53	158.74	0.48	218	3.18	25.66	25.86
5.00	222.15	0.49	259	3.81	34.30	34.51
5.51	304.73	0.51	291	3.91	41.69	41.87
6.00	402.72	0.52	300	5.23	50.55	50.82
6.49	518.18	0.53	288	6.09	57.38	57.70
7.00	652.56	0.53	251	8.49	65.55	66.10
7.49	791.18	0.53	240	10.35	69.56	70.32
7.99	935.29	0.51	182	12.70	79.25	80.26
8.48	1108.17	0.50	140	15.82	85.98	87.42
8.98	1274.40	0.49	119	21.95	95.54	98.03
9.50	1506.56	0.49	99	23.48	95.62	98.46
10.00	1653.45	0.46	73	25.11	85.64	89.24
10.51	1838.87	0.44	57	31.30	89.71	95.02
10.96	1969.99	0.41	32	35.85	62.32	71.90
11.55	2068.35	0.37	24	37.93	58.30	69.56
12.04	2196.15	0.35	13	20.01	41.22	45.82
12.54	2208.60	0.31	14	20.80	20.94	29.52
12.81	2168.40	0.28	4	58.70	11.61	59.84
13.59	2240.33	0.25	4	12.21	32.44	34.66
13.94	2287.74	0.23	4	2.07	25.49	25.57
14.44	2286.41	0.21	4	1.31	9.07	9.16

A.7 Annual Energy Production at standard air density (1.225 kg m-3)

Estimates of AEP are presented in Table 39 for standard air density. The final row in the table shows the site-specific AEP calculated using the Weibull shape and scale parameters found in §6.5. The value for the site-specific measured AEP represents 95.49% of the theoretical figure of 4677 MWh/year obtained using the reference power curve and the Weibull parameters from §6.5. The turbine would therefore pass the IEC performance test allowing for the deviations from the standard procedure described above.

Table 39: Sea-level AEP results

Wind speed (Rayleigh) (ms^{-1})	AEP measured (MWh/year)	Standard uncertainty in AEP		AEP extrapolated (MWh/year)	Status
		(MWh/year)	(%)		
4	1836	19	1.03	1837	
5	3404	25	0.73	3433	
6	5048	30	0.59	5259	
7	6376	33	0.52	7083	Incomplete
8	7214	34	0.47	8754	Incomplete
9	7590	34	0.45	10195	Incomplete
10	7617	32	0.42	11363	Incomplete
11	7414	30	0.4	12242	Incomplete
Weibull	4572	32	0.43	4598	

Appendix B: Eolos dataset

The core of the Eolos dataset was kindly provided by Eolos Wind Energy Research, a Minnesota-based wind energy group of university researchers and industry partners. The dataset includes SCADA data from the turbine itself and measurements from instruments mounted on the associated met mast. The Eolos data was supplemented with surface pressure data from Iowa Environmental Mesonet weather stations and data on local sunrise and sunset times from a reliable Internet source. In all, seven individual subsets of data were synchronised in order to create the final dataset.

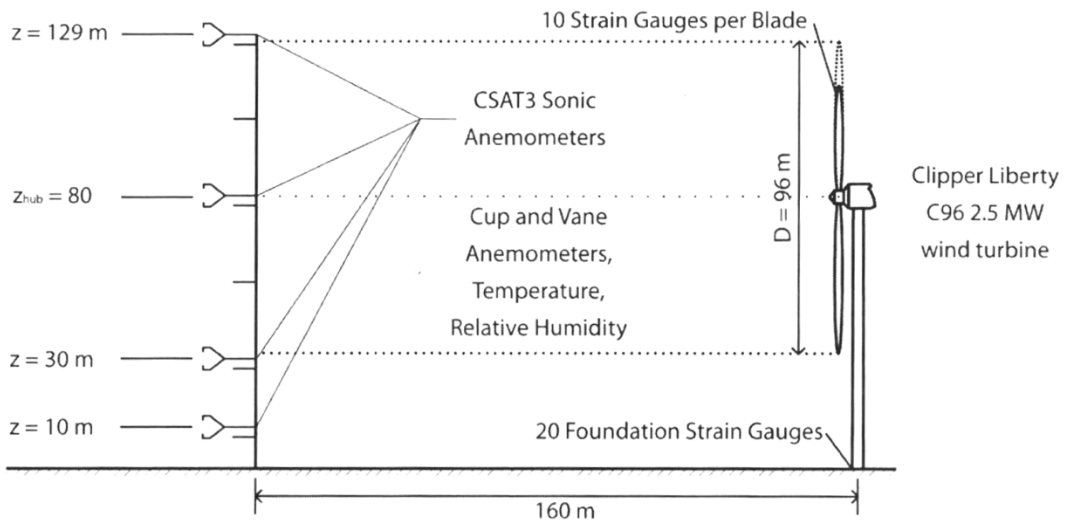

Figure 56: Schematic of data acquisition systems on the Eolos test site (Howard & Guala, 2014)

The turbine and met mast are located at Umore Park, a dedicated 80-acre site belonging to the University of Minnesota. The arrangement of instruments is illustrated in Figure 69, and the power curve is shown in Figure A2. The layout of the site does not comply fully with the requirements of IEC2017 since the horizontal distance between the turbine and the met mast is less than two rotor diameters.

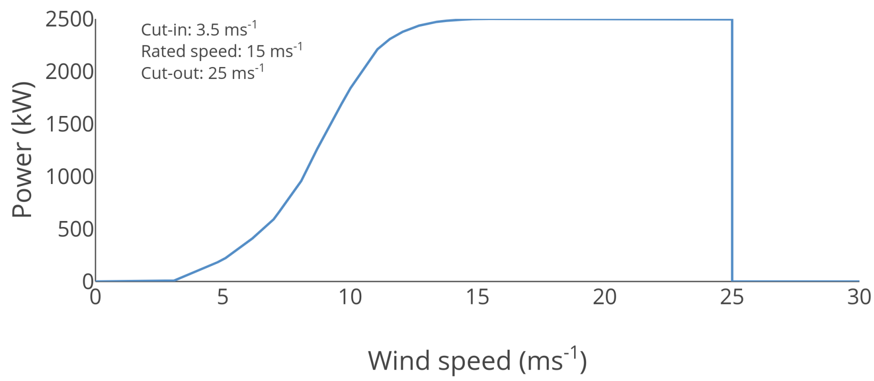

Figure 57: Clipper Liberty C96 power curve[21]

Basic details of the site are provided in Table 40.

Table 40: Location details

Terrain	Low rolling farmland
Location	44.728422°N, -93.048144°E (turbine)
	44.726774°N, -93.048131°E (mast)
	Elevation: 279.8m
Coriolis parameter	0.0001024
Roughness length	0.03 (from Table 2)
Mast height	130 m
Excluded sector	350 - 100°
Reference	(Howard & Guala, 2016)

There are three parameters contributing to disturbed airflow at the met mast in the sector 320° to 40°, the first of which is the wake of the turbine since the met mast is situated due south. The second parameter is the tower shadow from the met mast itself since the instrument booms are oriented at 210°. The boom orientation also gives rise

[21] https://www.thewindpower.net/turbine_en_296_clipper_liberty-c96.php

to the third parameter which is that at this angle, the arms and supporting structure of the sonic anemometers contaminate the flow of air through the sensors (Campbell Scientific, 1998). The sector 320° to 40° is therefore excluded from analyses leaving the free-stream sector as 50° to 310° after binning and averaging using the standard IEC bin size of 10° (IEC, 2017). Theoretically, there could be a small hysteresis effect at the edges of the free-stream sector if the standard deviation of the wind direction is large.

Table 41: File contents: MetA

Data subset identifier	MetA	
Time period (UTC)	2017-01-01 00:00:00 – 2017-12-31 23:59:59 Local time = UTC -6 (UTC -5 with DST)	
Type and frequency	Sonic anemometer data at 20 Hz	
Data items	Meridional wind speed (+ve: North ⇨ South) Zonal wind speed (+ve: West ⇨ East Vertical wind speed (+ve: upwards) Sonic temperature Diagnostic	
Instruments	CSAT1 (Campbell Scientific CSAT3) CSAT3 (Campbell Scientific CSAT3)	127.9m 79.1m

Table 42: File details: MetB

Data subset identifier	MetB	
Time period (UTC)	2017-01-01 00:00:00 – 2017-12-31 23:59:59 Local time = UTC -6 (UTC -5 with DST)	
Type and frequency	Sonic anemometer data at 20 Hz	
Data items	Meridional wind speed (+ve: North ⇨ South) Zonal wind speed (+ve: West ⇨ East Vertical wind speed (+ve: upwards) Sonic temperature Diagnostic	
Instruments	CSAT5 (Campbell Scientific CSAT3) CSAT6 (Campbell Scientific CSAT3)	29.6m 9.9m

Table 43: File details: RH

Data subset identifier	RH	
Time period (UTC)	2017-01-01 00:00:00 – 2017-12-31 23:59:59 Local time = UTC -6 (UTC -5 with DST)	
Type and frequency	Met mast data at 1 Hz	
Data items	Relative humidity Pressure	
Instruments	RH (Met One 083E-1-35) Bar (Met One 092)	79.1 m 79.1m

Table 44: File details: SCADA

Data subset identifier	SCADA	
Time period (UTC)	2017-01-01 00:00:00 – 2017-12-31 23:59:59 Local time = UTC -6 (UTC -5 with DST)	
Type and frequency	SCADA data at 1 Hz	
Data items	Real power (kW) Reactive power (kVAR) Rotor position (deg) Nacelle direction (deg) Wind direction (deg) Wind speed (m/s) Hub speed (rpm) Barometric pressure (hPa) Air density (kg/m^3)	Curtailment level (kW) Turbine state Fault level Fault code Yaw error (deg) Yaw mode Yaw state
Instruments	No details	80m (hub height – where applicable)

Valid SCADA records were identified by a turbine state value of *Run* (corresponding to internal code 8), and a fault code of either *0 (no fault) or 920 (feather check warning)* (Stone, 2015). Invalid records were suppressed before combination with the other datasets.

The curtailment level column contains values (e.g. 1,400 kW, 2,350 kW) which indicate an upper limit on the amount of power produced. Periods of curtailment introduce distortions into the power curve. Most of the affected records were rejected; however, those with a curtailment level of 2,300 kW were retained. This was to retain a reasonable number of records in the dataset. Checking against the published power curve, the wind speed corresponding to an output of 2,300 kW was exceeded on only four occasions. The risk was deemed acceptable.

Table 45: File details: Temp

Data subset identifier	Temp	
Time period (UTC)	2017-01-01 00:00:00 – 2017-12-31 23:59:59 Local time = UTC -6 (UTC -5 with DST)	
Type and frequency	Met mast data at 1 Hz	
Data items	Temperature	
Instruments	Temp (Met One 083E-1-35)	125.9m, 101.5m, 76.7m, 51.5m, 27.1m, 7.3m

Table 46: File details: ASOS

Data subset identifier	ASOS
Time period (UTC)	2017-01-01 00:00:00 – 2017-12-31 23:59:59 Local time = UTC -6 (UTC -5 with DST)
Type and frequency	Weather station data at 0.000278 Hz (hourly) Upsampled to 0.001667 Hz (every ten minutes) and padded
Location	Network of 13 weather stations in Minnesota at various locations and elevations
Data items	Mean surface pressure (adjusted for elevation)
Instruments	No details
Source	Iowa Environmental Mesonet http://mesonet.agron.iastate.edu/sites/networks.php?network=MN_ASOS

Table 47: File details: Solar

Data subset identifier	Solar
Time period (UTC)	2017-01-01 00:00:00 – 2017-12-31 23:59:59 Local time = UTC -6 (UTC -5 with DST)
Type and frequency	Solar geometry at 0.001667 Hz (every ten minutes)
Data items	Daylight saving time flag (0 = no DST, 1 = DST) UTC offset – difference in hours from UTC Sunrise azimuth Sunset azimuth Solar noon azimuth Local sunrise time Local sunset time Local solar noon UTC sunrise time UTC sunset time UTC solar noon Hour angle – solar direction as an angular offset from 0 at solar noon Day number – offset from 2017-01-01 00:00 including day fraction Declination – angle between the sun and the plane of the equator Solar elevation – angle between the sun and the local horizon
Source	timeanddate.com https://www.timeanddate.com/sun/usa/minneapolis

Uncertainty values for the raw meteorological data columns were either extracted from the instrument manuals (Ellis, 2013), or derived using the formulae for linear propagation of uncertainty if the values were calculated during pre-processing. No data on the accuracy of the SCADA variables was available, and estimates are based on similar data from other turbines and instruments. The full list is shown in Table 48.

Table 48 Uncertainty values used for raw data. * indicates a parameter calculated during pre-processing and therefore a calculated uncertainty; † indicates an estimated value.

Parameter	Instrument	Uncertainty
Wind speed	Met One Model 011 E-Class One cup anemometer	0.1 ms^{-1}
Wind speed component	Campbell Scientific CSAT3 3D sonic anemometer	0.04 ms^{-1}
Wind speed†	SCADA	0.24 ms^{-1}
Scalar wind speed 1 Hz*	Campbell Scientific CSAT3 3D sonic anemometer	0.03
Wind direction	Met One Model 024A Wind Direction Sensor	5°
Wind direction*	Campbell Scientific CSAT3 3D sonic anemometer	0.5°
Wind direction†	SCADA	3°
Temperature	Met One Model 038E/593A Relative Humidity/Temperature Sensor	0.1°C
Temperature	Campbell Scientific CSAT3 3D sonic anemometer	0.04°C
Relative humidity	Met One Model 038E/593A Relative Humidity/Temperature Sensor	2%
Pressure	Met One Barometric Pressure Sensor	0.75 hPa
Pressure†	SCADA	0.75 hPa
Real power†	SCADA	0.5 kW
Rotor position†	SCADA	0.5°
Nacelle direction†	SCADA	0.5°
Yaw error†	SCADA	3°
Hub speed†	SCADA	0.2 rpm
Air density*	SCADA	0.25 kg m^{-3}
Kinematic heat flux*	Campbell Scientific CSAT3 3D sonic anemometer	0.00001 K m s^{-1}
Kinematic momentum flux*	Campbell Scientific CSAT3 3D sonic anemometer	0.00001 m^2 s^{-2}

Appendix C: Python code to generate incommensurate numbers

```
def sumcheck(a, A):
    """ Returns True the parameter a is equal to the sum of a subset of A.
        Returns False otherwise
    """
    if len(A) == 0:                     # Return False when the list is empty
        return False
    if a == sum(A):                     # If a == sum of the members of A, return True
        return True
    if a - A[0] < A[-1]:                # If a - max(A) is less than min(A), ignore max(A)
        return sumcheck(a, A[1:])       # Call sumcheck recursively on the remainder of A
    for b in A:                         # Check each member of A
        B = A.copy()                    # Copy array to preserve the original
        B.remove(b)
        if sumcheck(a-b, B):            # Recursively check for the difference between the
            return True                 # selected value in the remainder of the list
    return False


def parametercheck(a, A, M=4):
    """ Returns True if parameter a has a multiple that is within +/-5 of another
        number in the list A. Multiples up to M are checked.
        Returns False otherwise
    """
    for m in range(2, M+1):
        for i in range(-5, 6):
            if m * a + i in A:
                return True
    return False


def incommensurate(seed, n, diff=7):
    """ Generate a list of n incommensurate values starting with seed, and reducing
        the value by diff each time. Each candidate value is checked for compatibility
        and if a clash is discovered, the value is reduced by 1 repeatedly until the
        next compatible value is found. If zero is reached before the required number
        of values has been generated, and error is raised.
    """
    freqs = [seed,]
    while len(freqs) < n:
        step=0
        num = freqs[-1] - diff
        if num <= 0:
            print(freqs, num, step)
            raise ValueError('Reached zero')
        while sumcheck(num-step, freqs) or parametercheck(num-step, freqs):
            step += 1
            if num-step <= 0:
                print(freqs, num, step)
                raise ValueError(''Reached  zero')
        freqs += [num-step]
    return freqs
```

Appendix D: Characteristics of datasets from winddata.com

The table below was compiled when assessing available datasets for the characteristics required for the current work. None of those at winddata.com were found to have the ideal combination of features.

Site	Wind speed	Wind direction	Temperature	Pressure	Relative humidity	Power	3D	Frequency (Hz)
abisko	Y	Y	Y				Y	20
ainswort	Y	Y					Y	5
alsvik	Y	Y	Y					1
andros	Y	Y	Y					1
aspruzza	Y	Y						1
bockstig	Y	Y	Y	Y		Y		17
cabauw	Y	Y						2
calwind	Y	Y					Y	5
ciba	Y	Y						5
clape	Y	Y					Y	8
ecn	Y	Y						4
emden	Y	Y						20
equinox	Y	Y						5
flowind	Y	Y						5
gedsrev	Y	Y						5
gorgonio	Y	Y						5
hanford	Y	Y					Y	5
holland	Y	Y	Y					5
hornsrev	Y	Y						12
hurghada	Y	Y						8
jericho	Y	Y	Y					5
jwe	Y	Y						20
kwkoog	Y	Y						2.5
lamme	Y	Y					Y	16
lavrio	Y	Y	Y				Y	8
lyse	Y	Y	Y					1
maglarp	Y	Y	Y				Y	20
marsta	Y	Y	Y				Y	21
mttsukub	Y	Y					Y	4

Site	Wind speed	Wind direction	Temperature	Pressure	Relative humidity	Power	3D	Frequency (Hz)
midgrund	Y	Y						5
nasudden	Y	Y						1
nm92	Y	Y	Y			Y	Y	25
nordtank	Y	Y	Y				Y	20
ntk1500	Y	Y						40
nwtc	Y	Y	Y				Y	40
oakcreek	Y	Y	Y				Y	16
orkney	Y	Y	Y					1
roedsand	Y	Y	Y				Y	20
rosiere	Y	Y	Y				Y	5
sjorge	Y	Y						40
ski	Y	Y						0.85
skyv27	Y	Y					Y	8
skyv39	Y	Y				Y		32
sle	Y	Y						0.85
sprogoe	Y	Y					Y	10
tarifa	Y	Y	Y				Y	4
tarifa_2	Y	Y					Y	20
tejona	Y	Y	Y				Y	4
tjare	Y	Y				Y		25
toboel_1	Y	Y						8
toboel_2	Y	Y						32
toplou	Y	Y	Y				Y	8
tsukuba	Y	Y						1
tughill	Y	Y					Y	5
utlangan	Y	Y	Y				Y	20
vindeby	Y	Y	Y				Y	20
vls	Y	Y						0.85
windland	Y	Y					Y	5
windy	Y	Y					Y	10
zeeb	Y	Y						2

Appendix E: Python methods

The code below defines a python class Calc and a set of associated class methods for performing standard calculations. These are an extract from the full set available from the code repository which can be accessed at https://bitbucket.org/coillarach/phd. The methods are arranged in alphabetical order.

```
From datetime import datetime

import numpy as np
import pandas as pd
import scipy.signal as sg
import statsmodels.tsa.stattools as tst
from math import pi, atan, cos, sin, isnan, sqrt, log, exp, acos, asin, atan2

T_c = 647.096       # Critical temperature (K) Wagner & Pruss (2001) p. 398
R = 8.3144598       # Universal gas constant (J mol^-1 K^-1) Jacobson (2001) p. 29
m_d = 28.966        # Molecular weight of dry air (g /mol) Jacobson (2001) p. 30
m_v = 18.02         # Molecular weight of water vapour (g /mol) Jacobson (2001) p. 712
c_pd = 1004.67      # Specific heat of dry air at constant pressure (J /kg/K) Jacobson (2001) p. 20
g = 9.81            # Acceleration due to gravity (ms^-2) Atkins, T. and Escudier, M. (2014)
P_c = 220640.0      # Critical pressure (hPa) Wagner & Pruss (2001) p. 398
R_v = 4.61526       # Gas constant of water vapour (m^3 hPa /kg /K) IAPWS97
R_d = 2.8704        # Gas constant of dry air (m^3 hPa /kg /K) Jacobson (2001) p. 712
P_0 = 1013.0        # Standard sea-level pressure (hPa) Jacobson (2001) p. 14
k = 0.4             # von Karman constant () Stull, 1988
gamma_d = 9.8       # Dry adiabatic lapse rate (K/km) Stull, 1988
Pr = 0.95           # Turbulent Prandtl number () Jacobson, 2005, p.242
L_v = 2500000       # Latent heat of condensation for water (J/kg) (Schotanus et al, 1983)
C_p = 1012          # Specific heat of air at constant pressure (J/kg/K) (Schotanus et al, 1983)


class Calc:

    @staticmethod
    def adf(df):
        """ Calculate a stationarity indicator using the Augmented Dickey-Fuller (adf) test.
            The data is stationary if the test statistic is less that the critical value of -2.88404
            for a 95% confidence. Between the critical value and zero, the statistic indicates non-
            stationarity, and above zero the series is explosive (unlikely). In the explosive case,
            this function returns 1. Otherwise the return value is the probability given by the test.
            Stationarity is therefore suggested when the return value is less than 0.95 and the closer
            to zero, the more stationary the data is.

        """
        adf, pvalue, usedlag, nobs, critical_values, icbest = tst.adfuller(df.dropna())
        if adf > 0:
            return 1.0
        return pvalue

    @staticmethod
    def airDensity(pressureInMillibars, temperatureInCelsius, relativeHumidityInPercent):
        """ Air density from temperature, pressure and relative humidity
            IEC (2005)
        """
        absoluteTemperature = Calc.celsiusToKelvin(temperatureInCelsius)
        relativeHumidity = relativeHumidityInPercent / 100
        vapourPressureInHectopascals = Calc.saturationVapourPressure(temperatureInCelsius)

        return ((pressureInMillibars / R_d) -
                relativeHumidity * vapourPressureInHectopascals *
                (1 / R_d - 1 / R_v)) / absoluteTemperature

    @staticmethod
    def airDensityFromSonic(pressureInMillibars, sonicTemperatureInCelsius):
        """ Air density from pressure and sonic temperature, which is almost identical to virtual temp
            Jacobson (2001) p. 33
        """
        absoluteTemperature = Calc.celsiusToKelvin(sonicTemperatureInCelsius)

        return pressureInMillibars / R_d / absoluteTemperature
```

```python
@staticmethod
def angularDifference(upperAngle, lowerAngle):
    """ Calculates the difference between two angles in degrees giving a negative answer where
        the lower angle is larger than the upper angle

    """
    newAngle = (upperAngle - lowerAngle) % 360
    if newAngle > 180:
        return newAngle - 360
    else:
        return newAngle

@staticmethod
def autocorrelation(data, stop='min', normalise=True):
    """ Calculates the autocorrelation for the supplied array, data, at all possible lags (0 - N-1).
        The stop parameter controls when the process is actually terminated. 'min' indicates the
        first minimum, 'zero' indicates the first zero-crossing, and '1/e' indicates 1/e
         (Tropea et al, 2007; Flay & Stevenson, 1988).
        Returns ndarray
    """
    if len(data) == 0:
        return None

    if stop not in ['min', 'zero', '1/e', 'none']:
        raise ValueError(
            '\'stop\' parameter should be one of \'min\', \'zero\', \'1/e\', \'none\', not \'' + \
            stop + '\'')

    df = pd.Series(sg.detrend(data, type='linear'))
    ac = np.array([])
    previous_value = 999
    for lag in range(0, len(data)):
        ac_at_lag = df.autocorr(lag)

        if stop == 'zero' and ac_at_lag <= 0.0:
            break
        elif stop == '1/e' and (ac_at_lag <= 1 / np.e or ac_at_lag <= 0.0):
            break
        elif stop == 'min' and (ac_at_lag > previous_value or ac_at_lag <= 0.0):
            break

        previous_value = ac_at_lag

        ac = np.append(ac, [ac_at_lag, ])

    if normalise:
        return ac / ac[0]
    else:
        return ac

@staticmethod
def boundaryLayerHeightRM(frictionVelocity, rossbyMontgomeryCoefficient, coriolis):
    """ Estimates the surface layer height based on the Rossby-Montgomery equation. This version
        uses a dynamic value of the Rossby-Montgomery coefficient.
        Rossby & Montgomery, 1935; Arya, 2001, p. 273
    """
    return rossbyMontgomeryCoefficient * frictionVelocity / coriolis

@staticmethod
def coriolis(latitudeInDegrees):
    """ Returns the Coriolis parameter value for a given latitude
    """
    latitude = np.radians(latitudeInDegrees)
    return 0.000145 * sin(latitude)

@staticmethod
def crossIsobarAngle(row, frictionVelocity, surfaceLayerHeight,
                     obukhovLength, roughnessLength, coriolis):
    """ Estimate of the rotation of the wind vector at the top of the surface layer compared to the
        direction of the geostrophic wind
        Emeis, 2013, p.46
    """
    gammaScale = sqrt(coriolis / (2 * k * row[frictionVelocity] * row[surfaceLayerHeight]))
    phi = Calc.universalStabilityFunction(row, obukhovLength, row[surfaceLayerHeight], 'M')
    psi = Calc.universalStabilityFunctionIntegrated(row, obukhovLength,
                                                     row[surfaceLayerHeight], 'M')
    radians = atan(1/(1 + 2 * gammaScale * row[surfaceLayerHeight] / phi * \
              (log(row[surfaceLayerHeight] / roughnessLength) - psi)))
    return Calc.radiansToDegrees(radians)
```

```
@staticmethod
def declination(day_number):
    """ Calculates the solar declination based on the day number.
    """
    return (-np.arctan(0.39779 * np.cos(0.98565 * (day_number + 10) * np.pi / 180) +
                       1.914 * np.sin(0.98565 * (day_number - 2) * np.pi / 180))) * 180 / np.pi
@staticmethod
def dissipation(structure2, mean_wind_speed, sampling_frequency):
    """ Calculate energy dissipation rate (m^2/s^3)
        (Stull, 2001, p. 300; Muñoz-Esparza et al , 2017).
        structure2 = second-order structure function at lag = 1 (this is equivalent to transience)

    """
    return (structure2 / 2) ** (3 / 2) / mean_wind_speed * sampling_frequency
@staticmethod
def extrapolate(value, gradient, height, targetHeight=0):
    """ Value of quantity at the target height assuming a linear lapse rate

    """
    return value + (gradient * (targetHeight - height))

@staticmethod
def frictionVelocity(kinematicMomentumFluxU, kinematicMomentumFluxV):
    """ Scaling parameter for wind speed in the surface layer - used in Monin-Obukhov theory
        Foken (2008) p. 31
    """
    return (kinematicMomentumFluxU**2 + kinematicMomentumFluxV**2)**0.25
@staticmethod
def geostrophicWindSpeed(frictionVelocity, coriolis, roughnessLength):
    """ Estimate of the wind speed in the free troposphere
        Hogstrom, 1998
    """
    return coriolis * roughnessLength * (frictionVelocity / \
           (sqrt(0.0123) * coriolis * roughnessLength)) ** (1/0.93)
@staticmethod
def haversineDistance(latitude1, longitude1, latitude2, longitude2):
    """ Returns the distance in kilometres between two points defined by their latitude and
        longitude.
        Implements the haversine formula: https://en.wikipedia.org/wiki/Haversine_formula
        Also returns the bearing of point2 from point1 calculated as the forward azimuth:
        https://www.movable-type.co.uk/scripts/latlong.html
    """
    earth_radius = 6373.0

    lat1 = np.radians(latitude1)
    lon1 = np.radians(longitude1)
    lat2 = np.radians(latitude2)
    lon2 = np.radians(longitude2)

    dlon = lon2 - lon1
    dlat = lat2 - lat1

    a = np.sin(dlat / 2) ** 2 + np.cos(lat1) * np.cos(lat2) * np.sin(dlon / 2) ** 2
    c = 2 * np.arctan2(np.sqrt(a), np.sqrt(1 - a))

    forward_azimuth = np.degrees(np.arctan2(np.sin(dlon) * np.cos(lat2), np.cos(lat1) * \
                      np.sin(lat2) - np.sin(lat1) * np.cos(lat2) * np.cos(dlon)))
    try:
        forward_azimuth = [360 + fa if fa < 0 else fa for fa in forward_azimuth]
    except TypeError:
        if forward_azimuth < 0:
            forward_azimuth = 360 + forward_azimuth

    return earth_radius * c, forward_azimuth

@staticmethod
def hour_angle(solar_noon, time):
    """ Calculates the solar hour angle given solar noon and the time to be evaluated as datetime
        objects
    """
    if time < solar_noon:
        seconds = -(solar_noon - time).total_seconds()
    else:
        seconds = (time - solar_noon).total_seconds()

    return seconds * 0.004167

@staticmethod
def inflowAngle(horizontalWindSpeed, verticalWindSpeed):
    """ Calculates inflow angle in degrees as the inverse tangent of vertical over horizontal wind
        speed
    """
    angles = np.degrees(np.arctan(verticalWindSpeed / horizontalWindSpeed))
    return Calc.signedAngle(angles)
```

```python
    @staticmethod
    def kinematicHeatFlux(flux, density, invert=False):
        """ Kinematic expression of heat flux density - measured in same units as the base quantity
          (mKs^-1)
            Jacobson (2001) p. 230
        """
        if invert:
            return -flux / density / c_pd
        return flux / density / c_pd

    @staticmethod
    def kinematicMomentumFlux(flux, density):
        """ Kinematic expression of momentum flux density - measured in same units as the base quantity
            (m^2s^-2)
            Jacobson (2001) p. 106
        """
        return flux / density

    @staticmethod
    def kinematicMomentumFluxResultant(zonalFlux, meridionalFlux, density):
        """ Kinematic expression of momentum flux density from flux components - measured in same units
            as the base quantity (m^2s^-2)

        """
        return sqrt(zonalFlux ** 2 + meridionalFlux ** 2) / density

    @staticmethod
    def kinematicViscosity(kelvin, density):
        """ Returns the kinematic viscosity of air based om the absolute temperature and density.
            Andreas (2005) ADDED MANUALLY 16 Sep 2018
        """
        return (1.458 * 10**-6 * kelvin**(3/2)) / (kelvin + 110.4)

    @staticmethod
    def kpss(df):
        """ Calculate a stationarity indicator using the KPSS test. This function returns the
            probability value
        """
        value, pvalue, lags, criticaleValues = tst.kpss(df.dropna())
        return pvalue

    @staticmethod
    def lapseRate(lowerValue, upperValue, lowerMeasurementHeight, upperMeasurementHeight, factor=1000):
        """ Returns lapse rate in units per metre. Typically used for temperatures.
            The default value for factor returns the result in units per kilometre. For units per metre
            run with factor=1
            Stull (2015) p. 59, 140
        """
        return -(upperValue - lowerValue) / (upperMeasurementHeight - lowerMeasurementHeight)

    @staticmethod
    def length_scale(time_scale, mean_speed):
        """ Calculates the integral length scale from a time scale by multiplying by the mean speed.
        """
        return time_scale * mean_speed

    def normalisedPower(power, airDensity, referenceAirDensity=1.225):
        """ Calculates the power normalised to a reference air density

        """
        return power * (referenceAirDensity / airDensity)

    @staticmethod
    def normalisedWindSpeed(windSpeed, airDensity, referenceAirDensity=1.225):
        """ Calculates wind speed normalised to a reference air density

        """
        return windSpeed * (airDensity / referenceAirDensity)**(1/3)


@staticmethod
    def obukhovLength(frictionVelocity, virtualPotentialTemperature, kinematicHeatFlux):
        """ Length scale (m) proportional to the height above the surface at which buoyant production of
            turbulence first dominates mechanical (shear) production of turbulence
            Stull (1989) p. 181
        """
        return -(frictionVelocity**3) * virtualPotentialTemperature / k / g / kinematicHeatFlux

    @staticmethod
    def obukhovStabilityParameter(obukhovLength, height):
        """ Measure of stability using Monin-Obukhov similarity theory

        """
        return height / obukhovLength
```

```python
    @staticmethod
    def planar_fit(df):
        """ Calculates the coefficients, b0, b1, b2, of the equation of a plane
            Z(x, y) = b0 + b1 x + b2 y which best fits a set of points in 3-dimensional space.
            (Wilczak et al, 2001; Lee et al, 2005).
            The return value is an array x = (b0, b1, b2). Parameters u, v and w are pandas Series
            objects. For use in rotating the coordinates of flux measurements, see unit_vector_k(),
            unit_vector_ij() and rotate()
        """
        df1 = df.dropna().copy()
        u = df1.iloc[:,0]
        v = df1.iloc[:,1]
        w = df1.iloc[:,2]

        flen = len(u)
        su = u.sum()
        sv = v.sum()
        sw = w.sum()
        suv = np.matmul(u, np.transpose(v)).sum()
        suw = np.matmul(u, np.transpose(w)).sum()
        svw = np.matmul(v, np.transpose(w)).sum()
        su2 = np.matmul(u, np.transpose(u)).sum()
        sv2 = np.matmul(v, np.transpose(v)).sum()

        H = [[flen, su, sv], [su, su2, suv], [sv, suv, sv2]]
        g = np.transpose([sw, suw, svw])
        x = np.matmul(np.linalg.inv(H), g)

        return x

    @staticmethod
    def planar_fit_three_points(p, q, r):
        """ Returns the fitted coefficients of the equation of a plane given three points in that plane.
            p, q, and r are assumed to be 2D numpy arrays of the form [[x0, y0, z0], [x1, y1, z1], ...]
            On return, the arrays a0, a1 and a2 can be assigned directly to columns in a dataframe.
        """
        v1 = np.subtract(p, q)
        v2 = np.subtract(p, r)
        n = np.cross(v1, v2)
        a0 = [(k[0]*c[0] + k[1]*c[1] + k[2]*c[2]) / k[2] for (k, c) in zip(n, p)]
        a1 = [-k[0] / k[2] for k in n]
        a2 = [-k[1] / k[2] for k in n]

        return a0, a1, a2


    @staticmethod
    def potentialTemperature(temperatureInCelsius, PressureInMillibars):
        """ Potential temperature from temperature and pressure
            Jacobson (2001) p 51
        """
        kelvin = Calc.celsiusToKelvin(temperatureInCelsius)
        return kelvin * (1000 / PressureInMillibars)**0.286

    @staticmethod
    def potentialTemperatureFromLapseRate(temperatureInCelsius, height):
        """ Calculates potential temperature using the dry adiabatic lapse rate. This avoids the need
            for a reference pressure.
            Stull, 2015 p. 61
        """
        return temperatureInCelsius + gamma_d / 1000 * height

    @staticmethod
    def potentialTemperatureScale(kinematicHeatFlux, frictionVelocity):
        """ Scaling parameter for temperature used in Monin-Obukhov theory
            Jacobson (2001) p. 241
        """
        return -kinematicHeatFlux / frictionVelocity

    @staticmethod
    def potentialVirtualTemperature(sonicTemperatureInCelsius, PressureInMillibars):
        """ Temperature adjusted for altitude and moisture content - calculated from sonic temperature
            which is almost identical to virtual temperature
            Foken (2008) p. 114;
        """
        kelvin = Calc.celsiusToKelvin(sonicTemperatureInCelsius)
        return kelvin * (1000 / PressureInMillibars)**0.286
    @staticmethod
    def powerDeviation(row, powerColumn, windSpeedColumn, powerCurve=None):
        """ Calculates the deviation in power output for a particular wind speed with respect to a power
            curve

        """
        expectedValue = powerCurve.getPower(row[windSpeedColumn])
        return Calc.percentageError(expectedValue, row[powerColumn])
```

```python
@staticmethod
def pressureDifferenceUnitLength(pressure1, pressure2, distance):
    """ Calculates the absolute pressure difference per unit length. Length units depend on the
        parameter supplied
    """
    return abs(pressure1 - pressure2) / distance

@staticmethod
def pressureNormalised(pressure1, height1, height2, temperatureInCelsius):
    """ Returns the pressure value adjusted for height by the hypsometric equation
        (Stull, 2015 p. 17)
    """
    return pressure1 * np.exp(g * (height1 - height2) / (R_d * 100) / \
            (temperatureInCelsius + 273.15))
@staticmethod
def rayleigh (x, mean):
    """ Calculates the Rayleigh statistic for a given value compared to the mean

    """
    return 1 - exp(-pi / 4 * (x / mean)**2)
@staticmethod
def reynolds(data):
    """ Decompose a sequence into a mean value and deviations.
    """
    data_mean = data.mean()
    return data_mean, data - data_mean

@staticmethod
def richardsonBulk(virtualPotentialTemperature,
                   virtualPotentialTemperatureAtSurface,
                   meanWindSpeed,
                   measurementHeight
                  ):
    """ Quantifies the ratio of buoyancy to mechanical shear - used as a measure of static
        stability. This version requires one measurement of temperature at height z and the
        temperature at the surface.
        Grachev & Fairall, 1997
    """

    return g * (virtualPotentialTemperature - virtualPotentialTemperatureAtSurface) * \
        measurementHeight / virtualPotentialTemperatureAtSurface / meanWindSpeed**2
@staticmethod
def richardsonFlux(virtualPotentialTemperature, kinematicHeatFlux,
                   kinematicMomentumFluxU, windSpeedGradientU,
                   kinematicMomentumFluxV, windSpeedGradientV):
    """ Quantifies the ratio of buoyancy to mechanical shear - used as a measure of static
        stability. This version requires wind speed components in the u and v dimensions.

    """
    return g * kinematicHeatFlux / virtualPotentialTemperature / \
            (kinematicMomentumFluxU * windSpeedGradientU + kinematicMomentumFluxV * \
            windSpeedGradientV)
@staticmethod
def richardsonGradient(virtualPotentialTemperature,
                       virtualPotentialTemperatureGradient,
                       windSpeedGradient):
    """ Quantifies the ratio of buoyancy to mechanical shear - used as a measure of static
        stability.

    """
    return g * virtualPotentialTemperatureGradient / \
               virtualPotentialTemperature / \
               windSpeedGradient**2
@staticmethod
def rossbyMontgomeryCoefficientStable(obukhovLength):
    """ Estimate a stability-dependent value of the Rossby-Montgomery coefficient based on the
        Obukhov length under stable conditions (L >= 0)
        Holtslag et al. 2017
    """
    return 0.04 + 0.05 / (1 + 200 / obukhovLength)

@staticmethod
def rossbyMontgomeryCoefficientUnstable(obukhovLength):
    """ Estimate a stability-dependent value of the Rossby-Montgomery coefficient based on the
        Obukhov length under stable conditions (L < 0)
        Holtslag et al. 2017
    """
    return 0.17 - 0.08 / (1 - 50 / obukhovLength)**3
```

```
    @staticmethod
    def rotateScalar(df, i, j, k):
        """ Takes a set of values in instrument coordinates and the unit vectors in a target coordinate
            frame and returns a set of values rotated into the new coordinates. Uses the approach of
            Lee et al (2005, p. 63).
            df is a pandas dataframe with three columns corresponding to the three components of the
            vector to be rotated. Eg. For sensible heat flux, columns are u't', v't', w't'
            i and j are arrays of vectors of the form [[x1, y1, z1], [x2, y2, z2], ...]
            k is a single vector in the form [x, y, z]
            For determining the unit vectors, see planar_fit(), unit_vector_k() and unit_vector_ij()
        """
        # return sum(i * df), sum(j * df), sum(k * df)
        return ([sum(i[c] * df.iloc[c]) for c in range(0, df.index.size)],
                [sum(j[c] * df.iloc[c]) for c in range(0, df.index.size)],
                [sum(k * df.iloc[c]) for c in range(0, df.index.size)]
                )

    @staticmethod
    def rotateTensor(df, i, j, k):
        """ Takes a set of values in instrument coordinates and the unit vectors in a target coordinate
            frame and returns a set of values rotated into the new coordinates. Uses the approach of Lee
            et al (2005, p. 63).
            df is a pandas dataframe with six columns corresponding to the six unique elements of the
            3x3 Reynolds stress tensor - ie. u'u', u'v', u'w', v'v', v'w', w'w'. The calculation uses
            the tensor coordinate transformation rule B = Q.A.Qt where A is the original tensor and B is
            the transformed tensor. Q is
            the transformation matrix [[iu, iv, iw], [ju, jv, jw], [ku, kv, kw]] and Qt is its
            transpose.
            See http://www.continuummechanics.org/coordxforms.html
            i and j are arrays of vectors of the form [[x1, y1, z1], [x2, y2, z2], ...]
            k is a single vector in the form [x, y, z]
            For determining the unit vectors, see planar_fit(), unit_vector_k() and unit_vector_ij()
        """
        # Recover omitted tensor elements
        c = df.columns
        df1 = df[[c[0], c[1], c[2], c[1], c[3], c[4], c[2], c[4], c[5]]].copy()
        transformed = []

        for row in range(0, df.index.size):
            Q = [i[row], j[row], k]
            A = df1.iloc[row].values.reshape(3,3)
            B = np.matmul(np.matmul(Q, A), np.transpose(Q))
            transformed.append(B.reshape(9))

        transformed = np.array(transformed)
        return transformed[:,0], transformed[:,1], transformed[:,2], transformed[:,4], transformed[:,5],
transformed[:,8]

    @staticmethod
    def rotorEquivalentWindSpeedWeightings(rewsColumns, hubHeight, diameter):
        """ Calculates the rotor equivalent wind speed weightings given a set of wind speed columns at
            different heights.
            rewsColumns is an array of dicts made up of column names and associated measurement heights.
            (IEC, 2017)
        """
        radius = diameter / 2
        upperTipHeight = hubHeight + radius
        lowerTipHeight = hubHeight - radius
        sweptArea = Calc.circleArea(diameter/2)
        rewsColumns = sorted(rewsColumns, key=lambda c: c['height'])

        heights = [column['height'] for column in rewsColumns]
        lowerEdges = [lowerTipHeight] + [(bottom + top) / 2 for bottom, top in zip(heights, heights[1:])]
        upperEdges = [(bottom + top) / 2 for bottom , top in zip(heights, heights[1:])] + [upperTipHeight]
        weightings = [Calc.stripeArea(radius, low-hubHeight, up-hubHeight)/sweptArea \
                      for (mh, low, up) in zip(heights, lowerEdges, upperEdges)]
        return weightings

    @staticmethod
    def rotorEquivalentWindSpeed(row, rewsColumns, weightings, hubHeightDirectionColumn=None):
        """ Calculates the rotor equivalent wind speed given a set of wind speed columns at different
            heights and the set of weightings to apply to each horizontal segment of the rotor disk.
            rewsColumns is an array of dicts made up of column names for wind speed and direction and
            associated measurement heights.
            (IEC, 2017)
        """
        windSpeedCubed = 0.

        for column, weighting in zip(rewsColumns, weightings):
            phi = 0
            if hubHeightDirectionColumn is not None:
                phi = np.radians(Calc.angularDifference(row[column['direction']],
                                                        row[hubHeightDirectionColumn]))
            windSpeedCubed += (row[column['wind_speed']] * np.cos(phi))**3 * weighting
        return windSpeedCubed**(1/3)
```

```python
@staticmethod
def saturationVapourPressure(temperatureInCelsius):
    """ Empirical approximation of saturation vapour pressure
        Jacobson (2005) p. 41
    """
    return 6.112 * np.exp(17.67 * temperatureInCelsius / (temperatureInCelsius + 243.5))

@staticmethod
def saturationVapourPressureIEC(absoluteTemperature):
    """ Vapour pressure from absolute temperature according to the approximation in IEC 61499-12
        (hPa)

    """
    return 0.0000205 * np.exp(0.0631846 * absoluteTemperature) / 100

@staticmethod
def scalarMomentumFlux(zonalFlux, meridionalFlux):
    """ Returns the magnitude of the horizontal flux vector based on the zonal and meridional
        components.
        (Nordbro et al 2012)
    """
    return np.sqrt(zonalFlux**2 + meridionalFlux**2)



@staticmethod
def schotanusFluxCorrection(sonicHeatFlux, verticalMomentumFlux, meanWindSpeed,
                            temperatureInCelsius, specificHumidity):
    """ Corrects the sensible heat flux calculated from sonic temperature for humidity
        (Schotanus et al, 1983)
    """
    gamma = 1.404   # Ratio of specific heat of dry air at constant pressure to that at constant
                    # volume (Campbell Scientific, 1996; Schotanus et al , 1983)
    beta = 0.4      # Bowen ratio approximation (Schotanus et al , 1983)
    kelvin = temperatureInCelsius + 273.15
    speed_of_sound_squared = gamma * R_d * 100 * kelvin * (1 - 0.51 * specificHumidity)
    offset = 2 * kelvin * meanWindSpeed * verticalMomentumFlux / speed_of_sound_squared
    denominator = 1 + 0.51 * kelvin * C_p / L_v / beta

    return (sonicHeatFlux + offset) / denominator

@staticmethod
def segmentArea(radius, chordHeight):
    """ Calculates the area of a segment of a circle based on the radius and chord height (distance
        from the circumference)

    """
    return radius**2 * acos(chordHeight / radius) - chordHeight * (
            (radius**2 - chordHeight**2))**0.5

@staticmethod
def solar_elevation(latitude, declination, hour_angle):
    """ Calculates the solar elevation based on latitude, declination and hour angle.
    """
    lat = latitude / 180 * np.pi
    dec = declination / 180 * np.pi
    ha = hour_angle / 180 * np.pi
    return (np.sin(lat) * np.sin(dec) + np.cos(lat) * np.cos(dec) * np.cos(ha)) * 180 / np.pi

@staticmethod
def specificEnergyProduction(row, windSpeedColumn, powerCurve, interpolate=True, decimalPlaces=3):
    """ Calculates specific energy production given a wind speed and a power curve

    """
    return powerCurve.getPower(row[windSpeedColumn], interpolate, decimalPlaces)
@staticmethod
def specificHumidity(temperatureInCelsius, pressureInMillibars, relativeHumidityInPercent):
    """ Specific humidity (qv) from measured temperature, pressure and relative humidity
        Jacobson (2001) p. 33
    """
    Pw = Calc.waterVapourPartialPressure(temperatureInCelsius, relativeHumidityInPercent)
    Pd = pressureInMillibars - Pw
    return (R_d / R_v) * Pw / (Pd + (R_d / R_v) * Pw)
```

```python
@staticmethod
def stabilityClassObukhov(obukhovLength, meanWindSpeed, thresholdWindSpeed=5):
    """ Returns the stability class for a specified set of conditions. Classes are
        strongly stable, weakly stable, neutral, unstable (Vogelezang & Holtslag, 1996).
        The Obukhov length is used as the main criterion for classifying conditions
        (Wharton & Lundquist, 2010):
        Stable: 0 < L < 200
        Neutral: -300 > L or L > 200
        Unstable: 0 > L > -300
        Mean horizontal wind speed U at an appropriate height (~40m) is used to differentiate
        between stable regimes (van Hooijdonk et al., 2015):
        Strongly stable: U < thresholdWindSpeed
        Weakly stable: U >= thresholdWindSpeed
    """
    a = pd.cut(obukhovLength, [-1000000, -500, 0, 500, 1000000],
               labels=['neutral', 'unstable', 'stable', 'neutral2'])
    a[a=='neutral2'] = 'neutral'
    b = pd.cut(meanWindSpeed, [0, thresholdWindSpeed, 100], labels=['strongly ', 'weakly '])
    return [adverb + name if name == 'stable' else name for adverb, name in zip(b,a)]
@staticmethod
def stripeArea(radius, lowerChordHeight, upperChordHeight):
    """ Calculates the area of a horizontal stripe through a circle given the upper and lower chord
        heights

    """
    if (lowerChordHeight < 0) != (upperChordHeight < 0):
        return pi * radius**2 - Calc.segmentArea(radius, abs(lowerChordHeight)) - \
               Calc.segmentArea(radius, abs(upperChordHeight))
    else:
        return abs(Calc.segmentArea(radius, abs(upperChordHeight)) - \
                   Calc.segmentArea(radius, abs(lowerChordHeight)))

@staticmethod
def structure(data, order, lag):
    """ Structure function (Pope, 2000, p. 191; Stull, 1988, p. 300). The second-order structure
        function at lag 1 is equivalent to transience (Clive, 2012)
    """
    return (data - data.shift(-lag)).pow(order).mean()

@staticmethod
def supplementaryAngle(angle1):
    """ Returns the supplementary angle in degrees for the parameter (ie sums to 180)
    """
    return 180 - angle1

@staticmethod
def surfaceGeostrophicU(pressure_gradient_v, density, coriolis):
    """ Returns the zonal component of the geostrophic wind given the meridional component of the
        mean horizontal pressure gradient in pascals per metre. (Stull, 2015, p. 302)
    """
    return -pressure_gradient_v / density / coriolis

@staticmethod
def surfaceGeostrophicV(pressure_gradient_u, density, coriolis):
    """ Returns the meridional component of the geostrophic wind given the zonal component of the
        mean horizontal pressure gradient in pascals per metre. (Stull, 2015, p. 302)
    """
    return pressure_gradient_u / density / coriolis
@staticmethod
def temperatureFromSonic(sonicTemperatureInCelsius, PressureInMillibars,
                         relativeHumidityInPercent, absolute=True):
    """ Calculates absolute temperature from sonic temperature
        Kaimal & Gaynor, 1991
    """
    kelvin = Calc.celsiusToKelvin(sonicTemperatureInCelsius)
    q_v = Calc.specificHumidity(sonicTemperatureInCelsius, PressureInMillibars,
                                relativeHumidityInPercent)
    T = kelvin / (1 + 0.51 * q_v)
    if absolute:
        return T
    return Calc.kelvinToCelsius(T)

@staticmethod
def thermalU(temperature_gradient_v, virtual_temperature, boundary_layer_height, coriolis):
    """ Returns the zonal component of the thermal wind given the meridional component of the mean
        horizontal gradient of virtual temperature and the height of the boundary layer.
        (Stull, 2015, p. 345)
        temperature gradient is in degrees per kilometre
    """
    rate_of_change = -g * temperature_gradient_v / (virtual_temperature + 273.15) / coriolis / 1000
    return rate_of_change * boundary_layer_height
```

```
@staticmethod
def thermalV(temperature_gradient_u, virtual_temperature, boundary_layer_height, coriolis):
    """ Returns the meridional component of the thermal wind given the zonal component of the mean
        horizontal gradient of virtual temperature and the height of the boundary layer.
        (Stull, 2015, p. 345)
        temperature gradient is in degrees per kilometre
    """
    rate_of_change = g * temperature_gradient_u / (virtual_temperature + 273.15) / coriolis / 1000
    return rate_of_change * boundary_layer_height
@staticmethod
def thermodynamicRoughnessLength(temperatureInCelsius, pressureInMillibars,
                                 relativeHumidityInPercent, density, frictionVelocity):
    """ Height at which sensible heat transfer falls to zero
        Jacobson (2001) p. 233
    """
    Dh = Calc.molecularThermalDiffusivity(temperatureInCelsius, pressureInMillibars,
                                          relativeHumidityInPercent, density)
    return Dh / k / frictionVelocity

@staticmethod
def time_scale(autocorrelation, sampling_frequency):
    """Calculates the integral time scale by integrating an autocorrelation sequence.
       (Pope, 2000, p. 197)
    """
    return autocorrelation.sum() / sampling_frequency

@staticmethod
def turbulenceIntensity(windSpeedMean, windSpeedStandardDeviation):
    """ Calculates turbulence intensity from wind speed mean and standard deviation

    """
    return windSpeedStandardDeviation / windSpeedMean

@staticmethod
def turbulenceKineticEnergy(varianceX, varianceY, varianceZ):
    """ Calculates TKE based on wind speed variance in three dimensions

    """
    return 0.5 * (varianceX + varianceY + varianceZ)

@staticmethod
def unit_vector_ij(df, k):
    """ Returns arrays of vector components which are orthogonal to component k for the vector
        defined by each row of the dataframe df. Df is assumed to have three columns representing
        coordinates in 3 dimensions in the order u, v, w. (Lee et al, 2005 p.62)
        see unit_vector_k(), planar_fit() and rotate()
    """
    j = np.cross(k, df)
    j = [list(v / np.sqrt(sum(np.multiply(v, v)))) for v in j]
    i = np.cross(j, k)
    return i, j

@staticmethod
def unit_vector_k(b1, b2):
    """ Returns the components of the vertical unit vector in a rotated coordinate frame defined by
        the terms b1 and b2. B1 and b2 are two of the three coefficients in the equation of a plane
        fitted to a set of points in 3-dimensional space (Lee at al, 2005 p.62) - see planar_fit(),
        unit_vector_ij() and rotate()
    """
    k3 = 1 / (1 + b1 ** 2 + b2 ** 2)
    k1 = -b1 * k3
    k2 = -b2 * k3

    return [k1, k2, k3]

@staticmethod
def universalStabilityFunction(row, obukhovLength, measurementHeight, momentumOrHeat):
    """ Monin-Obukhov universal stability function - the third parameter selects momentum or heat
        Kramm, 2013
    """
    _z = measurementHeight / row[obukhovLength]
    if momentumOrHeat.upper() == 'M':
        _a = 15
        _b = 6.1
        _g = 2.5
    else:
        _a = 35.7
        _b = 5.3
        _g = 1.1

    if row[obukhovLength] < 0:
        return 1 / Calc.cubeRoot(1 - _a * _z)
    else:
        return 1 + _b * ((_z + _z**_g * (1 + _z**_g)**((1-_g)/_g)) / (_z + (1 + _z**_g)**(1/_g)))
```

```python
@staticmethod
def universalStabilityFunctionIntegrated(row, obukhovLength, measurementHeight, momentumOrHeat):
    """ Integrated form of the Monin-Obukhov stability function - the third parameter selects
        momentum or heat
        Kramm, 2013
    """
    _z = measurementHeight / row[obukhovLength]
    if momentumOrHeat.upper() == 'M':
        _a = 15
        _b = 6.1
        _g = 2.5
    else:
        _a = 35.7
        _b = 5.3
        _g = 1.1

    y = Calc.cubeRoot(1 - _a * _z)
    x = (2 * y + 1) / sqrt(3)

    if row[obukhovLength] >= 0:
        return -_b * log(_z + (1 + _z**_g)**(1/_g))
    else:
        return (3/2) * log((y**2 + y + 1) / 3) - sqrt(3) * atan((x - sqrt(3)) / (1 + sqrt(3) * x))

@staticmethod
def virtualTemperature(temperatureInCelsius, PressureInMillibars, relativeHumidityInPercent):
    """ The temperature of a sample of dry air at the same density and pressure as a sample of moist
        air.
        Jacobson (2001) p. 33
    """
    kelvin = Calc.celsiusToKelvin(temperatureInCelsius)
    q_v = Calc.specificHumidity(temperatureInCelsius, PressureInMillibars,
                                relativeHumidityInPercent)
    return kelvin * (1 + 0.608 * q_v)

@staticmethod
def waterVapourPartialPressure(temperatureInCelsius, relativeHumidityInPercent):
    """ Water vapour partial pressure from measured temperature and relative humidity (0-100) (hPa)
        Vaisala (2013) p. 7
    """
    saturationVapourPressure = Calc.saturationVapourPressure(temperatureInCelsius)
    return relativeHumidityInPercent * saturationVapourPressure / 100

@staticmethod
def wavenumbers(frequencies, mean_speed):
    """ Convert a series of frequencies to wavenumbers using the mean speed of the wind flow.
    (De Kat & Ganapathisubramani, 2015; McNaughton et al., 2007; Tropea et al., 2007, p. 762)
    """
    return np.array([2 * np.pi * f / mean_speed for f in frequencies])

@staticmethod
def windDirectionFromComponents(zonal, meridional):
    """ Calculates wind direction based on zonal and meridional components. Assumes the positive
        directions are S->N and W->E. (Stull, 2015, p.3)
    """
    return np.degrees(np.arctan2(zonal, meridional)) + 180


@staticmethod
def windShearExponentTwoHeights(lowerWindSpeed, upperWindSpeed, lowerHeight=10.0, upperHeight=10.0):
    """ Calculates the wind shear exponent based on wind speed values at two heights

    """
    return np.log(upperWindSpeed / lowerWindSpeed) / np.log(upperHeight / lowerHeight)


@staticmethod
def windSpeedFromComponents(u, v):
    """ Calculates the resultant scalar wind speed from vector components by Pythagoras
    """
    return np.sqrt(u**2 + v**2)

@staticmethod
def windSpeedRatio(lowerWindSpeed, upperWindSpeed):
    """ Measure of shear that is independent of hub height.
        Colls 2014
    """
    return upperWindSpeed / lowerWindSpeed
```

Appendix F: Dataset details

F1. Introduction

This appendix provides a description of the format of the research dataset described in Chapter 5. Because of the large number of columns, the structure is presented in an abbreviated manner and the information below will be helpful in interpreting the information.

The descriptive information about the columns is shown in a large matrix in §F.2. The leftmost column of the matrix contains the root of a column heading and a description. The root may contain placeholders indicated with <angle brackets>. These can be replaced by a number of different values:

`<h>` indicates one of the heights listed in the `heights` column.

`<s>` is an abbreviated statistic name

`<n>` is an integer

For example, the root `Umean_<h>+<s>` should be interpreted as a series of columns such as `Umean_9.9+kpss`, `Umean_79.1+mean`, `Umean_127.9+skew`, etc. The substitution values for the statistic names come from the vertically-oriented column headings in the matrix and described in Table 51. A statistic may be substituted into the root if there is an `x` in the relevant cell in the matrix.

The last two vertically-oriented column headings have a slightly different meaning. If there is an `x` under `Variance` for a particular column, this shows that there is a variance column related to the column root whose format follows the pattern `root_<h>_d-root_<h>_d`. The `_d` is intended to indicate a deviation from the mean. If there is an `x` under the `Covariance` column, it means that there will be a series of columns similar to the autocovariance, but combining the root column with other similar columns. These include the 3d components of wind velocity at the relevant height and the sonic temperature. For example, if the root column is related to the meridional horizontal wind velocity component at a height of 127.9 m, the series of columns generated would be

```
n-s_127.9_d-ts_127.9_d

n-s_127.9_d-uz_127.9_d

n-s_127.9_d-w-e_127.9_d
```

The order of the column roots in the matrix matches the order in which they appear in the data file.

Table 49: Abbreviated statistic names

Statistic	Description	Range
adf	Augmented Dickie-Fuller test p-value	[0, 1]
count	Count of data points in TMA value	[0, 600]
cv	Coefficient of variation (TI with wind speeds)	[0, ∞]
cv2	Second-order coefficient of variation	[0, 1]
dissipation	Rate of dissipation of turbulence	
intermittency	Excess kurtosis of wind speed increments	
kpss	Kwiatkowski-Phillips-Schmidt-Shin test p-value	[0.01, 0.1]
kurtosis	Kurtosis	
length_sclae	Turbulence length scale	
max	Maximum value	
mean	Mean value	
min	Minimum value	
jb	Jarque-Bera test p-value	[0, 1]
skew	Skew	
spikes	Count of spikes removed within averaging period	[0, 600]
std	Standard deviation	
transience	Second-order structure function	
filter	Count of points removed by filter	[0, 600]

F2. File format matrix

Column Name (base parameter) or description (derived parameter)	**adf**	**count**	**cv**	**cv2**	**dissipation**	**intermittency**	**kpss**	**kurtosis**	**length scale**	**max**	**mean**	**min**	**jb**	**skew**	**spikes**	**std**	**transience**	**filter**	**Variance**	**Covariance**	**Heights**	**Units**
Timestamp Date and time at the start of the averaging period																						
DST Daylight saving time flag. 1 when DST is in operation; 0 otherwise																						
Fuu_<h> Autocovariance of longitudinal wind speed in rotated coordinate frame																					9.9, 29.6, 79.1, 127.9	$m^2\ s^{-2}$
Fuv_<h> Covariance of longitudinal and lateral wind speed in rotated coordinate frame																					9.9, 29.6, 79.1, 127.9	$m^2\ s^{-2}$
Fuw_<h> Covariance of longitudinal and vertical wind speed in rotated coordinate frame (kinematic vertical flux of horizontal momentum)																					9.9, 29.6, 79.1, 127.9	$m^2\ s^{-2}$
Fvv_<h> Autocovariance of lateral wind speed in rotated coordinate frame																					9.9, 29.6, 79.1, 127.9	$m^2\ s^{-2}$
Fvw_<h> Covariance of lateral and vertical wind speed in rotated coordinate frame																					9.9, 29.6, 79.1, 127.9	$m^2\ s^{-2}$
Fww_<h> Autocovariance of vertical wind speed in rotated coordinate frame																					9.9, 29.6, 79.1, 127.9	$m^2\ s^{-2}$
H_<h> Kinematic vertical flux of sensible heat in rotated coordinate frame including Schotanus humidity correction																					9.9, 29.6, 79.1, 127.9	$K\ m\ s^{-1}$
Hu_<h> Covariance of longitudinal wind speed and temperature in rotated coordinate frame																					9.9, 29.6, 79.1, 127.9	$K\ m\ s^{-1}$
Hv_<h> Covariance of lateral wind speed and temperature in rotated coordinate frame																					9.9, 29.6, 79.1, 127.9	$K\ m\ s^{-1}$
Hw_<h> Covariance of vertical wind speed and temperature in rotated coordinate frame (kinematic vertical flux of sensible heat)																					9.9, 29.6, 79.1, 127.9	$K\ m\ s^{-1}$
L Obukhov length																					9.9	Dimensionless
Local time Local clock time																						

Column Name (base parameter) or description (derived parameter)	**adf**	**count**	**cv**	**cv2**	**dissipation**	**intermittency**	**kpss**	**kurtosis**	**length scale**	**max**	**mean**	**min**	**jb**	**skew**	**spikes**	**std**	**transience**	**filter**	**Variance**	**Covariance**	**Heights**	**Units**
Rib Bulk Richardson number																					9.9 - 79.1	Dimensionless
Solar noon azimuth Solar noon azimuth																						Degrees
Solar_noon_local Solar noon (local time)																						
Solar_noon_utc Solar noon (UTC)																						
Sunrise azimuth Sunrise azimuth																						Degrees
Sunrise_local Sunrise (local time)																						
Sunrise_utc Sunrise (UTC)																						
Sunset azimuth Sunset azimuth																						Degrees
Sunset_local Sunset (local time)																						
Sunset_utc Sunset (UTC)																						
TKE_<h> Turbulence kinetic energy																					9.9, 29.6, 79.1, 127.9	$m^2\ s^{-2}$
T_<h>+<s> PT100 temperature	x	x				x	x	x		x	x	x	x	x		x	x	x	x		7.3, 27.1, 76.7, 125.9	
T_lapse PT100 temperature - Environmental lapse rate																					7.3 - 125.9	$K\ m^{-1}$
UTC offset Difference between local time and UTC																						hours
U_<h> Horizontal wind speed from sonic components after reduction to ten-minute averages																					9.9, 29.6, 79.1, 127.9	$m\ s^{-1}$
Umean_<h>+<s> Horizontal wind speed from sonic components	x	x	x	x	x	x	x	x	x	x	x	x	x	x		x	x	x	x		9.9, 29.6, 79.1, 127.9	
alpha																					9.9 - 127.9	

Column Name (base parameter) or description (derived parameter)	**adf**	**count**	**cv**	**cv2**	**dissipation**	**intermittency**	**kpss**	**kurtosis**	**length scale**	**max**	**mean**	**min**	**jb**	**skew**	**spikes**	**std**	**transience**	**filter**	**Variance**	**Covariance**	**Heights**	**Units**
Wind shear exponent (whole rotor)																						
alpha0_<h>																					9.9, 29.6, 79.1, 127.9	deg
alpha_lower Cross-isobar angle																					9.9 - 79.1	
alpha_upper Wind shear exponent (upper half of rotor)																					79.1 - 127.9	
curtailment_Curtailment_lost Count of values lost because of curtailment																						
day_number Julian day number																						
declination Solar declination																						deg
density Air density																					79.1	kg m^{-3}
diag<n>_Anemometer <n> fault_lost Count of values lost via sonic anemometer <n> fault filter																						
dir_<h> Wind direction																					9.9, 29.6, 79.1, 127.9	deg
dpm Meridional horizontal pressure gradient																					10	Pa m^{-1}
dpz Zonal horizontal pressure gradient																					10	Pa m^{-1}
dtm Meridional horizontal temperature gradient																					10	K m^{-1}
dtz Zonal horizontal temperature gradient																					10	K m^{-1}
fault_code_Turbine fault_lost Count of values lost via turbine fault filter																						
geostrophic																					10	m s^{-1}
geostrophic_dir Geostrophic wind speed																					10	deg
geostrophic_u Zonal component of geostrophic wind velocity																					10	m s^{-1}

Column Name (base parameter) or description (derived parameter)	**adf**	**count**	**cv**	**cv2**	**dissipation**	**intermittency**	**kpss**	**kurtosis**	**length scale**	**max**	**mean**	**min**	**jb**	**skew**	**spikes**	**std**	**transience**	**filter**	**Variance**	**Covariance**	**Heights**	**Units**
geostrophic_v Meridional component of geostrophic wind velocity																					10	m s^{-1}
hour_angle Solar hour angle																						deg
hub_speed+<s> Hub angular velocity	x	x	x	x		x	x	x		x	x	x	x	x		x	x					
inflow_<h> Inflow angle																					9.9, 29.6, 79.1, 127.9	deg
n-s_<h>+<s> Meridional component of wind velocity	x	x	x	x	x	x	x	x	x	x	x	x	x	x	x	x	x	x	x	x	9.9, 29.6, 79.1, 127.9	
power+<s> Power (despiked)	x	x	x	x		x	x	x		x	x	x	x	x	x	x	x					
power_raw+<s> Power	x	x	x	x		x	x	x		x	x	x	x	x		x	x					
pressure_80+<s> Barometric pressure	x	x	x	x		x	x	x		x	x	x	x	x	x	x	x				80	
rews Rotor equivalent wind speed																					9.9 - 127.9	m s^{-1}
rh_80+<s> Relative humidity	x	x	x	x		x	x	x		x	x	x	x	x	x	x	x				80	
rm Rossby-Montgomery coefficient																						
rotor+<s> Rotor angular velocity	x	x	x	x		x	x	x		x	x	x	x	x		x	x					
scada_density+<s> Air density from SCADA	x	x	x	x		x	x	x		x	x	x	x	x		x	x				80	
scada_pressure+<s> Barometric pressure from SCADA	x	x	x	x		x	x	x		x	x	x	x	x		x	x				80	
scada_u+<s> Wind speed from SCADA	x	x	x	x		x	x	x		x	x	x	x	x		x	x	x	x		80	
sh Specific humidity																					80	kg kg^{-1}

Column Name (base parameter) or description (derived parameter)	adf	count	cv	cv2	dissipation	intermittency	kpss	kurtosis	length scale	max	mean	min	jb	skew	spikes	std	transience	filter	Variance	Covariance	Heights	Units
sl_pressure Sea-level pressure																					80 normalised to sea level	mbar
solar_elevation Solar elevation																						deg
stability_obukhov Stability class from Obukhov length																					9.9	
stability_rib Stability class from bulk Richardson number																					0 - 79.1	
surface_geostrophic_u Zonal component of surface geostrophic wind speed																					10	$m\ s^{-1}$
surface_geostrophic_v Meridional component of surface geostrophic wind speed																					10	$m\ s^{-1}$
thermal_u Zonal component of thermal wind speed																					10	$m\ s^{-1}$
thermal_v Meridional component of thermal wind speed																					10	$m\ s^{-1}$
theta_<h> Potential virtual temperature																					9.9, 29.6, 79.1, 127.9	K
theta_lapse Potential virtual temperature - environmental lapse rate																					9.9 - 127.9	$K\ m^{-1}$
theta_surface Potential virtual temperature - extrapolated value at surface																					9.9 - 127.9 extrapolated to 0	K
ts_<h>+<s> Sonic temperature	x	x				x	x	x		x	x	x	x	x	x	x	x	x	x	x	127.9	
turbine_Turbine operating_lost Count of data points lost due to "Turbine operating" filter																						
ustar Friction velocity																					9.9	$m\ s^{-1}$
uxr_<h> Longitudinal component of wind velocity in rotated coordinate frame																					9.9, 29.6, 79.1, 127.9	$m\ s^{-1}$
uyr_<h> Lateral component of wind velocity in rotated coordinate frame																					9.9, 29.6, 79.1, 127.9	$m\ s^{-1}$
uz_<h>+<s>	x	x	x	x	x	x	x	x	x	x	x	x	x	x	x	x	x	x	x	x	9.9, 29.6, 79.1, 127.9	

Column Name (base parameter) or description (derived parameter)	adf	count	cv	cv2	dissipation	intermittency	kpss	kurtosis	length scale	max	mean	min	jb	skew	spikes	std	transience	filter	Variance	Covariance	Heights	Units
Vertical component of wind velocity																						
uzr_<h> Vertical component of wind velocity in rotated coordinate frame																					9.9, 29.6, 79.1, 127.9	m s^{-1}
veer_<h> Wind veer (calculated on difference between label height and 127.9 m) Degrees per 100 m (decametre)																					9.9, 29.6, 79.1	deg dm^{-1}
w-e_<h>+<s> Zonal component of wind velocity	x	x	x	x	x	x	x	x	x	x	x	x	x	x	x	x	x	x	x	x	127.9	
ws_ratio Wind speed ratio																					9.9 - 127.9	Dimensionless
zeta Obukhov stability parameter																					9.9	Dimensionless
zi_rm Boundary layer height																					9.9	m

F3. File excerpt

The file containing the research dataset has 727 columns including the timestamp and 52,560 rows. The excerpt below is therefore a small fraction of the whole. The entire file may be accessed at https://doi.org/10.13020/1etn-1q17

Timestamp	DST	Fuu_127.9	Fuu_29.6	Fuu_79.1	Fuu_9.9	Fuv_127.9	Fuv_29.6	…	w-e_9.9_d-uz_9.9_d	w-e_9.9_d-w-e_9.9_d	ws_ratio	zeta	zi_rm
01/01/2017 00:00	0	0.2493	0.2599	0.1753	0.204	-0.0284	-0.0102	…	-0.0288	0.1809	2.2296	0.2939	79.7035
01/01/2017 00:10	0	0.0207	0.2351	0.105	0.2146	-0.0083	-0.0157	…	-0.0401	0.2137	2.3319	0.2586	99.2145
01/01/2017 00:20	0	0.0271	0.2306	0.0759	0.1369	0.0115	-0.0143	…	-0.0154	0.1487	2.6126	0.2678	75.5548
01/01/2017 00:30	0	0.0212	0.3179	0.1247	0.2017	0.0144	-0.021	…	-0.008	0.128	2.3743	0.6575	52.095
01/01/2017 00:40	0	0.1468	0.2112	0.1565	0.1088	0.0046	-0.0188	…	-0.0076	0.091	2.6544	0.6429	51.4692
01/01/2017 00:50	0	0.0226	0.1989	0.1408	0.1723	-0.015	0.0121	…	-0.0047	0.0965	2.6783	0.6438	57.7342
01/01/2017 01:00	0	0.0328	0.3351	0.1867	0.1432	-0.0211	-0.004	…	-0.0065	0.1201	2.9634	1.243	40.1725
01/01/2017 01:10	0	0.028	0.2397	0.1707	0.1503	0.0016	-0.0207	…	-0.0119	0.144	2.6889	0.5616	51.6054
01/01/2017 01:20	0	0.0458	0.3273	0.1681	0.1942	-0.0053	-0.0301	…	-0.0164	0.1639	2.6355	0.2939	80.0563
01/01/2017 01:30	0	0.0492	0.4601	0.1631	0.2575	0.0113	-0.0401	…	-0.0093	0.2007	2.5623	0.2148	92.4837
01/01/2017 01:40	0	0.0525	0.4646	0.3277	0.2814	0.0023	0.0279	…	-0.0071	0.1897	2.4713	0.1812	100.2265
01/01/2017 01:50	0	0.1095	0.6002	0.5161	0.4538	-0.0329	-0.0106	…	-0.0461	0.3049	2.2801	0.1536	114.8733
01/01/2017 02:00	0	0.1694	0.7718	0.4843	0.5643	-0.046	0.0305	…	-0.042	0.4181	2.2238	0.0836	157.2446
01/01/2017 02:10	0	0.3863	0.8516	0.7113	0.4966	-0.0746	0.1001	…	-0.0481	0.35	2.2956	0.0469	181.6997
01/01/2017 02:20	0	0.3951	0.9617	0.8621	0.432	-0.0641	0.115	…	0.0089	0.5154	2.241	0.0773	138.4155
01/01/2017 02:30	0	0.4261	0.93	0.6416	0.6564	-0.0892	0.0733	…	-0.0533	0.7025	1.9675	0.0911	171.7712
01/01/2017 02:40	0	0.6229	1.2709	0.9267	0.8471	-0.1034	0.0066	…	-0.0718	0.5486	2.0461	0.0286	288.7522
01/01/2017 02:50	0	0.2491	0.895	0.636	0.4694	-0.0227	-0.0149	…	-0.0106	0.5213	2.0767	0.0986	146.1978
01/01/2017 03:00	0	0.2656	0.7744	0.6786	0.4465	-0.0787	-0.0494	…	-0.0279	0.4509	2.1269	0.0735	182.8451
01/01/2017 03:10	0	0.2548	0.7861	0.5672	0.4272	-0.0026	-0.053	…	-0.0637	0.3985	2.0535	0.1275	141.8447
…	…	…	…	…	…	…	…		…	…	…	…	…
31/12/2017 20:40	0	0.6188	0.427	0.6598	0.5291	-0.338	-0.1048	…	-0.0644	0.5212	1.2858	-0.1024	437.2095
31/12/2017 20:50	0	0.6589	0.9055	0.8239	0.6183	-0.3023	-0.2251	…	-0.0835	0.447	1.2707	-0.0492	514.7325
31/12/2017 21:00	0	1.2497	0.8068	0.8149	0.6787	-0.5543	-0.0375	…	-0.1531	0.7279	1.4616	-0.0074	416.6534
31/12/2017 21:10	0	1.0203	1.5269	1.4536	1.0987	0.055	0.239	…	-0.142	1.0717	1.334	-0.0072	357.6992
31/12/2017 21:20	0	0.1266	0.7393	0.2944	0.5488	-0.0221	0.0546	…	-0.1295	0.5975	1.4127	-0.0267	398.6263
31/12/2017 21:30	0	0.567	0.6662	0.5725	0.5125	-0.2883	-0.0057	…	-0.1045	0.5318	1.3457	-0.0002	290.5791
31/12/2017 21:40	0	0.3461	0.4326	0.6014	0.3953	-0.1507	-0.0014	…	-0.1001	0.3965	1.4002	0.0166	248.8696
31/12/2017 21:50	0	0.2165	1.0464	0.6611	0.8148	-0.0787	0.0235	…	-0.1864	0.8087	1.4038	0.0012	369.4454
31/12/2017 22:00	0	0.1308	0.5419	0.3108	0.5164	-0.0656	-0.0331	…	-0.1401	0.5122	1.475	0.0188	275.092
31/12/2017 22:10	0	0.2093	0.6199	0.3815	0.5373	-0.0623	-0.0467	…	-0.1336	0.5328	1.5078	0.0346	245.2084
31/12/2017 22:20	0	0.3058	0.5016	0.4339	0.5019	-0.0576	0.0438	…	-0.1137	0.4958	1.7351	0.0409	222.3969
31/12/2017 22:30	0	0.3959	0.5849	0.5831	0.4217	-0.0741	-0.0953	…	-0.0792	0.4159	1.5758	0.0905	157.294
31/12/2017 22:40	0	0.5481	0.7897	0.8603	0.529	-0.0222	0.0857	…	-0.107	0.5294	1.5925	0.0683	190.8442
31/12/2017 22:50	0	0.4023	0.7212	0.7471	0.5741	-0.1079	0.0098	…	-0.1399	0.5734	1.6258	0.0715	217.5741
31/12/2017 23:00	0	0.7555	0.6049	0.6731	0.3268	-0.3645	-0.1058	…	-0.0538	0.3273	1.5613	0.2079	113.5456
31/12/2017 23:10	0	0.3224	0.5268	0.5893	0.4314	-0.1257	-0.0376	…	-0.0906	0.4239	1.8252	0.0388	194.8521
31/12/2017 23:20	0	0.0938	0.7405	0.2508	0.5482	-0.0292	0.0123	…	-0.1433	0.5502	1.5902	0.0402	246.4889
31/12/2017 23:30	0	0.1846	0.6129	0.3747	0.4525	-0.0655	-0.0286	…	-0.1135	0.4477	1.6201	0.0648	204.4273
31/12/2017 23:40	0	0.3206	0.6681	0.6421	0.5589	-0.0406	0.1016	…	-0.1316	0.5542	1.6219	0.0457	229.8122
31/12/2017 23:50	0	0.1044	0.7427	0.2949	0.8832	0.0099	-0.0834	…	-0.2014	0.8776	1.6029	0.0369	295.0123

Appendix G: Parameter dependencies

Column	stats	count	left	right	closed	string	include	d1	d2	d3	d4	d5	d6
Rib								theta_127.9	theta_surface	U_127.9			
DST													
Fuu_<h>								w-e_<h>_d-w-e_<h>_d	n-s_<h>_d-w-e_<h>_d	w-e_<h>_d-uz_<h>_d	n-s_<h>_d-n-s_<h>_d	n-s_<h>_d-uz_<h>_d	uz_<h>_d-uz_<h>_d
Fuv_<h>								w-e_<h>_d-w-e_<h>_d	n-s_<h>_d-w-e_<h>_d	w-e_<h>_d-uz_<h>_d	n-s_<h>_d-n-s_<h>_d	n-s_<h>_d-uz_<h>_d	uz_<h>_d-uz_<h>_d
Fuw_<h>			-9999	0	1			w-e_<h>_d-w-e_<h>_d	n-s_<h>_d-w-e_<h>_d	w-e_<h>_d-uz_<h>_d	n-s_<h>_d-n-s_<h>_d	n-s_<h>_d-uz_<h>_d	uz_<h>_d-uz_<h>_d
Fvv_<h>								w-e_<h>_d-w-e_<h>_d	n-s_<h>_d-w-e_<h>_d	w-e_<h>_d-uz_<h>_d	n-s_<h>_d-n-s_<h>_d	n-s_<h>_d-uz_<h>_d	uz_<h>_d-uz_<h>_d
Fvw_<h>								w-e_<h>_d-w-e_<h>_d	n-s_<h>_d-w-e_<h>_d	w-e_<h>_d-uz_<h>_d	n-s_<h>_d-n-s_<h>_d	n-s_<h>_d-uz_<h>_d	uz_<h>_d-uz_<h>_d
Fww_<h>								w-e_<h>_d-w-e_<h>_d	n-s_<h>_d-w-e_<h>_d	w-e_<h>_d-uz_<h>_d	n-s_<h>_d-n-s_<h>_d	n-s_<h>_d-uz_<h>_d	uz_<h>_d-uz_<h>_d
Hu_<h>								w-e_<h>_d-ts_<h>_d	n-s_<h>_d-ts_<h>_d	uz_<h>_d-ts_<h>_d			
Hv_<h>								w-e_<h>_d-ts_<h>_d	n-s_<h>_d-ts_<h>_d	uz_<h>_d-ts_<h>_d			
Hw_<h>								w-e_<h>_d-ts_<h>_d	n-s_<h>_d-ts_<h>_d	uz_<h>_d-ts_<h>_d			
H_<h>								Hw_<h>	Fuw_<h>	uxr_<h>	sh		
L								ustar	theta_9.9	H_9.9			
Local time								UTC offset					
Solar noon azimuth													
Solar_noon_local													
Solar_noon_utc													
Sunrise azimuth													
Sunrise_local													
Sunrise_utc													
Sunset azimuth													
Sunset_local													
Sunset_utc													
TKE_<h>								n-s_<h>_d-n-s_<h>_d	w-e_<h>_d-w-e_<h>_d	uz_<h>_d-uz_<h>_d			
T_7.3			-40	40									
T_27.1			-40	40									
T_76.7			-40	40									
T_125.9			-40	40									
T_lapse								T_7.3	T_125.9				
UTC offset													
U_<h>			0	30				w-e_<h>	n-s_<h>				
Umean_<h>	1		0	30				w-e_<h>	n-s_<h>				
alpha								U_9.9	U_127.9				
alpha0_<h>								dir_<h>	geostrophic_dir				
alpha_lower								U_9.9	U_79.1				
alpha_upper								U_79.1	U_127.9				
day_number													
declination													
density								pressure_80	ts_79.1				
dir_<h>			40	320				w-e_<h>	n-s_<h>				
dpm													
dpz													
fault_code_Turbine fault_lost			0	60									

Column	stats	count	left	right	closed	string	include	d1	d2	d3	d4	d5	d6
geostrophic								geostrophic_u	geostrophic_v				
geostrophic_dir								geostrophic_u	geostrophic_v				
geostrophic_u								dpm	density				
geostrophic_v								dpz	density				
hour_angle													
hub_speed	1	600											
inflow_<h>								U_<h>	uz_<h>				
n-s_<h>	1	12000	-30	30									
n-s_<h>_d-n-s_<h>_d								n-s_<h>					
n-s_<h>_d-ts_<h>_d								n-s_<h>	ts_<h>				
n-s_<h>_d-uz_<h>_d								n-s_<h>	uz_<h>				
n-s_<h>_d-w-e_<h>_d								n-s_<h>	w-e_<h>				
power	1	600	-500	2800									
power_raw	1	600											
pressure_80	1	600	900	1100									
rews			0	30				U_29.6	U_79.1	U_127.9	dir_29.6	dir_79.1	dir_127.9
rh_80	1	600	0	99	0								
rm								L					
rotor	1	600											
scada_density	1	600											
scada_dir	1	600											
scada_pressure	1	600											
scada_u	1	600											
sh								T_76.7	pressure_80	rh_80			
sl_pressure								pressure_80	ts_79.1				
solar_elevation													
stability_obukhov								L	U_29.6				
stability_rib								Rib	U_29.6				
theta_<h>								ts_<h>	pressure_80				
theta_lapse								theta_9.9	theta_127.9				
theta_surface								theta_9.9	theta_lapse				
ts_<h>	1	12000	-40	40									
ts_<h>_d-ts_<h>_d								ts_<h>					
turbine_Turbine operating_lost			0	60									
ustar								Fuw_9.9	Fvw_9.9				
uxr_<h>								w-e_<h>	n-s_<h>	uz_<h>			
uyr_<h>								w-e_<h>	n-s_<h>	uz_<h>			
uz_<h>	1	12000	-10	10									
uz_<h>_d-ts_<h>_d								uz_<h>	ts_<h>				
uz_<h>_d-uz_<h>_d								uz_<h>					
uzr_<h>								w-e_<h>	n-s_<h>	uz_<h>			
veer_9.9								alpha0_127.9	alpha0_9.9				
veer_29.6								alpha0_127.9	alpha0_29.6				
veer_79.1								alpha0_127.9	alpha0_79.1				
w-e_<h>	1	12000	-30	30									
w-e_<h>_d-ts_<h>_d								w-e_<h>	ts_<h>				
w-e_<h>_d-uz_<h>_d								w-e_<h>	uz_<h>				
w-e_<h>_d-w-e_<h>_d								w-e_<h>					
ws_ratio								U_29.6	U_127.9				
zeta								L					
zi_rm								ustar	rm				

Appendix H: Correlation matrix

	Umean_79.1+adf	Umean_79.1+dissipation	Umean_79.1+intermittency	Umean_79.1+length_scale	Umean_79.1+mean	Umean_79.1+normality	Umean_79.1+std	Umean_79.1+transience	uz_79.1+adf	uz_79.1+cv	uz_79.1+cv2	uz_79.1+dissipation	uz_79.1+intermittency	uz_79.1+mean	uz_79.1+normality	uz_79.1+transience	T_76.7+kpss	T_76.7+mean	T_76.7+normality	T_76.7+transience	pressure_80+normality	pressure_80+transience	rh_80+mean	rh_80+transience	Fuw_79.1	H_79.1	TKE_79.1	theta_79.1	zeta	Rib	ws_ratio	T_lapse	theta_lapse	declination	rews	density
Umean_79.1+dissipation	-0.02																																			
Umean_79.1+intermittency	-0.02	0.01																																		
Umean_79.1+length_scale	-0.25	0.00	0.03																																	
Umean_79.1+mean	-0.15	0.08	0.02	0.33																																
Umean_79.1+normality	-0.02	0.00	0.05	0.00	0.01																															
Umean_79.1+std	-0.28	0.14	0.04	0.71	0.51	-0.01																														
Umean_79.1+transience	-0.09	0.92	0.03	0.13	0.30	0.00	0.39																													
uz_79.1+adf	0.54	-0.01	-0.01	-0.19	-0.14	-0.01	-0.20	-0.06																												
uz_79.1+cv	0.01	0.00	0.00	0.01	0.03	0.00	0.02	0.00	0.00																											
uz_79.1+cv2	-0.38	0.03	0.05	0.51	0.13	-0.02	0.61	0.16	-0.24	0.03																										
uz_79.1+dissipation	0.01	0.00	0.00	0.01	0.03	0.00	0.03	0.00	0.00	0.98	0.03																									
uz_79.1+intermittency	-0.11	0.01	0.68	0.10	0.00	0.05	0.09	0.04	-0.09	0.01	0.09	0.01																								
uz_79.1+mean	-0.09	-0.04	0.03	0.19	-0.07	-0.02	0.12	-0.05	-0.04	0.01	0.37	0.01	0.03																							
uz_79.1+normality	0.01	0.00	-0.01	0.00	-0.04	-0.01	-0.01	-0.01	-0.01	0.00	0.02	0.00	-0.02	0.00																						
uz_79.1+transience	-0.21	0.42	0.03	0.42	0.63	0.00	0.80	0.70	-0.13	0.00	0.39	0.00	0.05	-0.02	-0.01																					
T_76.7+kpss	-0.01	-0.01	-0.01	0.01	0.02	-0.01	0.00	-0.01	0.00	0.00	-0.01	0.00	-0.01	-0.02	0.00	0.00																				
T_76.7+mean	0.14	-0.01	-0.08	-0.16	-0.05	0.01	-0.20	-0.07	0.09	-0.05	-0.23	-0.05	-0.10	-0.21	0.00	-0.16	0.03																			
T_76.7+normality	0.06	-0.01	-0.01	-0.02	-0.03	-0.01	-0.03	-0.01	0.05	0.00	-0.01	0.00	-0.02	0.00	0.02	-0.02	0.04	-0.02																		
T_76.7+transience	-0.01	0.00	0.00	0.00	0.00	0.04	-0.02	-0.01	-0.01	-0.02	0.03	-0.02	-0.01	0.01	-0.01	-0.02	0.03	0.04	-0.05																	
pressure_80+normality	0.01	-0.01	-0.01	-0.04	0.05	-0.01	-0.08	-0.02	-0.03	-0.01	-0.06	0.00	-0.03	-0.02	-0.01	-0.05	-0.01	0.08	-0.02	0.00																
pressure_80+transience	-0.09	0.04	0.02	0.27	0.10	-0.03	0.35	0.13	-0.06	0.00	0.25	0.00	0.04	0.00	-0.01	0.28	-0.01	-0.16	-0.01	-0.03	-0.06															
rh_80+mean	-0.21	0.04	0.04	-0.10	-0.08	0.03	-0.06	0.05	-0.14	-0.02	-0.02	-0.03	0.05	-0.04	0.01	0.01	0.01	-0.07	-0.04	0.01	0.05	-0.01														
rh_80+transience	-0.11	0.00	-0.01	0.23	0.03	-0.02	0.31	0.05	-0.06	0.00	0.24	-0.01	0.03	0.08	-0.02	0.15	0.00	0.30	-0.03	-0.03	-0.06	0.13	-0.25													
Fuw_79.1	0.18	-0.14	-0.03	-0.57	-0.48	0.02	-0.87	-0.39	0.11	0.00	-0.48	0.00	-0.06	-0.08	0.03	-0.78	0.00	0.14	0.01	0.02	0.07	-0.33	0.10	-0.28												
H_79.1	-0.05	0.06	-0.02	0.26	-0.03	-0.03	0.31	0.06	-0.03	0.01	0.30	0.01	0.03	0.09	-0.03	0.11	0.04	0.09	-0.01	-0.03	-0.08	0.26	-0.23	0.37	-0.36											
TKE_79.1	-0.21	0.16	0.03	0.62	0.55	-0.02	0.94	0.43	-0.13	0.01	0.52	0.01	0.07	0.08	-0.02	0.86	0.01	-0.15	-0.02	-0.03	-0.08	0.36	-0.13	0.32	-0.92	0.38										
theta_79.1	0.14	0.00	-0.07	-0.16	-0.04	0.01	-0.20	-0.06	0.08	-0.05	-0.24	-0.05	-0.10	-0.21	0.00	-0.15	0.02	1.00	-0.02	0.03	0.08	-0.17	-0.06	0.30	0.14	0.07	-0.15									
zeta	0.14	-0.01	-0.01	-0.17	-0.06	-0.01	-0.20	-0.05	0.13	0.00	-0.19	0.00	-0.05	-0.03	0.00	-0.12	-0.02	0.06	-0.02	0.01	0.01	-0.07	-0.06	-0.07	0.13	-0.06	-0.15	0.06								
Rib	0.54	-0.03	-0.03	-0.46	-0.36	-0.01	-0.54	-0.14	0.51	-0.01	-0.52	-0.01	-0.10	-0.07	0.00	-0.35	-0.01	0.24	0.02	0.02	0.02	-0.18	-0.13	-0.15	0.36	-0.19	-0.42	0.24	0.25							
ws_ratio	0.05	-0.03	-0.02	-0.45	-0.04	0.01	-0.45	-0.11	0.00	-0.02	-0.34	-0.02	-0.08	-0.16	0.01	-0.26	0.00	0.20	0.01	0.04	0.10	-0.29	0.13	-0.13	0.36	-0.42	-0.42	0.21	0.14	0.27						
T_lapse	-0.45	0.04	0.04	0.55	0.06	0.01	0.63	0.16	-0.32	0.02	0.61	0.02	0.13	0.14	0.01	0.40	0.00	-0.28	-0.01	-0.02	-0.10	0.28	0.10	0.19	-0.45	0.29	0.52	-0.29	-0.23	-0.71	-0.59					
theta_lapse	-0.46	0.04	0.03	0.57	0.09	0.01	0.67	0.17	-0.33	0.02	0.62	0.02	0.12	0.17	0.01	0.43	0.01	-0.30	-0.01	-0.02	-0.10	0.29	0.09	0.20	-0.49	0.32	0.56	-0.30	-0.24	-0.75	-0.60	0.96				
declination	0.08	-0.03	-0.08	-0.14	-0.05	0.04	-0.21	-0.07	0.06	-0.03	-0.19	-0.03	-0.08	-0.12	0.01	-0.13	0.04	0.35	-0.02	0.08	0.03	0.02	0.26	-0.07	0.15	0.02	-0.18	0.33	0.09	0.17	0.08	-0.19	-0.19			
rews	-0.19	0.08	0.02	0.31	0.99	0.02	0.49	0.30	-0.17	0.02	0.13	0.03	0.00	-0.10	-0.03	0.62	0.02	-0.04	-0.03	0.01	0.06	0.08	-0.03	0.02	-0.46	-0.07	0.52	-0.03	-0.06	-0.37	0.05	0.05	0.08	-0.03		
density	-0.13	-0.01	0.07	0.16	0.02	-0.01	0.18	0.04	-0.08	0.05	0.23	0.05	0.09	0.20	0.00	0.12	-0.02	-0.99	0.03	-0.03	-0.09	0.16	0.05	-0.30	-0.12	-0.06	0.12	-1.00	-0.05	-0.24	-0.22	0.28	0.30	-0.30	0.01	
zi_rm	-0.26	0.06	0.02	0.63	0.38	-0.02	0.81	0.25	-0.17	0.04	0.60	0.04	0.09	0.08	-0.01	0.59	0.03	-0.14	-0.01	-0.04	-0.11	0.42	-0.16	0.39	-0.72	0.63	0.80	-0.15	-0.20	-0.52	-0.59	0.64	0.68	-0.18	0.35	0.14